ABSTRACT

Title of Dissertation: LIQUID CRYSTAL VARIATIONAL, PROBLEMS: MODELING, NUMERICAL ANALYSIS AND COMPUTATION

Lucas Christopher Bouck
Doctor of Philosophy, 2023

Dissertation Directed by: Professor Ricardo H. Nochetto
AMSC Program, Department of Mathematics

This dissertation is concerned with the numerical analysis and computation of variational models related to liquid crystals (LCs) and liquid crystal polymer networks (LCNs) as well as modeling of LCNs.

We first present a finite element method and projection free gradient flow to minimize the Frank-Oseen energy of nematic liquid crystals. The Frank-Oseen model is a continuum model that represents the liquid crystal with a vector field that must satisfy a nonconvex unit-length constraint pointwise. We prove convergence of minimizers of the discrete problem to minimizers of the continuous problem using the framework of Γ-convergence. The convergence analysis has no restrictions on the elastic constants or regularity of the solution beyond that required for existence of minimizers. Due to the low regularity requirement, the method can capture point defects. We also propose a projection free gradient flow algorithm to compute critical points of the discrete energy. The gradient flow is conditionally stable under a mild restriction on the

numerical parameters. We finally present computations illustrating the influence of the elastic constants on point defects as well as the influence of external magnetic fields.

The second part of this dissertation is concerned with modeling, numerical analysis, and computation of thin LCNs. We first begin from a classical 3D energy of LCN and use Kirchhoff-Love asymptotics to derive a reduced 2D membrane model. We then prove many properties of the membrane model including a pointwise metric condition that zero energy states must satisfy and construct a formal method to approximate configurations of LCN from higher degree defects that approximately match this pointwise condition. To conclude, we develop a finite element method to minimize the stretching energy. A key component of the discrete energy is to introduce a regularization that is inspired by a bending energy for LCN, which is also derived in this dissertation. We prove convergence of minimizers of the discrete problem to zero energy states of the continuous problem in the spirit of Γ-convergence. To compute critical points of the discrete problem, we propose a fully implicit gradient flow with Newton sub-iteration and study its superlinear convergence under suitable assumptions. We finish with many simulations that highlight interesting features of LCNs, including configurations arising from LC defects and nonisometric origami.

LIQUID CRYSTAL VARIATIONAL PROBLEMS: MODELING, NUMERICAL ANALYSIS, AND COMPUTATION

by

Lucas Christopher Bouck

Dissertation submitted to the Faculty of the Graduate School of the
University of Maryland, College Park in partial fulfillment
of the requirements for the degree of
Doctor of Philosophy
2023

Advisory Committee:
Professor Ricardo H. Nochetto, Chair/Advisor
Professor André Tits, Dean's Representative
Professor Howard Elman
Dr. Antonio De Rosa
Dr. Haizhao Yang

Acknowledgments

I first and foremost want to express my deepest gratitude to my advisor, Prof. Ricardo H. Nochetto, for his guidance, mentorship, and support throughout my PhD. There were many weekends, late nights, and long meetings where Ricardo was there to advise and discuss math and other topics with me. I am incredibly thankful for all of these things and more.

Thank you to my committee members: Prof. André Tits, Prof. Howard Elman, Dr. Antonio De Rosa, and Dr. Haizhao Yang for their feedback on this dissertation. I further want to thank Antonio for all our math discussions over the past few years. Another mentor I want to thank is Harbir Antil for his mentorship when I was an undergraduate student at George Mason University and his advice throughout my graduate studies.

Thank you to my friends and family, who have been crucial to my success and happiness over the past five years. I am grateful to my parents and sisters for their support. I want to express my deep gratitude to my girlfriend, Spencer Gee, for her love and support. I cherish our time together and am grateful for all the long trips you have made to see me in Maryland. Thank you to my graduate school and DC area friends, especially Luis Suárez, Brandon Kolstoe, Joe Russell, and Jim Gibson. I also want to thank my climbing partners, Andrew Laugharn and Ben Thesing, for our times in the mountains together.

I finally want to acknowledge the support of National Science Foundation Graduate Research Fellowship Program (DGE-1840340).

Table of Contents

List of Tables

List of Figures

List of Abbreviations

LC - liquid crystal
LCE - liquid crystal elastomer
LCN - liquid crystal polymer network
FEM - finite element method
DG - discontinuous Galerkin
$\mathcal{T}_h$ - triangulation (mesh, partition) of a domain Ω with mesh size h
$\mathcal{N}_h$ - nodes of a triangulation
$\mathcal{E}_h$ - internal edge set of a triangulation
$[v_h]$ - jump of v_h over an edge
$\mathbb{V}_h$ - finite element space of continuous piecewise affine functions $\mathbf{v}_h : \Omega \to \mathbb{R}^3$

Chapter 1: Introduction

Liquid crystals (LC) are a class of materials that can have intermediate phases between liquid and solid. One particular phase is the nematic phase, where LC molecules often retain an orientation order with their neighbors but no longer retain a positional order. As a result, the LC can flow like a liquid but retain desirable optical properties in the nematic phase, which is ideal for optical applications [106, 110]. When coupled with a rubbery network, the combination of LC and rubber becomes a liquid crystal elastomer (LCE) or liquid crystal polymer network (LCN). A LCE/LCN material can deform when heated or actuated, and the deformation depends on the orientation of the LC. An engineer can design (or blueprint) the orientation of the LC when forming the LCE/LCN material, which makes these materials natural candidates for use in soft robotics [26, 42, 72, 86, 117, 124].

The continuum modeling of LCs and LCE/LCNs results in nonlinear variational problems. We refer to the classic books [57, 114] for references on the modeling of LC and the book [121] for a reference on the modeling of LCE. These variational problems pose many challenges for numerical analysis and computation. This dissertation is concerned with the numerical analysis and computation of variational problems related to LC and LCN as well as modeling of LCN.

1.1 Framework for numerical analysis and computation

The variational problems under consideration share a similar structure. The problem is to seek $\mathbf{u} : \Omega \to \mathbb{R}^3$ such that

$$\mathbf{u} \in \mathrm{argmin}_{\mathbf{v}\in\mathcal{A}} E[\mathbf{v}].$$

where the domain $\Omega \subset \mathbb{R}^d$, $d = 2, 3$ is an open and bounded set and is the body occupied by the LC or LCN, $\mathcal{A} \subset H^1(\Omega; \mathbb{R}^3)$ is a closed admissible set of functions, and $E : \mathcal{A} \to \mathbb{R}$ is the energy we seek to minimize that is bounded from below.

For the problems addressed in this dissertation, a few challenges include: nonlinearity and nonconvexity present in the energy E, low regularity of minimizers $\mathbf{u}$, and nonlinearities that arise from the admissible set $\mathcal{A}$. As a result, we aim to solve such variational problems with a flexible approach. We now go over the two components to this approach.

1.1.1 Formulation of discrete minimization problem and convergence of minimizers

The first step is to formulate a discrete counterpart to the continuous problem. We discretize the problem with a finite element method (FEM) [39]. We first triangulate Ω with a sequence of triangulations $\{\mathcal{T}_j\}_{j=1}^{\infty}$. We now define what we mean by a triangulation of a set Ω following [39, Def. 3.3.11]. A triangulation $\mathcal{T} = \{T_i\}_{i=1}^{N}$, is a finite set of elements T_i. An element is a closed simplex, i.e. a triangle in 2D or tetrahedron in 3D. Additionally, the triangulation satisfies the following properties. First, the interiors of the elements are disjoint, i.e. if $i \neq k$ then $\mathrm{int}(T_i) \cap \mathrm{int}(T_k) = \emptyset$. Second, the union of the elements is the closure of Ω, i.e. $\overline{\Omega} = \cup_{T\in\mathcal{T}} T$.

The last property of a triangulation is that if z is a vertex of an element T_i, then z is not in the relative interior of an edge or face of any element. Note that if Ω has a polytopal boundary, then there is a triangulation of Ω. If $\partial\Omega$ is sufficiently smooth and does not have a polytopal boundary, then we approximate Ω arbitrarily closely with a suitable polytopal domain $\tilde{\Omega}$ and triangulate $\tilde{\Omega}$.

Since each triangulation has finitely many elements, we may define the *mesh size* of a triangulation $\mathcal{T}$ as $h = \max_{T\in\mathcal{T}} \operatorname{diam}(T)$. We work a sequence of triangulations $\{\mathcal{T}_j\}_{j=1}^{\infty}$ with mesh size h_j that satisfy $\lim_{j\to\infty} h_j = 0$ in order for the discrete problem to better approximate the continuous problem as $j \to \infty$. Throughout this dissertation, we assume the sequence of triangulations $\{\mathcal{T}_j\}_{j=1}^{\infty}$ is *quasi-uniform* (see [39, Def. 4.4.13]). For an element T, we denote $\rho_T := \sup\{\operatorname{diam}(B) : B \subset T \text{ and } B \text{ is a ball}\}$. A sequence of triangulations is quasi-uniform if there is $c > 0$ such that $ch_j \leq \min_{T\in\mathcal{T}_j} \rho_T$ for all j. Accordingly, quasi-uniformity implies that $c\operatorname{diam}(T) \leq \rho_T$ for all $T \in \cup_{j=1}^{\infty}\mathcal{T}_j$, which means that $\{\mathcal{T}_j\}_{j=1}^{\infty}$ is *shape-regular* or *regular* [39, (4.4.16)]. The intuition behind shape-regularity is that the elements cannot degenerate and become too skinny as $j \to \infty$. When a sequence of meshes is quasi-uniform, we simplify notation by indexing each triangulation with its mesh size h_j and drop the dependence on j. The resulting notation for a triangulation we use throughout this dissertation is $\mathcal{T}_h$ and a sequence of triangulations is $\{\mathcal{T}_h\}_h$.

Given a triangulation, $\mathcal{T}_h$, of mesh size h, we introduce the finite dimensional space $\mathbb{V}_h := \{\mathbf{v}_h \in C^0(\Omega;\mathbb{R}^3) : \mathbf{v}_h|_T \text{ is affine } \forall T \in \mathcal{T}_h\} \subset H^1(\Omega;\mathbb{R}^3)$ consisting of all continuous functions that are affine when restricted to an element T of $\mathcal{T}_h$. We chose a closed discrete admissible set $\mathcal{A}_h \subset \mathbb{V}_h$ that is a discrete analog to $\mathcal{A}$. The choice of $\mathcal{A}_h$ depends on the problem, and $\mathcal{A}_h$ may not necessarily be a subset of $\mathcal{A}$. As we will see in Chapter 2, the condition $\mathcal{A}_h \subset \mathcal{A}$ may be too restrictive. Hence, we do not require $\mathcal{A}_h \subset \mathcal{A}$. We finally formulate a discrete energy

$E_h : \mathcal{A}_h \to \mathbb{R}$ that is bounded from below and is lower semicontinuous in $\mathcal{A}_h$. The discrete energy will be a modification of E that makes it amenable to computation. We refer to Chapter 4 for an example where E_h is a modification of E that is more amenable to computation. The energy E_h and admissible set $\mathcal{A}_h$ are chosen such that the discrete minimization problem has a minimizer. The discrete problem is to find $\mathbf{u}_h \in \mathcal{A}_h$ such that $\mathbf{u}_h$ satisfies

$$\mathbf{u}_h \in \operatorname{argmin}_{\mathbf{v}_h \in \mathcal{A}_h} E_h[\mathbf{v}_h].$$

We then prove that minimizers of the discrete problem converge to the minimizers of the continuous problem as $h \to 0$. The framework follows that of Γ-convergence. We refer to [37, 38] for introductions to the theory of Γ-convergence. There is a growing literature on Γ-convergent finite element discretizations for problems arising in materials science. A non-exhaustive list includes work in liquid crystals [33, 95, 96, 115] as well as plate and shell models [14, 18, 19, 23, 29, 30, 30, 31, 32, 105].

There are two kinds of results that we need to prove in this framework. We first note that the framework is flexible with regard to the topology of the underlying space, and the choice of topology depends on the problem. Hence, in listing the results we would like to prove, we use the phrase "$\mathbf{u}_h \to \mathbf{u}$ either strongly or weakly in $H^1(\Omega; \mathbb{R}^3)$ as $h \to 0$" since the choice of the weak or strong topology on $H^1(\Omega; \mathbb{R}^3)$ will depend on the specific problem we are studying.

- *Recovery sequence*: If $\mathbf{u} \in \mathcal{A}$, there exists a sequence $\{\mathbf{u}_h\}_h$ such that $\mathbf{u}_h \in \mathcal{A}_h$ and $\mathbf{u}_h \to \mathbf{u}$ either strongly or weakly in $H^1(\Omega; \mathbb{R}^3)$ as $h \to 0$. Moreover,

$$\limsup_{h \to 0} E_h[\mathbf{u}_h] \leq E[\mathbf{u}].$$

A recovery sequence result is analogous to a consistency result in numerical analysis.

- *Compactness and lower bound*: Let $\{\mathbf{u}_h\}_h$ be a sequence as $h \to 0$ that satisfies $\mathbf{u}_h \in \mathcal{A}_h$ for each h and satisfy the uniform bound $E_h[\mathbf{u}_h] \leq C < \infty$. There is a subsequence (not relabeled) $\mathbf{u}_h$ such that $\mathbf{u}_h \to \mathbf{u} \in \mathcal{A}$ either strongly or weakly in $H^1(\Omega; \mathbb{R}^3)$ as $h \to 0$. We also have

$$E[\mathbf{u}] \leq \liminf_{h \to 0} E_h[\mathbf{u}_h].$$

The compactness and lower bound result is analogous to a stability result in numerical analysis.

These two ingredients combined lead to a subsequence of global minimizers of the discrete problem converging to a global minimizer of the continuous problem, which is often referred to as the Fundamental Theorem of Γ-convergence [38, Theorem 2.1]. We now state and prove convergence of minimizers.

Proposition 1.1 (convergence of minimizers)**.** *Suppose the recovery sequence property and compactness and lower bound properties outlined above hold for E_h and $\mathcal{A}_h$. For each h, let $\mathbf{u}_h^* \in \mathcal{A}_h$ be a minimizer of E_h over $\mathcal{A}_h$. Then as $h \to 0$, the sequence $\{\mathbf{u}_h^*\}_h$ has a convergent subsequence (not relabeled) whose limit, $\mathbf{u}^* \in \mathcal{A}$ is a minimizer of E over the admissible set $\mathcal{A}$, and* $\lim_{h \to 0} E_h[\mathbf{u}_h^*] = E[\mathbf{u}^*]$.

Proof. Let $\mathbf{u} \in \mathcal{A}$. We invoke the recovery sequence property to construct $\{\mathbf{u}_h\}_h$ such that each $\mathbf{u}_h \in \mathcal{A}_h$, $\mathbf{u}_h \to \mathbf{u}$ either weakly or strongly in $H^1(\Omega; \mathbb{R}^3)$ as $h \to 0$, and

$$\limsup_{h \to 0} E_h[\mathbf{u}_h] \leq E[\mathbf{u}].$$

By using the fact that $\mathbf{u}_h^*$ is a minimizer of E_h over $\mathcal{A}_h$, we have that

$$\limsup_{h\to 0} E_h[\mathbf{u}_h^*] \leq \limsup_{h\to 0} E_h[\mathbf{u}_h] \leq E[\mathbf{u}].$$

By the compactness and lower bound property, $\{\mathbf{u}_h^*\}_h$ has a convergent subsequence (not relabeled) such that its limit is $\mathbf{u}^* \in \mathcal{A}$. Additionally, we have

$$E[\mathbf{u}^*] \leq \liminf_{h\to 0} E_h[\mathbf{u}_h^*] \leq \limsup_{h\to 0} E_h[\mathbf{u}_h^*] \leq \limsup_{h\to 0} E_h[\mathbf{u}_h] \leq E[\mathbf{u}].$$

Since $\mathbf{u} \in \mathcal{A}$ is arbitrary, we take the infimum of the right hand side of the above inequality over all $\mathbf{u} \in \mathcal{A}$ to get $E[\mathbf{u}^*] \leq \inf_{\mathbf{u}\in\mathcal{A}} E[\mathbf{u}]$, and $\mathbf{u}^*$ is a minimizer of E over $\mathcal{A}$. Additionally, we have that $E[\mathbf{u}^*] \leq \liminf_{h\to 0} E_h[\mathbf{u}_h^*] \leq \limsup_{h\to 0} E_h[\mathbf{u}_h^*] \leq E[\mathbf{u}^*]$, whence $\lim_{h\to 0} E_h[\mathbf{u}_h^*] = E[\mathbf{u}^*]$. $\square$

We now make a few remarks before continuing. The functional framework for Gamma-convergence is much more general than $H^1(\Omega;\mathbb{R}^3)$, but the focus of this dissertation is on $H^1(\Omega;\mathbb{R}^3)$. Finally, the recovery sequence result requires that $\mathcal{A} \neq \emptyset$, which we either enforce with conditions on the data for the problem or other assumptions. Finally, for notational convenience, we often replace a sequence $\{\mathbf{u}_h\}_h$ with $\mathbf{u}_h$ to denote a sequence of discrete functions indexed by $h \to 0$.

1.1.2 Iterative solvers for discrete minimization problem

Once we have a discrete energy E_h and discrete admissible set $\mathcal{A}_h \subset \mathbb{V}_h$, we propose an iterative method to compute critical points of E_h over $\mathcal{A}_h$. Due to the nonlinearities and nonconvexity of the variational problems under study, we choose to implement a *gradient flow*. Given $\mathbf{u}_h^n \in \mathcal{A}_h$, we seek $\mathbf{u}_h^{n+1} \in \mathcal{A}_h$ to satisfy

$$\mathbf{u}_h^{n+1} \in \operatorname{argmin}_{\mathbf{v}_h \in \mathcal{A}_h} \frac{1}{2\tau} \|\mathbf{v}_h - \mathbf{u}_h^n\|_*^2 + E_h[\mathbf{v}_h],$$

where $\tau > 0$ is a pseudo-time step and $\|\cdot\|_*$ is a norm on $\mathbb{V}_h$ induced by an inner product $\langle \cdot, \cdot \rangle_*$, which is known as a flow metric. The above problem is well-posed because $\mathbf{v}_h \mapsto \frac{1}{2\tau}\|\mathbf{v}_h - \mathbf{u}_h^n\|_*^2 + E_h[\mathbf{v}_h]$ is bounded from below, lower semicontinuous, and coercive on $\mathbb{V}_h$.

The iterative scheme is formally a backward Euler discretization of the equation $\partial_t \mathbf{u}_h = -\nabla E_h[\mathbf{u}_h]$. One advantage of the gradient flow iteration is *energy stability*:

$$E_h[\mathbf{u}_h^{n+1}] + \frac{1}{2\tau}\|\mathbf{u}_h^{n+1} - \mathbf{u}_h^n\|_*^2 \leq E_h[\mathbf{u}_h^n],$$

which makes it a robust scheme provided we can solve the gradient flow subproblem. In Chapter 2, we actually linearize the gradient flow subproblem to make it computationally tractable while retaining energy stability. In Chapter 4, we implement a fully implicit gradient flow scheme, and discuss partial results of a Newton sub-itertation to solve the subproblem. We only expect a gradient flow scheme to converge to critical points of E_h, while the Γ-convergence theory is a statement about global minimizers of E_h over $\mathcal{A}_h$. We acknowledge this gap between the convergence of minimizers analysis and the properties of the iterative method, which is typical of nonconvex optimization problems. However, in some cases in Chapter 5, computational evidence suggests that the outputs of the iterative scheme achieve values of E_h that are close to the minimum of the discrete energy E_h.

1.2 Numerics for the full Frank-Oseen model of liquid crystals

Liquid crystals are materials that correspond to an intermediate phase of matter. In particular, they often retain optical properties of crystals, while being able to move freely like a fluid. They may also deform easily in the presence of external fields. These properties lead to the use of liquid crystals in liquid crystal displays [106]. More recently, physicists have been able to assemble smectic liquid crystals into what is known as a compound eye [110].

Mathematical modeling of liquid crystals has a long history. Two books on the subject include [57, 114]. One interesting aspect of the modeling of liquid crystal problems is that the stationary problem is a variational problem with a nonconvex pointwise unit length constraint, which leads to an interesting set of mathematical and numerical questions. For stationary continuum models of liquid crystals, there are typically 3 models to chose from. They are the Frank-Oseen model [64, 97], Ericksen model [63], and Landau de-Gennes or Q tensor model [57].

Chapter 2 develops a finite element method for the Frank-Oseen model [64, 97]. The orientation of LC molecules in Ω is represented with a *director field* $\mathbf{n} : \Omega \to \mathbb{S}^2 =: \{\mathbf{x} \in \mathbb{R}^3 : |\mathbf{x}| = 1\}$ and posits that the director field minimizes the following elastic energy:

$$E[\mathbf{n}] = \frac{1}{2} \int_{\Omega} k_1 (\mathrm{div}\mathbf{n})^2 + k_2 (\mathbf{n} \cdot \mathrm{curl}\mathbf{n})^2 + k_3 |\mathbf{n} \times \mathrm{curl}\mathbf{n}|^2 + (k_2 + k_4) \left(\mathrm{tr}((\nabla \mathbf{n})^2) - (\mathrm{div}\mathbf{n})^2 \right) d\mathbf{x},$$

where $k_i > 0$, $i = 1, 2, 3, 4$, are known as Frank's constants. In Chapter 2 we consider the admissible set

$$\mathcal{A}_{\mathbf{g}} := \{\mathbf{v} \in H^1(\Omega; \mathbb{S}^2) : \mathbf{v} = \mathbf{g} \text{ on } \partial\Omega\},$$

where $H^1(\Omega; \mathbb{S}^2) := \{\mathbf{v} \in H^1(\Omega; \mathbb{R}^3) : |\mathbf{v}| = 1 \text{ a.e. in } \Omega\}$. If the boundary data $\mathbf{g}$ is Lipschitz, then $\mathcal{A}_{\mathbf{g}} \neq \emptyset$, and there exists minimizers of E over $\mathcal{A}_{\mathbf{g}}$ [71]. There are a few challenges to this variational problem. Firstly, the vector field $\mathbf{n}$ must satisfy a pointwise unit-length constraint, which is nonconvex. Also, the terms $(\mathbf{n} \cdot \operatorname{curl}\mathbf{n})^2$ and $|\mathbf{n} \times \operatorname{curl}\mathbf{n}|^2$ present additional nonlinearities because of their nonquadratic nature. Partially due to these challenges, previous works on numerics for the Frank-Oseen model [1, 8, 9, 13, 16, 17, 50, 51, 67, 74, 75, 123] contain some limitations. One limitation in the works [8, 16, 67, 74, 75] is that they consider problems where Frank's constants are restricted beyond what is required in the existence theory in [71]. In order to prove convergence to a minimizer, [1, 74] assume higher regularity of a solution beyond $H^1(\Omega; \mathbb{S}^2)$, which is the natural regularity induced by the energy E. Also, higher regularity rules out modeling of point defects, like $\mathbf{x} \mapsto \mathbf{x}/|\mathbf{x}|$, which is important in the modeling of LC. Finally, the algorithm developed [8, 9, 13] requires that the mesh is *weakly acute*, which is a restrictive mesh condition in 3 dimensions. We go over the previous literature in more detail in Section 2.1.2.

Chapter 2 develops a finite element method for minimizing E over $\mathcal{A}_{\mathbf{g}}$. The discrete minimization problem we propose is as follows. Let $\{\mathcal{T}_h\}_h$ be a sequence of triangulations of Ω indexed by mesh size h, and let $\mathcal{N}_h$ be the nodes of $\mathcal{T}_h$. The discrete admissible set reads

$$\mathcal{A}_{\mathbf{g},h,\eta} := \{\mathbf{v}_h \in \mathbb{V}_h : \left\|I_h[|\mathbf{v}_h|^2 - 1]\right\|_{L^1(\Omega)} \leq \eta,\ \|\mathbf{v}_h|_{\partial\Omega} - \mathbf{g}\|_{L^2(\partial\Omega;\mathbb{R}^3)} \leq \eta, \|\mathbf{v}_h\|_{L^\infty(\Omega;\mathbb{R}^3)} \leq C\},$$

where $\mathbb{V}_h$ is the space of continuous piecewise linear functions, I_h is the Lagrange interpolation operator and $C > 1$ is an h independent constant. This discrete admissible set relaxes the pointwise unit length constraint by only enforcing it at nodes $z \in \mathcal{N}_h$ within a prescribed small tolerance $\eta = \eta_h > 0$. The discrete minimization problem is to find $\mathbf{n}_h \in \mathcal{A}_{\mathbf{g},h,\eta}$ such that $\mathbf{n}_h$

satisfies

$$\mathbf{n}_h \in \operatorname{argmin}_{\mathbf{v}_h \in \mathcal{A}_{\mathbf{g},h,\eta}} E[\mathbf{v}_h].$$

The main aspects of this work are listed below.

- *Convergence of discrete minimizers*: We show that a subsequence of discrete minimizers converges weakly in H^1 to a minimizer of the continuous problem as $h \to 0$. The techniques follow the Γ-convergence framework outlined above and require no regularity beyond $H^1(\Omega; \mathbb{R}^3)$. The theory thus includes the presence of defects, which are of paramount importance in practice, and has no restrictions on the Frank constants beyond what is required in the existence theory in [71]. The theory presented in Chapter 2 also allows for the addition on an external magnetic field.

- *Projection-free gradient flow*: We propose a projection free gradient flow in the spirit of [16, 23, 32], which applies to general shape-regular meshes that may not be weakly acute. This is a significant computational achievement. Each step of the gradient flow entails solving a linear algebraic system due to the explicit treatment of the nonlinearities. We prove conditional energy stability and control of unit length constraint under the mild condition $\tau h^{-1} \leq C$, where C depends on the Frank constants and initial data and τ is the pseudo-time step of the iterative scheme.

- *Computations*: We present computations on how the Frank constants influence the structure of defects. These seem to be the first such computations supported by theory. We also present computations of magnetic effects, including the interaction of a magnetic field on a liquid crystal around a colloid. This problem is notoriously difficult to assess with weakly acute meshes [96].

The work in this chapter corresponds to the paper [34].

1.3 Thin liquid crystal polymeric networks

LCNs are a coupling of liquid crystal molecules crosslinked with a rubbery polymer network. They are one of many possible materials that enable spontaneous mechanical motion under a stimulus. One common stimulus is heating [117, 124], and another potential stimulus is photoactuation [42]. The deformation of LCNs depend on the orientation of the LC director, and a practitioner can blueprint or program the LC director by stretching the rubber during formation [42], photoalignment [117], or additive manufacturing [80, 81] to achieve a desired shape or configuration [5, 92, 118, 122]. We refer the reader to [89, 122] for reviews of experimental work on LCEs/LCNs.

Due to these desirable properties, engineers create soft robots using LCNs/LCEs materials, such as LCE ribbons, which twist, deform, and move using thermal energy from the environment [124], soft materials that “swim” away from light [42], and LCN actuators that can lift an object tens of times its weight [117]. One advantage of soft robots is their resilience. For instance, the actuators in [68, Figure 3] were able to lift objects through 11 thermal cycles with only negligible reductions in performance.

There are two key commonalities of the soft robotics applications cited above. The first commonality is that the LCE/LCN often undergoes large deformations. For example, the voxelated LCE setup in [117, Figure 2A] deformed into an array of 9 sharp cones. Also, the soft robots in [124] deform into helical shapes and twist dramatically when actuated. In both these examples, a linear elastic model may not accurately describe the physics, since the deformations are large. As a result, a nonlinear elastic model is crucial.

The second commonality of many soft robotics applications is that the 3D body comprised of LCE/LCN is thin relative to its length and width. The swimmer in [42, Figure 3] consisted of a sheet that was 0.32 mm thick and 5 mm in diameter. The voxelated LCE setup in [117, Figure 2A] was a 15 mm by 15 mm square and was 50 μm thick. Finally, the face that was created in [5, Figure 5] was 20 mm long and 100 μm thick (see pg. 8 and Figure S9 of the Supplementary Information Appendix of [5]). The ratios of thickness to diameter in these three cases were 2×10^{-2}, 3×10^{-3}, and 5×10^{-3} respectively. In order to effectively model these materials, it is advantageous to dimensionally reduce the model from 3D to 2D.

1.3.1 Modeling of thin LCN

Chapter 3 is concerned with the modeling of thin LCNs. For 3D bodies, one of the most accepted elastic energies for modeling the interaction of the material deformation with the LCs is known as the *trace formula* [28, 120, 121]:

$$E_{3D,t}[\mathbf{u}] = \int_{-t/2}^{t/2} \int_{\Omega} \Big(\mathrm{tr}(\nabla \mathbf{u}^T \mathbf{L}_{\mathbf{n}}^{-1} \nabla \mathbf{u} \mathbf{L}_{\mathbf{m}}) - 3 \Big) \; d\mathbf{x}' dx_3$$

where $\mathcal{B}_t := \Omega \times (-t/2, t/2)$ is the thin 3D body, $\mathbf{u} : \mathcal{B}_t \to \mathbb{R}^3$ is the deformation of the rubber and is assumed to be incompressible, i.e. $\det \nabla \mathbf{u} = 1$. The vector field $\mathbf{m} : \mathcal{B}_t \to \mathbb{S}^2$ is the initial LC orientation, and $\mathbf{n} : \mathcal{B}_t \to \mathbb{S}^2$ is the current LC orientation. The matrices

$$\mathbf{L}_{\mathbf{n}} = (s+1)^{-1/3}(\mathbf{I}_3 + s\mathbf{n} \otimes \mathbf{n}), \quad \mathbf{L}_{\mathbf{m}} = (s_0+1)^{-1/3}(\mathbf{I}_3 + s_0\mathbf{m} \otimes \mathbf{m})$$

describe how the rubber stretches and shrinks relative to the LC orientations $\mathbf{m}, \mathbf{n}$. We discuss these matrices in more detail in Chapter 3. One distinguishing feature of LCNs over LCEs is that the LC is constrained by the rubber. We represent this with an algebraic constraint known as the kinematic constraint

$$\mathbf{n} = \frac{\nabla \mathbf{u}\, \mathbf{m}}{|\nabla \mathbf{u}\, \mathbf{m}|},$$

which was also considered in [47, 98]. This hard constraint can also be enforced weakly with a physically justified penalization [102, 113]. If we were interested in modeling LCEs, the cross-links would be less dense, and the model would allow $\mathbf{n}$ to be totally free [44, 59] or subject to a Frank elasticity term [12, 22, 87, 102]. We note that the constraint of the LC inside the rubber, whether subject to a kinematic constraint or penalization, is a key modeling difference between LCE/LCNs and nematic LCs, which is considered in Chapter 2. In computations in Chapter 2, (see Figure 2.4 and Figure 2.5 below), a degree 2 defect for a nematic LC is unstable. In fact, higher degree defects are unstable [40] for the one constant Frank model of nematic LCs. However in LCNs, higher degree defects do not split apart due to the constraining nature of the polymer network, and these higher degree defects can be realized in experiments [88].

We now give a broad overview of the contributions of Chapter 3. For a more detailed list of contributions, we refer to the introduction of Chapter 3 later. We begin by deriving the formal limit

$$E_{str} = \lim_{t \to 0} \frac{1}{t} E_{3D,t}$$

using Kirchhoff-Love asymptotics. This limit is a *stretching energy*. The Kirchhoff-Love ansatz $\mathbf{u}$ takes the form

$$\mathbf{u}(\mathbf{x}', x_3) = \mathbf{y}(\mathbf{x}') + \phi(\mathbf{x}', x_3)\boldsymbol{\nu}(\mathbf{x}')$$

where $\mathbf{x}' = (x_1, x_2)$, $\mathbf{y} : \Omega \to \mathbb{R}^3$ is the midplane deformation, $\boldsymbol{\nu}$ is the unit normal to the surface $\mathbf{y}(\Omega)$, and $\phi(\mathbf{x}', \cdot)$ is a polynomial in x_3. Choosing ϕ such that $\det \nabla \mathbf{u} = 1 + \mathcal{O}(x_3)$ and assuming $\mathbf{m}$ is planar, the resulting energy is

$$E_{str}[\mathbf{y}] = \int_\Omega \left[\lambda \left(\frac{1}{\det \mathrm{I}[\mathbf{y}]} + \frac{1}{s+1} \left(\mathrm{tr}\mathrm{I}[\mathbf{y}] + s_0 \mathbf{m} \cdot \mathrm{I}[\mathbf{y}]\mathbf{m} + s \frac{\det \mathrm{I}[\mathbf{y}]}{\mathbf{m} \cdot \mathrm{I}[\mathbf{y}]\mathbf{m}} \right) \right) - 3 \right] d\mathbf{x}',$$

where $\mathrm{I}[\mathbf{y}] = \nabla'\mathbf{y}^T \nabla'\mathbf{y}$ is the first fundamental form of $\mathbf{y}$, $\nabla' = (\partial_1, \partial_2)$, and $\lambda = \sqrt[3]{\frac{s+1}{s_0+1}}$ is the actuation parameter. This derivation follows the recent work of [98], but we relax a simplifying assumption made in [98]. The assumption in [98] is that $\mathbf{y}$ is inextensible (i.e. $\det \mathrm{I}[\mathbf{y}] = 1$), which simplifies the enforcement of incompressibility in 3D. Relaxing this simplifying assumption while still retaining incompressibility in 3D produces a slightly more physical model, which we discuss more in Chapter 3. We then prove that $\mathbf{y}$ satisfies $E_{str}[\mathbf{y}] = 0$ and is a minimizer of E_{str} if and only if $\mathrm{I}[\mathbf{y}] = g$ pointwise, where the matrix field $g : \Omega \to \mathbb{R}^{2\times 2}$ takes on symmetric positive definite values and only depends on the initial LC orientation $\mathbf{m}$ and the actuation parameter λ. This is known as a metric condition and is well known in the physics literature. There are many works that study configurations that satisfy this metric condition [4, 91, 92, 93, 94, 100, 101, 103, 118, 119] as well as works connecting the 3D trace formula to the target metric [102], [121, Chapter 6.2]. Our contribution connects the 2D energy E_{str} and the metric condition.

Once equipped with the target metric, we devise a new formal asymptotic method to construct configurations $\mathbf{y}$ that approximately match the target metric from blueprinted director fields $\mathbf{m}$ with a defect of degree $n > 1$. This formal construction helps explain the shapes that have been observed experimentally in [88] and computationally in Chapter 5 of this dissertation. We conclude Chapter 3 with a derivation of a bending energy of LCN, which is the formal limit $E_{bend} = \lim_{t\to\infty} \frac{1}{t^3} E_{3D,t}$. Our derivation also follows the recent work of [98] but relaxes the simplifying inextensibility assumption made in [98]. The bending energy serves as an inspiration for the design of the discrete energy in Chapter 4.

The content of Chapter 3, except for the bending energy derivation, corresponds to content in the papers [35, 36].

1.3.2 Numerical analysis and computations of thin LCN

Often, it is difficult to solve $\mathrm{I}[\mathbf{y}] = g$ with closed form solutions. Chapter 4 develops a finite element method to minimize the stretching energy E_{str}. The numerical minimization problem is to find $\mathbf{y}_h^* \in \mathbb{V}_h$ such that $\mathbf{y}_h^*$ satisfies

$$\mathbf{y}_h^* \in \operatorname{argmin}_{\mathbf{y}_h \in \mathbb{V}_h} \left(E_{str}[\mathbf{y}_h] + c_r h^2 |\mathbf{y}_h|^2_{H_h^2} \right).$$

where $|\cdot|_{H_h^2}$ is a discontinuous Galerkin (DG) H^2 seminorm for continuous piecewise linear functions. The second term in the discrete energy mimics the bending energy derived in Chapter 3. The contributions of Chapter 4 are as follows.

- *Convergence of minimizers:* We prove convergence of minimizers of the discrete problem to zero energy states of the continuous problem. The convergence theory follows the framework of Γ-convergence outlined in Section 1.1 and was also inspired by the seminal work [66].
- *Iterative scheme:* We devise a fully implicit gradient flow with Newton sub-iteration. We prove energy stability of the gradient flow outer iteration and convergence of the outer iteration

to critical points of E_h. We also prove partial results on the Newton sub-iteration under suitable assumptions.

Chapter 5 focuses on computations of configurations of LCN using the method outlined in Chapter 4. The computations include configurations arising from higher degree defects observed in lab experiments [88] and shapes of compatible nonisometric origami predicted by [100, 101, 102]. We also compute configurations with spatially varying actuation parameter λ and configurations of incompatible nonisometric origami.

The work in Chapters 4 and 5 corresponds to the papers [35, 36].

Chapter 2: Full Frank-Oseen Model of Liquid Crystals

2.1 Introduction

This chapter develops a finite element method for the Frank-Oseen model of liquid crystals [64, 97]. There are many computational and numerical analysis works pertaining to stationary continuum models of liquid crystals. The first works on the Frank-Oseen model were [50, 51]. Other works on Frank-Oseen include [8, 9, 13] for gradient flow which projects the solution to handle the constraint. One disadvantage of the projection is that triangulations are required to be *weakly acute* to guarantee the energy decrease of the projection. Methods for the Ericksen and uniaxial Q tensor models that use a projection method are [33, 96]. One way to fix this is to introduce a pseudo-time step and control the constraint by making the pseudo-time step size small. This results in a projection-free gradient flow. We point to the use of projection-free methods in [16] for harmonic maps, and [75] for a simplified Frank-Oseen model. Other uses of the projection-free method for liquid crystals includes work on the Ericksen model [95]. There has also been extensive work on the study of enforcing constraints via Lagrange multiplier. These include a study of the saddle point problem for harmonic maps in [74] as well as a Newton method for the Frank-Oseen energy in [1] and work on preconditioners for such Newton methods [123]. Other numerical works on stationary liquid crystal models include [56, 67, 107, 115] and recent work on harmonic maps includes error estimates [24] and algorithmic aspects [17]. For a review paper on numerical methods for liquid crystal problems, we point to [116].

2.1.1 Frank-Oseen model

The Frank-Oseen Model [64, 97] is a continuum model of liquid crystals. The liquid crystal occupies a bounded domain $\Omega \subset \mathbb{R}^3$. The Frank-Oseen model represents the liquid crystal with a director field $\mathbf{n} : \Omega \to \mathbb{S}^2 := \{\mathbf{v} \in \mathbb{R}^3 : |\mathbf{v}| = 1\}$. At a point $x \in \Omega$, the unit length vector $\mathbf{n}(x)$ describes the average orientation of the liquid crystal molecules. The model [64, 97] posits that $\mathbf{n}$ minimizes the following elastic energy:

$$E[\mathbf{n}] = \frac{1}{2}\int_\Omega k_1(\text{div}\mathbf{n})^2 + k_2(\mathbf{n}\cdot\text{curl}\mathbf{n})^2 + k_3|\mathbf{n}\times\text{curl}\mathbf{n}|^2 + (k_2+k_4)\left(\text{tr}((\nabla\mathbf{n})^2) - (\text{div}\mathbf{n})^2\right)d\mathbf{x} \tag{2.1}$$

over the admissible set class $H^1(\Omega;\mathbb{S}^2)$. The four constants k_i are known as Frank's constants.

Previous analytical work [71] proved existence of minimizers of E over the admissible set

$$\mathcal{A}_\mathbf{g} := \{\mathbf{n} \in H^1(\Omega;\mathbb{R}^3) : |\mathbf{n}| = 1 \text{ a.e. in } \Omega \text{ and } \mathbf{n}|_{\partial\Omega} = \mathbf{g}\}, \tag{2.2}$$

where $\mathbf{g} : \partial\Omega \to \mathbb{S}^2$ is Lipschitz and $k_i > 0$ for $i = 1, 2, 3$. The main idea for proving existence of minimizers is to write a modified but equivalent energy with modified coefficients $c_0 > 0$ and $c_i \geq 0$ for $i = 1, 2, 3$:

$$\tilde{E}[\mathbf{n}] = \frac{1}{2}\int_\Omega c_0|\nabla\mathbf{n}|^2 + c_1(\text{div}\mathbf{n})^2 + c_2(\mathbf{n}\cdot\text{curl}\mathbf{n})^2 + c_3|\mathbf{n}\times\text{curl}\mathbf{n}|^2 d\mathbf{x}. \tag{2.3}$$

We recall the relevant results and observations from the analysis in Section 2.2.

2.1.2 Previous related numerical works

There are many numerical methods to compute minimizers to the Frank-Oseen Energy [1, 8, 9, 13, 16, 17, 24, 51, 74, 75]. The various previous methods fall into a few camps. The collection of works [8, 9, 13, 16, 75] use a type of steepest descent method. At each step, the steepest descent only searches in tangent directions to linearize the unit length constraint. The violation of the constraint is then controlled either with a projection [8, 9, 13] or with a pseudo-timestep parameter to control the constraint violation [16, 75]. The use of a pseudo-time step is called a projection-free method. There is a large drawback to projecting the solution. In the finite element context, one needs *weakly acute triangulations*, so that the projection step does not increase the energy. This restriction can be hard to satisfy for 3 dimensional computations. The previous projection-free works have also dealt with simplifications of the Frank-Oseen energy. In [16], the one constant approximation $k = k_i$ for all $i = 1, 2, 3$ (also known as harmonic maps) is considered. In [75], the authors consider $k_2 = k_3$, which combines the bend and twist terms to $|\operatorname{curl} \mathbf{n}|^2$.

The other group of methods use a Lagrange multiplier to enforce the unit length constraint [1, 74]. These methods typically require additional regularity on the solution to allow for an analysis. For instance as noted by [1, Remark 3.9], their analysis requires that $\operatorname{curl} \mathbf{n} \in L^\infty$. Such regularity requirements can exclude interesting point defects. Finally, we make note of other Newton type methods explored recently in the literature. The work [17] compared the performance of Newton-type methods with steepest descent type methods and various finite element discretizations for harmonic maps. Also, the recent work [24] proved quasioptimal error estimates for a finite element discretization of harmonic maps as long as the solution is regular and stable. The theory in [24] also suggests super-linear convergence of Newton method if the initial guess is sufficiently close.

It should be noted that [115] proves a Γ-convergence type numerical analysis result for the full constant Ericksen model, while the focus of this Chapter is on the full Frank-Oseen model, where such an analysis has been absent in the literature.

2.1.3 Our contribution

This work presents a numerical method for computing minimizers the full Frank-Oseen energy, without additional restrictions on the elastic constants or triangulation. The method computes minimizers of the modified energy $\tilde{E}$ over the following discrete admissible set:

$$\mathcal{A}_{\mathbf{g},h,\eta} := \{\mathbf{v}_h \in \mathbb{V}_h : \left\| I_h[|\mathbf{v}_h|^2 - 1] \right\|_{L^1(\Omega)} \leq \eta, ; \|\mathbf{v}_h|_{\partial\Omega} - \mathbf{g}\|_{L^2(\partial\Omega;\mathbb{R}^3)} \leq \eta, \|\mathbf{v}_h\|_{L^\infty(\Omega;\mathbb{R}^3)} \leq C\},$$

where $\mathbb{V}_h$ is the space of continuous piecewise linear vector valued functions on a triangulation $\mathcal{T}_h$ with mesh size h, $\mathcal{N}_h$ is the nodes of the triangulation, and I_h is the Lagrange interpolation operator. Also, $C > 1$ is a constant that does not need to change with h. Our contributions are as follows.

- **Convergence of Discrete Minimizers** In Section 2.3, we prove that discrete minimizers converge up to a subsequence to a minimizer of the continuous problem. Our analysis is in the spirit of Γ-convergence. The analysis also only requires $k_i > 0$, which is what is required by the existence analysis in [71]. The analysis presented here extends the Γ-convergence analysis for harmonic maps discussed in [15, Example 4.6].

- **Projection-Free Gradient Flow** In Section 2.4, we propose projection-free gradient flow algorithm to compute critical points of $\tilde{E}$ over $\mathcal{A}_{\mathbf{g},h,\eta}$ inspired by [16, 23]. The gradient flow only requires solving linear systems, despite the quartic terms in the energy like $(\mathbf{n}\cdot\operatorname{curl}\mathbf{n})^2$ and $|\mathbf{n}\times\operatorname{curl}\mathbf{n}|^2$. We also prove the gradient flow is *energy stable* under a mild condition $\tau h^{-1} \le c$, for some constant c that depends on k_i and the initial data. We also show that although we need an L^∞ bound on $\mathbf{n}_h$, we can still achieve error estimates of the violation of the unit length constraint in L^1 that go to zero if $\tau h^{-1} \le c$.

- **Magnetic Effects** In Section 2.5, we explain how our results may be adapted for when there is a fixed magnetic field.

- **Computations** Finally in Section 2.6, we present computational results. We highlight quantitative properties of the algorithm, the effect of Frank's constants on defect configurations, as well as some examples with an external magnetic field.

2.2 Notation and preliminaries

2.2.1 Properties of Frank-Oseen model

We first begin by setting notation and summarize the results in [71] for the continuous problem. We first recall the Frank-Oseen energy:

$$E[\mathbf{n}] := \frac{1}{2}\int_\Omega k_1(\operatorname{div}\mathbf{n})^2 + k_2(\mathbf{n}\cdot\operatorname{curl}\mathbf{n})^2 + k_3|\mathbf{n}\times\operatorname{curl}\mathbf{n}|^2 \\ + (k_2+k_4)\left(\operatorname{tr}((\nabla\mathbf{n})^2) - (\operatorname{div}\mathbf{n})^2\right)d\mathbf{x}. \tag{2.4}$$

We then define the admissible set of director fields as

$$\mathcal{A}_{\mathbf{g}} := \{\mathbf{n} \in H^1(\Omega; \mathbb{S}^2) : \quad \mathbf{n}|_{\partial\Omega} = \mathbf{g}\} \tag{2.5}$$

where we consider g Lipschitz. We note that if g is Lipschitz, then $\mathcal{A}_{\mathbf{g}}$ is nonempty [71, Lemma 1.1].

Every term in E is not problematic from the computational point of view except for the last term $(k_2 + k_4)\left(\operatorname{tr}((\nabla\mathbf{n})^2) - (\operatorname{div}\mathbf{n})^2\right)$, which is known as saddle splay. At first glance, it is not entirely clear that this term is even bounded from below. This poses some challenge to prove existence of minimizers and computation. However, in the presence of Dirichlet boundary conditions, [71, Lemma 1.1] prove that the saddle splay term is constant.

Lemma 2.1 (saddle splay)**.** *There exists a constant $C_{\mathbf{g}}$ such that for all $\mathbf{n} \in \mathcal{A}_{\mathbf{g}}$, we have*

$$C_{\mathbf{g}} = \int_{\Omega} (k_2 + k_4)\left(\operatorname{tr}((\nabla\mathbf{n})^2) - (\operatorname{div}\mathbf{n})^2\right) d\mathbf{x} \tag{2.6}$$

The proof of this lemma relies on showing that the saddle splay can be written as a divergence, which means that the saddle splay contribution only depends on boundary data, which was first realized in [62]. In the presence of Dirichlet boundary conditions, this means that the saddle splay term is constant.

The above lemma is good news because now one can modify the energy by adding a multiple of $C_{\mathbf{g}}$ and not change the minimizers, which leads to the following proposition [71, Corollary 1.3].

Proposition 2.1 (modified energy)**.** *Let $c_0 = \min_{i=1,2,3}\{k_i\} > 0$ and let $c_i = k_i - c_0 \geq 0$. Define*

$\tilde{E} : \mathcal{A}_{\mathbf{g}} \to \mathbb{R}$ by

$$\tilde{E}[\mathbf{n}] := E[\mathbf{n}] + \frac{1}{2}(c_0 - k_2 - k_4)C_{\mathbf{g}} \tag{2.7}$$

Then, $\mathbf{n}^* \in \mathcal{A}_{\mathbf{g}}$ is a minimizer of $\tilde{E}$ in $\mathcal{A}_{\mathbf{g}}$ if and only if $\mathbf{n}^*$ is a minimizer of E in $\mathcal{A}_{\mathbf{g}}$.

It is clear that since $C_{\mathbf{g}}$ is a constant, then minimizers of $\tilde{E}$ are also minimizers of E. Currently, the explicit form of $\tilde{E}$ is not exactly amenable to computation. Below is a proposition that states an explicit form of $\tilde{E}$. The work for this was done in [71] however we state and prove the result for completeness.

Proposition 2.2 (explicit form of $\tilde{E}$)**.** *Let $c_0 = \min\{k_i\} > 0$ and let $c_i = k_i - c_0 \geq 0$ for $i = 1, 2, 3$. Then, for $\mathbf{n} \in H^1(\Omega; \mathbb{S}^2)$*

$$\tilde{E}[\mathbf{n}] = \frac{1}{2}\int_\Omega c_0|\nabla\mathbf{n}|^2 + c_1(\operatorname{div}\mathbf{n})^2 + c_2(\mathbf{n}\cdot\operatorname{curl}\mathbf{n})^2 + c_3|\mathbf{n}\times\operatorname{curl}\mathbf{n}|^2 d\mathbf{x} \tag{2.8}$$

Proof. Using the expression for $C_{\mathbf{g}}$ in (2.6), we write $\tilde{E}$ in (2.7) as

$$\begin{aligned}\tilde{E}[\mathbf{n}] &= E[\mathbf{n}] + (c_0 - k_2 - k_4)C_{\mathbf{g}} \\ &= \frac{1}{2}\int_\Omega c_0\operatorname{tr}((\nabla\mathbf{n})^2) + (k_1 - c_0)(\operatorname{div}\mathbf{n})^2 + k_2(\mathbf{n}\cdot\operatorname{curl}\mathbf{n})^2 + k_3|\mathbf{n}\times\operatorname{curl}\mathbf{n}|^2 d\mathbf{x}.\end{aligned}$$

Since $|\mathbf{n}| = 1$ a.e. in Ω, $(\mathbf{n}\cdot\operatorname{curl}\mathbf{n})^2 + |\mathbf{n}\times\operatorname{curl}\mathbf{n}|^2 = |\operatorname{curl}\mathbf{n}|^2$. Hence, adding and subtracting $c_0|\operatorname{curl}\mathbf{n}|^2$ to $\tilde{E}[\mathbf{n}]$ yields

$$\begin{aligned}\tilde{E}[\mathbf{n}] = \frac{1}{2}\int_\Omega c_0\left[\operatorname{tr}((\nabla\mathbf{n})^2) + |\operatorname{curl}\mathbf{n}|^2\right] &+ (k_1 - c_0)(\operatorname{div}\mathbf{n})^2 \\ &+ (k_2 - c_0)(\mathbf{n}\cdot\operatorname{curl}\mathbf{n})^2 + (k_3 - c_0)|\mathbf{n}\times\operatorname{curl}\mathbf{n}|^2 d\mathbf{x}.\end{aligned}$$

The result follows from the fact that $|\nabla \mathbf{n}|^2 = \operatorname{tr}((\nabla \mathbf{n})^2) + |\operatorname{curl} \mathbf{n}|^2$ and the definition of $c_i = k_i - c_0$ for $i = 1, 2, 3$. $\square$

The modified energy $\tilde{E}$ immediately looks friendlier than E. First off, it is easy to tell that $\tilde{E}$ is bounded from below. Secondly, $\tilde{E}$ is coercive in H^1 because $c_0 > 0$. Thirdly, $\tilde{E}$ is weakly lower semicontinuous in $\mathcal{A}_{\mathbf{g}}$ because each $c_i \geq 0$. These facts are proved in [71, Lemma 1.4] and are summarized by the following Lemma.

Lemma 2.2 (properties of $\tilde{E}$)**.** *The modified energy $\tilde{E}$ is w.l.s.c. in $H^1(\Omega; \mathbb{S}^2)$ and*

$$\frac{1}{2} c_0 \int_\Omega |\nabla \mathbf{n}|^2 d\mathbf{x} \leq \tilde{E}[\mathbf{n}] \leq 3(k_1 + k_2 + k_3) \int_\Omega |\nabla \mathbf{n}|^2 d\mathbf{x} \tag{2.9}$$

for all $\mathbf{n} \in H^1(\Omega; \mathbb{S}^2)$.

Remark 2.1 (modified energy $\tilde{E}$)**.** *The proof of the weak lower semicontinuity only relies on the fact that $c_i \geq 0$. Also the coercivity only relied on $c_0 > 0$. Hence the coercivity and weak lower semicontinuity of $\tilde{E}$ defined in (2.8) hold over the larger space $H^1(\Omega; \mathbb{R}^3)$. Thus, we will compute with $\tilde{E}$ as defined in (2.8).*

Remark 2.2 (Simplifications of $\tilde{E}$)**.** *Note that if $k_1 = k_2 = k_3 = 1$, then $\tilde{E}$ takes on the following form:*

$$\tilde{E}[\mathbf{n}] = \frac{1}{2} \int_\Omega |\nabla \mathbf{n}|^2 d\mathbf{x},$$

which is known as the one constant approximation. Also, if $k_2 = k_3 > k_1$, then $\tilde{E}$ takes on the following form

$$\tilde{E}[\mathbf{n}] = \frac{1}{2} \int_\Omega k_1 |\nabla \mathbf{n}|^2 + c_2 |\operatorname{curl} \mathbf{n}|^2 d\mathbf{x},$$

which was studied in [67, 75].

2.2.2 Discretization

We first define some notations for the discrete problem and summarize some useful results. We denote a sequence of quasiuniform, shape-regular triangulations of Ω as $\{\mathcal{T}_h\}_h$ and refer back to Section 1.1.1 for definitions of quasiuniform and shape-regular. The nodal set for $\mathcal{T}_h$ will be denoted by $\mathcal{N}_h$. The space of continuous piecewise linear vector fields is defined by

$$\mathbb{V}_h := \{\mathbf{v}_h \in C^0(\Omega; \mathbb{R}^3) : \mathbf{v}_h|_T \in \mathcal{P}_1 \quad \forall T \in \mathcal{T}_h\}.$$

Similarly, the space $\mathbb{Q}_h$ will denote the space of continuous piecewise linear real-valued functions:

$$\mathbb{Q}_h := \{v_h \in C^0(\Omega) : v_h|_T \in \mathcal{P}_1 \quad \forall T \in \mathcal{T}_h\}.$$

We also set $\mathbb{V}_{h,0} := \{\mathbf{v}_h \in \mathbb{V}_h : \mathbf{v}_h|_{\partial\Omega} = 0\}$ to be the discrete space with zero boundary conditions. Again, we use similar notation for $\mathbb{Q}_{h,0}$.

Another space that will be useful is a tangent space to $\mathbf{n}_h \in \mathbb{V}_h$, which will be used in the *gradient flow* algorithm. We denote $T_h(\mathbf{n}_h)$ as the space of tangent directions, namely,

$$T_h(\mathbf{n}_h) := \{\mathbf{v}_h \in \mathbb{V}_{h,0} : \mathbf{v}_h(z) \cdot \mathbf{n}_h(z) = 0 \quad \forall z \in \mathcal{N}_h\}.$$

Additionally, given a pseudo-time step $\tau > 0$, we denote the discrete time derivative as the backward difference:

$$d_t \mathbf{n}_h^{k+1} = \frac{1}{\tau}\left(\mathbf{n}_h^{k+1} - \mathbf{n}_h^k\right).$$

Since the $L^2(\Omega)$ norm and inner products are used frequently in this chapter, a norm should be assumed to be L^2 unless otherwise specified. For $u, v \in L^2(\Omega)$, the L^2 inner product will be denoted by $(u, v) = \int_\Omega uv\, d\mathbf{x}$. Also, $\|u\| = \sqrt{(u, u)}$. The same notation will be used for the inner product of vector valued functions. That is, for $\mathbf{u}, \mathbf{v} \in L^2(\Omega; \mathbb{R}^3)$, the L^2 inner product is denoted by $(\mathbf{u}, \mathbf{v}) = \int_\Omega \mathbf{u} \cdot \mathbf{v} d\mathbf{x}$, and the norm of $\mathbf{u}$ is denoted by $\|\mathbf{u}\| = \sqrt{(\mathbf{u}, \mathbf{u})}$. We further shorten notation by denoting $\|\mathbf{u}\|_{W^{k,p}(\Omega;\mathbb{R}^3)} = \|\mathbf{u}\|_{W^{k,p}}$ or $\|u\|_{W^{k,p}(\Omega)} = \|u\|_{W^{k,p}}$ when the domain of integration is clearly Ω.

We now overview two useful results that are needed for the numerical method. The first result is from [16].

Lemma 2.3 (discrete unit length constraint)**.** *Let* $\mathbf{n}_h$ *be a uniformly bounded sequence in* $H^1(\Omega; \mathbb{R}^3)$ *and further suppose* $\mathbf{n}_h \to \mathbf{n}$ *strongly in* $L^2(\Omega; \mathbb{R}^3)$*. If* $\lim_{h\to 0} \left\| I_h[|\mathbf{n}_h|^2 - 1] \right\|_{L^1} = 0$*, then* $|\mathbf{n}| = 1$ *a.e. in* Ω*.*

Proof. Let $\mathbf{n}_h$ be a uniformly bounded sequence in $H^1(\Omega; \mathbb{R}^3)$ such that $\mathbf{n}_h \to \mathbf{n}$ strongly in $L^2(\Omega; \mathbb{R}^3)$ and $\lim_{h\to 0} \left\| I_h[|\mathbf{n}_h|^2 - 1] \right\|_{L^1} = 0$. Our goal is to show $\||\mathbf{n}|^2 - 1\|_{L^1} = 0$. We first apply triangle inequality to bound

$$\||\mathbf{n}|^2 - 1\|_{L^1} \leq \||\mathbf{n}|^2 - |\mathbf{n}_h|^2\|_{L^1} + \||\mathbf{n}_h|^2 - 1\|_{L^1}.$$

The first term of the RHS goes to zero by the strong convergence $\mathbf{n}_h \to \mathbf{n}$ in $L^2(\Omega; \mathbb{R}^3)$. It is sufficient to show $\||\mathbf{n}_h|^2 - 1\|_{L^1} \to 0$ as $h \to 0$. We again apply triangle inequality to bound

$$\||\mathbf{n}_h|^2 - 1\|_{L^1} \lesssim \|I_h[|\mathbf{n}_h|^2] - 1\|_{L^1} + \|I_h[|\mathbf{n}_h|^2] - |\mathbf{n}_h|^2\|_{L^1}.$$

The first term of the RHS goes to zero as $h \to 0$ since $\lim_{h\to 0}\big\|I_h[|\mathbf{n}_h|^2 - 1]\big\|_{L^1} = 0$. What remains to show is $\|I_h[|\mathbf{n}_h|^2] - |\mathbf{n}_h|^2\|_{L^1} \to 0$ as $h \to 0$. Over an element T, we use an interpolation estimate in $L^1(T)$ and the fact that $\partial_{ij}^2|\mathbf{n}_h|^2 = 2\partial_i\mathbf{n}_h \cdot \partial_j\mathbf{n}_h$ a.e. in T because $\mathbf{n}_h$ is piecewise linear to obtain

$$\||\mathbf{n}_h|^2 - I_h[|\mathbf{n}_h|^2]\|_{L^1(T)} \lesssim h^2\|D^2[|\mathbf{n}_h|^2]\|_{L^1(T)} \lesssim h^2\|\nabla\mathbf{n}_h\|_{L^2(T)}^2.$$

Summing over elements yields

$$\||\mathbf{n}_h|^2 - I_h[|\mathbf{n}_h|^2]\|_{L^1(\Omega)} \lesssim h^2\|\nabla\mathbf{n}_h\|_{L^2(\Omega;\mathbb{R}^{3\times 3})}^2.$$

Notice that the RHS goes to 0 as $h \to 0$ because $\mathbf{n}_h$ is uniformly bounded in $H^1(\Omega;\mathbb{R}^3)$, which completes the proof. $\square$

The next Lemma is a discrete Sobolev inequality that connects the L^∞ norm and H^1 norm. This result is an easy consequence of a global inverse inequality and Sobolev imbedding and is well known (see for instance [15, Remark 3.8]).

Lemma 2.4 (discrete Sobolev inequality)**.** *Let $\mathbf{v}_h \in \mathbb{V}_{h,0}$. There is a constant c_{inv} independent of h such that for all $\mathbf{v}_h \in \mathbb{V}_{h,0}$:*

$$\|\mathbf{v}_h\|_{L^\infty} \le c_{inv}h^{-1/2}\|\nabla\mathbf{v}_h\|.$$

Proof. Let $\mathbf{v}_h \in \mathbb{V}_{h,0}$. Then a global inverse inequality in three dimensions gives $\|\mathbf{v}_h\|_{L^\infty} \le C_1h^{-\frac{1}{2}}\|\mathbf{v}_h\|_{L^6}$. In 3 dimensions, $L^6(\Omega)$ continuously imbeds into $H^1(\Omega)$, so there is a constant

C_2 such that $\|\mathbf{v}_h\|_{L^6} \leq C_2\|\mathbf{v}_h\|_{H^1}$. Due to the zero Dirichlet boundary conditions, $\|\mathbf{v}_h\|_{H^1} \leq C_p\|\nabla\mathbf{v}_h\|$ by Poincaré inequality. Combining these estimates and setting $c_{inv} = C_1C_2C_p$ gives the result. $\square$

2.3 Discrete minimization problem

The discrete minimization problem mimics the continuous problem. The main differences are that rather than enforcing the constraint $|\mathbf{n}_h| = 1$ pointwise, which would lead to locking, the constraint will be enforced at nodes of the triangulation but relaxed by a parameter $\eta > 0$. The discrete admissible set is then

$$\mathcal{A}_{\mathbf{g},h,\eta} := \{\mathbf{v}_h \in \mathbb{V}_h : \left\|I_h[|\mathbf{v}_h|^2 - 1]\right\|_{L^1} \leq \eta,\ \|\mathbf{v}_h|_{\partial\Omega} - \mathbf{g}\|_{L^2(\partial\Omega;\mathbb{R}^3)} \leq \eta,\ \|\mathbf{v}_h\|_{L^\infty} \leq C\}. \quad (2.10)$$

We note that $C > 1$ is some fixed constant. The parameter $\eta = \eta_h$ will satisfy $\eta_h \to 0$ as $h \to 0$. We only need a uniform L^∞ bound rather than L^∞ control of the constraint.

The discrete problem is to find $\mathbf{n}_{h,\eta}$ such that

$$\mathbf{n}_{h,\eta} \in \text{argmin}_{\mathbf{v}_h \in \mathcal{A}_{\mathbf{g},h,\eta}} \tilde{E}[\mathbf{v}_h].$$

The next task is to prove convergence of the discrete minimizers.

2.3.1 Convergence of minimizers

The framework follows that of Γ-convergence but not exactly. Recall that $\mathcal{A}_{\mathbf{g}}$ is nonempty if g is Lipschitz. We first state the recovery sequence result.

Lemma 2.5 (recovery sequence). *Let $\mathbf{n} \in \mathcal{A}_{\mathbf{g}}$. There exists a sequence $\eta_h \to 0$ and $\mathbf{n}_h \in \mathcal{A}_{\mathbf{g},h,\eta_h}$ such that $\mathbf{n}_h \to \mathbf{n}$ in $H^1(\Omega;\mathbb{R}^3)$ and $\tilde{E}[\mathbf{n}_h] \to \tilde{E}[\mathbf{n}]$ as $h \to 0$.*

Proof. Let $\mathbf{n} \in \mathcal{A}_{\mathbf{g}} \neq \emptyset$. We proceed in three steps.

1. Approximation: Let $\mathbf{n}_h = \mathcal{I}_h \mathbf{n}$ be the Clément interpolant [43, 48] of $\mathbf{n}$, i.e. $\mathbf{n}_h$ is defined by

$$\mathbf{n}_h := \sum_{z \in \mathcal{N}_h} \mathbf{n}_z \phi_z, \quad \mathbf{n}_z := |\omega_z|^{-1} \int_{\omega_z} \mathbf{n}$$

where $\{\phi_z\}_{z \in \mathcal{N}_h}$ is the nodal basis of $\mathbb{V}_h$, and $\mathbf{n}_z$ is the average of $\mathbf{n}$ over the patch ω_z.

We have that $\mathbf{n}_h \to \mathbf{n}$ in $H^1(\Omega;\mathbb{R}^3)$. We also have the uniform L^∞ bound:

$$\|\mathbf{n}_h\|_{L^\infty} \leq \|\mathbf{n}\|_{L^\infty} = 1$$

by Jensen's inequality for each $\mathbf{n}_z$. Due to continuity of the trace operator, there is a constant C such that $\|\mathbf{n}_h|_{\partial\Omega} - \mathbf{g}\|_{L^2(\partial\Omega;\mathbb{R}^3)} \leq C\|\mathbf{n}_h - \mathbf{n}\|_{H^1(\Omega;\mathbb{R}^3)} \leq \eta_h \to 0$.

2. *Constraint:* We next show that $\|I_h[|\mathbf{n}_h|^2 - 1]\|_{L^1} \to 0$. We first bound the error by triangle inequality

$$\|I_h[|\mathbf{n}_h|^2 - 1]\|_{L^1} \leq \||\mathbf{n}_h|^2 - I_h[|\mathbf{n}_h|^2]\|_{L^1} + \||\mathbf{n}_h|^2 - 1\|_{L^1} \tag{2.11}$$

We use $|\mathbf{n}|^2 = 1$ a.e., the vector identity $|\mathbf{a}|^2 - |\mathbf{b}|^2 = |\mathbf{a}-\mathbf{b}|^2 + 2\mathbf{b}\cdot(\mathbf{a}-\mathbf{b})$, and Cauchy-Schwarz inequality to bound the second term of the RHS of (2.11):

$$\||\mathbf{n}_h|^2 - 1\|_{L^1} \leq \|\mathbf{n}_h - \mathbf{n}\|^2 + 2\|\mathbf{n}\|\|\mathbf{n}_h - \mathbf{n}\|.$$

The L^2 error estimate for the Clement interpolant $\|\mathbf{n}_h - \mathbf{n}\| \leq h\|\mathbf{n}\|_{H^1}$ then gives the bound

$$\||\mathbf{n}_h|^2 - 1\|_{L^1} \lesssim h(\|\mathbf{n}\|_{H^1} + \|\mathbf{n}\|)\|\mathbf{n}\|_{H^1}. \tag{2.12}$$

The bound on the first term of the RHS of (2.11) follows arguments from [16] and arguments in the proof of Lemma 2.3. Over an element T, we use an interpolation estimate in $L^1(T)$ and the fact that $\partial^2_{\alpha\beta}|\mathbf{n}_h|^2 = 2\partial_\alpha \mathbf{n}_h \cdot \partial_\beta \mathbf{n}_h$ a.e. in Ω because $\mathbf{n}_h$ is piecewise linear to obtain

$$\||\mathbf{n}_h|^2 - I_h[|\mathbf{n}_h|^2]\|_{L^1(T)} \lesssim h^2\|D^2[|\mathbf{n}_h|^2]\|_{L^1(T;\mathbb{R}^{3\times3\times3})} \lesssim h^2\|\nabla\mathbf{n}_h\|^2_{L^2(T;\mathbb{R}^{3\times3})}$$

Summing over elements and using the H^1 stability of the Clement interpolant yields

$$\||\mathbf{n}_h|^2 - I_h[|\mathbf{n}_h|^2]\|_{L^1(\Omega)} \lesssim h^2\|\nabla\mathbf{n}_h\|^2_{L^2(\Omega;\mathbb{R}^{3\times3})} \lesssim h^2\|\nabla\mathbf{n}\|^2_{L^2(\Omega;\mathbb{R}^{3\times3})}. \tag{2.13}$$

Inserting the estimates (2.12) and (2.13) into (2.11) shows

$$\|I_h[|\mathbf{n}_h|^2 - 1]\|_{L^1} \lesssim h^2\|\nabla\mathbf{n}\|^2 + h\left(\|\mathbf{n}\|_{H^1} + \|\mathbf{n}\|\right)\|\mathbf{n}\|_{H^1}$$

Hence, $\|I_h[|\mathbf{n}_h|^2 - 1]\|_{L^1} \leq \eta_h \to 0$ as $h \to 0$.

3. Energy: What is left to show is that the energies converge. Clearly,

$$\int_\Omega c_0|\nabla\mathbf{n}_h|^2 + c_1(\operatorname{div}\mathbf{n}_h)^2 \to \int_\Omega c_0|\nabla\mathbf{n}|^2 + c_1(\operatorname{div}\mathbf{n})^2.$$

Hence we need to show the convergence of the energies for the other terms. We focus our attention on $\|\mathbf{n}_h \cdot \operatorname{curl} \mathbf{n}_h\|^2$ first. Note that it is sufficient to prove

$$\lim_{h\to 0} \|\mathbf{n}_h \cdot \operatorname{curl} \mathbf{n}_h\| = \|\mathbf{n} \cdot \operatorname{curl} \mathbf{n}\| \tag{2.14}$$

because $x \mapsto x^2$ is continuous. By triangle inequality, we have

$$\big| \|\mathbf{n}_h \cdot \operatorname{curl} \mathbf{n}_h\| - \|\mathbf{n} \cdot \operatorname{curl} \mathbf{n}\| \big| \leq \|\mathbf{n}_h \cdot (\operatorname{curl} \mathbf{n}_h - \operatorname{curl} \mathbf{n})\| + \|(\mathbf{n}_h - \mathbf{n}) \cdot \operatorname{curl} \mathbf{n}\|$$

The first term goes to zero because $\|\operatorname{curl} \mathbf{n}_h - \operatorname{curl} \mathbf{n}\| \to 0$ and a uniform L^∞ bound on $\mathbf{n}_h$. For the second term, we have a pointwise convergent subsequence $\mathbf{n}_{h_k} \to \mathbf{n}$ such that $\lim_{h_k\to 0} \|(\mathbf{n}_{h_k} - \mathbf{n}) \cdot \operatorname{curl} \mathbf{n}\| = \limsup_{h\to 0} \|(\mathbf{n}_h - \mathbf{n}) \cdot \operatorname{curl} \mathbf{n}\|$. By the uniform L^∞ bound $\|\mathbf{n}_{h_k}\|_{L^\infty(\Omega;\mathbb{R}^3)} \leq 1$, we have the pointwise bound $|(\mathbf{n}_{h_k} - \mathbf{n}) \cdot \operatorname{curl} \mathbf{n}| \leq |\mathbf{n}_{h_k} \cdot \operatorname{curl} \mathbf{n}| + |\mathbf{n} \cdot \operatorname{curl} \mathbf{n}| \leq 2|\operatorname{curl} \mathbf{n}| \in L^2(\Omega)$. Hence by dominated convergence theorem, $\|(\mathbf{n}_{h_k} - \mathbf{n}) \cdot \operatorname{curl} \mathbf{n}\| \to 0$, and $\limsup_{h\to 0} \|(\mathbf{n}_h - \mathbf{n}) \cdot \operatorname{curl} \mathbf{n}\| = 0$. Thus, $\lim_{h\to 0} \|(\mathbf{n}_h - \mathbf{n}) \cdot \operatorname{curl} \mathbf{n}\| = 0$, and (2.14) is proved. The same arguments go for the $\|\mathbf{n}_h \times \operatorname{curl} \mathbf{n}_h\|^2$ term and the proof is complete. □

Remark 2.3. *Note that the uniform L^∞ bound on $\mathbf{n}_h$ is important for Step 3 in the proof of Lemma 2.5. This is part of the reason for the enforcement of the L^∞ bound in the definition of $\mathcal{A}_{\mathbf{g},h,\eta}$*

Remark 2.4. *Although we need a L^∞ bound on $\mathbf{n}_h$, we only needed to estimate $I_h[|\mathbf{n}_h|^2 - 1]$ in L^1. This is part of the reason why the definition of $\mathcal{A}_{\mathbf{g},h,\eta}$ involves $\|I_h[|\mathbf{n}_h|^2 - 1]\|_{L^1}$. Also, the gradient flow studied in Section 2.4 will provide an L^∞ bounded and estimates on $\|I_h[|\mathbf{n}_h|^2 - 1]\|_{L^1}$.*

Remark 2.5. *The proof suggests that $\eta_h \to 0$ as $h \to 0$ very slowly due to $\|\mathbf{n}_h|_{\partial\Omega} - \mathbf{g}\|_{L^2(\partial\Omega;\mathbb{R}^3)} \to 0$ without a rate. However one can introduce a new parameter ξ as the tolerance of boundary* *condition violation in the definition of the discrete space. In this case, one can take $\eta \approx h$ and $\xi \to 0$ without a rate. In practice, we typically solve with $\mathbf{n}_h = I_h \mathbf{g}$ on $\partial\Omega$, which has error estimates in terms of h if $\mathbf{g}$ is Lipschitz.*

The next two results are important for compactness of minimizers as well as a liminf inequality in the Γ convergence framework.

Lemma 2.6 (equicoercivity)**.** *$\tilde{E}$ satisfies*

$$\frac{1}{2} c_0 \int_\Omega |\nabla \mathbf{n}_h|^2 d\mathbf{x} \leq \tilde{E}[\mathbf{n}_h] \tag{2.15}$$

for all $\mathbf{n}_h \in \mathcal{A}_{\mathbf{g},h,\eta}$.

Proof. The coercivity from Lemma 2.2 (properties of $\tilde{E}$) holds for any $\mathbf{n} \in H^1(\Omega; \mathbb{R}^3)$ and hence holds for any $\mathbf{n}_h \in \mathcal{A}_{\mathbf{g},h,\eta}$. See Remark 2.1. □

Lemma 2.7 (Weak lower semicontinuity)**.** *Let $\mathbf{n}_{h,\eta} \in \mathcal{A}_{\mathbf{g},h,\eta}$ be such that $\eta, h \to 0$, and $\mathbf{n}_{h,\eta} \rightharpoonup \mathbf{n}^*$, then*

$$\tilde{E}[\mathbf{n}^*] \leq \liminf_{h,\eta \to 0} \tilde{E}[\mathbf{n}_{h,\eta}] \tag{2.16}$$

Proof. This proof follows the proof of lower semicontinuity of [71, Lemma 1.4]. See Lemma 2.2 and Remark 2.1. □

Combining Lemmas 2.5 (recovery sequence), 2.6 (equicoercivity), and 2.7 (weak lower semicontinuity) leads to the main convergence result.

Theorem 2.1 (convergence of minimizers)**.** *Let $h \to 0$. There exists a sequence $\{\eta_h\}_h$ such that $\eta_h \to 0$ as $h \to 0$ such that the sequence of minimizers $\mathbf{n}^*_{h,\eta_h}$ of $\tilde{E}$ over the admissible set $\mathcal{A}_{\mathbf{g},h,\eta_h}$*

has a subsequence (not relabeled) $\mathbf{n}^*_{h,\eta_h}$ *such that* $\mathbf{n}^*_{h,\eta_h} \rightharpoonup \mathbf{n}^*$ *in* $H^1(\Omega;\mathbb{R}^3)$ *and* $\mathbf{n}^* \in \mathcal{A}_{\mathbf{g}}$ *is a minimizer of* $\tilde{E}$ *over* $\mathcal{A}_{\mathbf{g}}$. *Moreover,* $\tilde{E}[\mathbf{n}^*_{h,\eta_h}] \to \tilde{E}[\mathbf{n}^*]$ *as* $h \to 0$.

Proof. We proceed in 3 steps.

1. Convergence: Let $\mathbf{n} \in \mathcal{A}_{\mathbf{g}}$. By Lemma 2.5 (recovery sequence), we have that there is a sequence $\eta = \eta_h$ such that $\eta_h \to 0$ as $h \to 0$ and there is a sequence $\mathbf{n}_{h,\eta} \in \mathcal{A}_{\mathbf{g},h,\eta}$ such that $\mathbf{n}_{h,\eta} \to \mathbf{n}$ in $H^1(\Omega;\mathbb{R}^3)$ and $\limsup_{h\to 0} \tilde{E}[\mathbf{n}_{h,\eta}] \le \tilde{E}[\mathbf{n}]$.

Using the fact that $\mathbf{n}^*_{h,\eta}$ is a minimizer, we have that $\tilde{E}[\mathbf{n}^*_{h,\eta}] \le \tilde{E}[\mathbf{n}_{h,\eta}]$, and

$$\limsup_{h,\eta\to 0} \tilde{E}[\mathbf{n}^*_{h,\eta}] \le \limsup_{h,\eta\to 0} \tilde{E}[\mathbf{n}_{h,\eta}] \le \tilde{E}[\mathbf{n}].$$

Thus, $\tilde{E}[\mathbf{n}^*_{h,\eta}]$ is bounded, and by Lemma 2.6 (equicoercivity), we have that there exists a $\mathbf{n}^* \in H^1(\Omega;\mathbb{R}^3)$ such that there is a subsequence (not relabled) $\mathbf{n}^*_{h,\eta} \rightharpoonup \mathbf{n}^*$ in $H^1(\Omega;\mathbb{R}^3)$ as $h \to 0$. To see that $\mathbf{n}^* \in \mathcal{A}_{\mathbf{g}}$, we need to prove that $\mathbf{n}^*$ satisfies the unit length constraint pointwise a.e. and satisfies the boundary conditions. We first show that $|\mathbf{n}^*| = 1$ a.e. in Ω. Recall from Lemma 2.3 (discrete unit length constraint), it is sufficient to show that $\|I_h[|\mathbf{n}^*_{h,\eta}|^2 - 1]\|_{L^1} \to 0$, which immediately follows since $\eta \to 0$.

We now must show that $\mathbf{n}^*|_\Omega = \mathbf{g}$ in the sense of trace. Since the trace operator is weakly continuous in $H^1(\Omega)$ to $L^2(\partial\Omega;\mathbb{R}^3)$, it is sufficient to show that $\mathbf{n}^*_{h,\eta} \to \mathbf{g}$ in $L^2(\partial\Omega)$. By the definition for $\mathcal{A}_{\mathbf{g},h,\eta}$, we have $\|\mathbf{n}^*_{h,\eta} - \mathbf{g}\|_{L^2(\partial\Omega;\mathbb{R}^3)} \le \eta$. Hence, $\|\mathbf{n}^*_{h,\eta} - \mathbf{g}\|_{L^2(\partial\Omega;\mathbb{R}^3)} \to 0$.

2. Characterization of $\mathbf{n}^*$*:* We shall now proceed to show that $\mathbf{n}^*$ is a minimizer. By Lemma 2.7 (weak lower semicontinuity), $\liminf_{h,\eta\to 0} \tilde{E}[\mathbf{n}^*_{h,\eta}] \ge \tilde{E}[\mathbf{n}^*]$. We then have

$$\tilde{E}[\mathbf{n}^*] \le \liminf_{h,\eta\to 0} \tilde{E}[\mathbf{n}^*_{h,\eta}] \le \limsup_{h,\eta\to 0} \tilde{E}[\mathbf{n}^*_{h,\eta}] \le \limsup_{h,\eta\to 0} \tilde{E}[\mathbf{n}_{h,\eta}] \le \tilde{E}[\mathbf{n}].$$

Note that $\tilde{E}[\mathbf{n}^*] \leq \tilde{E}[\mathbf{n}]$ for all $\mathbf{n} \in \mathcal{A}_{\mathbf{g}}$, so $\mathbf{n}^*$ is a minimizer.

3. Energy: The final claim is $\lim_{h,\eta\to 0} \tilde{E}[\mathbf{n}^*_{h,\eta}] = \tilde{E}[\mathbf{n}^*]$. Since $\tilde{E}[\mathbf{n}^*] \leq \liminf_{h,\eta\to 0} \tilde{E}[\mathbf{n}^*_{h,\eta}]$, it is sufficient to prove $\limsup_{h,\eta\to 0} \tilde{E}[\mathbf{n}^*_{h,\eta}] \leq \tilde{E}[\mathbf{n}^*]$. By Lemma 2.5 (recovery sequence), we construct $\mathbf{n}'_{h,\eta} \to \mathbf{n}^*$ in $H^1(\Omega;\mathbb{R}^3)$ such that $\limsup_{h,\eta\to 0} \tilde{E}[\mathbf{n}'_{h,\eta}] \leq \tilde{E}[\mathbf{n}^*]$. We use the assumption that $\mathbf{n}^*_{h,\eta}$ is a minimizer to prove the desired bound:

$$\limsup_{h,\eta\to 0} \tilde{E}[\mathbf{n}^*_{h,\eta}] \leq \limsup_{h,\eta\to 0} \tilde{E}[\mathbf{n}'_{h,\eta}] \leq \tilde{E}[\mathbf{n}^*],$$

and the proof is complete. $\square$

Remark 2.6. *The theory here only required $H^1(\Omega;\mathbb{R}^3)$ regularity of the solution. Only requiring $H^1(\Omega;\mathbb{R}^3)$ regularity allows for point defects of LC. This contrasts with the theory in other papers [1, 24, 74], which require higher regularity. The higher regularity requirements in [24, 74] yield error estimates for harmonic maps and the higher regularity in [1] provide error estimates for solving the Newton linearizations of the Frank-Oseen energy. The Γ-convergence theory here does not provide error estimates.*

2.4 Projection-free gradient flow for discrete problem

In this section, we propose a gradient flow algorithm to compute critical points of $\tilde{E}$ over the discrete admissible set $\mathcal{A}_{\mathbf{g},h,\eta}$. The main idea follows that of [16, 23] to gain control of the violation of the unit length constraint. Recall the modified Full Frank energy:

$$\tilde{E}[\mathbf{n}_h] = \tilde{E}_1[\mathbf{n}_h] + \tilde{E}_2[\mathbf{n}_h],$$

where

$$\tilde{E}_1[\mathbf{n}_h] := \frac{1}{2}\int_\Omega c_0|\nabla \mathbf{n}|^2 + c_1(\operatorname{div}\mathbf{n})^2 d\mathbf{x},$$
$$\tilde{E}_2[\mathbf{n}_h] := \frac{1}{2}\int_\Omega c_2(\mathbf{n}\cdot \operatorname{curl}\mathbf{n})^2 + c_3|\mathbf{n}\times \operatorname{curl}\mathbf{n}|^2 d\mathbf{x}.$$

Here, $\tilde{E}_1$ is the quadratic part of the energy and $\tilde{E}_2$ contains the quartic contributions.

The gradient flow will involve a minimization problem at each step. Suppose we start with the iterate $\mathbf{n}_h^k \in \mathbb{V}_h$ such that $|\mathbf{n}_h^k(z)|^2 - 1 = 0$ at all nodes. Our goal is to find an increment $d_t\mathbf{n}_h^{k+1}$, and set $\mathbf{n}_h^{k+1} = \mathbf{n}_h^k + \tau d_t\mathbf{n}_h^{k+1}$. In order to make sure the minimization problem involves a linear problem to solve, there are two linearizations.

We first linearize the constraint. Rather than find $d_t\mathbf{n}_h^{k+1}$ such that $|\mathbf{n}_h^k(z)+\tau d_t\mathbf{n}_h^{k+1}(z)|^2 = 1$, we search for $d_t\mathbf{n}_h^{k+1} \in T(\mathbf{n}_h^k)$, which is the tangent space to the unit length constraint. Figure 2.1 shows what an increment $d_t\mathbf{n}_h^{k+1}$ looks like at a node z. Additionally, the addition of τ and searching in tangent directions allows for control over the constrain violation: $|\mathbf{n}_h^k(z) + \tau d_t\mathbf{n}_h^{k+1}(z)|^2 = 1 + \tau^2|d_t\mathbf{n}_h^{k+1}(z)|^2$.

The second linearization acts on $\tilde{E}_2$, which means the minimization problem for $d_t\mathbf{n}_h^{k+1}$ is

$$\tau d_t\mathbf{n}_h^{k+1} \in \operatorname{argmin}_{\mathbf{v}_h\in T_h(\mathbf{n}_h^k)} \frac{1}{2\tau}\|\mathbf{v}_h\|_*^2 + \tilde{E}_1[\mathbf{n}_h^k + \mathbf{v}_h] + \frac{\delta \tilde{E}_2[\mathbf{n}_h^k;\mathbf{v}_h]}{\delta \mathbf{n}} \tag{2.17}$$

where $\|\cdot\|_*^2$ is a norm induced by some flow metric. In order for $\frac{\delta \tilde{E}_2[\mathbf{n}_h^k;\tau d_t\mathbf{n}_h^{k+1}]}{\delta \mathbf{n}}$ to be a bounded and controlled quantity, we ought to control $d_t\mathbf{n}_h^{k+1}$ in H^1 , and the linearization of $\tilde{E}_2$ ought to be continuous on H^1, which means $\mathbf{n}_h^k$ needs to be bounded in L^∞. The desired control of $d_t\mathbf{n}_h^{k+1}$ in H^1 motivates the choice of the H^1 norm for the flow metric i.e. $\|\mathbf{v}_h\|_*^2 = \|\nabla \mathbf{v}_h\|^2$.

Control of $\|\nabla d_t \mathbf{n}_h^{k+1}\|^2$ and the inverse inequality from L^∞ to H^1 in Lemma 2.4 (discrete Sobolev inequality), will then determine a condition on h and τ. The resulting system is

$$(1 + c_0\tau)(\nabla d_t \mathbf{n}_h^{k+1}, \nabla \mathbf{v}_h) + c_1\tau(\operatorname{div} d_t\mathbf{n}_h^{k+1}, \operatorname{div} \mathbf{v}_h) = -\frac{\delta \tilde{E}[\mathbf{n}_h^k; \mathbf{v}_h]}{\delta \mathbf{n}} \tag{2.18}$$

To recap, there are three main ingredients.

- Control $\|\nabla d_t \mathbf{n}_h^{k+1}\|^2$ from the flow metric.
- Use a pseudo-time step to control the violation of the unit length constraint.
- Combine control of the unit length constraint and $\|\nabla d_t \mathbf{n}_h^{k+1}\|^2$ to control the linearization of $\tilde{E}_2$.

This kind of strategy originated in the context of bilayer plates [23] and was also used in [32].

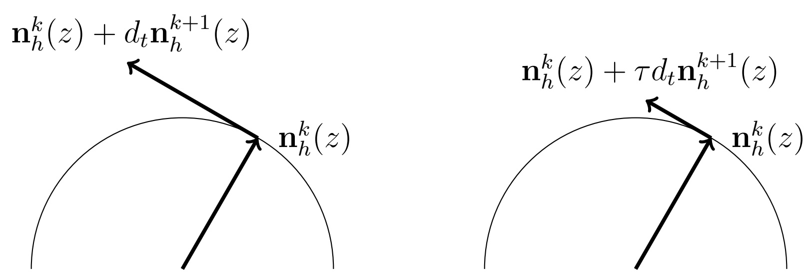

Figure 2.1: By searching in tangent directions, damping with τ yields $|\mathbf{n}_h^k(z) + \tau d_t \mathbf{n}_h^{k+1}(z)| = 1 + \tau^2 |d_t \mathbf{n}_h^{k+1}(z)|^2$

The resulting gradient flow algorithm is below.

Algorithm 1: Projection-free gradient flow

Data: Triangulation $\mathcal{T}_h$ with meshsize h, pseudo-time step τ, stopping tolerance ε, and initial guess $\mathbf{n}_h^0 \in \mathbb{V}_h$

Result: Approximate discrete local minimizer $\mathbf{n}^*_{h,\tau,\varepsilon}$

$k \leftarrow 0$

while $\tilde{E}^{k-1} - \tilde{E}^k \geq \tau\varepsilon$ **do**

  Compute increment $d_t\mathbf{n}_h^{k+1} \in T(\mathbf{n}_h^k)$ to solve (2.18)

  Update: $\mathbf{n}_h^{k+1} = \mathbf{n}_h^k + \tau d_t \mathbf{n}_h^{k+1}$

end

We see the following property of Algorithm 1 immediately from Figure 2.1.

Remark 2.7 (lower bound on $|\mathbf{n}_h^k(z)|^2$)**.** *Given $z \in \mathcal{N}_h$, we always have $|\mathbf{n}_h^k(z)|^2 \geq 1$ if $|\mathbf{n}_h^0(z)|^2 = 1$. This is because $d_t\mathbf{n}_h^k \in T(\mathbf{n}_h^k)$, and*

$$|\mathbf{n}_h^k(z)|^2 = |\mathbf{n}_h^k(z)|^2 + \tau^2|d_t\mathbf{n}_h^k(z)|^2 \geq |\mathbf{n}_h^k(z)|^2$$

Applying an induction argument yields $|\mathbf{n}_h^k(z)|^2 \geq |\mathbf{n}_h^0(z)|^2 \geq 1$.

2.4.1 Properties of gradient flow

The gradient flow Algorithm 1 has a few desirable properties. The most important property is the following energy stability.

Theorem 2.2 (energy stability and L^∞ control of constraint)**.** *Let $\mathbf{n}_h^0 \in \mathbb{V}_h$ be such that $|\mathbf{n}_h^0(z)|^2 = 1$ for all $z \in \mathcal{N}_h$. There is a constant $0 < C \leq 1$ which may depend on $\tilde{E}[\mathbf{n}_h^0]$, c_{inv}, and c_i for*

$i = 0, 1, 2, 3$ *such that if* $\tau h^{-1} \le C$ *then, for all* k

$$\tilde{E}[\mathbf{n}_h^{k+1}] + \frac{\tau}{2}\|\nabla d_t \mathbf{n}_h^{k+1}\|^2 \le \tilde{E}[\mathbf{n}_h^k],$$

and for all $z \in \mathcal{N}_h$

$$\left| |\mathbf{n}_h^{k+1}(z)|^2 - 1 \right| \le 4c_{inv}^2 \tau h^{-1} \tilde{E}[\mathbf{n}_h^0],$$

where c_{inv} *is the constant from Lemma 2.4 (discrete Sobolev inequality).*

Proof. We break the proof into two cases.

Case 1. $c_3 = c_1 = 0$*:* We proceed by induction. We assume for $k \ge 0$:

$$\tilde{E}[\mathbf{n}_h^k] + \frac{\tau}{2}\|\nabla d_t \mathbf{n}_h^k\|^2 \le \tilde{E}[\mathbf{n}_h^{k-1}] \tag{2.19}$$

$$0 \le |\mathbf{n}_h^k(z)|^2 - 1 \le 4c_{inv}^2 \tau h^{-1} \tilde{E}[\mathbf{n}_h^0] \tag{2.20}$$

with $\mathbf{n}_h^{-1} = \mathbf{n}_h^0$; this is trivially satisfied for $k = 0$. Testing (2.18) with $\tau d_t \mathbf{n}_h^{k+1}$:

$$\begin{aligned}(\tau + c_0\tau^2)\|\nabla d_t \mathbf{n}_h^{k+1}\|^2 = &- c_0\tau(\nabla \mathbf{n}_h^k, \nabla d_t \mathbf{n}_h^{k+1}) \\ &- c_2\tau(\mathbf{n}_h^k \cdot \operatorname{curl} \mathbf{n}_h^k, \mathbf{n}_h^k \cdot \operatorname{curl} d_t \mathbf{n}_h^{k+1} + d_t \mathbf{n}_h^{k+1} \cdot \operatorname{curl} \mathbf{n}_h^k)\end{aligned}$$

We split the proof into several steps.

1. Bound on $\|\nabla \mathbf{n}_h^{k+1}\|$: Recall that $\tau d_t \mathbf{n}_h^{k+1} = \mathbf{n}_h^{k+1} - \mathbf{n}_h^k$. By using the equality $(b, b-a) = \frac{1}{2}(\|b\|^2 - \|a\|^2 + \|b-a\|^2)$, we have

$$-c_0\tau(\nabla \mathbf{n}_h^k, \nabla d_t \mathbf{n}_h^{k+1}) = \frac{c_0}{2}\|\nabla \mathbf{n}_h^k\|^2 - \frac{c_0}{2}\|\nabla \mathbf{n}_h^{k+1}\|^2 + \frac{c_0\tau^2}{2}\|\nabla d_t \mathbf{n}_h^{k+1}\|^2$$

Inserting into the original equation and rearranging, we have

$$\left(\tau + c_0\frac{\tau^2}{2}\right)\|\nabla d_t \mathbf{n}_h^{k+1}\|^2 + \frac{c_0}{2}\|\nabla \mathbf{n}_h^{k+1}\|^2 = \frac{c_0}{2}\|\nabla \mathbf{n}_h^k\|^2 + I, \tag{2.21}$$

where

$$I = -c_2\tau(\mathbf{n}_h^k \cdot \operatorname{curl} \mathbf{n}_h^k, \mathbf{n}_h^k \cdot \operatorname{curl} d_t \mathbf{n}_h^{k+1} + d_t \mathbf{n}_h^{k+1} \cdot \operatorname{curl} \mathbf{n}_h^k)$$

To estimate I, we apply Cauchy-Schwartz and triangle inequalities

$$|I| \le \tau c_2 \|\mathbf{n}_h^k \cdot \operatorname{curl} \mathbf{n}_h^k\| \ \left(\|\mathbf{n}_h^k \cdot \operatorname{curl} d_t \mathbf{n}_h^{k+1}\| + \|d_t \mathbf{n}_h^{k+1} \cdot \operatorname{curl} \mathbf{n}_h^k\|\right).$$

Note that $c_2\|\mathbf{n}_h^k \cdot \operatorname{curl} \mathbf{n}_h^k\|^2 \le 2\tilde{E}[\mathbf{n}^{(0)}]$ by the inductive hypothesis (2.19). Hence,

$$\begin{aligned}
|I| &\le \tau\sqrt{2c_2\tilde{E}[\mathbf{n}^{(0)}]}\left(\|\mathbf{n}_h^k \cdot \operatorname{curl} d_t \mathbf{n}_h^{k+1}\| + \|d_t \mathbf{n}_h^{k+1} \cdot \operatorname{curl} \mathbf{n}_h^k\|\right) \\
&\le \tau\sqrt{2c_2\tilde{E}[\mathbf{n}^{(0)}]}\left(\|\mathbf{n}_h^k\|_{L^\infty}\|\operatorname{curl} d_t \mathbf{n}_h^{k+1}\| + \|d_t \mathbf{n}_h^{k+1}\|_{L^\infty}\|\operatorname{curl} \mathbf{n}_h^k\|\right) \\
&\le \tau\sqrt{2c_2\tilde{E}[\mathbf{n}^{(0)}]}\left(\|\mathbf{n}_h^k\|_{L^\infty}\|\nabla d_t \mathbf{n}_h^{k+1}\| + \|d_t \mathbf{n}_h^{k+1}\|_{L^\infty}\|\nabla \mathbf{n}_h^k\|\right).
\end{aligned}$$

The induction hypotheses (2.19), (2.20) imply $\|\mathbf{n}_h^k\|_{L^\infty} \le 1 + 4c_{inv}^2\tau h^{-1}\tilde{E}[\mathbf{n}_h^0] \le 1 + 4c_{inv}^2\tilde{E}[\mathbf{n}_h^0]$ as well as $\|\nabla \mathbf{n}_h^k\| \le \sqrt{\frac{2}{c_0}\tilde{E}[\mathbf{n}_h^0]}$. Incorporating these into the above estimate with Lemma 2.4 (discrete Sobolev inequality) yields

$$\begin{aligned}
|I| &\le \tau\sqrt{2c_2\tilde{E}[\mathbf{n}_h^0]}\left((1 + 4c_{inv}^2\tilde{E}[\mathbf{n}_h^0]) + c_{inv}h^{-1/2}\sqrt{\frac{2}{c_0}\tilde{E}[\mathbf{n}_h^0]}\right)\|\nabla d_t \mathbf{n}_h^{k+1}\| \\
&\le \tau c' h^{-1/2}\|\nabla d_t \mathbf{n}_h^{k+1}\|,
\end{aligned}$$

where c' depends on $\tilde{E}[\mathbf{n}_h^0], c_0, c_2$ and c_{inv}. We then apply Young's inequality to further estimate

$$|I| \le \frac{c'^2}{2} + \frac{\tau^2 h^{-1}}{2} \|\nabla d_t \mathbf{n}_h^{k+1}\|^2.$$

Since $\tau h^{-1} \le 1$, we absorb the last term into the left hand side of (2.21) and obtain again using the inductive hypothesis (2.19)

$$\frac{\tau}{2}\|\nabla d_t \mathbf{n}_h^{k+1}\|^2 + \frac{c_0}{2}\|\nabla \mathbf{n}_h^{k+1}\|^2 \le \frac{c_0}{2}\|\nabla \mathbf{n}_h^k\|^2 + \frac{c'^2}{2} \le \tilde{E}[\mathbf{n}_h^0] + \frac{c'^2}{2} \le c''. \tag{2.22}$$

Here, c'' only depends on $\tilde{E}[\mathbf{n}_h^0]$ and c'.

2. Estimate for $\|\mathbf{n}_h^{k+1}\|_{L^\infty}$: We shall now obtain an intermediate estimate on $\|\mathbf{n}_h^{k+1}\|_{L^\infty}$. Recall that $d_t \mathbf{n}_h^{k+1} \in T_h(\mathbf{n}_h^k)$. Hence, at nodes, $d_t \mathbf{n}_h^{k+1}(z) \cdot \mathbf{n}_h^k(z) = 0$, and

$$|\mathbf{n}_h^{k+1}(z)|^2 = |\mathbf{n}_h^k(z) + \tau d_t \mathbf{n}_h^{k+1}(z)|^2 = |\mathbf{n}_h^k(z)|^2 + \tau^2 |d_t \mathbf{n}_h^{k+1}(z)|^2.$$

By the inductive hypothesis (2.20) and and the assumption $\tau h^{-1} \le 1$, we deduce $\|\mathbf{n}_h^k\|_{L^\infty} \le 1 + 4c_{inv}^2 \tilde{E}[\mathbf{n}_h^0]$ and

$$|\mathbf{n}_h^{k+1}(z)|^2 \le \left(1 + 4c_{inv}^2 \tilde{E}[\mathbf{n}_h^0]\right)^2 + \tau^2 \|d_t \mathbf{n}_h^{k+1}\|_{L^\infty}^2.$$

Again applying Lemma 2.4 (discrete Sobolev inequality) and the assumption $\tau h^{-1} \le 1$, we now have an intermediate estimate on $|\mathbf{n}_h^{k+1}(z)|^2$:

$$
\begin{aligned}
|\mathbf{n}_h^{k+1}(z)|^2 &\leq \left(1 + 4c_{inv}^2 \tilde{E}[\mathbf{n}_h^0]\right)^2 + \tau^2 h^{-1} c_{inv}^2 \|\nabla d_t \mathbf{n}_h^{k+1}\|^2 \\
&\leq \left(1 + 4c_{inv}^2 \tilde{E}[\mathbf{n}_h^0]\right)^2 + \tau h^{-1} c_{inv}^2 c'' \leq c''',
\end{aligned} \tag{2.23}
$$

where c''' only depends on $\tilde{E}[\mathbf{n}_h^0]$, c_{inv}, and c''. This is the desired estimate for $\|\mathbf{n}_h^{k+1}\|_{L^\infty}^2$ but is not quite (2.20) for $k+1$. In this sense, (2.23) is an intermediate estimate.

3. Energy estimate: To prove the asserted energy estimate, we rewrite I in (2.21). To this end, let

$$
\mathbf{a}_k = \mathbf{n}_h^k, \quad \mathbf{b}_k = \operatorname{curl} \mathbf{n}_h^k
$$

and note that

$$
\begin{aligned}
\mathbf{a}_{k+1} \cdot \mathbf{b}_{k+1} - \mathbf{a}_k \cdot \mathbf{b}_k =& (\mathbf{a}_{k+1} - \mathbf{a}_k) \cdot \mathbf{b}_k \\
&+ \mathbf{a}_k \cdot (\mathbf{b}_{k+1} - \mathbf{b}_k) \\
&+ (\mathbf{a}_{k+1} - \mathbf{a}_k) \cdot (\mathbf{b}_{k+1} - \mathbf{b}_k).
\end{aligned}
$$

Squaring and rearranging terms, we end up with

$$
\begin{aligned}
|\mathbf{a}_{k+1} \cdot \mathbf{b}_{k+1}|^2 =& |\mathbf{a}_k \cdot \mathbf{b}_k|^2 \\
&+ 2\mathbf{a}_k \cdot \mathbf{b}_k \left[(\mathbf{a}_{k+1} - \mathbf{a}_k) \cdot \mathbf{b}_k + \mathbf{a}_k \cdot (\mathbf{b}_{k+1} - \mathbf{b}_k)\right] \\
&+ 2\mathbf{a}_k \cdot \mathbf{b}_k (\mathbf{a}_{k+1} - \mathbf{a}_k) \cdot (\mathbf{b}_{k+1} - \mathbf{b}_k) \\
&+ \left|(\mathbf{a}_{k+1} - \mathbf{a}_k) \cdot \mathbf{b}_k + \mathbf{a}_{k+1} \cdot (\mathbf{b}_{k+1} - \mathbf{b}_k)\right|^2.
\end{aligned}
$$

In view of the definition of $\mathbf{a}_k$ and $\mathbf{b}_k$, after multiplying by $\frac{c_2}{2}$ and integrating over Ω, this reads

$$
\begin{aligned}
\frac{c_2}{2}\left\|\mathbf{n}_h^{k+1}\cdot\operatorname{curl}\mathbf{n}_h^{k+1}\right\|^2 =& \frac{c_2}{2}\left\|\mathbf{n}_h^{k}\cdot\operatorname{curl}\mathbf{n}_h^{k}\right\|^2 && (2.24)\\
&+ c_2\tau(\mathbf{n}_h^k\cdot\operatorname{curl}\mathbf{n}_h^k, d_t\mathbf{n}_h^k\cdot\operatorname{curl}\mathbf{n}_h^k + \mathbf{n}_h^k\cdot\operatorname{curl} d_t\mathbf{n}_h^{k+1})\\
&+ c_2\tau^2(\mathbf{n}_h^k\cdot\operatorname{curl}\mathbf{n}_h^k, d_t\mathbf{n}_h^{k+1}\cdot\operatorname{curl} d_t\mathbf{n}_h^{k+1})\\
&+ \frac{c_2\tau^2}{2}\left\|d_t\mathbf{n}_h^{k+1}\cdot\operatorname{curl}\mathbf{n}_h^k + \mathbf{n}_h^{k+1}\cdot\operatorname{curl} d_t\mathbf{n}_h^{k+1}\right\|^2 && (2.25)
\end{aligned}
$$

Adding (2.21) and (2.25) and canceling the order τ terms, we have

$$
\left(\tau + c_0\frac{\tau^2}{2}\right)\|\nabla d_t\mathbf{n}_h^{k+1}\|^2 + \tilde{E}[\mathbf{n}_h^{k+1}] = \tilde{E}[\mathbf{n}_h^k] + II + III, \tag{2.26}
$$

where

$$
\begin{aligned}
II &= c_2\tau^2(\mathbf{n}_h^k\cdot\operatorname{curl}\mathbf{n}_h^k, d_t\mathbf{n}_h^{k+1}\cdot\operatorname{curl} d_t\mathbf{n}_h^{k+1})\\
III &= \frac{c_2\tau^2}{2}\left\|d_t\mathbf{n}_h^{k+1}\cdot\operatorname{curl}\mathbf{n}_h^k + \mathbf{n}_h^{k+1}\cdot\operatorname{curl} d_t\mathbf{n}_h^{k+1}\right\|^2.
\end{aligned}
$$

To achieve the energy inequality, we will estimate II and III separately. We first estimate II by Cauchy-Schwarz and the inductive hypothesis (2.19):

$$
|II| \le c_2\tau^2\left\|\mathbf{n}_h^k\cdot\operatorname{curl}\mathbf{n}_h^k\right\|\left\|d_t\mathbf{n}_h^{k+1}\cdot\operatorname{curl} d_t\mathbf{n}_h^{k+1}\right\| \le \tau^2\sqrt{2c_2\tilde{E}[\mathbf{n}_h^k]}\left\|d_t\mathbf{n}_h^{k+1}\cdot\operatorname{curl} d_t\mathbf{n}_h^{k+1}\right\|.
$$

We then apply Hölder inequality and Lemma 2.4 (discrete Sobolev inequality) to estimate $\|d_t\mathbf{n}_h^{k+1}\|_{L^\infty} \le$

$c_{inv} h^{-1/2} \|\nabla d_t \mathbf{n}_h^{k+1}\|$ and

$$
\begin{aligned}
|II| &\leq \sqrt{2c_2 \tilde{E}[\mathbf{n}_h^0]} \tau^2 \left\| d_t \mathbf{n}_h^{k+1} \right\|_{L^\infty} \left\| \nabla d_t \mathbf{n}_h^{k+1} \right\| \\
&\leq \sqrt{2c_2 \tilde{E}[\mathbf{n}_h^0]} c_{inv} \tau^2 h^{-1/2} \left\| \nabla d_t \mathbf{n}_h^{k+1} \right\|^2 \leq c^{iv} \tau^2 h^{-1} \left\| \nabla d_t \mathbf{n}_h^{k+1} \right\|^2,
\end{aligned}
$$

where c^{iv} depends on c_2, $\tilde{E}[\mathbf{n}_h^0]$, and c_{inv}. We also estimate III using the inequality $|a+b|^2 \leq 2|a|^2 + 2|b|^2$ and Hölder inequality:

$$
\begin{aligned}
|III| &\leq c_2 \tau^2 \left(\left\| d_t \mathbf{n}_h^{k+1} \cdot \operatorname{curl} \mathbf{n}_h^k \right\|^2 + \left\| \mathbf{n}_h^{k+1} \cdot \operatorname{curl} d_t \mathbf{n}_h^{k+1} \right\|^2 \right) \\
&\leq c_2 \tau^2 \left(\left\| d_t \mathbf{n}_h^{k+1} \right\|_{L^\infty}^2 \left\| \nabla \mathbf{n}_h^k \right\|^2 + \left\| \mathbf{n}_h^{k+1} \right\|_{L^\infty}^2 \left\| \nabla d_t \mathbf{n}_h^{k+1} \right\|^2 \right)
\end{aligned}
$$

The energy decrease from the inductive hypothesis (2.19), the intermediate estimate on $\|\mathbf{n}_h^{k+1}\|_{L^\infty}^2$ from (2.23), and Lemma 2.4 (discrete Sobolev inequality) helps us further bound III as follows:

$$
\begin{aligned}
|III| &\leq c_2 \tau^2 \left(\left\| d_t \mathbf{n}_h^{k+1} \right\|_{L^\infty}^2 \frac{2}{c_0} \tilde{E}[\mathbf{n}_h^{(0}] + (c''')^2 \left\| \nabla d_t \mathbf{n}_h^{k+1} \right\|^2 \right) \\
&\leq c_2 \tau^2 \left(c_{inv}^2 h^{-1} \frac{2}{c_0} \tilde{E}[\mathbf{n}_h^{(0}] + (c''')^2 \right) \left\| \nabla d_t \mathbf{n}_h^{k+1} \right\|^2 \\
&\leq \tau^2 h^{-1} c^v \left\| \nabla d_t \mathbf{n}_h^{k+1} \right\|^2,
\end{aligned}
$$

where c^v depends on c_2, c_{inv}, c''' and $\tilde{E}[\mathbf{n}_h^0]$. Inserting the estimates of II and III into (2.26) yields the following inequality:

$$
\left(\tau + c_0 \frac{\tau^2}{2} \right) \|\nabla d_t \mathbf{n}_h^{k+1}\|^2 + \tilde{E}[\mathbf{n}_h^{k+1}] \leq \tilde{E}[\mathbf{n}_h^k] + \tau c^{vi} \tau h^{-1} \left\| \nabla d_t \mathbf{n}_h^{k+1} \right\|^2.
$$

We pick τh^{-1} so that $\tau h^{-1} \leq \frac{1}{2c^{vi}} =: C$ where c^{vi} depends only on $c_{inv}, \tilde{E}[\mathbf{n}_h^0], c_0, c_2$. With this choice of τh^{-1}, we then have the desired energy inequality (2.19) for $k+1$:

$$\frac{\tau}{2}\|\nabla d_t \mathbf{n}_h^{k+1}\|^2 + \tilde{E}[\mathbf{n}_h^{k+1}] \leq \tilde{E}[\mathbf{n}_h^k].$$

4. Constraint for $\mathbf{n}_h^{k+1}$: Using the orthogonality of $\mathbf{n}_h^k$ and $d_t\mathbf{n}_h^{k+1}$, we have

$$|\mathbf{n}_h^{k+1}(z)|^2 = |\mathbf{n}_h^k(z)|^2 + \tau^2 |d_t \mathbf{n}_h^{k+1}(z)|^2.$$

Again applying the Lemma 2.4 (discrete Sobolev inequality), we have

$$\begin{aligned} |\mathbf{n}_h^{k+1}(z)|^2 &= |\mathbf{n}_h^k(z)|^2 + \tau^2 h^{-1} \left\| \nabla d_t \mathbf{n}_h^{k+1} \right\|^2 \\ &\leq |\mathbf{n}_h^k(z)|^2 + 2c_{inv}^2 \tau h^{-1} \left(\tilde{E}[\mathbf{n}_h^k] - \tilde{E}[\mathbf{n}_h^{k+1}] \right), \end{aligned}$$

whence,

$$|\mathbf{n}_h^{k+1}(z)|^2 - |\mathbf{n}_h^k(z)|^2 \leq 2c_{inv}^2 \tau h^{-1} \left(\tilde{E}[\mathbf{n}_h^k] - \tilde{E}[\mathbf{n}_h^{k+1}] \right).$$

Since $|\mathbf{n}_h^{k+1}(z)|^2 = |\mathbf{n}_h^k(z) + \tau d_t \mathbf{n}_h^{k+1}|^2 \geq |\mathbf{n}_h^k(z)|^2 \geq 1$, summing over k and using telescoping cancellation yields

$$|\mathbf{n}_h^{k+1}(z)|^2 - 1 \leq 2c_{inv}^2 \tau h^{-1} \left(\tilde{E}[\mathbf{n}_h^0] - \tilde{E}[\mathbf{n}_h^{k+1}] \right) \leq 2c_{inv}^2 \tau h^{-1} \tilde{E}[\mathbf{n}_h^0],$$

because $|\mathbf{n}_h^0(z)| = 1$ and $\tilde{E}[\mathbf{n}_h^{k+1}] \geq 0$. The lower bound $|\mathbf{n}_h^{k+1}(z)|^2 - 1 \geq 0$ follows immediately from $|\mathbf{n}_h^{k+1}(z)|^2 \geq |\mathbf{n}_h^k(z)|^2$ and the inductive hypothesis (2.20). See Remark 2.7. These two inequalities are the desired nodal length violation in (2.20) for $k+1$, and completes the inductive argument in the case $c_1 = c_3 = 0$

Case 2. $c_1 \neq 0, c_3 \neq 0$: We now sketch the remaining case when $c_1 \neq 0, c_3 \neq 0$.

First we deal with $c_1 \neq 0$. Since the splay term is dealt with implicitly, we immediately get the energy decrease of this term using similar quadratic identities.

If $c_3 \neq 0$, there are three steps that need to be checked. First, one would need to ensure that the intermediate estimates in (2.22) and (2.23) remains valid. This is indeed the case because an application of the techniques in the above proof would show there is a c' such that

$$c_3\tau \left| \left(\mathbf{n}_h^k \times \operatorname{curl} \mathbf{n}_h^k, \mathbf{n}_h^k \times \operatorname{curl} d_t\mathbf{n}_h^{k+1} + d_t\mathbf{n}_h^{k+1} \times \operatorname{curl} \mathbf{n}_h^k \right) \right| \leq c'\tau h^{-1/2} \|\nabla d_t \mathbf{n}_h^{k+1}\|,$$

and one can balance using Young's inequality to achieve a similar estimate like (2.22). Then the other intermediate estimate (2.23) would follow.

The next key step would be to achieve a version of (2.25). In fact, one can replace dot products with cross products in (2.25) due to the quartic structure of the bend term. Then the energy inequality would follow from the same techniques to estimate the remainder terms in (2.26). $\square$

An interesting observation is that once energy stability is achieved, one does not need to take $\tau h^{-1} \to 0$ to recover control of the unit length constraint violation. In fact, if we measure the constraint violation in a weaker norm, then taking $\tau \to 0$ would recover the unit length constraint as long as $\tau h^{-1} \leq C$ where C is the constant from Theorem 2.2 (energy stability and L^∞ control of constraint). We explore this next.

Corollary 2.1 (control of L^1 violation of constraint)**.** *Let $\mathbf{n}_h^0 \in \mathbb{V}_h$ such that $|\mathbf{n}_h^0(z)|^2 = 1$ for all $z \in \mathcal{N}_h$. Suppose $\tau h^{-1} \leq C$, where C is the constant from Theorem 2.2 (energy stability and L^∞ control of constraint). Then*

$$\left\| I_h[|\mathbf{n}_h^{k+1}|^2 - 1] \right\|_{L^1} \lesssim \tau \tilde{E}[\mathbf{n}_h^0]$$

Proof. Suppose $\tau h^{-1} \leq C$. Then the Theorem 2.2 (energy stability and L^∞ control of constraint) implies

$$\tilde{E}[\mathbf{n}_h^{k+1}] + \frac{\tau}{2}\|\nabla \mathbf{n}_h^k\|^2 \leq \tilde{E}[\mathbf{n}_h^k] \tag{2.27}$$

for all k. Recall that at nodes, we have

$$|\mathbf{n}_h^{k+1}(z)|^2 = |\mathbf{n}_h^k(z)|^2 + \tau^2 |d_t \mathbf{n}_h^{k+1}(z)|^2.$$

Multiplying by h, and summing over $z \in \mathcal{N}_h$, implies

$$h \sum_{z \in \mathbb{N}_h} |\mathbf{n}_h^{k+1}(z)|^2 = h \sum_{z \in \mathbb{N}_h} |\mathbf{n}_h^k(z)|^2 + \tau^2 h \sum_{z \in \mathbb{N}_h} |d_t \mathbf{n}_h^{k+1}(z)|^2.$$

Combining the norm equivalence $h \sum_{z \in \mathcal{N}_h} |d_t \mathbf{n}_h^{k+1}(z)|^2 \approx \|d_t \mathbf{n}_h^{k+1}\|^2$ and Poincaré inequality $\|d_t \mathbf{n}_h^{k+1}\|^2 \lesssim \|\nabla d_t \mathbf{n}_h^{k+1}\|^2$, we deduce

$$h \sum_{z \in \mathbb{N}_h} |\mathbf{n}_h^{k+1}(z)|^2 \lesssim h \sum_{z \in \mathbb{N}_h} |\mathbf{n}_h^k(z)|^2 + \tau^2 \|\nabla d_t \mathbf{n}_h^{k+1}\|^2.$$

Summing over $k = 0, \ldots, \ell$ yields

$$0 \le h \sum_{z \in \mathbb{N}_h} \left(|\mathbf{n}_h^{(\ell+1)}(z)|^2 - 1 \right) \lesssim \sum_{k=0}^{\ell} \tau^2 \|\nabla d_t \mathbf{n}_h^{k+1}\|^2.$$

The left hand side is equivalent to $\|I_h[|\mathbf{n}_h^{(\ell+1)}(z)|^2 - 1]\|_{L^1}$. Estimating the right hand side with the energy inequality (2.27) yields

$$\|I_h[|\mathbf{n}_h^{(\ell+1)}(z)|^2 - 1]\|_{L^1} \lesssim \tau \tilde{E}[\mathbf{n}_h^0],$$

which is the desired estimate. □

The next two corollaries state that Algorithm 1 computes a critical point of $\tilde{E}$ in the discrete admissible set $\mathcal{A}_{\mathbf{g},h,\eta}$. They mimic results for harmonic maps [13, Lemma 3.8.],[16, Proposition 3.1].

Corollary 2.2 (residual estimate)**.** *Given $\varepsilon > 0$, there is an integer k_ε such that $\tilde{E}[\mathbf{n}_h^{(k_\varepsilon - 1)}] - \tilde{E}[\mathbf{n}_h^{(k_\varepsilon)}] < \varepsilon\tau$. Moreover, $\mathbf{n}_h^{(k_\varepsilon)}$ satisfies*

$$\left| \frac{\delta \tilde{E}[\mathbf{n}_h^{(k_\varepsilon)}; \mathbf{v}_h]}{\delta \mathbf{n}} \right| \le (1 + \tau c_0 + \tau c_1)\sqrt{2\varepsilon}\|\nabla \mathbf{v}_h\| \tag{2.28}$$

for all $\mathbf{v}_h \in T(\mathbf{n}_h^{(k_\varepsilon)})$.

Proof. We recall the fundamental energy decay estimate

$$\tilde{E}[\mathbf{n}_h^{k+1}] + \frac{\tau}{2}\left\|\nabla d_t \mathbf{n}_h^{k+1}\right\|^2 \le \tilde{E}[\mathbf{n}_h^k].$$

The above implies that $\tilde{E}[\mathbf{n}_h^k] - \tilde{E}[\mathbf{n}_h^{k+1}] \geq 0$. Also note the telescoping sum, so

$$0 \leq \sum_{k=0}^{K} \left(\tilde{E}[\mathbf{n}_h^k] - \tilde{E}[\mathbf{n}_h^{k+1}]\right) = \tilde{E}[\mathbf{n}_h^0] - \tilde{E}[\mathbf{n}_h^{(K+1)}] \leq \tilde{E}[\mathbf{n}_h^0]$$

and each term is nonnegative. Therefore, the series $0 \leq \sum_{k=0}^{\infty}(\tilde{E}[\mathbf{n}_h^k] - \tilde{E}[\mathbf{n}_h^{k+1}])$ converges, and

$$\lim_{k\to\infty} \left(\tilde{E}[\mathbf{n}_h^k] - \tilde{E}[\mathbf{n}_h^{k+1}]\right) = 0.$$

Hence, there exists a k_ε such that $\tilde{E}[\mathbf{n}_h^{(k_\varepsilon)}] - \tilde{E}[\mathbf{n}_h^{(k_\varepsilon+1)}] \leq \varepsilon\tau$. Also, note that

$$\left\|\nabla d_t \mathbf{n}_h^{(k_\varepsilon+1)}\right\|^2 \leq \frac{2}{\tau}\left(\tilde{E}[\mathbf{n}_h^{(k_\varepsilon)}] - \tilde{E}[\mathbf{n}_h^{(k_\varepsilon+1)}]\right) \leq 2\varepsilon.$$

Using the gradient flow equation in (2.18), we have

$$\frac{\delta \tilde{E}[\mathbf{n}_h^{(k_\varepsilon)}, \mathbf{v}_h]}{\delta \mathbf{n}} = (1+\tau c_0)(\nabla d_t \mathbf{n}_h^{(k_\varepsilon+1)}, \nabla \mathbf{v}_h) + \tau c_1(\operatorname{div} d_t \mathbf{n}_h^{(k_\varepsilon+1)}, \operatorname{div} \mathbf{v}_h),$$

where the asserted estimate

$$\left|\frac{\delta \tilde{E}[\mathbf{n}_h^{(k_\varepsilon)}, \mathbf{v}_h]}{\delta \mathbf{n}}\right| \leq (1+\tau c_0+\tau c_1)\left\|\nabla d_t \mathbf{n}_h^{(k_\varepsilon+1)}\right\| \|\nabla \mathbf{v}_h\| \leq (1+\tau c_0+\tau c_1)\sqrt{2\varepsilon}\|\nabla \mathbf{v}_h\|$$

follows immediately. □

Theorem 2.3. *Let $\varepsilon \to 0$, and let $\mathbf{n}_h^{(k_\varepsilon)}$ be chosen from Corollary 2.2 (residual estimate). Firstly, there are cluster points of $\{\mathbf{n}_h^{(k_\varepsilon)}\}_{\varepsilon>0}$. Secondly, if $\mathbf{n}_h^*$ is a cluster point of $\{\mathbf{n}_h^{(k_\varepsilon)}\}_{\varepsilon>0}$, then it is a* *critical point of $\tilde{E}$ over $\mathbb{V}_h$ in tangential directions, namely*

$$\frac{\delta \tilde{E}[\mathbf{n}_h^*; \mathbf{v}_h]}{\delta \mathbf{n}} = 0 \tag{2.29}$$

for all $\mathbf{v}_h \in T(\mathbf{n}_h^*)$.

Proof. We first note that we have the uniform bound $\|\nabla \mathbf{n}_h^{(k_\varepsilon)}\| \leq \frac{2}{c_0} E[\mathbf{n}_h^0]$ due to Lemma 2.6 (equicoercivity) and the energy decreasing property of Theorem 2.2 (energy stability and L^∞ control of constraint). By compactness in the finite dimensional space $\mathbb{V}_h$, we deduce the first claim that there are cluster points of $\{\mathbf{n}_h^{(k_\varepsilon)}\}_{\varepsilon>0}$.

If $\mathbf{n}_h^*$ is a cluster point, we shall now prove that it is a critical point in the sense (4.50). Let $\mathbf{v}_h \in T(\mathbf{n}_h^*)$. Consider the discrete function $\boldsymbol{\phi}_h \in \mathbb{V}_h$ defined as $\boldsymbol{\phi}_h = I_h[|\mathbf{n}_h^*|^{-2}(\mathbf{v}_h \times \mathbf{n}_h^*)]$, which is well-defined because $|\mathbf{n}_h^*(z)| \geq 1$ for all $z \in \mathcal{N}_h$. Note that $\mathbf{n}_h^*(z) \times \boldsymbol{\phi}_h(z) = \mathbf{v}_h(z)$ at each $z \in \mathcal{N}_h$ because $\mathbf{v}_h \in T(\mathbf{n}_h^*)$ and the cross product identity $\mathbf{a} \times (\mathbf{b} \times \mathbf{c}) = (\mathbf{a} \cdot \mathbf{c})\mathbf{b} - (\mathbf{a} \cdot \mathbf{b})\mathbf{c}$. Moreover, $I_h[\mathbf{n}_h^{(k_\varepsilon)} \times \boldsymbol{\phi}_h] \in T(\mathbf{n}_h^{(k_\varepsilon)})$.

Consider a subsequence $\mathbf{n}_h^{(k_\varepsilon)} \to \mathbf{n}_h^*$ as $\varepsilon \to 0$ in any norm because $\mathbb{V}_h$ is finite dimensional. Then $I_h[\mathbf{n}_h^{(k_\varepsilon)} \times \boldsymbol{\phi}_h] \to \mathbf{v}_h$

$$\frac{\delta \tilde{E}[\mathbf{n}_h^{(k_\varepsilon)}; I_h[\mathbf{n}_h^{(k_\varepsilon)} \times \boldsymbol{\phi}_h]]}{\delta \mathbf{n}} \to \frac{\delta \tilde{E}[\mathbf{n}_h^*; \mathbf{v}_h]}{\delta \mathbf{n}}$$

because $\frac{\delta \tilde{E}}{\delta \mathbf{n}}$ is continuous in each argument. Also, from Corollary 2.2,

$$\left| \frac{\delta \tilde{E}[\mathbf{n}_h^{(k_\varepsilon)}; I_h[\mathbf{n}_h^{(k_\varepsilon)} \times \boldsymbol{\phi}_h]]}{\delta \mathbf{n}} \right| \leq (1 + \tau c_0 + \tau c_1)\sqrt{2\varepsilon} \|\nabla I_h[\mathbf{n}_h^{(k_\varepsilon)} \times \boldsymbol{\phi}_h]\| \leq C\sqrt{\varepsilon} \to 0,$$

whence

$$\frac{\delta \tilde{E}[\mathbf{n}_h^*; \mathbf{v}_h]}{\delta \mathbf{n}} = 0$$

for all $\mathbf{v}_h \in T(\mathbf{n}_h^*)$. $\square$

Remark 2.8 (cross product)**.** *The trick of the cross product to avoid the tangent space has been used before in both numerical analysis and analysis of related problems [8, 10, 13, 45]. However, it may not extend to showing that a discrete critical point of $\tilde{E}$ converges to a critical point of the continuous problem as $h \to 0$ like in [13]. This is because the product of two weakly convergent sequences may not converge weakly, which becomes an issue for the terms other than the Dirichlet energy. However, this is not an obstruction in the discrete setting with fixed h since the underlying space $\mathbb{V}_h$ is finite dimensional.*

2.4.2 Practical implementation: Lagrange multiplier

To practically implement the gradient flow step in (2.18) we introduce a Lagrange multiplier $\lambda_h \in \mathbb{Q}_{h,0}$ the space of scalare continuous piecewise linear functions that vanish on $\partial\Omega$, and the bilinear form for the linear constraint $\mathbf{u}_h \in T_h(\mathbf{n}_h^k)$, i.e. $(\mathbf{n}_h^k(z) \cdot \mathbf{u}_h(z) = 0)$

$$b^k(\lambda_h, \mathbf{v}_h) = \int_\Omega I_h[\lambda_h(\mathbf{v}_h \cdot \mathbf{n}_h^k)],$$

which is a mass lumped L^2 inner product between λ_h and $\mathbf{v}_h \cdot \mathbf{n}_h^k$. The gradient flow step is solved as a saddle point system:

$$a(d_t\mathbf{n}_h^{k+1}, \mathbf{v}_h) + b^k(\lambda_h, \mathbf{v}_h) = \langle \mathbf{f}^{(k)}, \mathbf{v}_h\rangle \qquad \forall \mathbf{v}_h \in \mathbb{V}_{h,0} \tag{2.30}$$

$$b^k(\rho_h, d_t\mathbf{n}_h^{k+1}) = 0 \qquad \forall \rho_h \in \mathbb{Q}_{h,0}, \tag{2.31}$$

where

$$a(\mathbf{u}_h, \mathbf{v}_h) := (1 + c_0\tau)(\nabla \mathbf{u}_h, \nabla \mathbf{v}_h) + c_1\tau(\operatorname{div} \mathbf{u}_h, \operatorname{div} \mathbf{v}_h)$$

and

$$\langle \mathbf{f}^{(k)}, \mathbf{v}_h\rangle := -\frac{\delta \tilde{E}[\mathbf{n}_h^k; \mathbf{v}_h]}{\delta \mathbf{n}}.$$

The saddle point system in (2.30) and (2.31) is well-posed. First, the bilinear form a is coercive over $\mathbb{V}_{h,0}$, and hence is coercive over the kernel of b^k. The bilinear form b^k satisfies the following h-dependent and potentially suboptimal inf-sup inequality. We point to [24, Lemma 3.1(i)] for an inf-sup for b^k measured in different norms.

Proposition 2.3 (inf-sup for linearized constraint)**.** *Let the hypothesis of Theorem 2.2 (energy stability and L^∞ control of constraint) hold i.e. $\tau h^{-1} \le C$ and $|\mathbf{n}_h^0(z)| = 1$ for all nodes $z \in \mathcal{N}_h$. Let $\mathbf{n}_h^k \in \mathbb{V}_h$ be the k-th iterate generated by Algorithm 1. Then the bilinear form $b^k : \mathbb{Q}_{h,0} \times \mathbb{V}_{h,0}$ satisfies the following inf-sup inequality*

$$\inf_{\lambda_h \in \mathbb{Q}_{h,0}\setminus\{0\}} \sup_{\mathbf{v}_h \in \mathbb{V}_{h,0}\setminus\{0\}} \frac{b^k(\lambda_h, \mathbf{v}_h)}{\|\mathbf{v}_h\|_{H^1(\Omega;\mathbb{R}^3)} \|\lambda_h\|_{L^2(\Omega)}} \ge c h^{3/2} \tag{2.32}$$

where $c > 0$ only depends on $\tilde{E}[\mathbf{n}_h^0]$ and shape regularity and quasiuniformity of the sequence of triangulations.

Proof. To prove the result, it is sufficient to prove that given a $\lambda_h \in \mathbb{Q}_{h,0}$ there exists $\mathbf{v}_h \in \mathbb{V}_{h,0}$ such that $b^k(\lambda_h, \mathbf{v}_h) \geq ch^{3/2}\|\mathbf{v}_h\|_{H^1(\Omega;\mathbb{R}^3)}\|\lambda_h\|$.

Let $\lambda_h \in \mathbb{Q}_{h,0}$. We choose $\mathbf{v}_h = I_h[\lambda_h \mathbf{n}_h^k] \in \mathbb{V}_{h,0}$. At each node, $z \in \mathcal{N}_h$, we have

$$\lambda_h(z)\mathbf{v}_h(z) \cdot \mathbf{n}_h^k = |\lambda_h(z)|^2 |\mathbf{n}_h^k(z)|^2.$$

Recall that Algorithm 1 produces $|\mathbf{n}_h^k(z)|^2 \geq 1$ at each node by the argument in Remark 2.7 (lower bound on $|\mathbf{n}_h^k(z)|^2$). Hence, $\lambda_h(z)\mathbf{v}_h(z) \cdot \mathbf{n}_h^k \geq \lambda_h(z)^2$, and there is a constant $c > 0$ independent of h such that

$$b^k(\lambda_h, \mathbf{v}_h) = \int_\Omega I_h[\lambda_h(\mathbf{v}_h \cdot \mathbf{n}_h^k)]\, d\mathbf{x} \geq \int_\Omega I_h[\lambda_h^2]\, d\mathbf{x} \geq c\|\lambda_h\|^2$$

by virtue of the norm equivalence $\|I_h[\lambda_h]\| \approx \|\lambda_h\|$ on $\mathbb{Q}_{h,0}$.

We are left to show $\|\mathbf{v}_h\|_{H^1(\Omega;\mathbb{R}^3)} \leq ch^{-3/2}\|\lambda_h\|_{L^2(\Omega)}$. We start with a generic element $T \in \mathcal{T}_h$ and apply triangle inequality

$$\|\nabla \mathbf{v}_h\|_{L^2(T,\mathbb{R}^{3\times 3})} \leq \|\nabla(\lambda_h \mathbf{n}_h^k - I_h[\lambda_h \mathbf{n}_h^k])\|_{L^2(T;\mathbb{R}^{3\times 3})} + \|\nabla(\lambda_h \mathbf{n}_h^k)\|_{L^2(T;\mathbb{R}^{3\times 3})}.$$

We handle the first term with an error estimate for the Lagrange interpolant and Hölder inequality

$$
\begin{aligned}
\|\nabla(\lambda_h \mathbf{n}_h^k - I_h[\lambda_h \mathbf{n}_h^k])\|_{L^2(T;\mathbb{R}^{3\times 3})} &\lesssim h\|D^2(\lambda_h \mathbf{n}_h^k)\|_{L^2(T;\mathbb{R}^{3\times 3\times 3})} \\
&\lesssim h\|\nabla\lambda_h\|_{L^2(T;\mathbb{R}^3)}\|\nabla \mathbf{n}_h^k\|_{L^\infty(T;\mathbb{R}^{3\times 3})}
\end{aligned}
$$

where the last inequality uses the fact that $\partial_{ij}^2(\lambda_h \mathbf{v}_h) = \partial_i\lambda_h\partial_j\mathbf{v}_h + \partial_j\lambda_h\partial_i\mathbf{v}_h$ for linear functions on T.

We handle the second term by applying a product rule and Hölder inequality

$$
\|\nabla(\lambda_h \mathbf{n}_h^k)\|_{L^2(T;\mathbb{R}^{3\times 3})} \lesssim \|\mathbf{n}_h^k\|_{L^\infty(T;\mathbb{R}^3)}\|\nabla\lambda_h\|_{L^2(T;\mathbb{R}^3)} + \|\lambda_h\|_{L^2(T)}\|\nabla\mathbf{n}_h^k\|_{L^\infty(T;\mathbb{R}^{3\times 3})}
$$

Theorem 2.2 (energy stability and L^∞ control of constraint) produces $\|\mathbf{n}_h^k\|_{L^\infty(T;\mathbb{R}^3)} \lesssim 1$. Hence,

$$
\|\nabla\left(\lambda_h \mathbf{n}_h^k\right)\|_{L^2(T;\mathbb{R}^{3\times 3})} \lesssim \|\nabla\lambda_h\|_{L^2(T;\mathbb{R}^3)} + \|\lambda_h\|_{L^2(T)}\|\nabla\mathbf{n}_h^k\|_{L^\infty(T;\mathbb{R}^{3\times 3})}
$$

Adding the estimates together yields

$$
\|\nabla\mathbf{v}_h\|_{L^2(T;\mathbb{R}^{3\times 3})} \leq \|\lambda_h\|_{L^\infty(T)}\|\nabla\mathbf{n}_h^k\|_{L^2(T;\mathbb{R}^{3\times 3})} + \|\nabla\lambda_h\|_{L^2(T;\mathbb{R}^3)} + \|\lambda_h\|_{L^2(T)}\|\nabla\mathbf{n}_h^k\|_{L^\infty(T;\mathbb{R}^{3\times 3})}
$$

Squaring, summing over elements, and taking a square root yields

$$
\|\nabla\mathbf{v}_h\| \leq \|\nabla\lambda_h\| + \|\lambda_h\|\|\nabla\mathbf{n}_h^k\|_{L^\infty}.
$$

We finally apply global inverse inequalities $\|\nabla\mathbf{n}_h^k\|_{L^\infty} \lesssim h^{-3/2}\|\nabla\mathbf{n}_h^k\|$ and $\|\nabla\lambda_h\| \lesssim h^{-1}\|\lambda_h\|$, Theorem 2.2 (energy stability and L^∞ control of constraint), and Lemma 2.6 (equicoercivity) to see that

$$\|\nabla \mathbf{v}_h\| \lesssim h^{-3/2}\|\lambda_h\|$$

with a hidden constant only depending on the initial energy $\tilde{E}[\mathbf{n}_h^0]$ and shape regularity and quasi-uniformity of the sequence of triangulations $\{\mathcal{T}_h\}_h$. □

Remark 2.9. If $\nabla \mathbf{n}_h^k$ was uniformly bounded in $L^\infty(\Omega;\mathbb{R}^{3\times 3})$, then the inf-sup condition reads

$$\inf_{\lambda_h \in \mathbb{Q}_{h,0}\setminus\{0\}} \sup_{\mathbf{v}_h \in \mathbb{V}_{h,0}\setminus\{0\}} \frac{b^k(\lambda_h, \mathbf{v}_h)}{\|\mathbf{v}_h\|_{H^1(\Omega;\mathbb{R}^3)}\|\lambda_h\|_{L^2(\Omega)}} \geq \frac{ch}{1 + h\|\nabla \mathbf{n}_h^k\|_{L^\infty}}$$

The assumption that $\nabla \mathbf{n}_h^k$ is uniformly bounded in $L^\infty(\Omega;\mathbb{R}^{3\times 3})$ is similar to the assumptions in [74] and [24]. In our context, [24, Lemma 3.1] would imply

$$\inf_{\lambda_h \in \mathbb{Q}_{h,0}\setminus\{0\}} \sup_{\mathbf{v}_h \in \mathbb{V}_{h,0}\setminus\{0\}} \frac{b^k(\lambda_h, \mathbf{v}_h)}{\|\mathbf{v}_h\|_{H^1(\Omega;\mathbb{R}^3)}\|\lambda_h\|_{H^{-1}(\Omega)}} \geq c\|\nabla \mathbf{n}_h^k\|_{L^\infty}^{-1}. \tag{2.33}$$

If $\Omega \subset \mathbb{R}^2$, then [74, Theorem 4.2] would also give an h-independent inf-sup constant.

In the presence of defects in $\Omega \in \mathbb{R}^3$, we do not expect $\nabla \mathbf{n}_h^k$ to be uniformly bounded in $L^\infty(\Omega;\mathbb{R}^{3\times 3})$. The inverse inequality and Theorem 2.2 (energy stability and L^∞ control of constraint) yields $\|\nabla \mathbf{n}_h^k\|_{L^\infty} \lesssim h^{-3/2}\|\nabla \mathbf{n}_h^k\| \leq Ch^{-3/2}$, and the h dependence in (2.33) would be on par with what we proved in (2.32). However, our result measures λ_h in a stronger norm than [24, 74].

Remark 2.10 (Newton iteration)**.** If we were to implement Newton's method to find critical points of $\tilde{E}$ over $\mathcal{A}_{\mathbf{g},h,0}$, the system for the Newton iterate $d_t\mathbf{n}_h^{k+1} = \mathbf{n}_h^{k+1} - \mathbf{n}_h^k$ and $d_t\lambda_h^{k+1} =$

$\lambda_h^{k+1} - \lambda_h^k$ would look like

$$\frac{\delta^2 \tilde{E}[\mathbf{n}_h^k; d_t \mathbf{n}_h^{k+1}, \mathbf{v}_h]}{\delta \mathbf{n}^2} + b^k(d_t \lambda_h^{k+1}, \mathbf{v}_h) = -\frac{\delta \tilde{E}[\mathbf{n}_h^k; \mathbf{v}_h]}{\delta \mathbf{n}} - b^k(\lambda_h^k, \mathbf{v}_h)$$
$$b^k(\rho_h, d_t \mathbf{n}_h^{k+1}) = -\frac{1}{2} \int_\Omega I_h \left[\left(|\mathbf{n}_h^k|^2 - 1 \right) \rho_h \right] \, d\mathbf{x}.$$

The above system has a similar structure to the system (2.30) and (2.31). First, the form b^k would satisfy the same h dependent inf-sup condition. Another issue is that it is not clear whether $\delta^2 E[\mathbf{n}_h^k; \cdot, \cdot]/\delta \mathbf{n}^2$ is coercive. One probably needs to further modify $\tilde{E}$ as was done in [1] to ensure coercivity. However, the work in [1, Remark 3.9] shows that a modification of $\delta^2 E[\mathbf{n}_h^k; \cdot, \cdot]/\delta \mathbf{n}^2$ is coercive if $k_2/k_3 \in (1 - \varepsilon_k, 1 + \varepsilon_k)$ for some ε_k that depends on $\mathbf{n}_h^k$, where $\varepsilon_k \to 0$ as $\|\nabla \mathbf{n}_h^k\|_{L^\infty} \to \infty$. As a result, we might expect to lose coercivity with mesh refinement if $k_2 \neq k_3$ and if there are defects present in the LC.

For solving the saddle point system, we use MINRES [99]. For preconditioning, we employ a block diagonal preconditioner motivated by preconditioned MINRES for Stokes' equations [61, Chapter 6.2]. We pick the upper left block to be an appropriate preconditioner of the Laplacian like the multigrid preconditioner implemented in NGSolve [108]. The lower right block of the preconditioner is the mass matrix $\mathbf{M}_{ij} = \int_\Omega \phi_i \phi_j \, d\mathbf{x}$, where ϕ_i are the nodal basis functions of $\mathbb{Q}_h$. The number of preconditioned MINRES iterations grows like $\mathcal{O}(h^{-1})$ as seen in Table 2.1 in Section 2.6. This computational evidence suggests that the preconditioning strategy we employ might be suboptimal. Additionally, the inf-sup condition in (2.32) is not uniform in h and the growth in MINRES iterations could be due to the lack of uniform stability of the system (2.30) and (2.31). We refer to [75, 123] for work on preconditioning systems similar to (2.30)-(2.31).

2.5 Magnetic effects

This section addresses how to adapt the previously discussed results in the presence of a *fixed* magnetic field $\mathbf{H} \in L^2(\Omega; \mathbb{R}^3)$,

For a fixed magnetic field $\mathbf{H}$ the magnetic energy is [114, Ch. 4.1]

$$E_m[\mathbf{n}] = -\frac{\chi_A}{2} \int_\Omega (\mathbf{n} \cdot \mathbf{H})^2 d\mathbf{x}$$

where χ_A is the diamagnetic anisotropy, which measures how much a liquid crystal wants to either align with the magnetic field or align orthogonally to the magnetic field. The parameter χ_A may be positive or negative depending on the material. For this chapter, we consider $\chi_A \geq 0$, which favors alignment of $\mathbf{n}$ with $\mathbf{H}$.

With the magnetic energy, the total energy becomes

$$E_{total}[\mathbf{n}] := \tilde{E}[\mathbf{n}] + E_m[\mathbf{n}]$$

Since the magnetic contribution is a lower order term, existence of minimizers is still true [70, Theorem 2.3]. We now summarize the numerical results in the presence of the extra magnetic field $\mathbf{H}$ and remark on how the proofs are modified.

2.5.1 Convergence of minimizers

The first proof to modify would be the proof of Lemma 2.5 (recovery sequence). Since $\mathbf{n}_h \to \mathbf{n}$ strongly in L^2 and $\mathbf{n}_h$ is uniformly bounded in L^∞, then $E_m[\mathbf{n}_h] \to E_m[\mathbf{n}]$ up to a subsequence by Lebesgue Dominated Convergence Theorem, and the recovery sequence result would carry over. For Lemma 2.6 (equicoercivity), the uniform bound in L^∞ in the definition of $\mathcal{A}_{\mathbf{g},h,\eta}$ would ensure that $E_m[\mathbf{n}_{h,\eta}] \geq -\frac{C|\chi_A|}{2}\|\mathbf{H}\|^2$, which does not impact equicoercivity. Finally, for Lemma 2.7 (weak lower semicontinuity), the liminf inequality also does not change with the magnetic field since if $\mathbf{n}_h \rightharpoonup \mathbf{n}$ in H^1, then a subsequence satisfies $\mathbf{n}_h \to \mathbf{n}$ strongly in L^2. Thus, $E_m[\mathbf{n}_h] \to E_m[\mathbf{n}]$ because $\mathbf{H}$ is fixed. Therefore, the following theorem holds with the magnetic field.

Theorem 2.4 (convergence of minimizers)**.** *Let $h, \eta \to 0$, and $\mathbf{n}^*_{h,\eta}$ be a sequence of minimizers of $\tilde{E} + E_m$ over the admissible set $\mathcal{A}_{\mathbf{g},h,\eta}$. Then there is a subsequence (not relabeled) $\mathbf{n}^*_{h,\eta}$ such that $\mathbf{n}^*_{h,\eta} \rightharpoonup \mathbf{n}^* \in \mathcal{A}_\mathbf{g}$ in $H^1(\Omega;\mathbb{R}^3)$ such that $\mathbf{n}^*$ is a minimizer of E_{total} over $\mathcal{A}_\mathbf{g}$.*

2.5.2 Gradient flow

Also, the gradient flow is only slightly modified. To guarantee energy decrease, we treat E_m explicitly in the gradient flow since $\chi_A \geq 0$. The resulting modification to the gradient flow equation is to find $d_t\mathbf{n}_h^{k+1} \in T_h(\mathbf{n}_h^k)$ that solves

$$(1+\tau c_0)(\nabla d_t \mathbf{n}_h^{k+1}, \nabla \mathbf{v}_h) + \tau c_1(\operatorname{div} d_t\mathbf{n}_h^{k+1}, \operatorname{div}\mathbf{v}_h) = -\frac{\delta E_{total}[\mathbf{n}^{(k)}; \mathbf{v}_h]}{\delta \mathbf{n}} \quad \forall \mathbf{v}_h \in T_h(\mathbf{n}_h^k). \tag{2.34}$$

The explicit treatment guarantees energy decrease due to the quadratic identity $(a, a-b) = \frac{1}{2}\|a\|^2 - \frac{1}{2}\|b\|^2 + \frac{1}{2}\|a-b\|^2$. We have

$$
\begin{aligned}
-\frac{\delta E_m[\mathbf{n}_h^k; \tau d_t \mathbf{n}_h^{k+1}]}{\delta \mathbf{n}} &= -\chi_A \frac{1}{2}\left\|\mathbf{n}_h^k \cdot \mathbf{H}\right\|^2 + \chi_A \frac{1}{2}\left\|\mathbf{n}_h^{k+1} \cdot \mathbf{H}\right\|^2 - \frac{\tau^2 \chi_A}{2}\left\|d_t \mathbf{n}_h^{k+1} \cdot \mathbf{H}\right\|^2 \\
&= E_m[\mathbf{n}_h^k] - E_m[\mathbf{n}_h^{k+1}] - \frac{\tau^2}{2}\left\|d_t \mathbf{n}_h^{k+1} \cdot \mathbf{H}\right\|^2
\end{aligned}
$$

Adding this to the proof of Theorem 2.2 (energy stability and L^∞ control of constraint) would still ensure total energy decrease, and the validity of the following theorem.

Theorem 2.5 (energy decrease with magnetic effects)**.** *Let $\mathbf{n}_h^0 \in \mathbb{V}_h$ such that $|\mathbf{n}_h^0(z)|^2 = 1$ for all $z \in \mathcal{N}_h$. There is a constant $0 < C \leq 1$ which may depend on $E_{total}[\mathbf{n}_h^0]$, c_{inv}, and c_i for $i = 0, 1, 2, 3$ such that if $\tau h^{-1} \leq C$ then, for all k*

$$
E_{total}[\mathbf{n}_h^{k+1}] + \frac{\tau}{2}\|\nabla d_t \mathbf{n}_h^{k+1}\|^2 \leq E_{total}[\mathbf{n}_h^{k+1}],
$$

and for all $z \in \mathcal{N}_h$

$$
||\mathbf{n}_h^{k+1}(z)|^2 - 1| \leq 4c_{inv}^2 \tau h^{-1} E_{total}[\mathbf{n}_h^0],
$$

where c_{inv} is the constant from Lemma 2.4 (discrete Sobolev inequality).

The other Corollaries in Section 2.4 would also hold.

2.6 Computational results

The algorithm proposed was implemented in the mutli physics software NGSolve [108] and visualizations were made with ParaView [6]. Since we are interested in the influence of Frank's constants. We introduce the following notation to denote splay, twist, and bend:

$$\begin{aligned}
\texttt{splay}(\mathbf{n}) &:= \int_\Omega (\operatorname{div}\mathbf{n})^2 d\mathbf{x}, \\
\texttt{twist}(\mathbf{n}) &:= \int_\Omega (\mathbf{n}\cdot\operatorname{curl}\mathbf{n})^2 d\mathbf{x}, \\
\texttt{bend}(\mathbf{n}) &:= \int_\Omega (\mathbf{n}\times\operatorname{curl}\mathbf{n})^2 d\mathbf{x}.
\end{aligned}$$

We also use short hand notation for the L^p discrete unit length constraint error

$$\texttt{err}_p(\mathbf{n}_h) := \left\| I_h[|\mathbf{n}_h|^2 - 1] \right\|_{L^p(\Omega)}.$$

Finally $\mathbf{n}_h^\infty$ will denote the solution produced by Algorithm 1 when the desired tolerance is reached.

2.6.1 Frank's constants and defects

This section presents how defects may change behavior under the influence of Frank's constants k_1 (splay), k_2 (twist), k_3 (bend). The first example is the instability of $x \mapsto x/|x|$ for k_2 sufficiently small, known as Hélein's condition. The second example is the instability of a degree two defect and the influence of Frank's constants on the resulting configuration.

2.6.1.1 Hélein's condition

This computation presents the instability of degree 1 defect depending on k_i known as Hélein's condition [73], which has also been computationally studied in [9]. Results in [77] state that the second variation of E over $\mathcal{A}_{\mathbf{g}}$ with $\Omega = B_1(0)$ at $\mathbf{n}_1(\mathbf{x}) = \mathbf{x}/|\mathbf{x}|$ is positive definite if and only if

$$8(k_2 - k_1) + k_3 \geq 0, \tag{2.35}$$

which is Hélein's condition. Note that $\mathtt{bend}(\mathbf{n}_1) = \mathtt{twist}(\mathbf{n}_1) = 0$, so $\mathbf{n}_1$ consists of pure splay. Hélein's condition states that there is a tradeoff between the splay and bend and twist energies. If the bend and twist constants k_2, k_3, are small relative to the splay constant k_1, then it is energetically favorable for a configuration to bend and twist a little; (2.35) does not hold. If k_1 is small relative to k_2, k_3, then (2.35) is valid and the energy cannot reduce by bending and twisting.

For the next set of computations, we let the parameters be

$$k_1 = k_3 = 1, \quad k_2 = 0.1, \quad \tau = h = 2^{-\ell/2}$$

and remesh Ω for $\ell = 4, \ldots, 9$ to see how the projection-free gradient flow behaves when decreasing h and τ. This simulation corresponds to a violation of (2.35). Note that from Theorem 2.2 (energy stability and L^∞ violation of constraint) and Corollary 2.1 (control of L^1 violation of constraint), we expect $\mathtt{err}_\infty(\mathbf{n}_h^\infty) \lesssim 1$, and $\mathtt{err}_1(\mathbf{n}_h^\infty) \lesssim h$. Figure 2.2 shows that $\mathtt{err}_1(\mathbf{n}_h^\infty) \lesssim h$ and $\mathtt{err}_\infty(\mathbf{n}_h^\infty)$ starts to decrease and perform slightly better than $\mathcal{O}(1)$. The table in Table 2.1 shows the initial and final energy as well as gradient flow iteration counts. Note that the number of gradient flow iterations grows like $\mathcal{O}(\tau^{-1})$. Table 2.1 also shows the number of MINRES iterations to compute the saddle point problem with residual error less than 10^{-8} for the first iterate of the gradient flow. The preconditioning strategy we employ is outlined in Section 2.4.2. The number of MINRES iterations grows like $\mathcal{O}(h^{-1})$. We note that the stairstep behavior of the

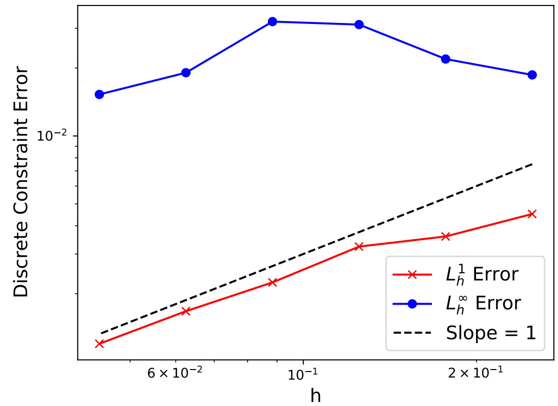

Figure 2.2: Plot of discrete unit length constraint errors $\|I_h[|\mathbf{n}_h^\infty|^2-1]\|_{L^p(\Omega)}$ for $p=1,\infty$. Note that Theorem 2.2 and Corollary 2.1 imply that $\mathtt{err}_1(\mathbf{n}_h^\infty)\lesssim h$ and $\mathtt{err}_\infty(\mathbf{n}_h^\infty)\lesssim 1$ provided $\tau h^{-1}\leq C$. The computational results corroborate the theory.

MINRES iterations is probably due to the fact that we are remeshing Ω rather than performing mesh refinement.

For the smallest meshsize and τ, we plot the initial and final configuration in Figure 2.3. We also present the initial and final splay, bend and twist in Table 2.3. Note that bend and twist increase by an order of magnitude from the initial to final configuration, which confirms the suspicion that the liquid crystal can decrease the energy by reducing splay at a modest cost of increasing twist and bend.

2.6.1.2 Influence of Frank's constants on instability of degree 2 defect

We now explore the influence of Frank's Constants on the instability of a degree 2 defect. All simulations were computed with the following parameters

$$\Omega=B_1(0),\quad h=\tau=\frac{1}{16},\quad \varepsilon=10^{-4}.$$

h	$\tilde{E}[\mathbf{n}_h^0]$	$\tilde{E}[\mathbf{n}_h^\infty]$	GF Iterations	MINRES Iterations
2^{-2}	21.686	21.147	396	40
$2^{-5/2}$	22.281	21.556	177	44
2^{-3}	23.067	21.883	264	72
$2^{-7/2}$	23.197	21.952	394	80
2^{-4}	23.491	21.998	562	144
$2^{-9/2}$	23.498	21.958	823	128

Table 2.1: Table of initial energies, final energies, number of gradient flow iterations for different values of h computing a degree 1 defect under Hélene's condition. Last column is the number of MINRES iterations to reach a residual error less than 10^{-8} for one step of the gradient flow for different values of h. We see that the number of gradient flow iterations grows like $\mathcal{O}(\tau^{-1}) = \mathcal{O}(h^{-1})$ and the number of MINRES iterations also grows like $\mathcal{O}(h^{-1})$.

ℓ	$\mathtt{err}_1(\mathbf{n}_h^\infty)$	$\mathtt{err}_\infty(\mathbf{n}_h^\infty)$	GF Iterations
1	1.19e-02	1.16e-01	74
2	6.29e-03	6.11e-02	138
3	3.24e-03	3.14e-02	265
4	1.64e-03	1.59e-02	520
5	8.27e-04	8.01e-03	1030
6	4.16e-04	4.028e-03	2051

Table 2.2: Discrete unit length constraint errors and number of gradient flow iterations for a degree 1 defect under Hélene's condition with $h = 1/8$, $\tau = \frac{1}{2^\ell}$ for $\ell = 1, \ldots, 6$ and $\varepsilon = 10^{-3}/2$. Both the L^1 and L^∞ errors for the discrete unit length constraint decreases linearly with τ, which is expected from Theorem 2.2 and Corollary 2.1 if h is fixed. Also, gradient flow iterations increase like $\mathcal{O}(\tau^{-1})$, which is also expected if ε is fixed.

	$\mathtt{splay}(\mathbf{n}_h)$	$\mathtt{twist}(\mathbf{n}_h)$	$\mathtt{bend}(\mathbf{n}_h)$
Initial	49.4	.0286	.138
Final	42.7	10.2	2.68

Table 2.3: Initial and final splay, twist, and bend for computed solution with $k_1 = k_3 = 1$ and $k_2 = .1$ and $h = \tau = 2^{-9/2}$ and $\varepsilon = 10^{-3}/2$ (the stopping parameter of Algorithm 1). Note that twist and bend increase by at least an order of magnitude while splay only decreases slightly. This sheds light on Hélein's condition being a tradeoff between splay and twist and bend.

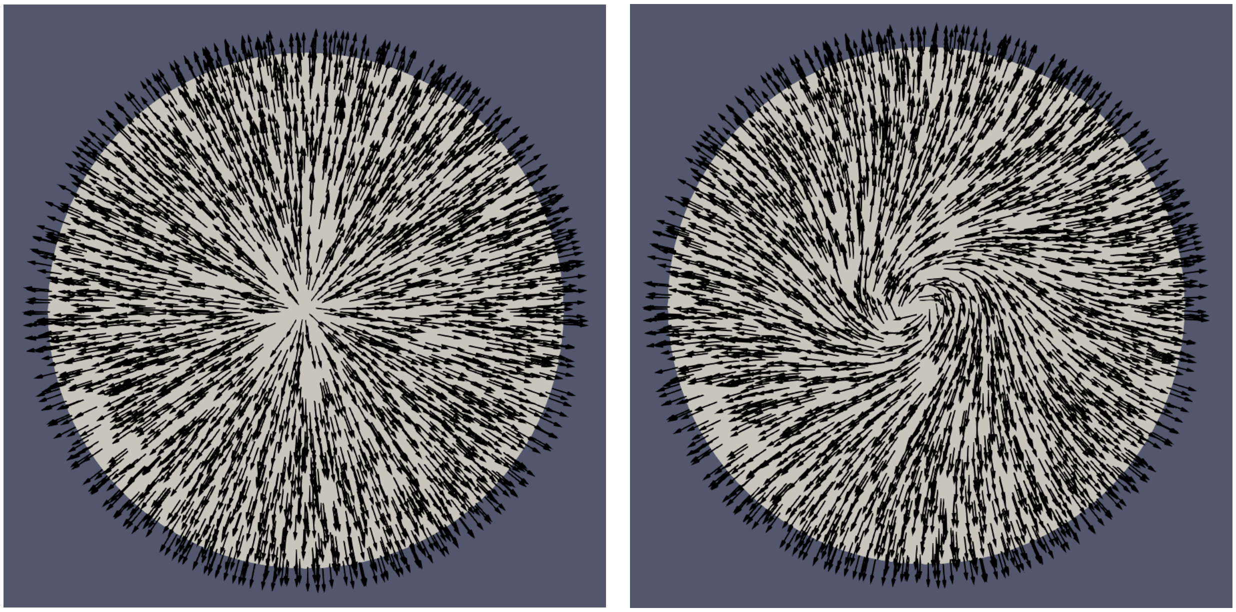

Figure 2.3: Above is the $\{y = 0\}$ slice of the projected director field. The right is the computed minimizer with $k_1 = k_3 = 1$ and $k_2 = .1$ and numerical parameters $h = 2^{-9/2}, \tau = h, \varepsilon = 10^{-3}/2$ (the stopping parameter of Algorithm 1)

The starting configuration and boundary conditions is given by the degree 2 defect:

$$\mathbf{n}_2(\mathbf{x}) = \pi^{-1}\left((\pi(\mathbf{x}/|\mathbf{x}|)^2\right).$$

where $\pi : \mathbb{S}^2 \to \mathbb{C}$ is the stereographic projection. This example has been explored previously in the one constant case [8, 13, 50]. The map $\mathbf{n}_2$ has a singularity at $\mathbf{x} \neq 0$ due to $\mathbf{x} \mapsto \mathbf{x}/|\mathbf{x}|$ in the argument of π. We sketch why $\mathbf{n}_2$ has a singularity of degree 2. Consider $\mathbf{x}_\theta = (\cos\theta, \sin\theta, 0)$. The stereographic projection π maps $\mathbf{x}_\theta$ to $z = e^{i\theta}$, so $\pi(\mathbf{x}_\theta)^2 = e^{2i\theta}$. Mapping back with π^{-1} yields $\mathbf{n}_2(\mathbf{x}_\theta) = (\cos 2\theta, \sin 2\theta, 0)$, which we can see has a winding number of 2 if we integrate the path integral around the unit circle $\mathbb{S}^2 \cap \{x_3 = 0\}$.

In fact, this technique also produces higher degree defects, i.e. $\mathbf{n}_m(\mathbf{x}) = \pi^{-1}(\pi(\mathbf{x}/|\mathbf{x}|)^m)$ would be the defect of degree m. For all numerical simulations, the initial configuration is $\mathbf{n}_h^0 =$

$I_h \mathbf{n}_2$. Figure 2.4 shows the initial condition and the result of the gradient flow for the one constant case $k_i = 1$. Figure 2.5 shows the final configurations for $k_1 = 1, k_2 = .75$ and $k_3 = 1, 3, 5$. Note in Figure 2.5 that as k_3 increases, the computed solution transitions from two bending defects to two splay defects. In fact, as $k_3 = 1, 3, 5$, the value of $8(k_2 - k_1) + k_3$ from Hélein's condition is $-1, 0, 1$. When $8(k_2 - k_1) + k_3 < 0$, we expect that bending and twist configurations are preferable based on Hélein's condition. Likewise for $8(k_2 - k_1) + k_3 \geq 0$, we expect splay configurations to be preferable. This is just a heuristic, but we see the different configurations arise in Figure 2.5.

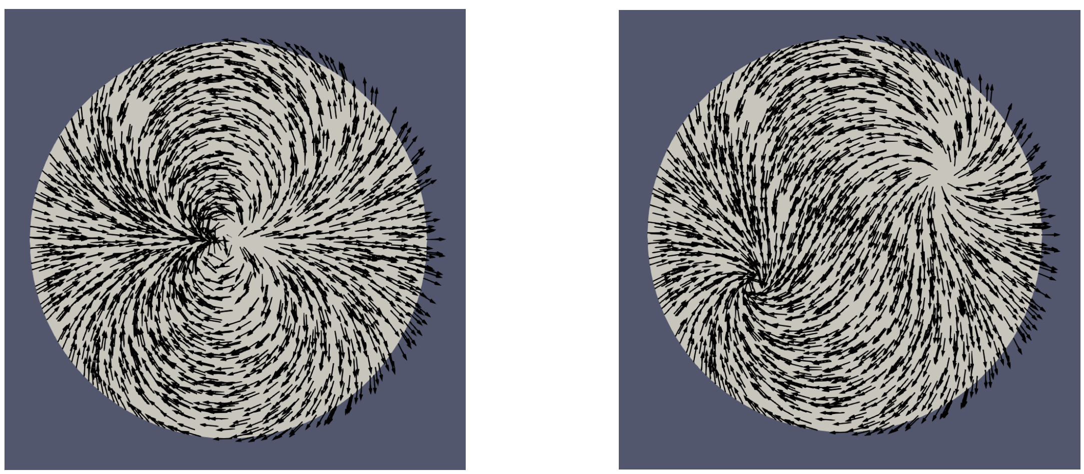

Figure 2.4: Initial and final configurations from Algorithm 1 with $k_i = 1$ for $i = 1, 2, 3$, $h = \tau = 1/16$ and $\varepsilon = 10^{-4}$. A degree 2 defect for the initial condition splits into two degree 1 defects.

2.6.2 Magnetic effects

2.6.2.1 Fréedericksz transition

We next study the Fréedericksz transition [65], which is an experimental technique to determine Frank's constants. We describe the set up to determine k_1. The domain is $\Omega = (-1, 1) \times (0, w)$ and Dirichlet boundary conditions are set on the top and bottom boundaries

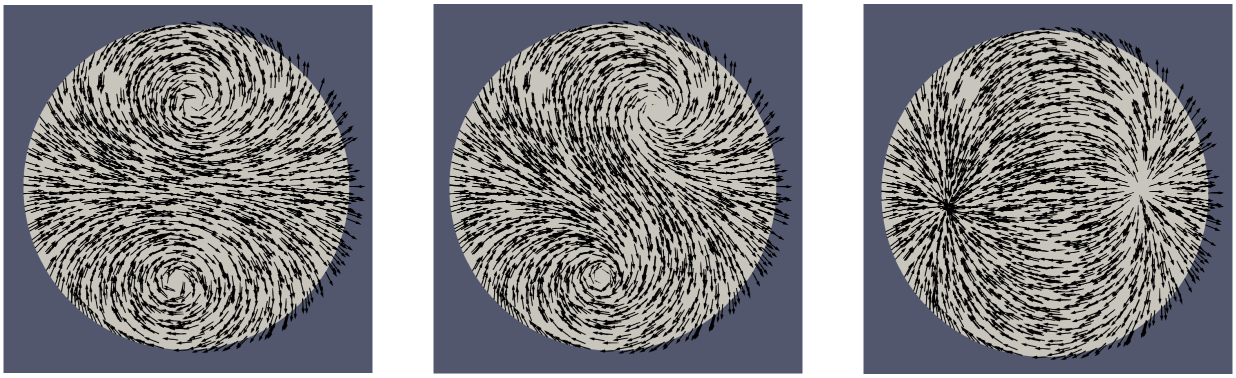

Figure 2.5: Initial and final configurations from Algorithm 1 and $k_1 = 1, k_2 = .75$ and $k_3 = 1, 3, 5$. As $k_3 = 1, 3, 5$, the equilibrium configuration changes from 2 bending degree 1 defects for $k_3 = 1$ to two degree 1 splay like defects for $k_3 = 5$.

$\Gamma_D = (-1, 1) \times \{0.w\}$. For the splay configuration, the boundary condition is $\mathbf{g}(x) = \mathbf{e}_1$. The applied magnetic field is $\mathbf{H} = H\mathbf{e}_3$ for H to be determined. Note that $\mathbf{n}_0 := \mathbf{g}$ has zero energy and is a critical point of $\tilde{E}$. However, analysis in [57, 114] show $\mathbf{n}_0$ becomes unstable when

$$H > \frac{1}{2w}\sqrt{\frac{k_1}{\chi_A}}.$$

For the numerical experiment, we take the following material parameters

$$w = \frac{1}{2},\ k_1 = 2.3,\ k_2 = 1.5,\ k_3 = 4.8,\ \chi_A = 1.21, H = 9.5,$$

where k_i are scaled constants for PAA at 125 degrees Celsius [114, pg 123] and χ_A is the scaled constant for PAA at 122 degrees Celsius [114, pg 174]. The numerical parameters are

$$h = \tau = \frac{1}{32}, \quad \varepsilon = \frac{10^{-4}}{2}.$$

For the initial condition, we consider a perturbation of the equilibrium state:

$$\mathbf{n}_h^0 = I_h\left[\frac{\mathbf{e}_1+\mathbf{u}}{|\mathbf{e}_1+\mathbf{u}|}\right], \qquad \mathbf{u} = 256[x(1-x)y(1-y)]^2 z(.5-z)\mathbf{e}_3.$$

Here, $\|\mathbf{u}\|_{L^\infty(\Omega;\mathbb{R}^3)} \approx .03$. Figure 2.6 shows the initial and final configurations of the gradient flow. Note that Dirichlet boundary conditions were note imposed on the sides, so our use of the modified energy $\tilde{E}$ may not be entirely faithful to E. However we still see energy decrease in the gradient flow algorithm as evidenced by Figure 2.7.

The reason why an experimenter can measure k_1 using this experiment is that the competition between the magnetic energy and the elastic energy only happens in the splay term. Table 2.4 shows that the splay is the dominant part of the energy that increases.

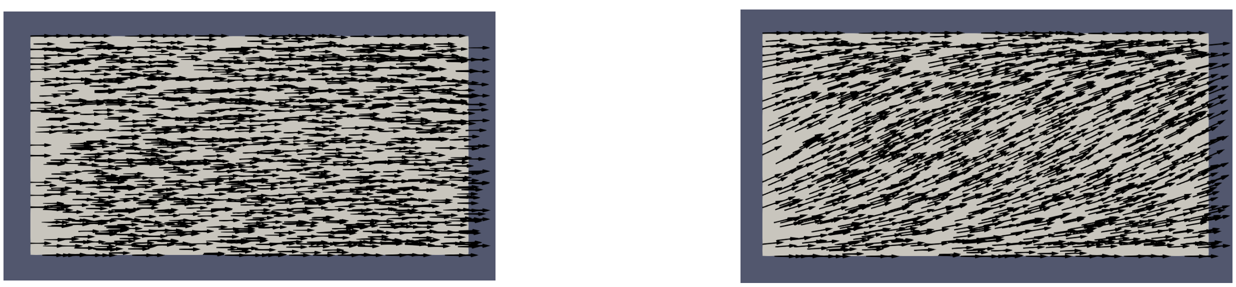

Figure 2.6: Initial and final configurations from Algorithm 1 and $k_1 = 2.3, k_2 = 1.5, k_3 = 4.8, \chi_A = 1.21, H = 9.5$.

	$\mathtt{splay}(\mathbf{n}_h)$	$\mathtt{twist}(\mathbf{n}_h)$	$\mathtt{bend}(\mathbf{n}_h)$
Initial	1.71e-03	5.15e-04	5.14e-04
Final	1.82	2.36e-02	8.06e-02

Table 2.4: Initial and final splay, twist, and bend for computed solution for the Fréedericksz transition experiment with $k_1 = 2.3, k_2 = 1.5, k_3 = 4.8, \chi_A = 1.21, H = 9.5$ and numerical parameters $h = \tau = \frac{1}{32}$, and $\varepsilon = \frac{10^{-4}}{2}$. Note the large increase in splay relative to bend and twist indicating that most of the increase in the elastic energy is due to splay.

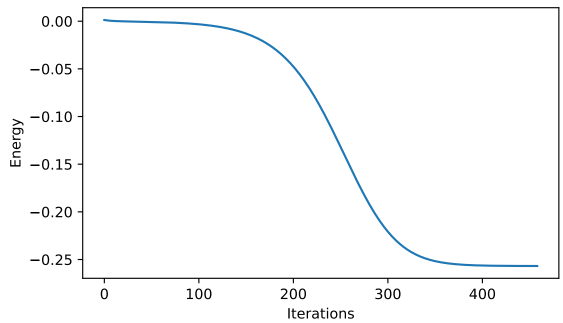

Figure 2.7: Energy decay for Fréedericksz transition experiment vs gradient flow iterations.

2.6.2.2 Magnetic effects and a colloid

This computational example reveals the influence of the magnetic field on a liquid crystal configuration around a colloid. One salient feature of computing with a colloid is the *inherent difficulty to mesh with weakly acute triangulations* due to the domain topology, and hence to realize projection methods that enforce energy decrease. This contrasts strikingly with the simplicity of the current projection-free approach. The setup is similar to what was done in [96]. The domain, boundary conditions, and magnetic field are

$$\Omega = [-2,2]^3 \setminus B_{3/4}(0), \quad \mathbf{g}(\mathbf{x}) = \begin{cases} \mathbf{x}/|\mathbf{x}|, & \mathbf{x} \in \partial B_{3/4}(0) \\ \mathbf{e}_3, & \mathbf{x} \in \partial[-2,2]^3 \end{cases}, \quad \mathbf{H} = H\mathbf{e}_2.$$

Here, $H = 0, 1, 2, 4$. Note that the magnetic field $\mathbf{H}$ is orthogonal to the outer boundary $\mathbf{g} = \mathbf{e}_3$. In this sense, this setup is similar to the Fréedericksz transition computed earlier. There is competition between matching the outer boundary condition and paying little elastic energy versus reducing the magnetic energy. The main difference with the Fréedericksz transition is twofold: first the Dirichlet boundary condition is enforced everywhere on $\partial\Omega$, and second the presence of the colloid. The numerical parameters are

$$h = \frac{1}{8}, \quad \tau = \frac{h}{4}, \quad \varepsilon = 10^{-4}$$

see Algorithm 1.

Figure 2.8 shows $\mathbf{n}_h^\infty$ with varying H. Note that for $H = 1, 2$, the computed minimizer looks quite similar to the $H = 0$ case. For $H = 4$, the computed $\mathbf{n}_h^\infty$ is nearly parallel to the magnetic field, except for near the boundary, where Dirichlet boundary conditions are imposed. We can see that $\mathbf{n}_h^\infty$ is nearly parallel to the magnetic field for $H = 4$ since the final energy is $E_{total}[\mathbf{n}_h^\infty] \approx -120$ while the final energies for $H = 0, 1, 2$ are approximately $28.4, 27.1, 18.9$ respectively. This suggests a transition similar to Fréederickz occurs where the magnetic field overcomes the elastic energy.

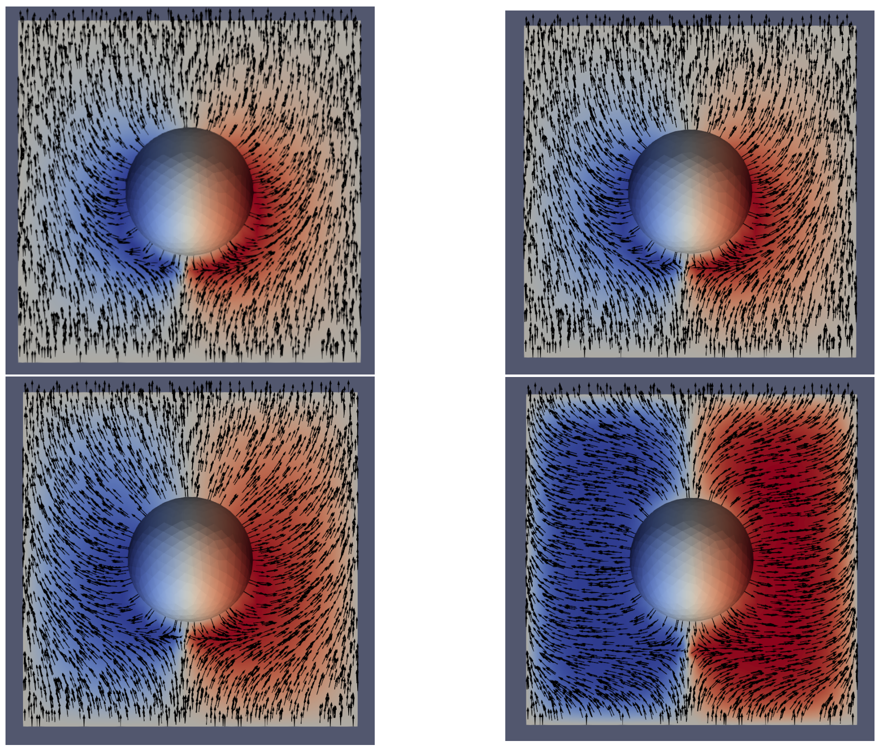

Figure 2.8: Influence of magnetic field on liquid crystal with colloid. Color is y component of $\mathbf{n}_h^\infty$ (Top left) $H = 0$, (Top right) $H = 1$, (Bottom left) $H = 2$, (Bottom right) $H = 4$. Note the large change in behavior from $H = 2$ to $H = 4$. The director field for $H = 2$ behaves more or less like $H = 0$. However for $H = 4$, the director field is almost totally parallel to $\mathbf{e}_2$ except near the boundary.

Chapter 3: Modeling of Thin Liquid Crystal Polymeric Networks

We recall from the discussion in Section 1.3 that the 3D body comprised of LCE/LCN in many applications [5, 42, 117] is thin relative to its length and width. As a result, it is advantageous to model such LCNs with dimensionally reduced models, which is the subject of this chapter. The scaling of thickness in models of thin $3D$ elastic bodies dictates the 2D models of LCNs/LCEs. If the energy is scaled linearly with the thickness, the resulting model is a membrane model: the energy is a function of the first fundamental form of the deformed surface and encodes stretching. Works that studied membrane models include [44, 54, 98]. For LCNs, the first fundamental form of zero stretching energy states satisfy a pointwise metric condition. Extensive work dedicated to examining configurations that satisfy this metric condition include [4, 91, 92, 93, 94, 100, 101, 103, 119]. For a review of these techniques, we refer to [118]. The second common scaling is a cubic scaling in the thickness, and results in a plate model driven by bending. The metric condition giving zero stretching energy becomes a constraint in the bending model. Some existing bending models include theory derived via formal asymptotics [98], a von Karman plate model derived in [90] using asymptotics, a rigorous Gamma convergence theory for a model of bilayer materials composed of LCEs and a classical isotropic elastic plate [22], or a plate model where the LC dramatically changes its orientation through the thickness [2]. Moreover, reduced $1D$ models for LCNs/LCEs have been explored as well; we refer to [21] for a rod model and to [3, 112] for ribbon models.

An outline and highlight of the contributions of this chapter are as follows.

- In Section 3.1, we present a derivation of a classical 3D elastic model of LCE, which was first derived by Bladon, Warner, and Terentjev [28]. The discussion follows discussions previously done in [121].

- In Section 3.2, we derive a 2D membrane model of LCN, prove numerous properties, and present a new technique for the construction of approximate configurations.

  - In Section 3.2.1, we derive a membrane model of LCN, following [98]. The key difference is that [98] assumes the midplane of the deformed surface is inextensible. This chapter drops this simplifying assumption by tuning the Kirchhoff-Love ansatz to conform to incompressibility in 3D.

  - In Section 3.2.2, motivated by [98], we derive the 2D membrane model from 3D rubber elasticity via an asymptotic analysis. We also connect W_{str} and W_{3D} with the notion of minimal energy extension which relates the model derived and a similar model in [47]. Moreover, we show that zero energy states of W_{str} satisfy a target metric condition. This metric condition is known throughout the physics literature and is typically derived for the $3D$ model [102], [121, Chapter 6.2].

  - We present a new formal construction of solutions for rotationally symmetric blueprinted director fields $\mathbf{m}$ with a defect of degree $n > 1$. Our technique hinges on the ideas of lifted surfaces (inspired by [101]), composition of defects and Taylor expansion.

- This chapter concludes by presenting a derivation of a bending model of LCN, following [98].

Again, we remove the simplifying inextensibility assumption in [98] by tuning the Kirchhoff-Love ansatz to conform to incompressibility in 3D.

3.1 3D elastic energy: neo-classical energy

3.1.1 Derivation of neo-classical energy

We begin with a derivation of the neo-classical energy density in (3.1) due to [28, 120, 121]. This initial discussion will follow discussion in [121].

We let $\mathcal{B} \subset \mathbb{R}^3$ be some 3 dimensional body and we consider $\mathbf{x} \in \mathcal{B}$. At $\mathbf{x}$, the polymer network is comprised of many strands as well as cross-links. Since the model we are considering is a continuum model, we consider many such strands in a small volume at $\mathbf{x}$. We first consider a set of vectors $\{\mathbf{r}^i\}_{i=1}^{n_s}$ to be comprised of end-to-end vectors of a strand at the point $\mathbf{x}$, and n_s denotes the number of strands per unit volume. Also, the current configuration of strands is obtained by $\mathbf{r}^i = \mathbf{F}\mathbf{r}^i_f$, where $\mathbf{F}$ is the deformation gradient, and $\mathbf{r}^i_f$ is the initial end-to-end vector that describes the crosslinks at the formation of the polymer network. Here, we assume the deformation gradient is incompressible and satisfies $\det \mathbf{F} = 1$. Additionally, we assume the initial strands are distributed normally as $\mathbf{r}_f \sim \mathcal{N}(\mathbf{0}, \mathbf{L_m})$, where $\mathbf{L_m}$ is a matrix of second moments determined by the initial LC director field $\mathbf{m}$, which is to be determined later. The entropic free energy at the point $\mathbf{x}$ is the sum of the entropic free energies of each strand

$$\mathcal{F} = \sum_{i=1}^{n_s} -k_b T \ln(N(\mathbf{r}^i))$$

where $N(\mathbf{r}^i)$ is the number of potential configurations the strand can take that results in the end-to-end vector $\mathbf{r}^i$, k_b is the Boltzmann constant, and T is the temperature. The number $N(\mathbf{r})$ is proportional to a Gaussian distribution whose second moments depends on the current liquid crystal orientation $\mathbf{n}$. In particular, we have that

$$N(\mathbf{r}) \propto (2\pi)^{-3/2}\det(\mathbf{L}_\mathbf{n}^{-1/2})\exp\left(-\frac{1}{2}\mathbf{r}^T\mathbf{L}_\mathbf{n}^{-1}\mathbf{r}\right),$$

where $\mathbf{L}_\mathbf{n}$ will be some symmetric positive definite matrix to be determined later. Inserting the normal distribution into the entropic free energy in place of $N(\mathbf{r})$ yields

$$\mathcal{F} = -k_b n_s T \ln\left((2\pi)^{-3/2}\det\mathbf{L}_\mathbf{n}^{-1/2}\right) + \sum_{i=1}^{n_s}\frac{k_bT}{2}(\mathbf{r}^i)^T\mathbf{L}_\mathbf{n}^{-1}\mathbf{r}^i.$$

We may drop the term $k_b n_s T \ln\left((2\pi)^{-3/2}\det\mathbf{L}_\mathbf{n}^{-1/2}\right)$ since it is a constant and will not impact minimizers of $\mathcal{F}$. The sum above can be well approximated by taking the average if n_s is large. Hence, we write

$$\mathcal{F} = \frac{k_bTn_s}{2}\int_{\mathbb{R}^3}\mathbf{w}^T\mathbf{L}_\mathbf{n}^{-1}\mathbf{w}\;d\mathbf{r}(\mathbf{w}),$$

where we are integrating with respect to the probability measure of the distribution of the $\mathbf{r}^i$'s. Recall $\mathbf{r}^i = \mathbf{F}\mathbf{r}_f^i$, so we apply a change of variables to the above integral to obtain

$$\begin{aligned}\mathcal{F} &= \frac{k_bTn_s}{2}\int_{\mathbb{R}^3}(\mathbf{F}\mathbf{v})^T\mathbf{L}_\mathbf{n}^{-1}(\mathbf{F}\mathbf{v})|\det\mathbf{F}|\;d\mathbf{r}_f(\mathbf{v})\\ &= \frac{k_bTn_s}{2}\int_{\mathbb{R}^3}(\mathbf{F}\mathbf{v})^T\mathbf{L}_\mathbf{n}^{-1}(\mathbf{F}\mathbf{v})(2\pi)^{-3/2}\det(\mathbf{L}_\mathbf{m}^{-1/2})\exp\left(-\frac{1}{2}\mathbf{v}^T\mathbf{L}_\mathbf{m}^{-1}\mathbf{v}\right)d\mathbf{v},\end{aligned}$$

where we used the assumption that $\mathbf{r}_f \sim \mathcal{N}(\mathbf{0}, \mathbf{L}_\mathbf{m})$, the formula for the probability density of $\mathcal{N}(0, \mathbf{L}_\mathbf{m})$, and the incompressibility assumption $\det\mathbf{F} = 1$.

Using the property that $\mathbf{a}^T\mathbf{b} = \text{tr}(\mathbf{a}\mathbf{b}^T)$, we may rewrite the integral as

$$\mathcal{F} = \frac{k_b T n_s}{2} \int_{\mathbb{R}^3} \text{tr}(\mathbf{F}^T \mathbf{L}_{\mathbf{n}}^{-1} \mathbf{F} \mathbf{v} \mathbf{v}^T)(2\pi)^{-3/2} \det(\mathbf{L}_{\mathbf{m}}^{-1/2}) \exp\left(-\frac{1}{2}\mathbf{v}^T \mathbf{L}_{\mathbf{m}}^{-1} \mathbf{v}\right) d\mathbf{v}.$$

Moving the integral inside the trace, noting that $\mathbf{F}^T \mathbf{L}_{\mathbf{n}}^{-1} \mathbf{F}$ is constant in terms of $\mathbf{v}$, we have

$$\mathcal{F} = \frac{k_b T n_s}{2} \text{tr}\left(\mathbf{F}^T \mathbf{L}_{\mathbf{n}}^{-1} \mathbf{F} \int_{\mathbb{R}^3} \mathbf{v}\mathbf{v}^T (2\pi)^{-3/2} \det(\mathbf{L}_{\mathbf{m}}^{-1/2}) \exp\left(-\frac{1}{2}\mathbf{v}^T \mathbf{L}_{\mathbf{m}}^{-1} \mathbf{v}\right) d\mathbf{v}\right).$$

Note that

$$\int_{\mathbb{R}^3} \mathbf{v}\mathbf{v}^T (2\pi)^{-3/2} \det(\mathbf{L}_{\mathbf{m}}^{-1/2}) \exp\left(-\frac{1}{2}\mathbf{v}^T \mathbf{L}_{\mathbf{m}}^{-1} \mathbf{v}\right) d\mathbf{v} = \mathbf{L}_{\mathbf{m}}$$

because $\mathbf{L}_{\mathbf{m}}$ is the second moments matrix of $\mathcal{N}(0, \mathbf{L}_{\mathbf{m}})$. Therefore, the energy becomes

$$\mathcal{F} = \frac{k_b T n_s}{2} \text{tr}(\mathbf{F}^T \mathbf{L}_{\mathbf{n}}^{-1} \mathbf{F} \mathbf{L}_{\mathbf{m}}).$$

Writing $\mu = k_b T n_s$ as the shear modulus, we have the neo-classical trace formula in (3.1) except for the form of $\mathbf{L}_{\mathbf{n}}, \mathbf{L}_{\mathbf{m}}$. Since, $\mathbf{L}_{\mathbf{m}}$ and $\mathbf{L}_{\mathbf{n}}$ are interpreted as second moments, we require that both tensors are symmetric positive definite. We also assume that the liquid crystal director fields $\mathbf{m}, \mathbf{n}$ are eigenvectors of $\mathbf{L}_{\mathbf{m}}$ and $\mathbf{L}_{\mathbf{n}}$ respectively. Finally, we assume that $\mathbf{L}_{\mathbf{m}}$ is uniaxial as in $\mathbf{L}_{\mathbf{m}}$ has two equal eigenvalues. We likewise assume $\mathbf{L}_{\mathbf{n}}$ is uniaxial. Combining these assumptions leads to $\mathbf{L}_{\mathbf{m}}$ and $\mathbf{L}_{\mathbf{n}}$ taking the form

$$\mathbf{L}_{\mathbf{m}} = a_0(\mathbf{I}_3 + s_0 \mathbf{m} \otimes \mathbf{m}), \quad \mathbf{L}_{\mathbf{n}} = a(\mathbf{I}_3 + s\mathbf{n} \otimes \mathbf{n})$$

where s_0, s describes the degree of orientation of the strands around $\mathbf{m}$ and $\mathbf{n}$ respectively. If $a, a_0 > 0$, then s, s_0 satisfy

$$s, s_0 > -1$$

to respect the positive definiteness assumption of $\mathbf{L_m}$ and $\mathbf{L_n}$. See also Section 3.1.3. Note that we do not see $\mathbf{L_n}$ in the energy but rather

$$\mathbf{L}_\mathbf{n}^{-1} = a^{-1}\left(\mathbf{I}_3 - \frac{s}{s+1}\mathbf{n}\otimes\mathbf{n}\right).$$

To have some intuition as to why we should expect to use $\mathbf{L}_\mathbf{n}^{-1}$, we consider a specific case. As $s \to \infty$, the strands become better aligned with $\mathbf{n}$. If an end-to-end vector $\mathbf{r}^i$ is parallel to $\mathbf{n}$, then there are many more potential strand configurations leading to $\mathbf{r}^i$. As a result the entropy increases and the entropic energy should decrease. One final remark is that a, a_0 only influence the energy by becoming multiplicative constants. Hence, for the rest of this chapter and dissertation, we shall set

$$a_0 = (s_0+1)^{-1/3}, \quad a = (s+1)^{-1/3}$$

so that $\det \mathbf{L_m} = \det \mathbf{L_n} = 1$.

3.1.2 3D elastic energy

To summarize, we have discussed the molecular basis for the neo-classical *trace formula* [28, 120, 121]. We shall now denote this energy density by

$$W_{3D}(\mathbf{x}, \mathbf{F}) := \frac{\mu}{2}\left[\operatorname{tr}\left(\mathbf{F}^T\mathbf{L}_\mathbf{n}^{-1}\mathbf{F}\mathbf{L_m}\right) - 3\right], \tag{3.1}$$

where $\mathbf{x} := (\mathbf{x}', x_3) := (x_1, x_2, x_3) \in \mathcal{B}$ is the space variable and $\mathbf{F} \in \mathbb{R}^{3\times 3}$ is the deformation gradient. Note that we are interested in thin films of LCNs, and mathematically slender materials are usually modeled as $3D$ hyper-elastic bodies $\mathcal{B} := \Omega \times (-t/2, t/2)$, with $\Omega \subset \mathbb{R}^2$ being a bounded Lipschitz domain and $t > 0$ being a small thickness parameter. We denote by $\mathbf{u} : \mathcal{B} \to \mathbb{R}^3$ the 3D deformation of the LCNs material, so that $\nabla \mathbf{u} = \mathbf{F}$. Since the shear modulus μ, is a multiplicative constant, we set $\mu = 2$ for the rest of this dissertation. The constant -3 was added to ensure that the energy density is nonnegative, we refer to Corollary 3.1 (nondegeneracy of W_{3D}) below.

We define $\mathbf{m} : \mathcal{B} \to \mathbb{S}^2$ the *blueprinted* nematic director field on the reference configuration. The director field $\mathbf{n} : \mathcal{B} \to \mathbb{S}^2$ is the director field on the deformed configuration, to be defined below, whereas

$$\mathbf{L}_{\mathbf{m}} := (s_0 + 1)^{-1/3}(\mathbf{I}_3 + s_0 \mathbf{m} \otimes \mathbf{m}) \tag{3.2}$$

is the reference step length tensor, and

$$\mathbf{L}_{\mathbf{n}} := (s + 1)^{-1/3}(\mathbf{I}_3 + s \mathbf{n} \otimes \mathbf{n}) \tag{3.3}$$

are the tensors recently discussed. Recall from the previous discussion, $s_0, s \in L^\infty(\Omega)$ are nematic order parameters that refer to the *reference* configuration and *deformed* configuration respectively. They are typically constant and depend on temperature, but may vary in Ω if the liquid crystal polymers are actuated non-uniformly. These parameters have a physical range

$$-1 < s_0, s \leq C < \infty. \tag{3.4}$$

We emphasize that the energy density $W_{3D}(\mathbf{x}, \mathbf{F})$ defined in (3.1) depends explicitly on coordinates $\mathbf{x}$, due to the dependence of $\mathbf{m}, \mathbf{n}, s, s_0$ on $\mathbf{x}$.

In the case where $s = s_0 = 0$, the step length tensors become $\mathbf{L}_\mathbf{m} = \mathbf{L}_\mathbf{n} = \mathbf{I}_3$, the identity matrix $\mathbf{I}_3 \in \mathbb{R}^{3\times 3}$, and the formula (3.1) reduces to the classical neo-Hookean energy density for rubber-like materials $W_{3D}(\mathbf{F}) = |\mathbf{F}|^2 - 3$. Recall, we have assumed that the material is incompressible, i.e,

$$\det \mathbf{F} = 1. \tag{3.5}$$

The density of crosslinks between the mesogens and polymer network differentiate LCNs (also called liquid crystal glasses) and liquid crystals elastomers (LCEs): the former has moderate to dense crosslinks, while in the latter the density of crosslinks is low [122]. In this chapter, we focus on LCNs and leave a study of LCEs for future research. Mathematically, the strong coupling in LCNs is reflected in terms of director fields via a *kinematic constraint* [98]:

$$\mathbf{n} := \frac{\mathbf{F}\mathbf{m}}{|\mathbf{F}\mathbf{m}|}. \tag{3.6}$$

This implies that, in contrast to LCEs [22, 121], $\mathbf{n}$ is *not* a free variable for models of LCNs; in fact it is also called frozen director [47]. For LCEs the energy density may be minimized over $\mathbf{n}$ first and next over $\mathbf{F}$, like in [44, 52], or a Frank elastic energy for $\mathbf{n}$ may be introduced (c.f. [12, 22, 87]). Moreover, we note that a director field description may not be the only choice for modeling LC components. One can also formulate a model with Q-tensor descriptions like in [41].

Using the energy density (3.1), the 3D elastic energy is given by

$$E_{3D,t}[\mathbf{u}] = \int_{-t/2}^{t/2} \int_{\Omega} W_{3D}(\mathbf{x}, \nabla \mathbf{u}) \, d\mathbf{x}' dx_3, \tag{3.7}$$

where $\mathbf{x}' \in \Omega$, $x_3 \in (-t/2, t/2)$, subject to incompressibility and kinematic constraints $\det \nabla \mathbf{u} = 1$ and $\mathbf{n} = \frac{\nabla \mathbf{u}\, \mathbf{m}}{|\nabla \mathbf{u}\, \mathbf{m}|}$.

3.1.3 Properties of 3D elastic energy

This subsection is dedicated to proving some properties of the 3D elastic energy (3.1), which will be useful later.

In view of definition (3.2) and (3.3) for step length tensors, we first observe that $\mathbf{L_m}$ can be equivalently expressed as follows in the orthonormal basis $\{\mathbf{m}, \mathbf{w}_1, \mathbf{w}_2\}$:

$$\mathbf{L_m} = (s_0 + 1)^{2/3} \mathbf{m} \otimes \mathbf{m} + (s_0 + 1)^{-1/3} \mathbf{w}_1 \otimes \mathbf{w}_1 + (s_0 + 1)^{-1/3} \mathbf{w}_2 \otimes \mathbf{w}_2, \tag{3.8}$$

where $(\mathbf{w}_1, \mathbf{w}_2)$ are orthonormal vectors spanning the space orthogonal to $\mathbf{m}$. Likewise $\mathbf{L_n}$ may be expressed in the basis $\{\mathbf{n}, \mathbf{v}_1, \mathbf{v}_2\}$ for orthonormal vectors $(\mathbf{v}_1, \mathbf{v}_2)$ spanning the space orthogonal to $\mathbf{n}$:

$$\mathbf{L_n} = (s + 1)^{2/3} \mathbf{n} \otimes \mathbf{n} + (s + 1)^{-1/3} \mathbf{v}_1 \otimes \mathbf{v}_1 + (s + 1)^{-1/3} \mathbf{v}_2 \otimes \mathbf{v}_2. \tag{3.9}$$

The assumptions (3.4) together with $s_0, s \in L^\infty(\Omega)$ imply that the eigenvalues of $\mathbf{L_m}$ and $\mathbf{L_n}$ are bounded away from 0 and ∞, and $\mathbf{L_m}, \mathbf{L_n}$ are thus invertible. Moreover, the dyadic representation

(3.9) provides an explicit inverse for $\mathbf{L_n}$

$$\mathbf{L_n}^{-1} = (s+1)^{-2/3}\mathbf{n}\otimes\mathbf{n} + (s+1)^{1/3}\mathbf{v}_1\otimes\mathbf{v}_1 + (s+1)^{1/3}\mathbf{v}_2\otimes\mathbf{v}_2\,,$$

or equivalently

$$\mathbf{L_n}^{-1} = (s+1)^{1/3}\left(\mathbf{I}_3 - \frac{s}{s+1}\mathbf{n}\otimes\mathbf{n}\right). \tag{3.10}$$

Since both $\mathbf{L_m}$ and $\mathbf{L_n}^{-1}$ are symmetric positive definite, the energy density in (3.1) can be rewritten as a neo-Hookean energy density:

$$W_{3D}\big((\mathbf{x},z),\mathbf{F}\big) = \left|\mathbf{L_n}^{-1/2}\mathbf{F}\mathbf{L_m}^{1/2}\right|^2 - 3. \tag{3.11}$$

We stress the importance of (3.11) because it is critical for the energy scaling argument in Proposition 4.3. To see the non-negativity of (3.11), we first observe that a basic linear algebra argument exploiting eigenvalues of $\mathbf{F}^T\mathbf{F}$ yields $W_{3D}^H(\mathbf{F}) = |\mathbf{F}|^2 - 3 \geq 0$ provided $\det\mathbf{F} = 1$. Consequently, since $\det\mathbf{L}_m = \det\mathbf{L}_n^{-1} = 1$ according to (3.8) and (3.10), the constraint $\det\mathbf{F} = 1$ implies that (3.11) is non-negative.

More precisely, $W_{3D}^H(\mathbf{F})$ is non-degenerate in the sense that it is bounded from below by $\mathrm{dist}(\mathbf{F}, SO(3))^2 := \inf_{\mathbf{R}\in SO(3)} |\mathbf{F}-\mathbf{R}|^2$. We now state and prove lower and upper bounds for $W_{3D}^H(\mathbf{F})$. The former can also be found in [102, Proposition A.3]. The latter will be used in the numerical analysis in Lemma 4.1.

Proposition 3.1 (bounds for $W_{3D}^H(\mathbf{F})$). *Let* $\mathbf{F}\in\mathbb{R}^{3\times3}$ *satisfy* $\det\mathbf{F} = 1$. *Then,*

$$\mathrm{dist}\big(\mathbf{F}, SO(3)\big)^2 \leq |\mathbf{F}|^2 - 3 \leq 3\,\mathrm{dist}\big(\mathbf{F}, SO(3)\big)^2\,. \tag{3.12}$$

Proof. Let $\mathbf{F} \in \mathbb{R}^{3\times 3}$ be such that $\det \mathbf{F} = 1$. We first use the polar decomposition, $\mathbf{F} = \mathbf{R}\mathbf{U}$ for $\mathbf{U}$ symmetric positive definite (SPD) and $\mathbf{R} \in SO(3)$, to write $|\mathbf{F}|^2 - 3 = |\mathbf{R}\mathbf{U}|^2 - 3 = |\mathbf{U}|^2 - 3$, and $\mathrm{dist}(\mathbf{R}\mathbf{U}, SO(3))^2 = \mathrm{dist}(\mathbf{U}, SO(3))^2$.

1. *Lower bound*: It is thus sufficient to prove

$$|\mathbf{U}|^2 - 3 \geq \mathrm{dist}(\mathbf{U}, SO(3))^2.$$

Since $\mathbf{U}$ is SPD there exists $\mathbf{Q} \in SO(3)$ such that $\mathbf{U} = \mathbf{Q}^T \mathbf{\Lambda} \mathbf{Q}$ with $\mathbf{\Lambda}$ a diagonal matrix with the eigenvalues $\lambda_1, \lambda_2, \lambda_3 > 0$ of $\mathbf{U}$. Moreover, $\det \mathbf{U} = 1$ yields $\lambda_3 = \frac{1}{\lambda_1 \lambda_2}$, and $|\mathbf{U}| = |\mathbf{\Lambda}|$ implies

$$|\mathbf{U}|^2 - 3 = \lambda_1^2 + \lambda_2^2 + \frac{1}{\lambda_1^2 \lambda_2^2} - 3.$$

On the other hand, $\mathrm{dist}(\mathbf{U}, SO(3)) = |\mathbf{U} - \mathbf{I}_3|$ because $|\mathbf{U} - \mathbf{R}| = |\mathbf{\Lambda} - \mathbf{Q}\mathbf{R}\mathbf{Q}^T|$ with $\mathbf{R} \in SO(3)$ is minimized by $\mathbf{Q}\mathbf{R}\mathbf{Q}^T = I_3$, whence $\mathbf{R} = I_3$. Consequently,

$$\begin{aligned}
\mathrm{dist}(\mathbf{U}, SO(3))^2 &= (\lambda_1 - 1)^2 + (\lambda_2 - 1)^2 + \left(\frac{1}{\lambda_1 \lambda_2} - 1\right)^2 && (3.13)\\
&= \lambda_1^2 + \lambda_2^2 + \frac{1}{\lambda_1^2 \lambda_2^2} - 2\left(\lambda_1 + \lambda_2 + \frac{1}{\lambda_1 \lambda_2}\right) + 3\\
&= \lambda_1^2 + \lambda_2^2 + \frac{1}{\lambda_1^2 \lambda_2^2} - 3 + 2\left(3 - \lambda_1 - \lambda_2 - \frac{1}{\lambda_1 \lambda_2}\right)\\
&= |\mathbf{U}|^2 - 3 + 2\left(3 - \lambda_1 - \lambda_2 - \frac{1}{\lambda_1 \lambda_2}\right). && (3.14)
\end{aligned}$$

A basic calculus argument gives $\sup_{\lambda_1, \lambda_2 > 0} \left(3 - \lambda_1 - \lambda_2 - \frac{1}{\lambda_1 \lambda_2}\right) \leq 0$, whence

$$\mathrm{dist}(\mathbf{U}, SO(3))^2 \leq |\mathbf{U}|^2 - 3,$$

and the lower bound is proved.

2. *Upper bound*: In view of (3.13) and (3.14) it suffices to prove

$$(\lambda_1 - 1)^2 + (\lambda_2 - 1)^2 + \left(\frac{1}{\lambda_1\lambda_2} - 1\right)^2 \geq \lambda_1 + \lambda_2 + \frac{1}{\lambda_1\lambda_2} - 3.$$

Without loss of generality, let us assume $\lambda_3 = \frac{1}{\lambda_1\lambda_2} \geq 1$ and write

$$\lambda_1 + \lambda_2 + \frac{1}{\lambda_1\lambda_2} - 3 = \Big(\frac{1}{\lambda_1\lambda_2} - 1\Big) - \Big(1 - \lambda_1\lambda_2\Big) + \lambda_1 + \lambda_2 - \lambda_1\lambda_2 - 1.$$

The first two terms satisfy the following relation

$$\Big(\frac{1}{\lambda_1\lambda_2} - 1\Big) - \Big(1 - \lambda_1\lambda_2\Big) = \lambda_1\lambda_2\Big(\frac{1}{\lambda_1\lambda_2} - 1\Big)^2 \leq \Big(\frac{1}{\lambda_1\lambda_2} - 1\Big)^2$$

because $\lambda_1\lambda_2 \leq 1$. The remaining terms, instead, obey the relation

$$\lambda_1 + \lambda_2 - \lambda_1\lambda_2 - 1 = -(\lambda_1 - 1)(\lambda_2 - 1) \leq (\lambda_1 - 1)^2 + (\lambda_2 - 1)^2$$

by virtue of Young's inequality. This proves the desired upper bound. □

An immediate consequence of Proposition 3.1 (bounds on $W_{3D}^H(\mathbf{F})$) is that the 3D energy density is nondegenerate and thereby nonnegative.

Corollary 3.1 (nondegeneracy of W_{3D})**.** *Let* $\mathbf{x} \in \mathcal{B}$*. If* $\mathbf{F} \in \mathbb{R}^{3\times 3}$ *satisfies* $\det \mathbf{F} = 1$*, then*

$$W_{3D}(\mathbf{x}, \mathbf{F}) \geq \operatorname{dist}(\mathbf{L}_\mathbf{n}^{-1/2}\mathbf{F}\mathbf{L}_\mathbf{m}^{1/2}, SO(3))^2. \tag{3.15}$$

Proof. Recall that by (3.8) and (3.10), $\det(\mathbf{L}_{\mathbf{n}}^{-1/2}\mathbf{F}\mathbf{L}_{\mathbf{m}}^{1/2}) = 1$ is valid. Applying Proposition 3.1 with the form (3.11) yields (3.15). □

3.2 Membrane model of liquid crystals polymer networks

In this section, we introduce a formal asymptotic derivation of a membrane model of LCNs, discuss properties of the model related to its global minimizers, and present a technique for formal construction of solution profiles with defects.

We assume the $3D$ director field $\mathbf{m} : \mathcal{B} \to \mathbb{S}^2$ is planar and it depends only on $\mathbf{x}'$, and therefore, with a slight abuse of notations, we define $\mathbf{m} : \Omega \to \mathbb{S}^1$ to be the $2D$ *blueprinted* director field. We denote by $\mathbf{y} : \Omega \to \mathbb{R}^3$ the 3D deformation of the 2D midplane Ω.

The $2D$ membrane model is the following formal minimization problem: find $\mathbf{y}^* \in H^1(\Omega;\mathbb{R}^3)$ that solves

$$\mathbf{y}^* \in \operatorname{argmin}_{\mathbf{y}\in H^1(\Omega;\mathbb{R}^3)} E_{str}[\mathbf{y}], \quad E_{str}[\mathbf{y}] := \int_\Omega W_{str}(\mathbf{x}', \nabla\mathbf{y}) d\mathbf{x}', \tag{3.16}$$

where W_{str} is a stretching energy density that is only a function of $\mathbf{x}' \in \Omega$ and the first fundamental form $\mathrm{I}[\mathbf{y}] = \nabla\mathbf{y}^T\nabla\mathbf{y}$. It is defined as

$$W_{str}(\mathbf{x}', \nabla\mathbf{y}) := \lambda\left[\frac{1}{J[\mathbf{y}]} + \frac{1}{s+1}\left(\mathrm{tr}(\mathrm{I}[\mathbf{y}]) + s_0 C_{\mathbf{m}}[\mathbf{y}] + s\frac{J[\mathbf{y}]}{C_{\mathbf{m}}[\mathbf{y}]}\right)\right] - 3, \tag{3.17}$$

where the *actuation parameter* $\lambda : \Omega \to \mathbb{R}^+$ is given and well-defined by

$$\lambda = \lambda_{s,s_0} := \sqrt[3]{\frac{s+1}{s_0+1}}, \tag{3.18}$$

because $s, s_0 > -1$. If the material is heated, then $\lambda < 1$, whereas if it is cooled, then $\lambda > 1$. Moreover, $J[\mathbf{y}], C_{\mathbf{m}}[\mathbf{y}]$ are among the following abbreviations:

$$J[\mathbf{y}] = \det \mathrm{I}[\mathbf{y}], \quad C_{\mathbf{m}}[\mathbf{y}] = \mathbf{m} \cdot \mathrm{I}[\mathbf{y}]\mathbf{m}, \quad C_{\mathbf{m}_\perp}[\mathbf{y}] = \mathbf{m}_\perp \cdot \mathrm{I}[\mathbf{y}]\mathbf{m}_\perp. \tag{3.19}$$

We employ a similar notation when the second argument of W_{str} is $\mathbf{F} \in \mathbb{R}^{3\times 2}$

$$\begin{aligned} \mathrm{I}(\mathbf{F}) := \mathbf{F}^T\mathbf{F}, \quad J(\mathbf{F}) := \det \mathrm{I}(\mathbf{F}), \\ C_{\mathbf{m}}(\mathbf{F}) := \mathbf{m} \cdot \mathrm{I}(\mathbf{F})\mathbf{m}, \quad C_{\mathbf{m}_\perp}(\mathbf{F}) := \mathbf{m}_\perp \cdot \mathrm{I}(\mathbf{F})\mathbf{m}_\perp. \end{aligned} \tag{3.20}$$

We stress that at this stage is not clear that (3.16) is well posed; hence the expression "formal minimization problem".

3.2.1 Derivation of stretching energy from asymptotics

This section is dedicated to deriving a 2D stretching or membrane energy from (3.7) via formal asymptotics as the thickness t goes to zero. In particular, we shall derive the formal limit $E_{str} = \lim_{t\to 0} \frac{1}{t} E_{3D}[\mathbf{u}]$. This procedure will follow closely the derivation of [98], but we will relax the simplifying assumption $\det \mathrm{I}[\mathbf{y}] = 1$ made in [98]. We also contrast the asymptotic method presented here with the more analytical method presented in [47]. The connection between the two will be explored in Section 3.2.2.1.

3.2.1.1 Kirchhoff-Love assumption and overview of strategy

We assume that the 3D deformation $\mathbf{u} : \mathcal{B} := \Omega \times (-t/2, t/2) \to \mathbb{R}^3$ takes the form

$$\mathbf{u}(\mathbf{x}', x_3) = \mathbf{y}(\mathbf{x}') + \phi(\mathbf{x}', x_3)\, \boldsymbol{\nu}(\mathbf{x}') \tag{3.21}$$

where $\mathbf{y} : \Omega \to \mathbb{R}^3$ is the reduced deformation and $\boldsymbol{\nu} : \Omega \to \mathbb{R}^3$ is the normal to the deformed midplane $\mathbf{y}(\Omega)$. We posit that ϕ takes the form:

$$\phi(\mathbf{x}', x_3) = \alpha(\mathbf{x}')x_3 + \mathcal{O}(x_3^2), \tag{3.22}$$

which is a modified *Kirchhoff-Love assumption*. The higher order terms would be useful for deriving the bending energy, but we do not need them for the stretching energy. Note that α is undetermined for the moment. Later, α will be chosen so that $\mathbf{u}$ is incompressible in an asymptotic sense, i.e. $\det \nabla\mathbf{u}(\mathbf{x}', x_3) = 1 + \mathcal{O}(x_3)$.

The goal of asymptotics is to write the energy $W_{3D}(\mathbf{x}, \nabla\mathbf{u})$ given in (3.1) for the deformation $\mathbf{u}$ in terms of powers of t and the reduced stretching energy $W_{str}(\mathbf{x}', \nabla'\mathbf{y})$

$$\int_{-t/2}^{t/2} \int_\Omega W_{3D}(\mathbf{x}, \nabla\mathbf{u})\, d\mathbf{x}' dx_3 = t \int_\Omega W_{str}(\mathbf{x}', \nabla'\mathbf{y})\, d\mathbf{x}' + \mathcal{O}(t^3), \tag{3.23}$$

where $\nabla' := (\partial_1, \partial_2)$ denotes the gradient with respect to $\mathbf{x}'$. The stretching energy W_{str} in (3.23) gives the leading order effects of the energy as the body thickness t vanishes in the sense that formally

$$\lim_{t\to 0} \frac{1}{t} \int_{-t/2}^{t/2} \int_\Omega W_{3D}(\mathbf{x}, \nabla\mathbf{u})\, d\mathbf{x}' dx_3 = \int_\Omega W_{str}(\mathbf{x}', \nabla'\mathbf{y})\, d\mathbf{x}'.$$

The third order term in (3.23) corresponds to the bending energy W_{ben} and will be examined later in Section 3.4. Combined with the modified Kirchhoff-Love assumption (3.21), the process to derive the stretching energy is as follows:

1. Write the Cauchy tensor $\mathbf{C} = \mathbf{F}^T\mathbf{F}$ in terms of leading order terms.

2. Write W_{3D} in terms of $\mathbf{C}$ and powers of x_3.

3. Collect $\mathcal{O}(1)$ terms of W_{3D} which contribute to the stretching energy.

4. Determine α so that $\mathbf{u}$ satisfies incompressibility in an asymptotic sense.

3.2.1.2 Cauchy tensor

Substituting (3.21) into $\mathbf{C} := \nabla\mathbf{u}^T\nabla\mathbf{u}$ yields

$$\mathbf{C} = \nabla\mathbf{u}^T\nabla\mathbf{u} = \begin{bmatrix} \mathbf{C}_\phi & \mathbf{C}_{1\times 2}^T \\ \mathbf{C}_{1\times 2} & \mathbf{C}_{1\times 1} \end{bmatrix}, \tag{3.24}$$

where

$$\mathbf{C}_\phi = \nabla'\mathbf{y}^T\nabla'\mathbf{y} + \phi(\nabla'\boldsymbol{\nu}^T\nabla'\mathbf{y} + \nabla'\mathbf{y}^T\nabla'\boldsymbol{\nu}) + \phi^2\nabla'\boldsymbol{\nu}^T\nabla'\boldsymbol{\nu} + \nabla'\phi\otimes\nabla'\phi \tag{3.25}$$

$$\mathbf{C}_{1\times 2} = (\boldsymbol{\nu}\otimes\nabla'\phi)^T\partial_3\phi\boldsymbol{\nu} = \partial_3\phi\nabla'\phi \tag{3.26}$$

$$\mathbf{C}_{1\times 1} = (\partial_3\phi)^2. \tag{3.27}$$

Here, we have used the facts that $\nabla'\mathbf{y}^T\boldsymbol{\nu} = 0$, $\nabla'\boldsymbol{\nu}^T\boldsymbol{\nu} = 0$ and $|\boldsymbol{\nu}| = 1$. Since $\nabla'\phi(\mathbf{x}', x_3) = \nabla'\alpha x_3 + \mathcal{O}(x_3^2)$ and $\partial_3\phi(\mathbf{x}', x_3) = \alpha + \mathcal{O}(x_3)$, we have $C_{1\times 2} = \mathcal{O}(x_3)$, and hence we may drop

$C_{1\times 2}$ as a higher order term.

Also ignoring any terms higher than constant order, we have

$$\mathbf{C}_\phi = \mathrm{I}[\mathbf{y}] + \mathcal{O}(x_3),$$

where $\mathrm{I}[\mathbf{y}] = \nabla'\mathbf{y}^T\nabla'\mathbf{y}$ is the first fundamental form of $\mathbf{y}$. Since

$$\big(\partial_3\phi(\mathbf{x}', x_3)\big)^2 = \alpha(\mathbf{x}')^2 + \mathcal{O}(x_3),$$

we find

$$\mathbf{C} = \begin{bmatrix} \mathrm{I}[\mathbf{y}] & 0 \\ 0 & \alpha(\mathbf{x}')^2 \end{bmatrix} + \mathcal{O}(x_3). \tag{3.28}$$

3.2.1.3 Expanding W_{3D}

Recall that we assume that the $3D$ blueprinted director field $\mathbf{m}$ *lies in the plane* i.e.

$$\mathbf{m}(\mathbf{x}) = (\widetilde{\mathbf{m}}(\mathbf{x}'), 0)^T. \tag{3.29}$$

First, substituting the kinematic constraint (3.6) into (3.1) with $\mathbf{F} = \nabla\mathbf{u}$ and using the explicit expressions (3.8) for $\mathbf{L_m}$ and (3.10) for $\mathbf{L_n^{-1}}$, we obtain

$$W_{3D}(\mathbf{x}', \nabla\mathbf{u}) = \lambda\Big(\operatorname{tr}\mathbf{C} + \frac{s_0}{s+1}\mathbf{m}\cdot\mathbf{C}\mathbf{m} - \frac{s}{s+1}\frac{\mathbf{m}\cdot\mathbf{C}^2\mathbf{m}}{\mathbf{m}\cdot\mathbf{C}\mathbf{m}}\Big) - 3, \tag{3.30}$$

where λ is defined in (3.18), and we notice that from now on W_{3D} depends on $\mathbf{x}'$ instead of $\mathbf{x}$, due to the assumption (3.29). Then plugging the asymptotic form (3.28) of $\mathbf{C}$ into (3.30) and using (3.29), the energy density $W_{3D}(\mathbf{x}', \nabla\mathbf{u})$ becomes

$$\begin{aligned} &W_{3D}(\mathbf{x}', \nabla\mathbf{u}) \\ &\quad = \lambda\left[\operatorname{tr}\mathrm{I}[\mathbf{y}] + \alpha(\mathbf{x}')^2 + \frac{s_0}{s+1}\widetilde{\mathbf{m}}\cdot\mathrm{I}[\mathbf{y}]\widetilde{\mathbf{m}} - \frac{s}{s+1}\frac{\widetilde{\mathbf{m}}\cdot\mathrm{I}[\mathbf{y}]^2\widetilde{\mathbf{m}}}{\widetilde{\mathbf{m}}\cdot\mathrm{I}[\mathbf{y}]\widetilde{\mathbf{m}}}\right] - 3 + \mathcal{O}(x_3). \end{aligned}$$

Since $\mathrm{I}[\mathbf{y}]$ is a 2×2 matrix, the Cayley-Hamilton Theorem gives

$$\mathrm{I}[\mathbf{y}]^2 = \big(\operatorname{tr}\mathrm{I}[\mathbf{y}]\big)\,\mathrm{I}[\mathbf{y}] - \det\mathrm{I}[\mathbf{y}]\,I_2,$$

so that the energy now reads

$$\begin{aligned} &W_{3D}(\mathbf{x}', \nabla\mathbf{u}) \\ &\quad = \lambda\left[\alpha(\mathbf{x}')^2 + \frac{1}{s+1}\left(\operatorname{tr}\mathrm{I}[\mathbf{y}] + s_0\widetilde{\mathbf{m}}\cdot\mathrm{I}[\mathbf{y}]\widetilde{\mathbf{m}} + s\frac{\det\mathrm{I}[\mathbf{y}]}{\widetilde{\mathbf{m}}\cdot\mathrm{I}[\mathbf{y}]\widetilde{\mathbf{m}}}\right)\right] - 3 + \mathcal{O}(x_3). \end{aligned}$$

We now have all the constant order terms of $W_{3D}(\mathbf{x}', \nabla\mathbf{u})$. The only remaining task is to determine $\alpha(\mathbf{x}')$. We do this next.

3.2.1.4 Incompressibility

Since we would like $\mathbf{u}$ to satisfy incompressibility $\det\nabla\mathbf{u} = 1+\mathcal{O}(x_3)$, we impose $\det\mathbf{C} = 1 + \mathcal{O}(x_3)$. By (3.28), we see that

$$\det\mathbf{C} = \det\mathrm{I}[\mathbf{y}]\,\alpha(\mathbf{x}')^2 + \mathcal{O}(x_3), \tag{3.31}$$

whence

$$\alpha(\mathbf{x}') = \frac{1}{\sqrt{\det \mathrm{I}[\mathbf{y}]}} \tag{3.32}$$

gives us the desired equality $\det \mathbf{C} = 1 + \mathcal{O}(x_3)$ in view of (3.21) and (3.22). This further implies

$$\nabla \mathbf{u} = [\nabla' \mathbf{y}, (\det \mathrm{I}[\mathbf{y}])^{-1/2} \boldsymbol{\nu}] + \mathcal{O}(x_3). \tag{3.33}$$

3.2.1.5 Stretching energy

For convenience of presentation, from now on we slightly abuse notation and drop the prime for ∇' and tilde for $\widetilde{\mathbf{m}}$. Therefore, we will denote

$$\mathbf{m} = \widetilde{\mathbf{m}} \in \mathbb{R}^2, \quad \mathbf{m} = (\widetilde{\mathbf{m}}, 0)^T \in \mathbb{R}^3 \tag{3.34}$$

depending on whether we regard $\mathbf{m}$ as a vector in $\mathbb{R}^2$ or $\mathbb{R}^3$. We conclude that, with the steps built in Sections 3.2.1.1-3.2.1.4, we finally derive the stretching energy in (3.17), namely

$$\int_\Omega \lambda \left[\frac{1}{J[\mathbf{y}]} + \frac{1}{s+1} \left(\mathrm{tr}(\mathrm{I}[\mathbf{y}]) + s_0 C_{\mathbf{m}}[\mathbf{y}] + s \frac{J[\mathbf{y}]}{C_{\mathbf{m}}[\mathbf{y}]} \right) \right] - 3 \, d\mathbf{x}'.$$

3.2.1.6 Comparison with inextensibility constrained stretching energy

If we assume $\det \mathrm{I}[\mathbf{y}] = 1$, then the stretching energy density (3.16) reduces to that of [98, Eq. (14)]. However, the stretching energy density (3.16) is slightly more physical. In particular, relaxing the inextensibility constraint means that minimizers of E_{str} produce a Kirchhoff-Love ansatz that has lower 3D energy compared with minimizers subject to the inextensibility constraint $\det \mathrm{I}[\mathbf{y}] = 1$.

We shall see from Corollary 3.4 (immersions of g are minimizers with vanishing energy) below that $E_{str}[\mathbf{y}] = 0$ and $\mathbf{y}$ is a global minimizer to E_{str} if and only if

$$\mathrm{I}[\mathbf{y}] = \lambda^2 \mathbf{m} \otimes \mathbf{m} + \lambda^{-1} \mathbf{m}_\perp \otimes \mathbf{m}_\perp.$$

Suppose $\mathbf{y}$ satisfies the above metric condition. Combining the above metric condition with the Kirchhoff Love assumption from (3.21), we have that

$$\mathbf{u}(\mathbf{x}', x_3) = \mathbf{y}(\mathbf{x}') + \frac{x_3}{\sqrt{\lambda}} \boldsymbol{\nu}(\mathbf{x}'), \tag{3.35}$$

whose Cauchy tensor is

$$\mathbf{C} = \nabla \mathbf{u}^T \nabla \mathbf{u} = \begin{pmatrix} \mathrm{I}[\mathbf{y}] & \mathcal{O}(x_3) \\ \mathcal{O}(x_3) & \lambda^{-1} \end{pmatrix}.$$

Inserting $\mathbf{C}$ into the 3D energy density (3.30) we obtain,

$$W_{3D}(\mathbf{x}, \nabla \mathbf{u}) = 0.$$

We now enforce the inextensibility assumption $\det \mathrm{I}[\mathbf{y}] = 1$. Suppose $\mathbf{F} \in \mathbb{R}^{3\times 2}$ minimizes $W_{str}(\mathbf{x}', \cdot)$ subject to the constraint $\det \mathbf{F}^T\mathbf{F} = 1$. Using standard calculus techniques, one can show that

$$\mathbf{F}^T\mathbf{F} = \sqrt{\frac{s+1}{s_0+1}} \mathbf{m} \otimes \mathbf{m} + \sqrt{\frac{s_0+1}{s+1}} \mathbf{m}_\perp \otimes \mathbf{m}_\perp =: \tilde{\mathbf{G}},$$

which is a target metric condition derived in [98, Eq (17)]. Now suppose $\tilde{\mathbf{y}} : \Omega \to \mathbb{R}^3$ satisfies the metric condition $\mathrm{I}[\tilde{\mathbf{y}}] = \tilde{\mathbf{G}}$ pointwise. Combining the above metric condition with the Kirchhoff Love assumption from (3.21), we have that

$$\tilde{\mathbf{u}}(\mathbf{x}', x_3) = \tilde{\mathbf{y}}(\mathbf{x}') + x_3 \tilde{\boldsymbol{\nu}}(\mathbf{x}'),$$

whose Cauchy tensor is

$$\tilde{\mathbf{C}} = \nabla \tilde{\mathbf{u}}^T \nabla \tilde{\mathbf{u}} = \begin{pmatrix} \tilde{\mathbf{G}} & 0 \\ 0 & 1 \end{pmatrix}.$$

Defining $\tilde{\lambda} = \sqrt{\frac{s+1}{s_0+1}}$ and inserting $\tilde{\mathbf{C}}$ into the 3D energy density (3.30) we obtain,

$$W_{3D}(\mathbf{x}, \nabla \tilde{\mathbf{u}}) = \lambda \left(\left(\frac{s_0+1}{s+1} \right) \tilde{\lambda} + \tilde{\lambda}^{-1} + 1 \right) - 3.$$

We then using the relation $\tilde{\lambda} = \lambda^{3/2}$ to compute

$$W_{3D}(\mathbf{x}, \nabla \tilde{\mathbf{u}}) = 2\lambda^{-1/2} + \lambda - 3.$$

If $\lambda \neq 1$, there is actuation of the LCN, and

$$W_{3D}(\mathbf{x}, \nabla \tilde{\mathbf{u}}) = 2\lambda^{-1/2} + \lambda - 3 > 0 = W_{3D}(\mathbf{x}, \nabla \mathbf{u}),$$

where $\mathbf{u}$ was given by (3.35). What this example shows is that when there is actuation of the LCN, configurations with $E_{str}[\mathbf{y}] = 0$ always have lower 3D energy than configurations that minimize $E_{str}[\mathbf{y}]$ subject to the inextensibility constraint $\det \mathrm{I}[\mathbf{y}] = 1$.

3.2.2 Properties of Stretching Energy

3.2.2.1 Minimal energy extension.

In this section we show that the stretching energy density (3.17) is the minimal energy extension of the 3D energy (3.1). The proof is similar to that of [44, Lemma 5.3] and is related to how [47] derives the model.

Proposition 3.2 (minimal energy extension)**.** *Let* $\mathbf{F} \in \mathbb{R}^{3\times 2}$ *have rank 2. The following equality between* W_{str} *defined in* (3.17) *and* W_{3D} *given in* (3.1) *is valid*

$$W_{str}(\mathbf{x}', \mathbf{F}) = \inf_{\mathbf{b}\in\mathbb{R}^3:\det[\mathbf{F},\ \mathbf{b}]=1} W_{3D}(\mathbf{x}', [\mathbf{F},\ \mathbf{b}])\,. \tag{3.36}$$

Moreover, the unique minimizer $\mathbf{b}$ *is*

$$\frac{\mathbf{F}_1 \times \mathbf{F}_2}{|\mathbf{F}_1 \times \mathbf{F}_2|^2} =: \operatorname{argmin}_{\mathbf{b}\in\mathbb{R}^3:\det[\mathbf{F},\ \mathbf{b}]=1} W_{3D}(\mathbf{x}', [\mathbf{F},\ \mathbf{b}]), \tag{3.37}$$

where $\mathbf{F}_1, \mathbf{F}_2$ *are columns of* $\mathbf{F}$.

Proof. The incompressibility constraint reads $\det[\mathbf{F}, \mathbf{b}] = \mathbf{b}^T(\mathbf{F}_1 \times \mathbf{F}_2) = 1$. Using (3.30) and (3.34) to determine $W_{3D}(\mathbf{x}', [\mathbf{F}, \mathbf{b}])$ for $\mathbf{b} \in \mathbb{R}^3$ yields

$$W_{3D}(\mathbf{x}', [\mathbf{F}, \mathbf{b}]) = \lambda\Big(\operatorname{tr}\mathrm{I}(\mathbf{F}) + |\mathbf{b}|^2 + \frac{s_0}{s+1}C_{\mathbf{m}}(\mathbf{F}) - \frac{s}{s+1}\frac{|\mathrm{I}(\mathbf{F})\mathbf{m}|^2 + (\mathbf{b}\cdot\mathbf{F}\mathbf{m})^2}{C_{\mathbf{m}}(\mathbf{F})}\Big) - 3.$$

If we append the term $\mu\big(\mathbf{b}^T(\mathbf{F}_1 \times \mathbf{F}_2) - 1\big)$ to $W_{3D}(\mathbf{x}', [\mathbf{F}, \mathbf{b}])$, with Lagrange multiplier μ, we see that $\mathbf{b}$ and μ solve the following saddle point system

$$\begin{pmatrix} 2\lambda\Big(\mathbf{I}_3 - \frac{s}{(s+1)C_{\mathbf{m}}(\mathbf{F})}\mathbf{Fm}\otimes\mathbf{Fm}\Big) & \mathbf{F}_1\times\mathbf{F}_2 \\ (\mathbf{F}_1\times\mathbf{F}_2)^T & 0 \end{pmatrix}\begin{pmatrix}\mathbf{b}\\ \mu\end{pmatrix} = \begin{pmatrix}0\\1\end{pmatrix},$$

whose unique solution is $\mathbf{b} = (\mathbf{F}_1\times\mathbf{F}_2)/|\mathbf{F}_1\times\mathbf{F}_2|^2$ and $\mu = -\frac{2\lambda}{|\mathbf{F}_1\times\mathbf{F}_2|^2}$. Note that the uniqueness of $\mathbf{b}$ follows from the invertibility of the upper-left 3×3 block matrix, which follows from the fact that $\frac{s}{s+1} < 1$. Since $|\mathbf{F}_1\times\mathbf{F}_2|^2 = \det \mathrm{I}(\mathbf{F}) = J(\mathbf{F})$, substituting the minimizing $\mathbf{b}$ into the 3D energy yields

$$W_{3D}\big(\mathbf{x}', [\mathbf{F},\mathbf{b}]\big) = \lambda\Big(\operatorname{tr}\mathrm{I}(\mathbf{F}) + \frac{1}{J(\mathbf{F})} + \frac{s_0}{s+1}C_{\mathbf{m}}(\mathbf{F}) - \frac{s}{s+1}\frac{|\mathrm{I}(\mathbf{F})\mathbf{m}|^2}{C_{\mathbf{m}}(\mathbf{F})}\Big) - 3. \tag{3.38}$$

Applying the Cayley Hamilton Theorem for a 2×2 matrix $\mathbf{A}$, namely $\mathbf{A}^2 - \operatorname{tr}(\mathbf{A})\mathbf{A} + (\det\mathbf{A})\mathbf{I}_2 = \mathbf{0}$, to the last term inside bracket on the RHS of (3.38) yields

$$\frac{|\mathrm{I}(\mathbf{F})\mathbf{m}|^2}{C_{\mathbf{m}}(\mathbf{F})} = \frac{\mathbf{m}\cdot\mathrm{I}(\mathbf{F})^2\mathbf{m}}{C_{\mathbf{m}}(\mathbf{F})} = \operatorname{tr}\mathrm{I}(\mathbf{F}) - \frac{J(\mathbf{F})}{C_{\mathbf{m}}(\mathbf{F})}. \tag{3.39}$$

We then insert (3.39) into the RHS of (3.38) to obtain

$$W_{3D}\big(\mathbf{x}', [\mathbf{F},\mathbf{b}]\big) = \lambda\Big(\frac{1}{J(\mathbf{F})} + \frac{1}{s+1}\Big[\operatorname{tr}\mathrm{I}(\mathbf{F}) + s_0 C_{\mathbf{m}}(\mathbf{F}) + s\frac{J(\mathbf{F})}{C_{\mathbf{m}}(\mathbf{F})}\Big]\Big) - 3 = W_{str}(\mathbf{x}', \mathbf{F}),$$

which is the desired equality. □

Remark 3.1 (asymptotics vs minimal energy extension)**.** If $\mathbf{F} = \nabla\mathbf{y}$, then the minimizing $\mathbf{b}$ in

Proposition 3.2 (minimal energy extension) is

$$\mathbf{b} = \frac{\boldsymbol{\nu}}{\sqrt{\det I[\mathbf{y}]}}.$$

This corroborates that the asymptotic expression (3.33) gives the correct extension. However, this formula for $\mathbf{b}$ relies on the fact that $\mathbf{m}$ is planar; see (3.34). If $\mathbf{m}$ were not planar, then the formula for $\mathbf{b}$ would be more complicated: we refer to [102].

An immediate consequence of the above result and the neo-Hookean form of the 3D energy in (3.11) is that the stretching energy also has a neo-Hookean structure. We will exploit this structure in the numerical analysis in Section 4.3

Corollary 3.2 (neo-Hookean form of the stretching energy)**.** *Let* $\mathbf{F} \in \mathbb{R}^{3\times 2}$ *have rank 2,* $\mathbf{b} = \frac{\mathbf{F}_1 \times \mathbf{F}_2}{|\mathbf{F}_1 \times \mathbf{F}_2|^2}$*, and* $\mathbf{n} = \frac{\mathbf{F}\mathbf{m}}{|\mathbf{F}\mathbf{m}|}$*. Then* $\det[\mathbf{F},\ \mathbf{b}] = 1$ *and* $W_{str}(\mathbf{x}', \mathbf{F})$ *satisfies*

$$W_{str}(\mathbf{x}', \mathbf{F}) = \left|\mathbf{L}_{\mathbf{n}}^{-1/2}[\mathbf{F},\ \mathbf{b}]\mathbf{L}_{\mathbf{m}}^{1/2}\right|^2 - 3. \tag{3.40}$$

The next corollary is an easy consequence of Proposition 3.2 (minimal energy extension of W_{3D}) and Corollary 3.1 (nondegeneracy of W_{3D}).

Corollary 3.3 (nondegeneracy of W_{str})**.** *The stretching energy* $W_{str}(\mathbf{x}', \mathbf{F})$ *satisfies*

$$W_{str}\big(\mathbf{x}', \mathbf{F}\big) \geq \operatorname{dist}\big(\mathbf{L}_{\mathbf{n}}^{-1/2}[\mathbf{F},\ \mathbf{b}]\mathbf{L}_{\mathbf{m}}^{1/2}, SO(3)\big)^2 \geq 0 \tag{3.41}$$

for all $\mathbf{F} \in \mathbb{R}^{3\times 2}$ *such that* $\operatorname{rank}(\mathbf{F}) = 2$ *and* $\mathbf{b} = \frac{\mathbf{F}_1 \times \mathbf{F}_2}{|\mathbf{F}_1 \times \mathbf{F}_2|^2}$.

Proof. Combine Proposition 3.2 and Corollary 3.1 (nondegeneracy of W_{3D}). □

Remark 3.2 (special rotations)**.** An important by-product of Corollary 3.3 is that any solution $\mathbf{y} \in H^1(\Omega; \mathbb{R}^3)$ of $E_{str}[\mathbf{y}] = 0$ must satisfy the pointwise relation

$$\mathbf{L}_{\mathbf{n}}^{-1/2}[\nabla \mathbf{y},\ \mathbf{b}]\mathbf{L}_{\mathbf{m}}^{1/2} \in SO(3)$$

a.e. in Ω where $\mathbf{b} = \frac{\partial_1 \mathbf{y} \times \partial_2 \mathbf{y}}{|\partial_1 \mathbf{y} \times \partial_2 \mathbf{y}|^2}$ is a scaled normal. This observation will turn out to be useful later in the proof of Proposition 3.3 and Proposition 4.3.

3.2.2.2 Global minimizers and target metrics.

In this section, we characterize global minimizers of (3.16). We show that minimizing the stretching energy density W_{str} is equivalent to satisfying the target metric constraint pointwise. We point to [102, Appendix A] for a similar result, but for a related 3 dimensional model.

Proposition 3.3 (target metric)**.** *The stretching energy density* $W_{str}(\mathbf{x}', \mathbf{F}) = 0$ *vanishes at* $\mathbf{F} \in \mathbb{R}^{3\times 2}$ *if and only if* $\mathrm{I}(\mathbf{F}) = g$ *where* $g \in \mathbb{R}^{2\times 2}$ *is given by*

$$g = \lambda^2 \mathbf{m} \otimes \mathbf{m} + \lambda^{-1} \mathbf{m}_\perp \otimes \mathbf{m}_\perp, \tag{3.42}$$

λ *is defined in* (3.18) *and* $\mathbf{m}_\perp : \Omega \to \mathbb{S}^1$ *is perpendicular to* $\mathbf{m}$.

Proof. First suppose that $\mathrm{I}(\mathbf{F}) = g$. Inserting (3.42) into (3.17) gives

$$\begin{aligned}
W_{str}(\mathbf{x}', \mathbf{F}) &= \lambda\left(\frac{1}{\det g} + \frac{1}{s+1}\left(\mathrm{tr} g + s_0 \mathbf{m}\cdot g\mathbf{m} + s\frac{\det g}{\mathbf{m}\cdot g\mathbf{m}}\right)\right) - 3 \\
&= \lambda\left(\lambda^{-1} + \frac{1}{s+1}\left(\lambda^2 + \lambda^{-1} + s_0\lambda^2 + s\lambda^{-1}\right)\right) - 3 \\
&= \lambda\left(\lambda^{-1} + \frac{1}{s+1}\left((s_0+1)\lambda^2 + (s+1)\lambda^{-1}\right)\right) - 3 \\
&= \lambda\left(2\lambda^{-1} + \frac{s_0+1}{s+1}\lambda^2\right) - 3.
\end{aligned}$$

Note that $\frac{s_0+1}{s+1} = \lambda^{-3}$ according (3.18), whence

$$W_{str}(\mathbf{x}', \mathbf{F}) = \lambda\left(2\lambda^{-1} + \lambda^{-3}\lambda^2\right) - 3 = 0.$$

Now suppose that $W_{str}(\mathbf{x}', \mathbf{F}) = 0$. Corollary 3.3 (nondegeneracy of W_{str}) guarantees

$$0 = W_{str}(\mathbf{x}', \mathbf{F}) \geq \mathrm{dist}(\mathbf{L}_{\mathbf{n}}^{-1/2}[\mathbf{F},\ \mathbf{b}]\mathbf{L}_{\mathbf{m}}^{1/2}, SO(3))^2 \geq 0,$$

for $\mathbf{b} = \frac{\mathbf{F}_1\times\mathbf{F}_2}{|\mathbf{F}_1\times\mathbf{F}_2|^2}$. This implies there is a rotation $\mathbf{R} \in SO(3)$ such that

$$\mathbf{L}_{\mathbf{n}}^{-1/2}[\mathbf{F},\ \mathbf{b}]\mathbf{L}_{\mathbf{m}}^{1/2} = \mathbf{R}.$$

Multiplying both sides by $\mathbf{R}^T$ yields

$$\mathbf{L}_{\mathbf{m}}^{1/2}[\mathbf{F},\ \mathbf{b}]^T\mathbf{L}_{\mathbf{n}}^{-1}[\mathbf{F},\ \mathbf{b}]\mathbf{L}_{\mathbf{m}}^{1/2} = \mathbf{I}_3.$$

We shall now perform some algebraic operations to determine what $\mathrm{I}(\mathbf{F}) = \mathbf{F}^T\mathbf{F}$ should satisfy. First, multiplying on the left and right by $\mathbf{L}_{\mathbf{m}}^{-1/2}$ gives

$$[\mathbf{F},\ \mathbf{b}]^T\mathbf{L}_{\mathbf{n}}^{-1}[\mathbf{F},\ \mathbf{b}] = \mathbf{L}_{\mathbf{m}}^{-1}.$$

The definitions (3.2) and (3.3) of $\mathbf{L}_{\mathbf{m}}$ and $\mathbf{L}_{\mathbf{n}}$, with $\mathbf{m} \in \mathbb{R}^3$ given by (3.34), imply

$$\mathbf{L}_{\mathbf{m}}^{-1} = (s_0+1)^{1/3}\Big(\mathbf{I}_3 - \frac{s_0}{s_0+1}\mathbf{m}\otimes\mathbf{m}\Big), \quad \mathbf{L}_{\mathbf{n}}^{-1} = (s+1)^{1/3}\Big(\mathbf{I}_3 - \frac{s}{s+1}\mathbf{n}\otimes\mathbf{n}\Big),$$

and combined with the kinematic constraint $\mathbf{n} = \frac{\mathbf{Fm}}{|\mathbf{Fm}|}$, this further yields

$$\begin{aligned}\mathbf{L}_{\mathbf{m}}^{-1} = [\mathbf{F},\ \mathbf{b}]^T\mathbf{L}_{\mathbf{n}}^{-1}[\mathbf{F},\ \mathbf{b}] = (s+1)^{1/3} &\begin{pmatrix} \mathrm{I}(\mathbf{F}) & 0 \\ 0 & \frac{1}{J(\mathbf{F})} \end{pmatrix} \\ &- \frac{s}{(s+1)^{2/3}C_{\mathbf{m}}(\mathbf{F})}\begin{pmatrix} \mathrm{I}(\mathbf{F})\mathbf{m}\otimes\mathrm{I}(\mathbf{F})\mathbf{m} & 0 \\ 0 & 0\end{pmatrix}.\end{aligned} \tag{3.43}$$

We express $\mathrm{I}(\mathbf{F})$ in terms of the orthonormal basis $\mathbf{m}, \mathbf{m}_\perp \in \mathbb{R}^2$ and scalars a_1, a_2, a_3

$$\mathrm{I}(\mathbf{F}) = a_1\mathbf{m}\otimes\mathbf{m} + a_2\mathbf{m}_\perp\otimes\mathbf{m}_\perp + a_3(\mathbf{m}_\perp\otimes\mathbf{m} + \mathbf{m}\otimes\mathbf{m}_\perp).$$

We may do this because $\{\mathbf{m}\otimes\mathbf{m}, \mathbf{m}_\perp\otimes\mathbf{m}_\perp, \mathbf{e}_3\otimes\mathbf{e}_3\}$ is the basis of the 3 dimensional space of symmetric 2×2 matrices. We also extend $\mathbf{m}$ to $\mathbb{R}^3$, according to (3.34), and represent $\mathbf{L}_{\mathbf{m}}^{-1}$ on the orthonormal basis $(\mathbf{m}, 0)^T, (\mathbf{m}_\perp, 0)^T, \mathbf{e}_3$ of $\mathbb{R}^3$. We next compare the upper-left 2×2 blocks of the matrix representations of the left and right-hand sides of (3.43) to obtain

$$\begin{pmatrix} (s_0+1)^{-2/3} & 0 \\ 0 & (s_0+1)^{1/3} \end{pmatrix} = (s+1)^{1/3}\begin{pmatrix} a_1 & a_3 \\ a_3 & a_2 \end{pmatrix} - \frac{s}{(s+1)^{2/3}}\begin{pmatrix} a_1 & a_3 \\ a_3 & a_3^2/a_1 \end{pmatrix}.$$

By matching entries, a_3 must vanish and $(s+1)^{1/3}a_2 = (s_0+1)^{1/3}$, which entails that $a_2 = \left(\frac{s_0+1}{s+1}\right)^{1/3} = \lambda^{-1}$. Finally,

$$(s_0+1)^{-2/3} = \big((s+1)^{1/3} - s(s+1)^{-2/3}\big)a_1 = (s+1)^{-2/3}a_1,$$

whence $a_1 = \left(\frac{s+1}{s_0+1}\right)^{2/3} = \lambda^2$. Therefore, we get

$$\mathrm{I}(\mathbf{F}) = \lambda^2\mathbf{m}\otimes\mathbf{m} + \lambda^{-1}\mathbf{m}_\perp\otimes\mathbf{m}_\perp = g,$$

which is the desired expression of $\mathrm{I}(\mathbf{F})$. □

A direct consequence of the characterization of the target metric is that H^1 isometric immersions of g are minimizers to the stretching energy.

Corollary 3.4 (immersions of g are minimizers with vanishing energy)**.** *Let* $\mathbf{y} \in H^1(\Omega;\mathbb{R}^3)$ *be a deformation. Then* $\mathbf{y}$ *satisfies*

$$\mathrm{I}[\mathbf{y}] = g \text{ a.e. in } \Omega, \tag{3.44}$$

i.e., $\mathbf{y}$ *is an* isometric immersion *of the metric* g *defined in* (3.42)*, if and only if* $\mathbf{y}$ *is a global minimizer to* (3.16) *with* $E_{str}[\mathbf{y}] = 0$.

Therefore, the solvability of (3.16) is related to the long standing open problem in differential geometry of existence of isometric immersions in $\mathbb{R}^3$ for a general metric $g : \Omega \to \mathbb{R}^{2\times 2}$. Smooth isometric immersions in $\mathbb{R}^3$ are known to exist for certain metrics with positive or negative curvatures, while there are also examples of metrics that have no C^2 isometric immersions; we refer to the book [69] for discussions and further references. Corollary 3.4 requires the minimal regularity $\mathbf{y} \in H^1(\Omega; \mathbb{R}^3)$, but we further assume the existence of an H^2 isometric immersion to prove convergence of our FEM with regularization (4.12) in Section 4.3. The existence of either H^1 or H^2 isometric immersions seems to be an open question, to the best of our knowledge. Finally, it is conceivable that g is not immersible and yet there is a global minimizer $\mathbf{y}$ of (3.16) with $E_{str}[\mathbf{y}] > 0$; this justifies the requirement $E_{str}[\mathbf{y}] = 0$ in Corollary 3.4. We explore this matter computationally in Section 5.4. Therefore, if there exists an H^1 isometric immersion of g, a pure geometric fact unrelated to LCN, global minimizers of $E_{str}[\mathbf{y}]$ over $H^1(\Omega; \mathbb{R}^3)$ are guaranteed to exist; otherwise, $E_{str}[\mathbf{y}]$ may not vanish over $H^1(\Omega; \mathbb{R}^3)$. On the other hand, minimizers of $E_{str}[\mathbf{y}]$ might not be unique, because g could have many isometric immersions in general. From another point of view, this issue is also related to lack of convexity and is discussed in Section 4.1.1.

3.3 Asymptotic profiles of defects

We now construct asymptotic profiles for blueprinted director fields $\mathbf{m}$ with defects of several degrees. We are not aware of studies of shapes beyond the Gauss curvature obtained in [92] for higher degree defects. Our approximate solutions provide insight on the complicated shapes that can be programmed upon actuation. We reproduce these profiles computationally later in Section 5.1.

3.3.1 Lifted surfaces

Lifted surfaces for LCNs/LCEs are originally introduced in [102]. We adapt the idea to the reduced model (3.16) in this subsection. To this end, we consider the following parameterization of lifted surfaces

$$\mathbf{y}^l(\mathbf{x}') = \big(\alpha\mathbf{x}', \phi(\alpha\mathbf{x}')\big)^T \quad \forall\mathbf{x}' \in \Omega, \tag{3.45}$$

where $\alpha \in \mathbb{R}$ will be determined later. Here, $\phi : \alpha\Omega \to \mathbb{R}$ represents the graph of the lifted surfaces. Our goal is to match the metric g in (3.42) with $\mathrm{I}[\mathbf{y}^l]$, i.e,

$$\mathrm{I}[\mathbf{y}^l] = g = \lambda^2\mathbf{m}\otimes\mathbf{m} + \lambda^{-1}\mathbf{m}_\perp \otimes \mathbf{m}_\perp = (\lambda^2 - \lambda^{-1})\mathbf{m}\otimes\mathbf{m} + \lambda^{-1}\mathbf{I}_2. \tag{3.46}$$

Since (3.45) yields

$$\mathrm{I}[\mathbf{y}^l] = \alpha^2\nabla\phi(\alpha\mathbf{x}') \otimes \nabla\phi(\alpha\mathbf{x}') + \alpha^2\mathbf{I}_2, \tag{3.47}$$

(3.46) is valid if ϕ satisfies $|\nabla\phi| = \sqrt{\lambda^3 - 1}$ a.e. in Ω, and $\alpha = \lambda^{-1/2}$, with the properties that $\lambda > 1$ and λ is *constant* over Ω. Substituting them into (3.45) gives

$$\mathbf{y}^l(\mathbf{x}') = \Big(\mathbf{x}'_\lambda, \phi(\mathbf{x}'_\lambda)\Big)^T, \quad \mathbf{x}'_\lambda := \lambda^{-1/2}\mathbf{x}'. \tag{3.48}$$

Since this deformation is an isometric immersion of the metric (3.42), it is also an equilibrium configuration provided $\mathbf{m}(\mathbf{x}') = \pm(\lambda^3-1)^{-1/2}\nabla\phi(\mathbf{x}'_\lambda)$ according to Corollary 3.4. We observe that the discussion so far has restricted $\lambda > 1$, which means the LCN is being cooled. If $\lambda < 1$

and ϕ satisfies $\pm\sqrt{\lambda^{-3}-1}\nabla\phi(\lambda\mathbf{x}') = \mathbf{m}_\perp(\mathbf{x}')$, then a lifted surface of the form

$$\mathbf{y}^l(\mathbf{x}') = \Big(\lambda\mathbf{x}', \phi(\lambda\mathbf{x}')\Big)^T, \tag{3.49}$$

satisfies $\mathrm{I}[\mathbf{y}^l] = g$. Since a lifted surface may be constructed for $\lambda < 1$ in a similar fashion as for $\lambda > 1$, we restrict the remaining discussion of this section to $\lambda > 1$. However, we note that the computations in Section 5.1 typically set $\lambda < 1$.

3.3.2 Surfaces for defects of degree 1 and $1/2$

To set the stage, we first go over known lifted surfaces that arise from degree 1 and degree 1/2 defects. These solutions will match the metric g exactly, and will help us later in constructing approximate solutions for higher order defects in Sections 3.3.5 and 3.3.6.

A director field $\mathbf{m}_1$ with a *defect of degree* 1 reads

$$\mathbf{m}_1(\mathbf{x}') = \frac{\mathbf{x}'}{|\mathbf{x}'|}. \tag{3.50}$$

If $\mathbf{R}_1$ is a rotation of $\pm\pi/2$, the corresponding exact solution $\mathbf{y}_1$ for $\mathbf{R}_1\mathbf{m}_1$ reads

$$\mathbf{y}_1(\mathbf{x}') = \Big(\mathbf{x}'_\lambda, \phi_1(\mathbf{x}'_\lambda)\Big)^T \tag{3.51}$$

where

$$\phi_1(\mathbf{x}') = \sqrt{\lambda^3-1}\,(1-|\mathbf{x}'|); \tag{3.52}$$

$\mathbf{y}_1$ is a *cone* with vertex at the origin as long as $\lambda > 1$ [91]. If $\lambda < 1$, then the cone solution in (3.52) is no longer well defined. In fact, the director field $\mathbf{m}_1$ in (3.50) will produce what is known as an *anticone* configuration [91]. The solution for a degree 1 defect will be a cone or anti-cone depending on the angle α_r between $\mathbf{m}_1$ and $\mathbf{x}'$ as well as λ [94]. See Fig. 3.1 for the cone and anti-cone shapes computed by our algorithm.

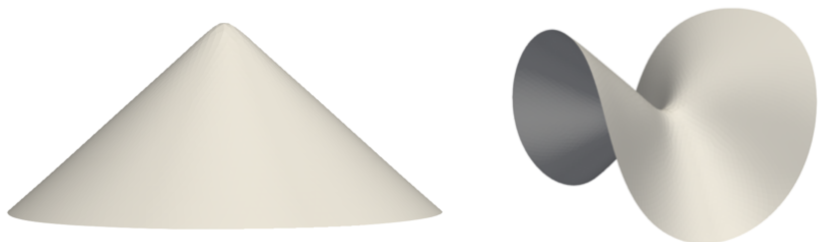

Figure 3.1: Computed solution with the blueprinted director field $\mathbf{m}_1$ that has degree 1 defect, $\lambda < 1$ and $\alpha_r = 0$ (right), $\pi/2$ (left). The left configuration is a cone, and the right configuration is an anticone. We refer to Section 5.1 for details of these numerical simulations.

Next, we introduce a solution induced by a director field with a *degree* $1/2$ *defect*, which will help us construct an approximate solution for a degree $3/2$ defect in Section 3.3.6. Motivated by [92], we consider the director field

$$\mathbf{m}_{1/2}(\mathbf{x}') = \begin{cases} \text{sign}(x_2)\mathbf{e}_2, & x_1 \geq 0 \\ \frac{\mathbf{x}'}{|\mathbf{x}'|}, & x_1 < 0\,, \end{cases} \tag{3.53}$$

and note that $\mathbf{m}_\perp \otimes \mathbf{m}_\perp$ is the typical line field for a defect of degree $1/2$ at the origin. Since $\mathbf{m}_{1/2}(\mathbf{x}') = \mathbf{m}_1(\mathbf{x}')$ when $x_1 < 0$, we expect a cone configuration forming in the left half-plane. For $\lambda > 1$, an exact solution is given by the lifted surface configuration

$$\mathbf{y}_{1/2}(\mathbf{x}') = \Big(\mathbf{x}'_\lambda, \phi_{1/2}(\mathbf{x}'_\lambda)\Big)^T, \tag{3.54}$$

where

$$\phi_{1/2}(\mathbf{x}') = \begin{cases} \sqrt{\lambda^3 - 1}\,(1 - |x_2|), & x_1 \geq 0 \\ \sqrt{\lambda^3 - 1}\,(1 - |\mathbf{x}'|), & x_1 < 0 \end{cases}. \tag{3.55}$$

This entails stretching in the direction $\mathbf{m}_{1/2}$ and shrinking in the perpendicular direction $\mathbf{m}_{1/2}^{\perp}$, which in turn explains the shape of $\mathbf{y}_{1/2}$ in Fig. 3.2 for $x_1 > 0$. We see that when $x_1 < 0$, the map $\mathbf{y}_{1/2}$ coincides with the cone in (3.51). We plot $\mathbf{m}_{1/2}$ (left), $\mathbf{y}_{1/2}$ (middle) and our computed solution (right) in Fig.3.2.

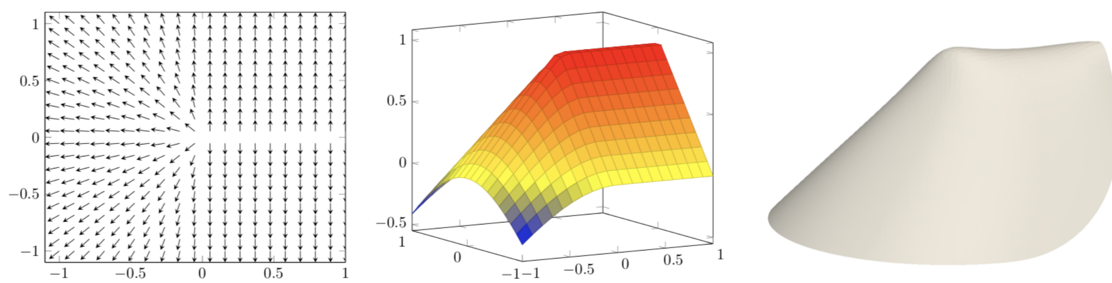

Figure 3.2: Director field $\mathbf{m}_{1/2}$ from (3.53) (left), lifted surface $\mathbf{y}_{1/2}$ from (3.54)-(3.55) for $\lambda = 2^{1/3}$ (middle), and computed solution in a unit disc domain with $\mathbf{m} = \mathbf{m}_{1/2}$ and a Dirichlet boundary condition that is compatible with (3.54)-(3.55) (right). Note that the gradient of $\phi_{1/2}$ is parallel to $\mathbf{m}_{1/2}$ whereas $\mathbf{m}_{1/2}^{\perp}$ is the typical director field for a $1/2$ defect.

3.3.3 Higher degree defects: main idea and idealized construction

We now consider rotationally symmetric blueprinted director fields $\mathbf{m}_n$ with defects of integer degree $n > 1$. Such director fields are given in polar coordinates by

$$\mathbf{m}_n(r, \theta) = \big(\cos(n\theta), \sin(n\theta)\big). \tag{3.56}$$

We observe that the line field $\mathbf{m}_n \otimes \mathbf{m}_n$ in (3.46) exhibits a discontinuity at the origin. We denote by g_n the metric generated by $\mathbf{m}_n$ and arbitrary λ via (3.42). Ideally, the goal is to build on the solution (3.51) for $n = 1$ and composition of defects to obtain a solution $\mathbf{y}_n$ with degree n defect. The main idea is as follows.

We exploit the relation to the complex-valued function $f_n(z) = e^{in\arg(z)}$ to write

$$\mathbf{m}_n(\mathbf{x}') = p^{-1}\big(f_n(p(\mathbf{x}'))\big),$$

where $z = |z|e^{i\arg(z)}$ for any $z \in \mathbb{C}$ and $p : \mathbb{R}^2 \to \mathbb{C}$ is the map $p(\mathbf{x}') = x_1 + ix_2$. From this perspective, we can write a director field with degree n defect as the multiplication or composition of two director fields with degree 1 and $n-1$ defects

$$e^{in\mathrm{arg}(z)} = e^{i\mathrm{arg}(z)}e^{i(n-1)\mathrm{arg}(z)}.$$

If $\mathbf{m}_1 := (\mu_1, \mu_2)$ and $\mathbf{m}_{n-1} := (\xi_1, \xi_2)$, then $\mu_1 + i\mu_2 = e^{i\arg(p(\mathbf{m}_1))}$ and $\xi_1 + i\xi_2 = e^{i\arg(p(\mathbf{m}_{n-1}))}$ imply

$$e^{i\arg(p(\mathbf{m}_n))} = (\mu_1 + i\mu_2)(\xi_1 + i\xi_2) = (\mu_1\xi_1 - \mu_2\xi_2) + i(\mu_1\xi_2 + \mu_2\xi_1).$$

Applying p^{-1} to both sides yields

$$\mathbf{m}_n = \begin{pmatrix} \mu_1 & -\mu_2 \\ \mu_2 & \mu_1 \end{pmatrix} \begin{pmatrix} \xi_1 \\ \xi_2 \end{pmatrix} = \mathbf{R}_1\mathbf{m}_{n-1}, \tag{3.57}$$

where $\mathbf{R}_1 := \big(\mathbf{m}_1, \mathbf{m}_1^{\perp}\big)$ is a rotation matrix that depends on $\mathbf{x}'$. In view of (3.46) we may write the metric g_n at $\mathbf{x}'$ as

$$g_n = (\lambda^2 - \lambda^{-1})\mathbf{R}_1\big(\mathbf{m}_{n-1} \otimes \mathbf{m}_{n-1}\big)\mathbf{R}_1^T + \lambda^{-1}\mathbf{I}_2. \tag{3.58}$$

Assuming $\lambda > 1$, we compare (3.58) with the metric that arises from function composition of two defects of degree 1 and $n-1$. With $\mathbf{x}'_\lambda = \lambda^{-1/2}\mathbf{x}'$ already defined in (3.48), we consider the following modified lifted surface

$$\mathbf{y}_n(\mathbf{x}') := \Big(\mathbf{x}'_\lambda, \phi_n\big(\mathbf{v}(\mathbf{x}'_\lambda)\big)\Big)^T. \tag{3.59}$$

Compared to either (3.51) or (3.54) of Section 3.3.1, we now compose ϕ_n with an unknown function $\mathbf{v} : \lambda^{-1/2}\Omega \to \lambda^{-1/2}\Omega$. We then apply the chain rule to determine

$$\mathrm{I}[\mathbf{y}_n(\mathbf{x}')] = \lambda^{-1}\mathbf{I}_2 + \lambda^{-1}\nabla\mathbf{v}(\mathbf{x}'_\lambda)^T\big(\nabla\phi_n(\mathbf{v}(\mathbf{x}'_\lambda)) \otimes \nabla\phi_n(\mathbf{v}(\mathbf{x}'_\lambda))\big)\nabla\mathbf{v}(\mathbf{x}'_\lambda). \tag{3.60}$$

To match (3.58) an ideal construction would be to find ϕ_n and $\mathbf{v}$ so that

$$\nabla\phi_n(\mathbf{v}(\mathbf{x}'_\lambda)) = \sqrt{\lambda^3 - 1}\,\mathbf{m}_{n-1}(\mathbf{x}')$$

and $\nabla\mathbf{v}(\mathbf{x}'_\lambda) = \mathbf{R}_1(\mathbf{x}')^T$. We will find ϕ_n in terms of ϕ_{n-1}, but before we do so we need to argue with $\mathbf{v}$. An ideal $\mathbf{v}$ should have a gradient whose rows are $\mathbf{m}_1$ and $\mathbf{m}_1^\perp$. Since $\mathbf{m}_1$ points radially outward and $\mathbf{m}_1^\perp$ is tangent to concentric circles, the choice of $\mathbf{v}$ in polar coordinates should be $\mathbf{v}(r,\theta) = (v_1(r), v_2(\theta))$ in order for the rows of $\nabla\mathbf{v}$ to be parallel to $\mathbf{m}_1$ and $\mathbf{m}_1^\perp$. One such choice of $\mathbf{v}$ is

$$\mathbf{v}(r,\theta) = \begin{pmatrix} a\log r \\ \\ a\,\theta \end{pmatrix} \tag{3.61}$$

for $a > 0$, whose gradient in Euclidean coordinates is formally

$$\nabla\mathbf{v}(\mathbf{x}') = \frac{a}{|\mathbf{x}'|}\mathbf{R}_1(\mathbf{x}')^T. \tag{3.62}$$

The choice of $v_1(r) = a\log r$ is so that the scaling of $\frac{1}{r}$ matches the gradient of $v_2(\theta) = a\theta$. Here, $\nabla\mathbf{v}$ matches $\mathbf{R}_1(\mathbf{x})^T$ up to the scaling $\frac{a}{|\mathbf{x}'|}$, and we nearly recover the ideal $\mathbf{v}$. Finding a vector field $\mathbf{v}$ whose gradient equals a space-dependent rotation $\mathbf{R}_1(\mathbf{x}')^T$ is questionable. In fact, in order for $\operatorname{curl}\big(\psi(r)\mathbf{m}_1^{\perp}(\mathbf{x})\big) = 0$ and potentially have an antiderivative, the only choice of ψ is $\psi(r) = \frac{a}{r}$. Therefore, $\psi(|\mathbf{x}'|) = \frac{a}{|\mathbf{x}'|}$ is the only scaling for which one may hope to find an antiderivative of $\psi(|\mathbf{x}'|)\mathbf{R}_1(\mathbf{x}')^T$. The choice of ϕ_n is designed to compensate for this scaling. If

$$\phi_n(\mathbf{x}') := \frac{\sqrt{\lambda^3 - 1}}{n\,a^{n-1}}\,|\mathbf{x}'|^n \quad \Rightarrow \quad \nabla\phi_n(\mathbf{x}') = \frac{|\mathbf{x}'|}{a}\nabla\phi_{n-1}(\mathbf{x}'), \tag{3.63}$$

which is consistent with (3.52) for $n = 1$. Combining the inductive hypothesis

$$\nabla\phi_{n-1}\big(\mathbf{v}(\mathbf{x}'_\lambda)\big) = \sqrt{\lambda^3 - 1}\,\mathbf{m}_{n-1}(\mathbf{x}'),$$

with the recursion relation (3.63) yields

$$\nabla\big[\phi_n\big(\mathbf{v}(\mathbf{x}'_\lambda)\big)\big] = \nabla\mathbf{v}(\mathbf{x}'_\lambda)^T\nabla\phi_n\big(\mathbf{v}(\mathbf{x}'_\lambda)\big) = \frac{|\mathbf{v}(\mathbf{x}'_\lambda)|}{|\mathbf{x}'_\lambda|}\mathbf{R}_1(\mathbf{x}'_\lambda)\nabla\phi_{n-1}\big(\mathbf{v}(\mathbf{x}'_\lambda)\big)$$
$$= \frac{|\mathbf{v}(\mathbf{x}'_\lambda)|}{|\mathbf{x}'_\lambda|}\sqrt{\lambda^3-1}\mathbf{R}_1(\mathbf{x}')\mathbf{m}_{n-1}(\mathbf{x}') = \frac{|\mathbf{v}(\mathbf{x}'_\lambda)|}{|\mathbf{x}'_\lambda|}\sqrt{\lambda^3-1}\,\mathbf{m}_n(\mathbf{x}').$$

This shows that we need $|\mathbf{v}(\mathbf{x}')| = |\mathbf{x}'|$ to close the argument, which may not be possible unless $\mathbf{v}(\mathbf{x}') = \mathbf{R}(\mathbf{x}')^T\mathbf{x}'$ with $\mathbf{R}(\mathbf{x}')$ a rotation. This in turn would not lead to (3.62). Finally, the cone solution for $n=1$ satisfies $\nabla\phi_1(\mathbf{x}'_\lambda) = \pm\sqrt{\lambda^3-1}\;\mathbf{m}_1(\mathbf{x}')$, whereas the ideal construction requires $\nabla\phi_1\big(\mathbf{v}(\mathbf{x}'_\lambda)\big) = \pm\sqrt{\lambda^3-1}\;\mathbf{m}_1(\mathbf{x}')$. The sign does not matter because g_1 is invariant under $\mathbf{m}_1 \mapsto -\mathbf{m}_1$, but there is a mismatch in the argument of $\nabla\phi_1$ since $\mathbf{v}(\mathbf{x}'_\lambda)$ may not be equal to $\mathbf{x}'_\lambda$ everywhere. We next discuss how to circumvent these obstructions to the idealized construction via approximation.

3.3.4 Formal approximation of idealized construction

We now build an approximate deformation $\mathbf{y}_n$ such that $\mathrm{I}[\mathbf{y}_n] \approx g_n$. To this end, we modify $\mathbf{v}$ from (3.61), so that $\mathbf{v}(\mathbf{x}'_\lambda) \approx \mathbf{x}'_\lambda$ near the point $\mathbf{x}^* = (a,0)^T$ for $a>0$; this avoids a singularity at $\mathbf{0}$. To guarantee that $\mathbf{v}(\mathbf{x}^*) = \mathbf{x}^*$ and $\nabla\mathbf{v}(\mathbf{x}^*) = I_2$, we choose

$$\mathbf{v}(\mathbf{x}') = \begin{pmatrix} \frac{a}{2}\log(x_1^2+x_2^2) + C_a \\ a\arctan(x_2/x_1) \end{pmatrix}, \tag{3.64}$$

where $C_a = a - a\log(a)$. Hence, $\mathbf{v}$ satisfies (3.62) and the formal Taylor expansion

$$\mathbf{v}(\mathbf{x}') = \mathbf{x}^* + (\mathbf{x}' - \mathbf{x}^*) + \mathcal{O}\big(|\mathbf{x}' - \mathbf{x}^*|^2\big) = \mathbf{x}' + \mathcal{O}\big(|\mathbf{x}' - \mathbf{x}^*|^2\big),$$

or equivalently the following expression in the rescaled coordinates $\mathbf{x}'_\lambda$

$$\mathbf{v}(\mathbf{x}'_\lambda) = \mathbf{x}'_\lambda + \mathcal{O}\big(|\mathbf{x}' - \mathbf{x}^*|^2\big), \tag{3.65}$$

because $\lambda = \mathcal{O}(1)$. Using (3.65), we approximately satisfy the three crucial requirements

$$\begin{aligned} |\mathbf{v}(\mathbf{x}'_\lambda)|^2 &= |\mathbf{x}'_\lambda|^2 + \mathcal{O}(|\mathbf{x}' - \mathbf{x}^*|^2), \\ \mathbf{m}_1(\mathbf{v}(\mathbf{x}'_\lambda)) &= \mathbf{m}_1(\mathbf{x}'_\lambda) + \mathcal{O}(|\mathbf{x}' - \mathbf{x}^*|^2), \\ \nabla\big[\phi_n\big(\mathbf{v}(\mathbf{x}'_\lambda)\big)\big] &= \sqrt{\lambda^3 - 1}\,\mathbf{m}_n(\mathbf{x}') + \mathcal{O}(|\mathbf{x}' - \mathbf{x}^*|^2). \end{aligned}$$

Inserting these formal approximations into (3.60) yields a map $\mathbf{y}_n$ defined by (3.59) for $n \geq 2$ that approximately satisfies the metric constraint in a vicinity of $\mathbf{x}^*$

$$\mathrm{I}[\mathbf{y}_n(\mathbf{x}')] = g_n(\mathbf{x}') + \mathcal{O}(|\mathbf{x}' - \mathbf{x}^*|^2). \tag{3.66}$$

3.3.5 Approximate surfaces for defects of degree two

We now specialize the above construction for $n = 2$. In view of (3.63), we realize that

$$\phi_2(\mathbf{x}') := \frac{\sqrt{\lambda^3 - 1}}{2a}|\mathbf{x}'|^2 \quad \Rightarrow \quad \nabla\phi_2(\mathbf{x}') = \frac{\sqrt{\lambda^3 - 1}}{a}\mathbf{x}' = \frac{\sqrt{\lambda^3 - 1}}{a}|\mathbf{x}'|\mathbf{m}_1(\mathbf{x}'),$$

Hence, (3.59) gives an approximate map $\mathbf{y}_2$ with

$$\phi_2\big(\mathbf{v}(\mathbf{x}')\big) = \frac{\sqrt{\lambda^3-1}}{2a}\left(\left(\frac{a}{2}\log\left(x_1^2+x_2^2\right)+a-a\log a\right)^2+a^2\text{arctan}^2\left(\frac{x_2}{x_1}\right)\right),$$

for $x_1 > 0$ and any $a > 0$ not be too large so that $\mathbf{y}_2$ captures the correct defect configuration. We display $\phi_2 \circ \mathbf{v}$ for $a = .75, \lambda = 1.1$ in Fig. 3.3, reflected for $x_1 < 1$ to account for symmetry, along with the computed solution from Section 5.1.

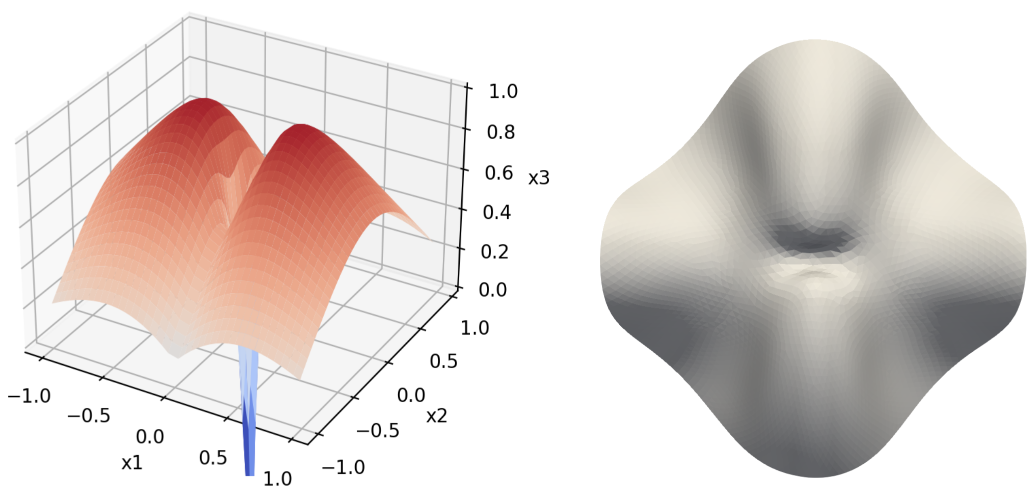

Figure 3.3: Approximate lifted surface for degree 2 defect (left) and computed solution with the director field $\mathbf{m}_2$ in Section 5.1 (right). Our derivation requires $x_1 > 0$, but the solution should be symmetric across the x_2x_3 plane, which is why we plot a reflected solution for $x_1 < 0$. We recover two bumps, consistent with the simulation but at the cost of a singularity at the origin.

3.3.6 Approximate surface for degree 3/2 defect

We now apply the above approach of composing defects, but for a defect of degree $3/2$. We intend to explain the intriguing "bird beak" shape observed in our computations displayed in Figures 3.4 and 5.1. We first observe that the explicit expressions (3.54) and (3.55) for a defect of degree $1/2$ do not quite conform with (3.56) for $n = 1/2$, except in the vicinity of the origin.

Motivated by the recursion relation (3.57), we still write the degree $3/2$ director field as

$$\mathbf{m}_{3/2}(\mathbf{x}') = \mathbf{R}_1(\mathbf{x}')\mathbf{m}_{1/2}(\mathbf{x}'), \tag{3.67}$$

with $\mathbf{m}_{1/2}$ given in (3.53). We now construct an approximate map $\mathbf{y}_{3/2}$ such that

$$\mathrm{I}[\mathbf{y}_{3/2}(\mathbf{x}')] \approx g_{3/2}(\mathbf{x}') = (\lambda^2 - \lambda^{-1})\mathbf{m}_{3/2}(\mathbf{x}') \otimes \mathbf{m}_{3/2}(\mathbf{x}') + \lambda^{-1}\mathbf{I}_2,$$

according to (3.58) for $\lambda > 1$. The deformation $\mathbf{y}_{3/2}$ satisfies in turn (3.59), namely

$$\mathbf{y}_{3/2}(\mathbf{x}') = \big(\mathbf{x}'_\lambda, \phi_{3/2}(\mathbf{v}(\mathbf{x}'_\lambda))\big)^T \tag{3.68}$$

with $\phi_{3/2}$ related to $\phi_{1/2}$ via (3.63). Since we are interested in an approximation for $x_1 > 0$ to capture the "bird beak" structure, we deduce from (3.55)

$$\nabla\phi_{3/2}(\mathbf{x}') = \frac{|\mathbf{x}'|}{a}\nabla\phi_{1/2}(\mathbf{x}') \quad \Rightarrow \quad \nabla\phi_{3/2}(\mathbf{x}') = \sqrt{\lambda^3 - 1}\,\frac{|\mathbf{x}'|}{a}\,\mathrm{sign}(x_2)\,\mathbf{e}_2.$$

Unfortunately, this ideal relation is incompatible because $\mathrm{curl}\,\big(\frac{|\mathbf{x}'_\lambda|}{a}\mathrm{sign}(x_2)\mathbf{e}_2\big) \neq 0$ and we need to amend the construction of $\phi_{3/2}$ by approximation. To this end, we define for $x_1 > 0$ the following modification of $\phi_{3/2}$

$$\phi_{3/2}(\mathbf{x}') = \sqrt{\lambda^3 - 1}\Big(1 - \frac{1}{a}\int_0^{|x_2|} \sqrt{s^2 + x_1^2}\, ds\Big), \tag{3.69}$$

whose gradient is

$$\nabla\phi_{3/2}(\mathbf{x}') = -\sqrt{\lambda^3-1}\frac{|\mathbf{x}'|}{a}\mathrm{sign}(x_2)\mathbf{e}_2 - \sqrt{\lambda^3-1}\frac{1}{a}\left(\int_0^{|\mathbf{x}_2|}\frac{x_1}{\sqrt{s^2+x_1^2}}\,ds\right)\mathbf{e}_1.$$

Exploiting that the integrand in the second term is bounded by 1 yields

$$\nabla\phi_{3/2}(\mathbf{x}) = -\sqrt{\lambda^3-1}\,\frac{|\mathbf{x}|}{a}\,\mathrm{sign}(x_2)\,\mathbf{e}_2 - \frac{\sqrt{\lambda^3-1}}{a}\mathcal{O}(|x_2|).$$

To approximate the first fundamental form $\mathrm{I}[\mathbf{y}_{3/2}]$, we recall (3.60) and compute

$$\nabla\mathbf{v}(\mathbf{x}'_\lambda)^T\nabla\phi(\mathbf{v}(\mathbf{x}'_\lambda)) = \sqrt{\lambda^3-1}\mathbf{R}_1(\mathbf{x}'_\lambda)\frac{|\mathbf{v}(\mathbf{x}'_\lambda)|}{|\mathbf{x}'_\lambda|}\mathrm{sign}(\mathbf{v}(\mathbf{x}'_\lambda)_2)\mathbf{e}_2 + \mathcal{O}(|\mathbf{v}(\mathbf{x}'_\lambda)_2|),$$

where $\mathbf{v}(\mathbf{x}'_\lambda)_2 = a\arctan(x_2/x_1)$ denotes the second component of $\mathbf{v}(\mathbf{x}'_\lambda)$ written in (3.64). We thus deduce $\mathrm{sign}(\mathbf{v}(\mathbf{x}'_\lambda)_2) = \mathrm{sign}(x_2)$ for $x_1 > 0$ and, employing that $\mathbf{m}_{1/2}(\mathbf{x}) = \mathrm{sign}(x_2)\,\mathbf{e}_2$ for $x_1 > 1$ along with (3.67), we arrive at

$$\nabla\mathbf{v}(\mathbf{x}'_\lambda)^T\nabla\phi(\mathbf{v}(\mathbf{x}'_\lambda)) = \sqrt{\lambda^3-1}\,\mathbf{m}_{3/2}(\mathbf{x}') + \mathcal{O}(|x_2|) + \mathcal{O}(|\mathbf{x}'-\mathbf{x}^*|^2),$$

because $\arctan(x_2/x_1) = \mathcal{O}(|x_2|)$ for x_1 away from 0. The expression (3.68) for $\mathbf{y}_{3/2}$ with $\phi_{3/2}$ defined in (3.69) gives an approximate shape profile that satisfies

$$\mathrm{I}[\mathbf{y}_{3/2}(\mathbf{x}')] = g_{3/2}(\mathbf{x}') + \mathcal{O}(|x_2|) + \mathcal{O}(|\mathbf{x}-\mathbf{x}^*|^2).$$

The contour plot of the corresponding lifted surface $\phi_{3/2}\big(\mathbf{v}(\mathbf{x}'_\lambda)\big)$ is displayed in Fig. 3.4 (left) for $a = .75$. We note that the profile has a similar bird beak shape to the computational result reported in Fig. 3.4 (right) and Fig. 5.1. For the $x_1 < 0$, $\mathbf{m}_{1/2}(\mathbf{x}') = \mathbf{m}_1(\mathbf{x}')$, and one can apply the arguments in Section 3.3.5 to get the asymptotic profile for $x_1 < 0$.

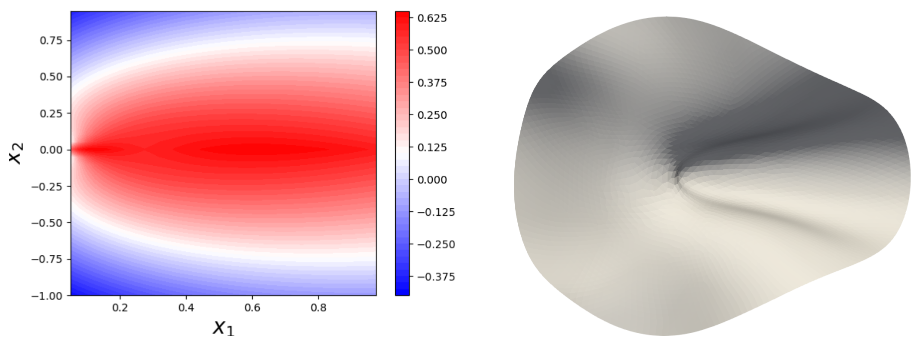

Figure 3.4: Contour plot of approximate lifted surface for degree 3/2 defect for $a = .75$ and $x_1 > 0$ (left) and computational result for a degree 3/2 defect obtained in Section 5.1. The profile matches the computed "bird beak" shape. To see this, notice that contour lines pinch off as $x_1 \to 0$. As a result, the lifted surface gets steeper near the origin. This helps explains the "bird beak" shape.

The compositional method explains why we should expect the intriguing "bird beak". We now provide a heuristic explanation. If a is fixed but x_1 is small, we drop x_1 in the integrand of (3.69), and $\phi_{3/2}(\mathbf{x}')$ behaves like $\tilde{\phi}_{3/2}(\mathbf{x}') := \sqrt{\lambda^3 - 1}\big(1 - \frac{1}{2a}|x_2|^2\big)$. We see that level sets of this function are straight lines $|x_2| =$ constant that increase as $|x_2|$ decreases to 0, very much like level sets of $\phi_{1/2}(\mathbf{x}')$ in (3.55) for $x_1 > 0$. On the other hand, the lifted surface $\phi_{3/2}(\mathbf{v}(\mathbf{x}'_\lambda))$ from (3.68) behaves like

$$\tilde{\phi}_{3/2}(\mathbf{v}(\mathbf{x}'_\lambda)) = \sqrt{\lambda^3 - 1}\Big(1 - \frac{a}{2} \arctan\Big(\frac{|x_2|}{x_1}\Big)^2\Big), \tag{3.70}$$

whose level sets are radial lines $\frac{|x_2|}{x_1} =$ constant that increase as $\frac{|x_2|}{x_1}$ decreases to 0. Therefore, the lifted surface $\tilde{\phi}_{3/2}(\mathbf{v}(\mathbf{x}'_\lambda))$ pinches off at the origin in the sense that it develops a discontinuity. In Section 3.3.3 we advocated that a defect of degree $3/2$ could be viewed as a composition of degree $1/2$ and 1 defects. The effect of the degree 1 defect on (3.54) is to twist or compress the horizontal level sets of $\phi_{1/2}(\mathbf{v}(\mathbf{x}'_\lambda))$ into radial level sets of $\tilde{\phi}_{3/2}(\mathbf{v}(\mathbf{x}'_\lambda))$. This is due to the action of the vector-valued map $\mathbf{v}$ and boils down to the replacement of $|x_2|$ in (3.55) by $\frac{a}{2}\,\arctan\left(\frac{|x_2|}{x_1}\right)^2$ in (3.70).

3.4 Bending energy for LCN

This section deals with computing the formal limit of vanishing thickness scaled with t^3. One reason to introduce a bending energy is that due to lack of convexity, minimizing the stretching energy may induce wrinkling and the membrane problem may be ill-posed. We point to Section 4.1.1 for a discussion of this phenomenon. One remedy is to introduce a bending energy, which will be well-posed due to convexity in the highest order terms. In particular, we compute the formal limit via Kirchhoff-Love asymptotics:

$$E_{bend}[\mathbf{y}] = \lim_{t\to\infty} \frac{1}{t^3} E_{3D,t}[\mathbf{u}]$$

where $E_{3D,t}$ is from (3.7) The bending energy would correspond the second term in the expansion

$$E_{3D,t}[\mathbf{u}] = \int_{-t/2}^{t/2}\int_\Omega W_{str}(\mathbf{x}', \nabla'\mathbf{y}) + x_3^2 W_{bend}(\mathbf{x}', \nabla'\mathbf{y}, D^2\mathbf{y})\; d\mathbf{x}' dx_3 + \mathcal{O}(t^5).$$

Similar to the stretching energy, we follow closely the work of [98].

3.4.1 Review of relevant differential geometry

This section briefly reviews the relevant differential geometry needed to derive a bending energy. We refer the reader to books [60, 78] for references on differential geometry. The LCE energy will depend on products of the gradient of $\mathbf{y}$ and $\boldsymbol{\nu}$, which is to be seen. These products will correspond to first, second, and third fundamental forms of $\mathbf{y}$. We now define them below

$$\mathrm{I}[\mathbf{y}] = \nabla'\mathbf{y}^T\nabla'\mathbf{y}, \quad \mathrm{II}[\mathbf{y}] = -\nabla'\boldsymbol{\nu}^T\nabla'\mathbf{y}, \quad \mathrm{III}[\mathbf{y}] = \nabla'\boldsymbol{\nu}^T\nabla'\boldsymbol{\nu}. \tag{3.71}$$

It is easy to tell that $\mathrm{I}[\mathbf{y}]$, and $\mathrm{III}[\mathbf{y}]$ are symmetric. The second fundamental form, $\mathrm{II}[\mathbf{y}]$ is also symmetric, but it is not obvious. Recall that $\partial_i\mathbf{y}\cdot\boldsymbol{\nu} = 0$. Applying ∂_i to this expression leads to $(\partial_j\partial_i\mathbf{y})\cdot\boldsymbol{\nu} = -\partial_i\mathbf{y}\cdot\partial_j\boldsymbol{\nu}$. Hence, $\mathrm{II}[\mathbf{y}]_{ij} = (\partial_j\partial_i\mathbf{y})\cdot\boldsymbol{\nu} = \mathrm{II}[\mathbf{y}]_{ji}$, and $\mathrm{II}[\mathbf{y}]$ is symmetric.

Another nice feature of these fundamental forms is that they relate to the shape operator and the curvatures of a surface. We first recall some definitions of the curvatures of a surface.

Definition 3.1 (Shape operator)**.** *Let* $\mathbf{y}:\Omega\to\mathbb{R}^3$ *be the parameterization of a surface* $\mathbf{y}(\Omega)$ *embedded in* $\mathbb{R}^3$ *(i.e.* $\mathbf{y}$ *is one-to-one). Let* $\mathbf{N}:\mathbf{y}(\Omega)\to\mathbb{R}^3$ *be defined by* $\mathbf{N}(\mathbf{z}) = \boldsymbol{\nu}(\mathbf{y}^{-1}(\mathbf{x}))$ *because* $\boldsymbol{\nu}:\Omega\to\mathbb{R}$ *according to* (3.21)*. For a smooth enough surface and sufficiently small* $\varepsilon > 0$*, we may consider a tubular neighborhood of width* ε*, denoted* $U(\mathbf{y}(\Omega))_\varepsilon$*, so that we may extend* $\mathbf{N}: U(\mathbf{y}(\Omega))_\varepsilon\to\mathbb{R}^3$ *normally. We define the shape operator as* $\mathbf{S} = \nabla\mathbf{N}(\mathbf{I}_3 - \mathbf{N}\otimes\mathbf{N})$.

Note that $\mathbf{S}$ is a symmetric matrix with at least one zero eigenvalue corresponding to the vector $\mathbf{N}$. To see this, we introduce the distance function:

$$d(\mathbf{z}) = \mathrm{dist}(\mathbf{z}, \mathbf{y}(\Omega)).$$

Note that $\nabla d = \mathbf{N}$, so we have $D^2 d = \nabla \mathbf{N}$. Combined with the fact that $\mathbf{N}^T \nabla \mathbf{N} = 0$, we have that $\mathbf{S} = D^2 d$ is symmetric, and $\mathbf{N}$ is in the kernel of $\mathbf{S}$. The other eigenvalues are known as the principle curvatures of $\mathbf{y}(\Omega)$. We now define the principle curvatures as well as the mean and Gauss curvature.

Definition 3.2 (mean and Gauss curvature)**.** *The eigenvalues corresponding to tangent eigenvectors of* $\mathbf{S}$ *are known as the principle curvatures and are denoted as* κ_1, κ_2*. The mean curvature,* H*, and Gauss curvature,* K*, are defined as*

$$H = \frac{\kappa_1 + \kappa_2}{2}, \quad K = \kappa_1 \kappa_2. \tag{3.72}$$

The corresponding fundamental forms also relate to the mean and Gauss curvature. These results are well known, and we refer the reader to the book chapter [60, Chapter 3-3] as well as [78, Proposition 3.5.5] and [78, Proposition 3.5.6]. For completeness, we state and prove the relevant results in the following lemma.

Lemma 3.1 (second and third fundamental form relations)**.** *The mean and Gauss curvature are also expressed as the following*

$$\mathrm{tr}(-\mathrm{I\!I}[\mathbf{y}]\mathrm{I}[\mathbf{y}]^{-1}) = 2H, \quad \det(-\mathrm{I\!I}[\mathbf{y}]\mathrm{I}[\mathbf{y}]^{-1}) = K \tag{3.73}$$

and the third fundamental form can be expressed as

$$\mathrm{I\!I\!I}[\mathbf{y}] = -2H\mathrm{I\!I}[\mathbf{y}] - K\mathrm{I}[\mathbf{y}] \tag{3.74}$$

Proof. We begin with (3.73). Let $\mathbf{x}' \in \Omega$ and let $\mathbf{z} = \mathbf{y}(\mathbf{x}')$. We assume every function in this calculation is evaluated at $\mathbf{x}'$ unless further specified. We first claim that $\mathrm{I\!I}[\mathbf{y}] = -\nabla'\mathbf{y}^T\mathbf{S}(\mathbf{z})\nabla'\mathbf{y}$. Using the definition of $\mathbf{S}$, we have

$$\mathbf{S}(\mathbf{z}) = \nabla\mathbf{N}(\mathbf{z})(\mathbf{I}_3 - \mathbf{N}(\mathbf{z}) \otimes \mathbf{N}(\mathbf{z})).$$

We multiply on the left by $\nabla'\mathbf{y}^T$ and on the right by $\nabla'\mathbf{y}$ so then

$$\nabla'\mathbf{y}^T\mathbf{S}(\mathbf{z})\nabla'\mathbf{y} = \nabla'\mathbf{y}^T\nabla\mathbf{N}(\mathbf{z})\nabla'\mathbf{y}.$$

where we used the fact that $\mathbf{N}(\mathbf{z})^T\nabla'\mathbf{y}(\mathbf{x}) = \boldsymbol{\nu}^T\nabla'\mathbf{y} = 0$. Since $\mathbf{N}(\mathbf{y}(\mathbf{x}')) = \boldsymbol{\nu}(\mathbf{x}')$, taking the derivative with respect to $\mathbf{x}'$ of both sides and using chain rule yields $\nabla\mathbf{N}(\mathbf{z})\nabla'\mathbf{y}(\mathbf{x}') = \nabla'\boldsymbol{\nu}(\mathbf{x}')$. Hence

$$\nabla'\mathbf{y}^T\mathbf{S}(\mathbf{z})\nabla'\mathbf{y} = \nabla'\mathbf{y}^T\nabla'\boldsymbol{\nu} = -\mathrm{I\!I}[\mathbf{y}]. \tag{3.75}$$

Since $\mathbf{S}(\mathbf{z})\mathbf{N}(\mathbf{z}) = 0$, the shape operator $\mathbf{S}(\mathbf{z})$ aacts on the tangent space to $\mathbf{y}(\Omega)$, and it can thus be represented in the basis $(\partial_1\mathbf{y}, \partial_2\mathbf{y})$ via a matrix $\tilde{S} \in \mathbb{R}^{2\times 2}$, namely

$$\mathbf{S}(\mathbf{z})\partial_i\mathbf{y} = \sum_{j=1}^{2}\tilde{\mathbf{S}}_{ji}\partial_j\mathbf{y}(\mathbf{z}) \implies \nabla'\mathbf{y}\tilde{S} = \mathbf{S}\nabla'\mathbf{y}$$

The matrix $\tilde{\mathbf{S}}$ is well defined since $\nabla'\mathbf{y}$ has full rank, and the range of $\mathbf{S}(\mathbf{z})\nabla'\mathbf{y}$ is the range of $\nabla'\mathbf{y}$. Suppose $(\mathbf{v}_i, \mu_i) \in \mathbb{R}^2 \times \mathbb{R}$, is an eigenpair of $\tilde{\mathbf{S}}$, then

$$\tilde{S}\mathbf{v}_i = \mu_i\mathbf{v}_i \implies \mathbf{S}(\mathbf{z})\nabla'\mathbf{y}\mathbf{v}_i = \mu_i\nabla'\mathbf{y}\mathbf{v}_i,$$

whence μ_i is an eigenvalue of $\mathbf{S}(\mathbf{z})$ with an eigenvector $\nabla'\mathbf{y}\mathbf{v}_i$ in the tangent plane of $\mathbf{y}(\Omega)$ at $\mathbf{z}$. Hence, the eigenvalues of $\tilde{\mathrm{S}}$ are κ_1, κ_2. Note that since $\tilde{\mathrm{S}}$ solves $\nabla'\mathbf{y}\tilde{\mathbf{S}} = \mathbf{S}(\mathbf{z})\nabla'\mathbf{y}$, then we have

$$\tilde{\mathbf{S}} = \mathrm{I}[\mathbf{y}]^{-1}\nabla'\mathbf{y}^T\mathbf{S}(\mathbf{z})\nabla'\mathbf{y} = -\mathrm{I}[\mathbf{y}]^{-1}\mathrm{II}[\mathbf{y}]$$

by virtue of (3.75). Hence,

$$\mathrm{tr}(-\mathrm{II}[\mathbf{y}]\mathrm{I}[\mathbf{y}]^{-1}) = \mathrm{tr}(\tilde{\mathbf{S}}) = \kappa_1 + \kappa_2 = 2H,$$

$$\det(-\mathrm{II}[\mathbf{y}]\mathrm{I}[\mathbf{y}]^{-1}) = \det(\tilde{\mathbf{S}}) = \kappa_1\kappa_2 = K,$$

which proves (3.73).

For (3.74), it is sufficient to prove $\tilde{\mathbf{S}}^2 = \mathrm{I}[\mathbf{y}]^{-1}\mathrm{III}[\mathbf{y}]$. To see this, we first utilize Cayley-Hamilton Theorem for $\tilde{\mathrm{S}}$:

$$\tilde{\mathbf{S}}^2 - \mathrm{tr}(\tilde{\mathbf{S}})\tilde{\mathbf{S}} + (\det\tilde{\mathbf{S}})\mathbf{I}_2 = 0$$

We then use the fact that $\mathrm{tr}(\tilde{\mathbf{S}}) = 2H$, $\det(\tilde{\mathbf{S}}) = K$, and $\tilde{\mathbf{S}} = -\mathrm{I}[\mathbf{y}]^{-1}\mathrm{II}[\mathbf{y}]$ to write

$$\tilde{\mathbf{S}}^2 + 2H\mathrm{I}[\mathbf{y}]^{-1}\mathrm{II}[\mathbf{y}] + K\mathbf{I}_2 = 0 \tag{3.76}$$

If we prove, $\tilde{\mathrm{S}}^2 = \mathrm{I}[\mathrm{y}]^{-1}\mathrm{III}[\mathrm{y}]$, then (3.74) immediately follows from (3.76).

We first show that $\nabla'\mathbf{y}^T\mathbf{S}(\mathbf{z})^2\nabla'\mathbf{y} = \mathrm{III}[\mathrm{y}]$. Recall that $\mathbf{S}(\mathbf{z}) = \nabla\mathbf{N}(\mathbf{z})(\mathbf{I}_3 - \mathbf{N}(\mathbf{z}) \otimes \mathbf{N}(\mathbf{z}))$ is symmetric, and $\mathbf{N}(\mathbf{z})^T\nabla'\mathbf{y} = 0$. Hence,

$$\nabla'\mathbf{y}^T\mathbf{S}(\mathbf{z})^2\nabla'\mathbf{y} = \nabla'\mathbf{y}^T\nabla\mathbf{N}(\mathbf{z})^T\nabla\mathbf{N}(\mathbf{z})\nabla'\mathbf{y}.$$

We also have computed that $\nabla\mathbf{N}(\mathbf{z})\nabla'\mathbf{y} = \nabla'\boldsymbol{\nu}$, so

$$\nabla'\mathbf{y}^T\mathbf{S}(\mathbf{z})^2\nabla'\mathbf{y} = \nabla'\boldsymbol{\nu}^T\nabla\boldsymbol{\nu} = \mathrm{I\!I\!I}[\mathbf{y}].$$

Thus, it is sufficient to show $\tilde{S}^2 = \mathrm{I}[\mathbf{y}]^{-1}\nabla'\mathbf{y}^T\mathbf{S}(\mathbf{z})^2\nabla'\mathbf{y}$. We use the relation $\tilde{\mathbf{S}} = \mathrm{I}[\mathbf{y}]^{-1}\nabla'\mathbf{y}^T\mathbf{S}(\mathbf{z})\nabla'\mathbf{y}$ to compute

$$\tilde{\mathbf{S}}^2 = \mathrm{I}[\mathbf{y}]^{-1}\nabla'\mathbf{y}^T\mathbf{S}(\mathbf{z})\nabla'\mathbf{y}\mathrm{I}[\mathbf{y}]^{-1}\nabla'\mathbf{y}^T\mathbf{S}(\mathbf{z})\nabla'\mathbf{y}.$$

Note that $\nabla'\mathbf{y}\mathrm{I}[\mathbf{y}]^{-1}\nabla'\mathbf{y}^T\nabla'\mathbf{y}\mathbf{v} = \nabla'\mathbf{y}\mathbf{v}$ for all $\mathbf{v} \in \mathbb{R}^2$, so $\nabla'\mathbf{y}\mathrm{I}[\mathbf{y}]^{-1}\nabla'\mathbf{y}^T$ acts like the identity in the range of $\nabla'\mathbf{y}$. Since the range of $\mathbf{S}(\mathbf{z})$ is the range of $\nabla'\mathbf{y}$, we have $\mathbf{S}(\mathbf{z})\nabla'\mathbf{y}\mathrm{I}[\mathbf{y}]^{-1}\nabla'\mathbf{y}^T\mathbf{S}(\mathbf{z}) = \mathbf{S}(\mathbf{z})^2$, and

$$\tilde{\mathbf{S}}^2 = \mathrm{I}[\mathbf{y}]^{-1}\nabla'\mathbf{y}^T\mathbf{S}(\mathbf{z})^2\nabla'\mathbf{y},$$

which completes the proof of (3.74). □

3.4.2 Kirchhoff-Love assumption

We now expand the modified Kirchhoff-Love assumption (3.21) to include higher order terms

$$\mathbf{u}(\mathbf{x}', x_3) = \mathbf{y}(\mathbf{x}') + \phi(\mathbf{x}', x_3)\boldsymbol{\nu}(\mathbf{x}'). \tag{3.77}$$

$$\phi(\mathbf{x}', x_3) = \alpha(\mathbf{x}') + \beta(\mathbf{x}')x_3^2 + \gamma(\mathbf{x}')x_3^3 + \mathcal{O}(x_3^4). \tag{3.78}$$

The process to derive bending energy follows similarly to the stretching energy and is as follows:

1. Write the Cauchy tensor $\mathbf{C} = \mathbf{F}^T\mathbf{F}$ in terms of powers of ϕ.

2. Write W_{3D} in terms of $\mathbf{C}$ and powers of x_3.

3. Collect $\mathcal{O}(x_3^2)$ terms of W_{3D} which contribute to the bending energy.

4. Determine α, β, γ so that $\mathbf{u}$ satisfies incompressibility in an asymptotic sense.

Since we are computing the formal limit $E_{bend}[\mathbf{y}] = \lim_{t\to 0} \frac{1}{t^3} E_{t,3D}[\mathbf{y}]$, we assume that $\mathbf{y}$ already satisfies $E_{str}[\mathbf{y}] = 0$, so that the limit is finite. This means that by Corollary 3.4 (immersions of g are minimizers with vanishing energy), we have that

$$\mathrm{I}[\mathbf{y}] = \lambda^2 \tilde{\mathbf{m}} \otimes \tilde{\mathbf{m}} + \lambda^{-1} \tilde{\mathbf{m}} \otimes \tilde{\mathbf{m}}, \quad \lambda = \sqrt[3]{\frac{s+1}{s_0+1}}.$$

Moreover, for the purposes of this chapter we deal with s, s_0 as constants in space. Hence $\alpha = \det \mathrm{I}[\mathbf{y}] = \lambda$ is a constant.

3.4.3 Cauchy tensor

Using (3.77), we have

$$\nabla \mathbf{u} = [\nabla' \mathbf{y} + \phi \nabla' \boldsymbol{\nu} + \boldsymbol{\nu} \otimes \nabla' \phi, \partial_3 \phi \boldsymbol{\nu}].$$

Computing $\mathbf{C} = \nabla \mathbf{u}^T \nabla \mathbf{u}$, we have

$$\mathbf{C} = \nabla \mathbf{u}^T \nabla \mathbf{u} = \begin{pmatrix} \mathbf{C}_\phi + \nabla'\phi \otimes \nabla'\phi & \partial_3\phi \nabla'\phi \\ \partial_3 \phi \nabla' \phi^T & (\partial_3\phi)^2 \end{pmatrix},$$

where

$$\mathbf{C}_\phi = \mathrm{I}[\mathbf{y}] - 2\phi\mathrm{II}[\mathbf{y}] + \phi^2\mathrm{III}[\mathbf{y}], \tag{3.79}$$

and we used the fact that $\boldsymbol{\nu}^T\boldsymbol{\nu} = 1, \boldsymbol{\nu}^T\nabla'\mathbf{y} = 0$, and $\boldsymbol{\nu}^T\nabla'\boldsymbol{\nu} = 0$.

Recall that $\alpha = \lambda$, which is constant, so

$$\nabla'\phi = \nabla'(\alpha(\mathbf{x}') + \beta(\mathbf{x}')x_3^2 + \gamma(\mathbf{x}')x_3^3 + \mathcal{O}(x_3^4)) = \nabla'\beta(\mathbf{x}')x_3^2 + \mathcal{O}(x_3^3).$$

Hence, $\nabla'\phi \otimes \nabla'\phi = \mathcal{O}(x_3^4)$. Thus,

$$\mathbf{C} = \begin{pmatrix} \mathbf{C}_\phi & \partial_3\phi\nabla'\phi \\ \partial_3\phi\nabla'\phi^T & (\partial_3\phi)^2 \end{pmatrix} + \mathcal{O}(x_3^4). \tag{3.80}$$

3.4.4 Incompressibility

For incompressibility, we want to determine α, β, γ such that $\det \mathbf{C} = 1 + \mathcal{O}(x_3^3)$. Note that we already determined that $\alpha = (\det \mathrm{I}[\mathbf{y}])^{-1/2}$, so that $\det \mathbf{C} = 1 + \mathcal{O}(x_3)$. Hence, we will determine β, γ so that the $\mathcal{O}(x_3)$ and $\mathcal{O}(x_3^2)$ terms of $\det \mathbf{C}$ are 0.

We first compute $\det \mathbf{C}$:

$$\det \mathbf{C} = \det \mathbf{C}_\phi(\partial_3\phi)^2 + D + \mathcal{O}(x_3^3),$$

where

$$D = \partial_3\phi\partial_1\phi \begin{vmatrix} (\mathbf{C}_\phi)_{2,1} & (\mathbf{C}_\phi)_{2,2} \\ \partial_3\phi\partial_1\phi & \partial_3\phi\partial_1\phi \end{vmatrix} - \partial_3\phi\partial_1\phi \begin{vmatrix} (\mathbf{C}_\phi)_{1,1} & (\mathbf{C}_\phi)_{1,2} \\ \partial_3\phi\partial_1\phi & \partial_3\phi\partial_1\phi \end{vmatrix}.$$

Note that since $\nabla'\phi = \mathcal{O}(x_3^2)$, then $D = \mathcal{O}(x_3^4)$. Hence,

$$\det \mathbf{C} = \det \mathbf{C}_\phi (\partial_3\phi)^2 + \mathcal{O}(x_3^3).$$

We now compute $\det \mathbf{C}_\phi$ as

$$\begin{aligned} \det \mathbf{C}_\phi &= J[\mathbf{y}] \det \left(\mathbf{C}_\phi \mathrm{I}[\mathbf{y}]^{-1}\right) \\ &= J[\mathbf{y}] \det \left(\mathbf{I}_2 - 2\phi \mathrm{II}[\mathbf{y}]\mathrm{I}[\mathbf{y}]^{-1} + \phi^2 \mathrm{III}[\mathbf{y}]\mathrm{I}[\mathbf{y}]^{-1}\right), \end{aligned}$$

where $J[\mathbf{y}] = \det \mathrm{I}[\mathbf{y}]$ as previously defined in (3.19). Since $-2\phi\mathrm{II}[\mathbf{y}]\mathrm{I}[\mathbf{y}]^{-1} + \phi^2\mathrm{III}[\mathbf{y}]\mathrm{I}[\mathbf{y}]^{-1}$ is a 2×2 matrix, we use the expansion $\det(\mathbf{I}_2 + \mathbf{A}) = 1 + \mathrm{tr}\mathbf{A} + \det \mathbf{A}$, to write

$$\det \mathbf{C}_\phi = J[\mathbf{y}] \left(1 - 2\phi \mathrm{tr}(\mathrm{II}[\mathbf{y}]\mathrm{I}[\mathbf{y}]^{-1}) + \phi^2 \mathrm{tr}(\mathrm{III}[\mathbf{y}]\mathrm{I}[\mathbf{y}]^{-1}) + 4\phi^2 \det(\mathrm{II}[\mathbf{y}]\mathrm{I}[\mathbf{y}]^{-1})\right) + \mathcal{O}(\phi^3).$$

Applying Lemma 3.1 (second and third fundamental form relations) yields

$$\begin{aligned} \det \mathbf{C}_\phi &= J[\mathbf{y}](1 + 4\phi H + \phi^2(4H^2 + 2K)) + \mathcal{O}(\phi^3) \\ &= J[\mathbf{y}](1 + 4\alpha H x_3 + (4\beta H + \alpha^2(4H^2 + 2K))x_3^2) + \mathcal{O}(x_3^3). \end{aligned}$$

Multiplying $\det \mathbf{C}_\phi$ and $(\partial_3\phi)^2 = \alpha^2 + 4\beta\alpha x_3 + (6\alpha\gamma + 4\beta^2)x_3^2 + \mathcal{O}(x_3^3)$ results in

$$\det \mathbf{C}_\phi(\partial_3\phi)^2 = J[\mathbf{y}]\Big[\alpha^2 + (4\alpha^3 H + 4\beta\alpha)x_3 \\ + (6\alpha\gamma + 4\beta^2 + 4\beta\alpha^2 H + \alpha^4(4H^2 + 2K) + 16\alpha^2 H\beta)x_3^2\Big] + O(x_3^3). \tag{3.81}$$

To ensure that the $\mathcal{O}(x_3)$ term in (3.81) is 0, we need $4\alpha^3 H + 4\beta\alpha = 0$, which implies $\beta = -H\alpha^2$. To set the $\mathcal{O}(x_3^2)$ order term in (3.81) to zero we require

$$6\alpha\gamma + 4\beta^2 + 4\beta\alpha^2 H + \alpha^4(4H^2 + 2K) + 16\alpha^2 H\beta = 0.$$

Substituting $\beta = -H\alpha^2$ and solving for γ, yields $\gamma = \frac{\alpha^3}{3}(6H^2 - K)$. To summarize, we determined

$$\alpha = J[\mathbf{y}]^{-1/2} \tag{3.82}$$

$$\beta = -J[\mathbf{y}]^{-1}H = -H\alpha^2 \tag{3.83}$$

$$\gamma = \frac{J[\mathbf{y}]^{-3/2}}{3}(6H^2 - K) = \frac{\alpha^3}{3}(6H^2 - K), \tag{3.84}$$

which ensures $\det \mathbf{C} = 1 + \mathcal{O}(x_3^3)$.

Remark 3.3 (comparison with [98])**.** *Note that if we assume* $\det \mathrm{I}[\mathbf{y}] = 1$*, then* $\alpha = 1$*,* $\beta = -H$*, and* $\gamma = \frac{1}{3}(6H^2 - K)$*, which agrees with [98]. This is the key difference in our derivation compared with that of [98]: we relax the inextensibility constraint* $\det \mathrm{I}[\mathbf{y}] = 1$*, which makes the model a bit more realistic in practice. We refer to Section 3.2.1.6.*

3.4.5 Expanding W_{3D}

Recall that we computed W_{3D} in terms of $\mathbf{C}$ back in (3.30) when deriving the stretching energy. Inserting $\mathbf{C}$ from (3.80) into (3.30) yields:

$$W_{3D}(\mathbf{x}', \nabla\mathbf{u}) = \lambda\left((\partial_3\phi)^2 + \mathrm{tr}\mathbf{C}_\phi + \frac{s_0}{s+1}\mathbf{m}\cdot\mathbf{C}_\phi\mathbf{m} - \frac{s}{s+1}\frac{\mathbf{m}\cdot\mathbf{C}_\phi^2\mathbf{m}}{\mathbf{m}\cdot\mathbf{C}_\phi\mathbf{m}}\right) - 3 + \mathcal{O}(x_3^4), \quad (3.85)$$

where $\mathbf{m} : \Omega \to \mathbb{S}^1$ is the planar director field denoting the initial LC orientation. Note that $\mathbf{C}_\phi$ is a 2×2 matrix, and we may apply Cayley Hamilton again to see that

$$\mathbf{C}_\phi^2 = \mathrm{tr}\mathbf{C}_\phi\mathbf{C}_\phi - \det(\mathbf{C}_\phi)\mathbf{I}_2.$$

Rearranging the energy density now reads:

$$W_{3D}(\mathbf{x}', \nabla\mathbf{u}) = \lambda(\partial_3\phi)^2 + \frac{\lambda}{s+1}\left(\mathrm{tr}\mathbf{C}_\phi + s_0\mathbf{m}\cdot\mathbf{C}_\phi\mathbf{m} + s\frac{\det\mathbf{C}_\phi}{\mathbf{m}\cdot\mathbf{C}_\phi\mathbf{m}}\right) - 3 + \mathcal{O}(x_3^4). \quad (3.86)$$

We shall now expand W_{3D} in terms of powers of ϕ. Note that the $\mathrm{tr}\mathbf{C}_\phi$ and the $\mathbf{m}\cdot\mathbf{C}_\phi\mathbf{m}$ terms are linear in $\mathbf{C}_\phi$, so their asymptotic expansion will be easy. We use the expansion of $\mathbf{C}_\phi$ in (3.79) to compute

$$\mathrm{tr}\mathbf{C}_\phi = \mathrm{tr}\mathrm{I}[\mathbf{y}] - 2\phi\mathrm{tr}\mathrm{II}[\mathbf{y}] + \phi^2\mathrm{tr}\mathrm{III}[\mathbf{y}], \quad (3.87)$$

and

$$\mathbf{m}\cdot\mathbf{C}_\phi\mathbf{m} = C_{\mathbf{m}}[\mathbf{y}] - 2\phi C_{\mathrm{II}}[\mathbf{y}] + \phi^2 C_{\mathrm{III}}[\mathbf{y}], \quad (3.88)$$

where $C_{\mathbb{II}}[\mathbf{y}] = \mathbf{m} \cdot \mathbb{II}[\mathbf{y}]\mathbf{m}$, and $C_{\mathbb{III}}[\mathbf{y}] = \mathbf{m} \cdot \mathbb{III}[\mathbf{y}]\mathbf{m}$, and $C_{\mathbf{m}}[\mathbf{y}] = \mathbf{m} \cdot \mathbb{I}[\mathbf{y}]\mathbf{m}$ as defined in (3.19). We turn our attention to the last term. The numerator is

$$\det \mathbf{C}_\phi = J[\mathbf{y}](1 + 4\phi H + \phi^2(4H^2 + 2K)) + \mathcal{O}(\phi^3).$$

We now look at the denominator. We write out

$$\frac{1}{\mathbf{m} \cdot \mathbf{C}_\phi \mathbf{m}} = \frac{1}{C_{\mathbf{m}}[\mathbf{y}]} \frac{1}{1 - 2\phi C_{\mathbb{II}}[\mathbf{y}] C_{\mathbf{m}}[\mathbf{y}]^{-1} + \phi^2 C_{\mathbb{III}}[\mathbf{y}] C_{\mathbf{m}}[\mathbf{y}]^{-1}},$$

With use of the expansion $\frac{1}{1+x} = 1 - x + x^2 + \mathcal{O}(x^3)$ for $|x| < 1$, we write the above equality as

$$\frac{1}{\mathbf{m} \cdot \mathbf{C}_\phi \mathbf{m}} = \frac{1}{C_{\mathbf{m}}[\mathbf{y}]} \Big(1 + 2\phi C_{\mathbb{II}}[\mathbf{y}] C_{\mathbf{m}}[\mathbf{y}]^{-1} - \phi^2 \phi C_{\mathbb{III}}[\mathbf{y}] C_{\mathbf{m}}[-1] + 4\phi^2 C_{\mathbb{II}}[\mathbf{y}]^2 C_{\mathbf{m}}[\mathbf{y}]^{-2}\Big) + \mathcal{O}(\phi^3).$$

Note that this expansion is valid for sufficiently small thickness t. Dividing $\mathbf{m} \cdot \mathbf{C}_\phi \mathbf{m}$ from $\det \mathbf{C}_\phi$ yields

$$\frac{\det \mathbf{C}_\phi}{\mathbf{m} \cdot \mathbf{C}_\phi \mathbf{m}} = \frac{J[\mathbf{y}]}{C_{\mathbf{m}}[\mathbf{y}]} A. \tag{3.89}$$

where

$$A = 1 + \phi(4H + 2C_{\mathbb{II}}[\mathbf{y}] C_{\mathbf{m}}[\mathbf{y}]^{-1})$$
$$+ \phi^2(8HC_{\mathbb{II}}[\mathbf{y}] - C_{\mathbb{III}}[\mathbf{y}] C_{\mathbf{m}}[\mathbf{y}]^{-1} + (4H^2 + 2K) + 4C_{\mathbb{II}}[\mathbf{y}]^2 C_{\mathbf{m}}[\mathbf{y}]^{-2}).$$

Inserting (3.87), (3.88), and (3.89) into (3.86), we have the expansion of W_{3D} in terms of ϕ:

$$W_{3D}(\mathbf{x}', \nabla\mathbf{u}) = \lambda(\partial_3\phi)^2 + \frac{\lambda}{s+1}\Bigg[\mathrm{tr}\mathrm{I}[\mathbf{y}] - 2\phi\mathrm{tr}\mathrm{II}[\mathbf{y}] + \phi^2\mathrm{tr}\mathrm{III}[\mathbf{y}] + s_0 C_{\mathbf{m}}[\mathbf{y}] - 2\phi s_0 C_{\mathrm{II}}[\mathbf{y}] + \phi^2 s_0 C_{\mathrm{III}}[\mathbf{y}] + s\frac{J[\mathbf{y}]}{C_{\mathbf{m}}[\mathbf{y}]}A\Bigg] - 3 + O(x_3^3). \tag{3.90}$$

We now collect the $\mathcal{O}(x_3^2)$ terms for $W_{3D}(\mathbf{x}', \nabla\mathbf{u})$ to derive the bending energy. To do this, we replace powers of ϕ or $\partial_3\phi$ with their respective $\mathcal{O}(x_3^2)$ term. Hence, we replace $(\partial_3\phi)^2$ with $(6\alpha\gamma + 4\beta^2)$, ϕ with β, and ϕ^2 is α^2 in (3.90) to deduce the bending energy density

$$W_{bend}(\mathbf{x}', \nabla\mathbf{y}, D^2\mathbf{y}) = \lambda(6\alpha\gamma + 4\beta^2) + \frac{\lambda}{s+1}\left[-2\beta(\mathrm{tr}\mathrm{II}[\mathbf{y}] + s_0 C_{\mathrm{II}}[\mathbf{y}]) + \alpha^2(\mathrm{tr}\mathrm{III}[\mathbf{y}] + s_0 C_{\mathrm{III}}[\mathbf{y}]) + s\frac{J[\mathbf{y}]}{C_{\mathbf{m}}[\mathbf{y}]}A\right], \tag{3.91}$$

where A now reads:

$$A = \beta(4H + 2C_{\mathrm{II}}[\mathbf{y}]C_{\mathbf{m}}[\mathbf{y}]^{-1}) + \alpha^2\Big(8HC_{\mathrm{II}}[\mathbf{y}]C_{\mathbf{m}}[\mathbf{y}]^{-1} - C_{\mathrm{III}}[\mathbf{y}]C_{\mathbf{m}}[\mathbf{y}]^{-1} + (4H^2 + 2K) + 4C_{\mathrm{II}}[\mathbf{y}]^2 C_{\mathbf{m}}[\mathbf{y}]^{-2}\Big).$$

Utilizing the expressions of β, γ in (3.83) and (3.84), we have that A simplifies to

$$A = \alpha^2\Big((-2HC_{\mathrm{II}}[\mathbf{y}]C_{\mathbf{m}}[\mathbf{y}]^{-1}) + 8HC_{\mathrm{II}}[\mathbf{y}]C_{\mathbf{m}}[\mathbf{y}]^{-1} - C_{\mathrm{III}}[\mathbf{y}]C_{\mathbf{m}}[\mathbf{y}]^{-1} + 2K + 4C_{\mathrm{II}}[\mathbf{y}]^2 C_{\mathbf{m}}[\mathbf{y}]^{-2}\Big).$$

Applying Lemma 3.1 (Second and third fundamental form relations), we have $C_{\mathrm{III}}[\mathbf{y}] = -2HC_{\mathrm{II}}[\mathbf{y}] - KC_{\mathbf{m}}[\mathbf{y}]$ and may further simplify

$$A = \alpha^2(8HC_{\mathrm{II}}[\mathbf{y}]C_{\mathbf{m}}[\mathbf{y}]^{-1} + 3K + 4C_{\mathrm{II}}[\mathbf{y}]^2C_{\mathbf{m}}[\mathbf{y}]^{-2}). \tag{3.92}$$

We now use the expressions of β, γ in (3.83) and (3.84) to obtain

$$(6\alpha\gamma + 4\beta^2) = \alpha^4(16H^2 - 2K). \tag{3.93}$$

Using the equality $\mathrm{III}[\mathbf{y}] = -2H\mathrm{II}[\mathbf{y}] - K\mathrm{I}[\mathbf{y}]$ from Lemma 3.1 (second and third fundamental form relations) and the expressions of β, γ in (3.83) and (3.84), we simplify

$$\alpha^2\left(\mathrm{tr}\mathrm{III}[\mathbf{y}] + s_0C_{\mathrm{III}}[\mathbf{y}]) - 2\beta(\mathrm{tr}\mathrm{II}[\mathbf{y}] + s_0C_{\mathrm{II}}[\mathbf{y}]\right) = -K\alpha^2\left[\mathrm{tr}\mathrm{I}[\mathbf{y}] + s_0C_{\mathbf{m}}[\mathbf{y}]\right]. \tag{3.94}$$

We use the fact that $\lambda\alpha^2 = 1$ and insert (3.92), (3.93), and (3.94) into (3.91) to obtain the final form of the bending energy density:

$$\begin{aligned} W_{bend}(\mathbf{x}', \nabla\mathbf{y}, D^2\mathbf{y}) = \frac{(16H^2 - 2K)}{J[\mathbf{y}]} + \frac{1}{s+1}\Bigg[&- K\mathrm{tr}\mathrm{I}[\mathbf{y}] - s_0KC_{\mathbf{m}}[\mathbf{y}] \\ &+ s\frac{\det \mathrm{I}[\mathbf{y}]}{C_{\mathbf{m}}[\mathbf{y}]}\left(8H\frac{C_{\mathrm{II}}[\mathbf{y}]}{C_{\mathbf{m}}[\mathbf{y}]} + 4\frac{C_{\mathrm{II}}[\mathbf{y}]^2}{C_{\mathbf{m}}[\mathbf{y}]^2} + 3K\right)\Bigg]. \end{aligned} \tag{3.95}$$

3.4.6 Final bending energy

We integrate the energy in the x_3 direction and use $\int_{-t/2}^{t/2} x_3^2 dx_3 = \frac{1}{12}$ to derive the final bending energy

$$E_{bend}[\mathbf{y}] = \frac{1}{12} \int_\Omega W_{bend}(\mathbf{x}', \nabla \mathbf{y}, D^2 \mathbf{y}) d\mathbf{x}' \tag{3.96}$$

We shall now do some comparison with [98]. Note that if we enforce an inextensibility assumption, $J[\mathbf{y}] = 1$, then the energy (3.96) coincides with the energy of [98, Eq (74)]. The bending energy (3.96) is slightly more realistic than [98, Eq (74)], we refer to Section 3.2.1.6 for more discussion.

Further suppose that $\mathbf{y}$ satisfies $E_{str}[\mathbf{y}] = 0$. Then, $\mathrm{I}[\mathbf{y}] = g$ due to Corollary 3.4 (immersions of g are minimizers with vanishing energy). The bending energy then simplifies to

$$E_{bend}[\mathbf{y}] = \frac{1}{12} \int_\Omega \frac{16H^2}{J[\mathbf{y}]} + \frac{s}{s+1} \frac{J[\mathbf{y}]}{C_{\mathbf{m}}[\mathbf{y}]} \left(8H \frac{C_{\mathrm{II}}[\mathbf{y}]}{C_{\mathbf{m}}[\mathbf{y}]} + 4 \frac{C_{\mathrm{II}}[\mathbf{y}]^2}{C_{\mathbf{m}}[\mathbf{y}]^2} \right) d\mathbf{x}' + C(g)$$

where $C(g)$ is a constant that only depends on the metric g. Note that the Gauss curvature K only depends on g due to Gauss's Theorema Egregium [60, Ch. 4-3].

An important point to make is that often the bending energy can be rewritten as quadratic in the Hessian rather than a quadratic in terms of the second fundamental form. Suppose we further simplify the energy to the case $s = 0$. We also have $J[\mathbf{y}] = \lambda$, and the bending energy reduces to

$$E_{bend}[\mathbf{y}] = \frac{4}{3\lambda} \int_\Omega H^2 d\mathbf{x}' = \frac{4}{3\lambda} \int_\Omega \mathrm{tr}(g^{-1/2} \mathrm{II}[\mathbf{y}] g^{-1/2})^2 d\mathbf{x}'$$

which is special case of the energy found in prestrained plates [27, 30]. Due to work done in [30, Proposition 1], we may write

$$E_{bend}[\mathbf{y}] = \frac{4}{3\lambda}\int_{\Omega} \mathrm{tr}(g^{-1/2}\mathrm{I\!I}[\mathbf{y}]g^{-1/2})^2 d\mathbf{x}' = \frac{4}{3\lambda}\int_{\Omega} |\mathrm{tr}(g^{-1/2}D^2\mathbf{y}g^{-1/2})|^2 d\mathbf{x}' + C(g)$$

where $C(g)$ is again a constant that depends on g and its derivatives. We point to similar results in the case of bending energies for isometries [14] as well as shells [105]. This simplification is important because it means that we should expect the bending energy to behave like a quadratic function of $D^2\mathbf{y}$, which motivates the choice of regularization in the numerics in Chapter 4. This rewriting of the bending energy also makes numerics for a bending energy more tractable, but we leave numerics for the bending energy for future study.

Chapter 4: Numerical Analysis of Thin Liquid Crystal Polymeric Networks

The concern of this chapter is to develop a numerical method to solve the membrane problem of LCNs. Recall from Corollary 3.4 (immersions of g are minimizers with vanishing energy), that $E_{str}[\mathbf{y}] = 0$ if and only if $\mathbf{y}$ is an isometric immersion of g, namely $\mathrm{I}[\mathbf{y}] = g$ a.e. in Ω. Most of the attention in the physics literature has focused on satisfying this metric condition to predict shapes of LCNs [4, 91, 92, 93, 94, 100, 101, 103, 118, 119]. However, as we saw in Section 3.3, constructing an exact solution for more complicated metrics, like those arising from higher degree LC defects, can be quite difficult. Also, solving the metric condition exactly becomes even more difficult if the actuation parameter varies spatially. Finally, some metrics may not admit immersions, so the metric condition will not be a useful tool in predicting the shapes when actuated. These reasons suggest the need for numerical methods to solve the membrane problem, which we develop in this chapter.

Computation of LCEs/LCNs have received some attention. Publications include computations of various membrane models [103], a membrane model with regularization [47], a bending model of LCE bilayer structure [22], a relevant 2D model for LCEs [87], 3D models [46, 52], and LCE rods [21]. Literature involving numerical analysis is limited, to the best of our knowledge. Paper [87] proves well-posedness of a mixed method for a 2D model with Frank-Oseen regularization.

An outline and highlight of the contributions of this chapter are as follows.The main contribution of this chapter is a new finite element method for solving a membrane model of LCNs presented in Chapter 3.

- In Section 4.1, we recall the membrane model developed in Section 3.2. We also prove lack of quasiconvexity in Section 4.1.1, which motivates the need for regularization.

- Section 4.2 presents the FEM. The key is to add a regularization that is inspired by the bending energy derived in Chapter 3. This regularization circumvents the quasiconvexity issues presented in Section 4.1.1.

- In Section 4.3, we present a convergence analysis of the numerical method inspired by the seminal work [66]. In particular, we prove that a subsequence of minimizers of the discrete energy converges to minimizers of the continuous energy in the framework of Γ-convergence. The main result is Theorem 4.1. We also note that the proof of this result is technical, and the main challenge lies in the construction of the recovery sequence. In particular, the recovery sequence needs to remain bounded away from a singularity in the energy. To meet this challenge, we employ a Lusin truncation argument and prove additional results needed for the construction in Lemmas 4.2, 4.3, and 4.5.

- In Section 4.4, we discuss how to introduce folds or creases into the numerical model. This section is motivated by previous works on folding [18] and [20]. For physical applications, the motivation comes from nonisometric origami [100, 101, 102].

- In Section 4.4 we present a gradient flow iteration with Newton sub-iteration to solve for critical points of the discrete energy. We prove various properties of the Newton sub-iteration.

4.1 Problem statement: a membrane model

The focus of this chapter is on solving the $2D$ membrane model of LCNs introduced in Section 3.2. We now recall the membrane model as well as relevant parameters.

The $2D$ membrane model consists of the following formal minimization problem: find $\mathbf{y}^* \in H^1(\Omega; \mathbb{R}^3)$ such that

$$\mathbf{y}^* \in \operatorname{argmin}_{\mathbf{y} \in H^1(\Omega;\mathbb{R}^3)} E_{str}[\mathbf{y}], \quad E_{str}[\mathbf{y}] := \int_\Omega W_{str}(\mathbf{x}, \nabla \mathbf{y}) d\mathbf{x}. \tag{4.1}$$

Recall the stretching energy density W_{str} is only a function of $\mathbf{x} \in \Omega$ and the first fundamental form $\mathrm{I}[\mathbf{y}] := \nabla \mathbf{y}^T \nabla \mathbf{y}$ of the surface $\mathbf{y}(\Omega)$ and is given by

$$W_{str}(\mathbf{x}, \nabla \mathbf{y}) = \lambda \left[\frac{1}{J[\mathbf{y}]} + \frac{1}{s+1} \left(\operatorname{tr}(\mathrm{I}[\mathbf{y}]) + s_0 C_{\mathbf{m}}[\mathbf{y}] + s \frac{J[\mathbf{y}]}{C_{\mathbf{m}}[\mathbf{y}]} \right) \right] - 3\,; \tag{4.2}$$

hereafter $J[\mathbf{y}], C_{\mathbf{m}}[\mathbf{y}]$ are among the following notational abbreviations:

$$J[\mathbf{y}] := \det \mathrm{I}[\mathbf{y}], \quad C_{\mathbf{m}}[\mathbf{y}] := \mathbf{m} \cdot \mathrm{I}[\mathbf{y}]\mathbf{m}, \quad C_{\mathbf{m}_\perp}[\mathbf{y}] := \mathbf{m}_\perp \cdot \mathrm{I}[\mathbf{y}]\mathbf{m}_\perp. \tag{4.3}$$

Note that if $J[\mathbf{y}], C_{\mathbf{m}}[\mathbf{y}]$ are bounded away from 0, then $\int_\Omega W_{str}(\mathbf{x}, \nabla \mathbf{y}) d\mathbf{x}$ is finite. If the second argument of W_{str} is a generic matrix $\mathbf{F} \in \mathbb{R}^{3\times 2}$ instead, then we define $\mathrm{I}(\mathbf{F})$, $J(\mathbf{F})$, $C_{\mathbf{m}}(\mathbf{F})$, and $C_{\mathbf{m}_\perp}(\mathbf{F})$ similarly as

$$\begin{aligned} \mathrm{I}(\mathbf{F}) = \mathbf{F}^T\mathbf{F}, \quad J(\mathbf{F}) = \det \mathrm{I}(\mathbf{F})\,, \\ C_{\mathbf{m}}(\mathbf{F}) = \mathbf{m} \cdot \mathrm{I}(\mathbf{F})\mathbf{m}, \quad C_{\mathbf{m}_\perp}(\mathbf{F}) = \mathbf{m}_\perp \cdot \mathrm{I}(\mathbf{F})\mathbf{m}_\perp\,. \end{aligned} \tag{4.4}$$

We observe that $J[\mathbf{y}]$ can be written in terms of $C_{\mathbf{m}}[\mathbf{y}], C_{\mathbf{m}_\perp}[\mathbf{y}]$ and $\partial_1\mathbf{y} \times \partial_2\mathbf{y}$ as

$$J[\mathbf{y}] = C_{\mathbf{m}}[\mathbf{y}]C_{\mathbf{m}_\perp}[\mathbf{y}] - (\mathbf{m}_\perp \cdot \mathrm{I}[\mathbf{y}]\mathbf{m})^2\,, \tag{4.5}$$

$$J[\mathbf{y}] = |\partial_1\mathbf{y} \times \partial_2\mathbf{y}|^2. \tag{4.6}$$

We note that (4.2) is consistent with the stretching energy in [98] after additionally assuming an inextensibility constraint $J[\mathbf{y}] = 1$ and incorporating the multiplicative parameter λ and the constant -3.

Throughout this chapter, we do not impose any boundary condition so that the materials under consideration have *free boundaries*. If necessary, one can take Dirichlet boundary conditions into account with a simple modification on theories and simulations. Moreover, $s_0, s \in L^\infty(\Omega)$ are nematic order parameters that refer to the *reference* configuration and *deformed* configuration respectively. These parameters are typically constant in time and depend on temperature, but may vary in Ω if the liquid crystal polymers are actuated non-uniformly by a light source. Their physical range is $s_0, s > -1$ and s_0, s are bounded away from -1 i.e.

$$\mathrm{essinf}_{x\in\Omega} s_0(x) > -1, \quad \mathrm{essinf}_{x\in\Omega} s(x) > -1\,. \tag{4.7}$$

The actuation parameter of the model is

$$\lambda = \lambda_{s,s_0} = \sqrt[3]{\frac{s+1}{s_0+1}}\,. \tag{4.8}$$

If the material is heated, then $\lambda < 1$. Likewise, if cooled, then $\lambda > 1$. For s, s_0 non-constant, the assumption on s, s_0 in (4.7) implies that $\lambda : \Omega \to \mathbb{R}$ satisfies

$$0 < \mathrm{essinf}_{x\in\Omega}\lambda(x) \leq \mathrm{esssup}_{x\in\Omega}\lambda(x) < \infty. \tag{4.9}$$

The energy density (4.2) lacks convexity, which raises the question of the actual meaning of a minimizer $\mathbf{y}^* \in H^1(\Omega; \mathbb{R}^3)$ in (4.1). It also presents the main difficulty for discretization, convergence analysis, and design of efficient iterative solvers for the discrete minimization problem.

4.1.1 Challenges: lack of convexity

The lack of convexity of the stretching energy (4.2) translates into lack of weak lower semicontinuity of (4.2) and prevents one from using the direct method of calculus of variations to prove the existence of minimizers, and is also responsible for serious computational challenges.

To stress the importance of convexity or lack there-of, we present a modification of a classical 1D example known as the Bolza example [55, Example 4.8]; see also [11, Example 2.1]. We next extend this situation to 2D.

Example 4.1. We consider the double well energy defined on $W_0^{1,4}((0,1))$

$$E_{1D}[u] = \int_0^1 ((u')^2 - 1)^2 + cu^2 d\mathbf{x}, \tag{4.10}$$

with some nonnegative c, and define a sequence of sawtooth functions starting with

$$u_1(x) = \begin{cases} x, & x < \frac{1}{2} \\ 1 - x, & x \geq \frac{1}{2}. \end{cases}$$

To construct u_2, we subdivide the intervals $[0, 1/2]$ and $[1/2, 1]$ into $[0, 1/4]$, $[1/4, 1/2]$ and $[1/2, 3/4]$, $[3/4, 1]$ and then alternating the derivative between ± 1 on the 4 subintervals. The function u_2 is a sawtooth with derivative of ± 1 and maximum height $\frac{1}{4}$. Given u_n, we do the same subdividing procedure to get a u_{n+1} to get a sawtooth of height $\frac{1}{2^{n+1}}$. The resulting sequence consists of u_n that satisfy $|u_n'(x)| = 1$. The first few elements are plotted in Figure 4.1. The sequence $u_n \rightharpoonup 0$ in $W^{1,4}((0,1))$, but

$$0 = \lim_{n \to \infty} E_{1D}[u_n] < E_{1D}[0] = 1$$

Thus, the energy E_{1D} is not weakly lower semicontinuous on $W^{1,4}$, and if $c > 0$ the direct method of the calculus of variations would fail to provide the existence of a minimizer. If $c = 0$, then any u_n is a minimizer to E_{1D} over $W^{1,4}$.

Figure 4.1: Example 4.1: First four elements u_n of the minimizing sequence of (4.10).

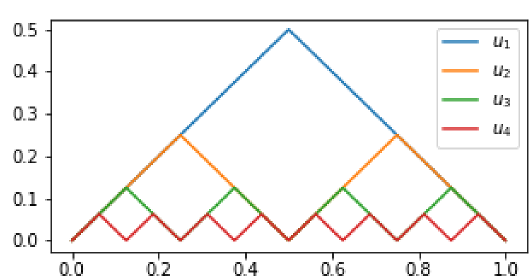

On the discrete level, the above example is also important, because the lack of convexity means that a standard weak compactness result in H^1 will not be enough to prove convergence of minimizers. We shall see in Proposition 4.1 that the stretching energy does not satisfy the relevant convexity condition for us to expect weak lower semicontinuity. To illustrate this point, we present an example of some minimizers to E that extends Example 4.1 to 2D. The first element of the sequence of minimizers is a pyramid from [92]. We later display several pyramid configurations in Section 5.3.1 computed with our FEM.

Example 4.2. Let $\Omega = [-1,1]^2$ and let $\mathbf{m}$ be the blueprinted director field depicted in Figure 4.2(a) and let $\mathbf{y}_1$ be the solution in Figure 4.2(b) with $\lambda < 1$. The surface $\mathbf{y}_1(\Omega)$ is a square pyramid with base width 2λ and height $\sqrt{\lambda^{-1} - \lambda^2}$, and first fundamental form $\mathrm{I}[\mathbf{y}] = g$ with target metric g given by (3.42). We can mimic the subdivision procedure of Example 4.1 to produce a sequence $\mathbf{y}_n$ such that $\mathrm{I}[\mathbf{y}_n] = g$, and $\mathbf{y}_n \rightharpoonup \mathbf{y}^*$ in $H^1(\Omega;\mathbb{R}^3)$, where $\mathbf{y}^*(x) = (\lambda x_1, \lambda x_2, 0)$. The first three elements of the sequence are displayed in Figure 4.3. Since $\mathrm{I}[\mathbf{y}_n] = g$, we deduce $E[\mathbf{y}_n] = 0$ for all n, according to Corollary 3.4 (immersions of g are minimizers). Moreover, $\mathrm{I}[\mathbf{y}^*] = \lambda^2\mathbf{I} \neq g$ a.e. in Ω because $\lambda \neq 1$. Inserting $\nabla\mathbf{y}^*$ into W_{str} yields $W_{str}(\mathbf{x}, \nabla\mathbf{y}^*) > 0$ a.e. in Ω due to Proposition 3.3 (target metric), whence

$$\liminf_{n\to\infty} E[\mathbf{y}_n] = 0 < E[\mathbf{y}^*].$$

We thus conclude that E is not weakly lower semicontinuous in $H^1(\Omega;\mathbb{R}^3)$.

Figure 4.2: Example 4.2: Blueprinted director field $\mathbf{m}$ and pyramid surface $\mathbf{y}_1(\Omega)$ for $\lambda = \frac{1}{2}$ from [92].

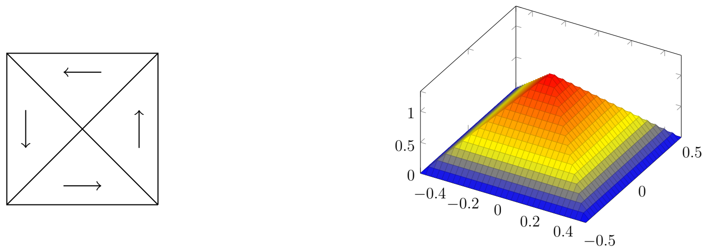

Figure 4.3: Example 4.2: First three elements $\mathbf{y}_n(\Omega)$ of a minimizing sequence with foldings on dyadic squares concentric with Ω.

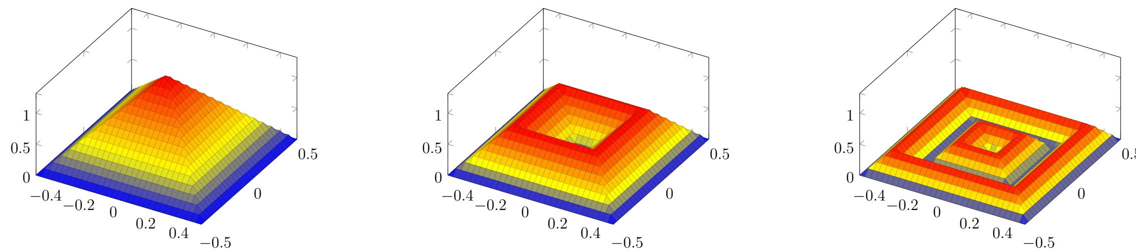

The notions of quasiconvexity and rank-one convexity, defined next, are relevant in this context. We refer to the book [55] for background on this topic. The first concept is quasiconvexity [55, Def. 1.5(ii)].

Definition 4.1 (quasiconvexity). *A function $f : \mathbb{R}^{m\times n} \to \mathbb{R}$ is quasiconvex if*

$$f(\mathbf{F}) \leq \inf_{\phi \in W_0^{1,\infty}((0,1)^n;\mathbb{R}^m)} \int_{(0,1)^n} f(\mathbf{F} + \nabla\phi(z))dz,$$

for all $\mathbf{F} \in \mathbb{R}^{m\times n}$.

The intuition behind the above definition is that one cannot decrease the energy by adding laminations, which are Lipschitz perturbations $\phi \in W_0^{1,\infty}((0,1)^2;\mathbb{R}^3)$ in our case. Going back to

Example 4.1, we can see that if $f_{1D}(p) = (p^2 - 1)^2$, then adding u_n' to 0 decreases the energy

$$f_{1D}(0) = 1 > 0 = \int_{(0,1)} f_{1D}(u_n'(z))dz \geq \inf_{\phi \in W_0^{1,\infty}((0,1),\mathbb{R})} \int_{(0,1)} f_{1D}(0 + \nabla\phi(z))dz.$$

Hence, f_{1D} is not quasiconvex. This is in fact obvious because for $f : \mathbb{R} \to \mathbb{R}$, convexity and quasiconvexity are equivalent [55, Theorem 1.7(ii)].

The notion of rank-one convexity is weaker than quasiconvexity [55, Def. 1.5(i)].

Definition 4.2 (rank-one convexity)**.** *A function $f : \mathbb{R}^{m\times n} \to \mathbb{R}$ is rank-one convex if*

$$z \mapsto f(\mathbf{F} + z\mathbf{a} \otimes \mathbf{c})$$

is convex for all $\mathbf{F} \in \mathbb{R}^{m\times n}$, $\mathbf{a} \in \mathbb{R}^m$, $\mathbf{c} \in \mathbb{R}^n$ and $z \in \mathbb{R}$.

For real-valued $f : \mathbb{R}^{m\times n} \to \mathbb{R}$, quasiconvexity implies rank-one convexity [55, Thm 1.7(i)]. We show next that the stretching energy density found in (4.2) is not rank-one convex. An intuition behind is as follows. A necessary condition for a piecewise affine map to be continuous is that the gradient is rank-one connected across the folds ($\mathbf{F}_1, \mathbf{F}_2 \in \mathbb{R}^{m\times n}$ are rank-one connected if $\operatorname{rank}(\mathbf{F}_1 - \mathbf{F}_2) = 1$). If an energy is not rank-one convex, then we can make a fold preserving continuity and without increasing the energy. In Example 4.2, $\nabla\mathbf{y}_n$ is rank-one connected across folds.

Proposition 4.1 (lack of rank-one convexity)**.** *Let $s, s_0 > -1$ and fix $\mathbf{x} \in \Omega$. Then there exists a $\mathbf{F} \in \mathbb{R}^{3\times 2}$ and rank-one perturbation $\mathbf{a} \otimes \mathbf{c}$ such that*

$$z \mapsto W_{str}(\mathbf{x}, \mathbf{F} + z\mathbf{a} \otimes \mathbf{c})$$

is not convex at $z = 0$.

Proof. Let $\mathbf{F} \in \mathbb{R}^{3\times 2}$ be so that $\mathbf{F}^T\mathbf{F} = \mu^2 \mathbf{m}\otimes\mathbf{m} + \frac{1}{\mu^2}\mathbf{m}_\perp \otimes \mathbf{m}_\perp = \mathbf{A}_\mu$ for some μ to be determined later. Let $\mathbf{a} \in \mathbb{R}^3$ be a unit vector orthogonal to the range of $\mathbf{F}$. Then, the rank-one perturbation $\widehat{\mathbf{F}} = \mathbf{F} + z\mathbf{a}\otimes\mathbf{m}$ of $\mathbf{F}$ satisfies

$$\begin{aligned}\mathrm{I}(\widehat{\mathbf{F}}) = \widehat{\mathbf{F}}^T\widehat{\mathbf{F}} = \mathbf{F}^T\mathbf{F} + z^2\mathbf{m}\otimes\mathbf{m} = \mathbf{A}_\mu + z^2\mathbf{m}\otimes\mathbf{m} \\ = \mathbf{A}_\mu\left(\mathbf{I}_2 + z^2\mathbf{A}_\mu^{-1}\mathbf{m}\otimes\mathbf{m}\right) = \mathbf{A}_\mu\left(\mathbf{I}_2 + \frac{z^2}{\mu^2}\mathbf{m}\otimes\mathbf{m}\right).\end{aligned}$$

Since the eigenpairs of this rank-one perturbation of identity are $(1, \mathbf{m}_\perp)$ and $(1 + \frac{z^2}{\mu^2}, \mathbf{m})$, its determinant reads $\det\left(\mathbf{I}_2 + \frac{z^2}{\mu^2}\mathbf{m}\otimes\mathbf{m}\right) = 1 + \frac{z^2}{\mu^2}$, whence $J(\widehat{\mathbf{F}}) = (\det\mathbf{A}_\mu)(1 + \frac{z^2}{\mu^2}) = 1 + \frac{z^2}{\mu^2}$. Inserting this into the stretching energy (4.2) gives

$$W_{str}(\mathbf{x}, \widehat{\mathbf{F}}) = \lambda\left[\frac{1}{1+\frac{z^2}{\mu^2}} + \frac{s_0+1}{s+1}z^2 + \frac{s_0+1}{s+1}\mu^2 + \frac{1}{\mu^2}\right] - 3$$

which as a function of z reads equivalently

$$W_{str}(\mathbf{x}, \mathbf{F} + z\mathbf{a}\otimes\mathbf{m}) = \lambda\left(\frac{1}{1+\frac{z^2}{\mu^2}} + \frac{s_0+1}{s+1}z^2\right) + C_{s,s_0,\mu},$$

with a constant $C_{s,s_0,\mu}$ that depends on s, s_0, and μ. Computing the second derivative with respect to z, we have

$$\frac{d^2}{dz^2}W_{str}(\mathbf{x}, \mathbf{F} + z\mathbf{a}\otimes\mathbf{m}) = \lambda\left[\frac{8z^2}{\mu^4(1+z^2/\mu^2)^3} - \frac{2}{\mu^2(1+z^2/\mu^2)^2} + 2\frac{s_0+1}{s+1}\right].$$

Evaluating at $z = 0$, yields

$$\frac{d^2}{dz^2} W_{str}(\mathbf{x}, \mathbf{F} + z\mathbf{a} \otimes \mathbf{m})\Big|_{z=0} = 2\lambda \left[\frac{s_0 + 1}{s + 1} - \frac{1}{\mu^2} \right].$$

Taking μ sufficiently small ensures that $\frac{d^2}{dz^2} W_{str}(\mathbf{x}, \mathbf{F} + z\mathbf{a} \otimes \mathbf{m})\big|_{z=0} < 0$, which means that $z \mapsto W_{str}(\mathbf{x}, \mathbf{F} + z\mathbf{a} \otimes \mathbf{m})$ is not convex at $z = 0$, as asserted. □

4.1.2 Strategies to deal with lack of convexity

In this section, we discuss two strategies to deal with the lack of convexity and the literature related to LCEs/LCNs. For an introduction on numerics for nonconvex variational problems, we refer to [15, Chapter 9]. The first strategy consists of computing the quasiconvex envelope of the energy density. For nonnegative, Borel measurable, and locally bounded $f : \mathbb{R}^{m \times n} \to \mathbb{R}$, the quasiconvex envelope can be expressed as follows using [55, Theorem 1.9]:

$$f^{qc}(\mathbf{F}) = \inf_{\phi \in W_0^{1,\infty}((0,1)^n;\mathbb{R}^m)} \int_{(0,1)^n} f(\mathbf{F} + \nabla \phi(z)) dz. \tag{4.11}$$

Note that this formula is the right hand side of Definition 4.1. The integral of the quasiconvex envelope f^{qc} is sometimes the relaxed or effective energy. For a 1D energy, the procedure reduces to computing the convex envelope. In Example 4.1 without the lower order term, the weak limit of u_n is 0 and turns out to be a minimizer of the relaxed energy. For 1D problems, working with the convex envelope fixes the weak lower semicontinuity issue. In the context of LCNs/LCEs, the authors of [44, 59] derive explicit expressions of quasiconvex envelopes, which is a rare occurrence. If the quasiconvex envelope is not known, then approximating the rank-one convex envelope might be an alternative; we point to [54] for work on approximating rank-1 convex envelopes with applications in LCNs/LCEs.

There are advantages to work with the quasiconvex envelope. The first one is that it can be derived as the rigorous mathematical limit in a Γ-convergence dimension reduction theory. For example, if $s = s_0 = 0$, recall that W_{3D} reduces to $W_{3D}^H(\mathbf{F}) = |\mathbf{F}|^2 - 3$, and the rigorous Γ-convergence theory [53, Theorem 2.4] applies: the ensuing Γ-limit of $\frac{1}{t}E_{3D,t}$ is the quasiconvex envelope of

$$W_{2D}^H(\mathbf{F}') = \frac{1}{\det \mathbf{F}'^T\mathbf{F}'} + |\mathbf{F}'|^2 - 3,$$

where $\mathbf{F}' \in \mathbb{R}^{3\times 2}$; see also [44] for another example. We also refer to classical works [83, 84], which are membrane theories without the constraint of incompressibility in 3D and also result in the Γ-limit being a quasiconvex envelope. Moreover, dealing with the relaxed energy is preferable in some physically relevant situations, such as the study of microstructures. One such situation is a stretched sheet experiment [82], which was also studied in [52].

On the other hand, computing with the quasiconvex envelope presents several disadvantages. First, it is difficult to derive explicit expressions for quasiconvex envelopes, especially when the energy is anisotropic, such as the stretching energy in (4.2); the energies studied by [44, 52, 59] were all isotropic. We refer to the book [55], which covers known strategies for computing quasiconvex envelopes. Another issue is that there may be many minimizers to the relaxed energy. In Example 4.1, without boundary conditions and lower order terms, any $u : (0, 1) \to \mathbb{R}$ whose derivative satisfies $u'(x) \in [-1, 1]$ for a.e. $x \in (0, 1)$ would be a minimizer to the *relaxed energy*. Existence of many minimizers may occur in higher dimensions as well. For the stretching energy (4.2), we expect that the zero level set of relaxed energy density would be *short maps*, i.e. $\mathbf{y} \in H^1(\Omega;\mathbb{R}^3)$ such that $g - \mathrm{I}[\mathbf{y}] \geq 0$ is positive semidefinite. Our conjecture is motivated by the results of [83, 104]. If short maps are minimizers to the relaxed problem, then the weak limit of $\mathbf{y}_n \rightharpoonup \mathbf{y}^*$ from Example 4.2 would be a minimizer to the relaxed problem.

Afterall, our interest in this chapter is in the shapes and configurations that LCNs can produce rather than in microstructures. One example is the experimental work [88], which studies the configurations that arise from liquid crystal defects. As a result, we employ the second possible strategy, which is *regularization.*

In Example 4.1, regularizing would entail adding the term $\varepsilon|u''|^2$ to the energy. For $\varepsilon > 0$ fixed, the regularization would gain additional compactness, and a minimizing sequence would converge strongly in $W^{1,4}((0,1))$, thereby bypassing the lack of convexity of the double well. The model of [47] utilizes the regularized energy

$$\int_\Omega W_{str}(\mathbf{x}, \nabla\mathbf{y}) + \varepsilon|\operatorname{div}\nabla\mathbf{y}|^2,$$

where $\varepsilon > 0$ is a positive fixed constant. This is a dimensionally reduced model from the 3D model of [25], which incorporates a Hessian term to the energy.

We are interested in the membrane model and would like to recover the target metric in the limit. We consider the regularized energy

$$E_\varepsilon[\mathbf{y}] = E_{str}[\mathbf{y}] + \varepsilon\int_\Omega \left|D^2\mathbf{y}\right|^2, \tag{4.12}$$

where ε scales likes h^2. One may view this as analogous to a higher order bending term. This kind of energy blending is studied by [98]. An alternative approach from [111] develops a membrane theory from a 3D model with regularization term $\varepsilon|D^2\mathbf{u}|^2$ and studies the limit $\varepsilon \to 0$ as the thickness $t \to 0$.

Yet another physically motivated approach would be to consider a pure bending theory, where the nonconvexity lives inside the constraint. A recent example of a bending theory for LCEs is [22]. We also refer to works on prestrained plates for rigorous Γ-convergence theories [27, 85] and numerics [29, 30].

4.2 Discrete minimization problem

Let $\{\mathcal{T}_h\}_h$ be a shape regular sequence of triangulations with mesh size h. We denote by $\mathcal{E}_h$ the set of interior edges to of each triangulation, and by $\mathcal{N}_h$ the set of nodes of the triangulation. The space for discrete deformations consists of continuous piecewise linear functions:

$$\mathbb{V}_h := \{\mathbf{y}_h \in C^0(\Omega;\mathbb{R}^3) : \quad \mathbf{y}_h|_T \in \mathcal{P}_1 \quad \forall\, T \in \mathcal{T}_h\}. \tag{4.13}$$

We propose the regularized discrete energy $E_h : \mathbb{V}_h \to \mathbb{R}$ defined by

$$E_h[\mathbf{y}_h] = \int_\Omega W_{str}(\mathbf{x}, \nabla\mathbf{y}_h)\, d\mathbf{x} + R_h[\mathbf{y}_h] \tag{4.14}$$

where the regularization term

$$R_h[\mathbf{y}_h] := c_r h^2 \underbrace{\sum_{e\in\mathcal{E}_h} \frac{1}{h}\int_e |[\nabla\mathbf{y}_h]|^2}_{=|\mathbf{y}_h|^2_{H^2_h}} \tag{4.15}$$

is a rescaling of the DG discrete H^2-seminorm for continuous piecewise linear functions:

$$|\mathbf{y}_h|^2_{H^2_h} := \sum_{e\in\mathcal{E}_h} \frac{1}{h} \int_e |[\nabla \mathbf{y}_h]|^2, \tag{4.16}$$

and $c_r : \Omega \to \mathbb{R}^+$ is a non-negative *regularization* parameter of our choice. The notation $[\nabla \mathbf{y}_h]$ denotes the jump of $\nabla \mathbf{y}_h$ across edges $e \in \mathcal{E}_h$

$$[\nabla \mathbf{y}_h]\big|_e = \nabla \mathbf{y}_h^+ - \nabla \mathbf{y}_h^-, \tag{4.17}$$

where $\nabla \mathbf{y}_h^{\pm}(x) := \lim_{s\to 0} \nabla \mathbf{y}_h(x \pm s\mathbf{n}_e)$ and $\mathbf{n}_e$ is a unit normal vector to e (the choice of its direction is arbitrary but fixed).

We point out that, in the discontinuous Galerkin (DG) contexts (for instance [29, 49]), a discrete H^2 semi-norm is defined as

$$|\mathbf{y}_h|^2_{H^2_h(\Omega)} := \|D^2_h \mathbf{y}_h\|^2_{L^2(\Omega)} + \sum_{e\in\mathcal{E}_h} h_e^{-1} \|[\nabla \mathbf{y}_h]\|^2_{L^2(e)} + \sum_{e\in\mathcal{E}_h} h_e^{-3} \|[\mathbf{y}_h]\|^2_{L^2(e)}, \tag{4.18}$$

where D^2_h denotes a piecewise Hessian on every element. Substituting continuous piecewise affine $\mathbf{y}_h \in \mathbb{V}_h$ into (4.18), we can see that only the second term remains while other terms vanish, leaving us with (4.16). This motivates our choice (4.15) for the regularization term (4.15), which in fact further satisfies $R_h[\mathbf{y}_h] \approx h^2 |\mathbf{y}_h|^2_{H^2_h(\Omega)}$ provided c_r is uniformly positive and $\{\mathcal{T}_h\}_h$ is a quasi-uniform sequence of triangulations. We note that $|\mathbf{y}_h|^2_{H^2_h(\Omega)}$ scales oscillations of the elementwise constant $\nabla \mathbf{y}_h$ between adjacent elements of $\mathcal{T}_h$ for $\mathbf{y}_h \in \mathbb{V}_h$ and, consequently, can be viewed as a discrete approximation of the *Hessian* of $\mathbf{y}_h$.

To justify that (4.16) is indeed a discrete H^2-seminorm, we argue heuriscally as follows.

Since $\mathbf{y}_h$ is elementwise affine, we view $H_h[\mathbf{y}_h]|_e := \frac{[\nabla \mathbf{y}_h]|_e}{h}$ as a finite difference Hessian of $\mathbf{y}_h$. If one extends the definition of $H_h[\mathbf{y}_h]|_e$ to elements $T \in \mathcal{T}_h$ so that $e \subset \partial T$, the discrete nature of $H_h[\mathbf{y}_h]$ guarantees the validity of the inverse estimate $h \int_e \left|H_h[\mathbf{y}_h]\right|^2 \approx \int_T \left|H_h[\mathbf{y}_h]\right|^2$ and results in the equivalence

$$
\begin{aligned}
|\mathbf{y}_h|^2_{H^2_h(\Omega)} &= \sum_{e\in\mathcal{E}_h} \frac{1}{h}\int_e |[\nabla \mathbf{y}_h]|^2 = \sum_{e\in\mathcal{E}_h} h^2 \frac{1}{h}\int_e \left|\frac{[\nabla \mathbf{y}_h]}{h}\right|^2 \\
&= \sum_{e\in\mathcal{E}_h} h \int_e \left|H_h[\mathbf{y}_h]\right|^2 \approx \sum_{T\in\mathcal{T}_h} \int_T \left|H_h[\mathbf{y}_h]\right|^2 = \int_\Omega \left|H_h[\mathbf{y}_h]\right|^2.
\end{aligned}
$$

The regularization term $h^2 \int_\Omega \left|H_h[\mathbf{y}_h]\right|^2$ thus mimics the higher order bending energy (4.12) where h is proportional to the thickness of a thin 3D body.

We emphasize that a full model of LCNs is a blending of stretching energy and bending energy, which comes from higher order terms in the thickness t in the expansion (3.23) [22, 98, 102, 121]. This leads to a bending energy that incorporates the second fundamental form $\mathrm{I\!I}[\mathbf{y}]$, and thus to a nonlinear combination of second order derivatives of the deformations $\mathbf{y}$. Ideally, one is able to express this energy in terms of the Hessian of $\mathbf{y}$ [15, 19, 29, 31]. In the context of piecewise affine deformations $\mathbf{y}_h \in \mathbb{V}_h$, second order derivative information is contained in $|\mathbf{y}_h|_{H^2_h(\Omega)}$ and so in $R_h[\mathbf{y}_h]$. Therefore, for c_r uniformly positive and $\{\mathcal{T}_h\}_h$ quasi-uniform, one can compare $R_h[\mathbf{y}_h] \approx h^2|\mathbf{y}_h|^2_{H^2_h(\Omega)}$ with the scaled bending energy $t^2 E_{ben}[\mathbf{y}] := t^2\|D^2\mathbf{y}\|^2_{L^2(\Omega)}$, and realize that the meshsize parameter h plays a similar role to the thickness parameter t in the expansion of $\frac{1}{t}E_{3D}$ using (3.23) [22, 98, 102, 121]. Moreover, allowing c_r to vanish over a polygonal Γ made of edges of $\mathcal{E}_h$ mimics discretely a material amenable to folding across Γ [18, 20]. We prove convergence of minimizers of (4.1) over $\mathbb{V}_h$, including creases.

We regard (4.15) as a discrete regularization mechanism rather than a discrete form of the bending energy $E_{bend}[\mathbf{y}]$, even though such a simplified form of $E_{bend}[\mathbf{y}]$ has been considered widely in the literature; we refer for instance [47, 102]. The true bending energy [98, 102, 121] involves $\mathrm{I\!I}[\mathbf{y}]$ and its reduction to $D^2\mathbf{y}$ is a matter of current research. We leave the numerics for E_{bend} for a future study.

Moreover, we view (4.15) as a mechanism for equilibria selection. In the absence of regularization, i.e. $c_r = 0$ in (4.15), minimizers $\mathbf{y}_h^* \in \mathbb{V}_h$ of (4.1) can exhibit extra bumps and wrinkling which have negligible influence on the stretching energy. This is a manifestation of lack of convexity of W_{str}, and thus of uniqueness, and leads to the formation of micro-structure [15]. This topic is well studied in the theory and computation of nonlinear elasticity, but it is not the focus of this chapter. We invoke (4.15) to suppress numerical oscillations in Section 5.6 as well as to allow for folding in the development of compatible origami-structures in Section 5.3 and incompatible origami-structures in Section 5.4. The latter lead to weak limits $y^* \in H^1(\Omega; \mathbb{R}^3)$ with $E_{str}[\mathbf{y}^*] > 0$, so it is unclear whether they are minimizers of the stretching energy E_{str}.

Our next task is to solve the discrete counterpart of (4.1), namely

$$\mathbf{y}_h^* \in \mathrm{argmin}_{\mathbf{y}_h \in \mathbb{V}_h} E_h[\mathbf{y}_h]. \tag{4.19}$$

According to the discussions in Section 4.1.1, we can also expect lack of quasi-convexity in the first term of $E_h[\mathbf{y}_h]$ in (4.14). This feature brings the main difficulty to solve the discrete minimization problem (4.19) and to analyze convergence of $\mathbf{y}_h^*$ towards a minimizer $\mathbf{y}^*$ of (4.1). These topics are discussed in Section 4.3.

4.3 Convergence of discrete minimizers

This section is dedicated to proving convergence of discrete minimizers under the following regularity assumption.

Assumption 4.1. *The metric g defined in (3.42) admits an H^2 isometric immersion. That is, there exists a $\mathbf{y} \in H^2(\Omega;\mathbb{R}^3)$ such that $\nabla\mathbf{y}^T\nabla\mathbf{y} = g$ a.e. in Ω.*

Under the regularity Assumption 4.1, the main result can be stated as follows.

Theorem 4.1 (convergence of minimizers)**.** *Let Assumption 4.1 hold and let $\mathbf{y}_h$ be a minimizer of E_h. Then there is a subsequence (not relabeled) of $\mathbf{y}_h - \overline{\mathbf{y}}_h$ that converges in $H^1(\Omega,\mathbb{R}^3)$ strongly to a function $\mathbf{y}^* \in H^2(\Omega;\mathbb{R}^3)$ that satisfies $E[\mathbf{y}^*] = 0$, i.e. $\mathbf{y}^*$ is an isometric immersion $\mathrm{I}[\mathbf{y}^*] = \nabla\mathbf{y}^{*T}\nabla\mathbf{y}^* = g$.*

We start with a roadmap to the proof of convergence of discrete minimizers, which is inspired by the seminal work [66]. The first step is to build a recovery sequence $\mathbf{y}_h$ for the isometric immersion $\mathbf{y} \in H^2(\Omega;\mathbb{R}^3)$ in Assumption 4.1, that exhibits the desired energy scaling $E_h[\mathbf{y}_h] \lesssim h^2$ (see Proposition 4.3.) For such a $\mathbf{y}$ we know that $J[\mathbf{y}] = \lambda \geq c_{s,s_0} > 0$ for a constant c_{s,s_0} depending on s, s_0, so the challenge is to show a similar lower bound for $J[\mathbf{y}_h]$. To address this challenge, we resort to a Lusin approximation argument for Sobolev functions similar to that is used in [66]. To achieve the desired energy scaling of $E_h[\mathbf{y}_h] \lesssim h^2$, we exploit both frame indifference and the neo-Hookean structure of the stretching energy in Corollary 3.2. We proceed as follows starting with Corollary 3.2

$$\int_\Omega W_{str}(\mathbf{x},\nabla\mathbf{y}_h)d\mathbf{x} = \int_\Omega \left(\left|\mathbf{L}_{\mathbf{n}_h}^{-1/2}[\nabla\mathbf{y}_h,\ \mathbf{b}_h]\mathbf{L}_{\mathbf{m}}^{1/2}\right|^2 - 3\right)\ d\mathbf{x}, \tag{4.20}$$

where $\mathbf{n}_h = \frac{\nabla \mathbf{y}_h \mathbf{m}}{|\nabla \mathbf{y}_h \mathbf{m}|}$ and $\mathbf{b}_h = \frac{\partial_1 \mathbf{y}_h \times \partial_2 \mathbf{y}_h}{|\partial_1 \mathbf{y}_h \times \partial_2 \mathbf{y}_h|^2}$. We next recall that Remark 3.2 implies that $\mathbf{R} = \mathbf{L}_{\mathbf{n}}^{-1/2}[\nabla \mathbf{y},\ \mathbf{b}]\mathbf{L}_{\mathbf{m}}^{1/2} \in SO(3)$, because $E_{str}[\mathbf{y}] = 0$ according to Proposition 3.3 (target metric). This enables us to use the rotation $\mathbf{R}$ to rewrite the integrand as

$$\left|\mathbf{L}_{\mathbf{n}_h}^{-1/2}[\nabla \mathbf{y}_h,\ \mathbf{b}_h]\mathbf{L}_{\mathbf{m}}^{1/2}\right| = \left|\mathbf{R} + \mathbf{A}_h\right|, \quad \mathbf{A}_h := \mathbf{L}_{\mathbf{n}_h}^{-1/2}[\nabla \mathbf{y}_h,\ \mathbf{b}_h]\mathbf{L}_{\mathbf{m}}^{1/2} - \mathbf{R},$$

and invoke frame indifference. Multiplying by $\mathbf{R}^T$ does not change the energy, i.e.

$$\int_\Omega W_{str}(\mathbf{x}, \nabla \mathbf{y}_h) d\mathbf{x} = \int_\Omega \left(\left|\mathbf{R}^T\mathbf{R} + \mathbf{R}^T\mathbf{A}_h\right|^2 - 3\right)\, d\mathbf{x} = \int_\Omega \left(\left|\mathbf{I}_3 + \mathbf{R}^T\mathbf{A}_h\right|^2 - 3\right)\, d\mathbf{x}.$$

Lemma 4.1 below leads to a quadratic expansion around $\mathbf{I}_3$:

$$\int_\Omega W_{str}(\mathbf{x}, \nabla \mathbf{y}_h) d\mathbf{x} = \int_\Omega \left(\left|\mathbf{I}_3 + \mathbf{R}^T\mathbf{A}_h\right|^2 - 3\right)\, d\mathbf{x} \lesssim \|\mathbf{A}_h\|_{L^2(\Omega)}^2.$$

Finally, an error estimate on $\mathbf{y} - \mathbf{y}_h$ and properties of $\mathbf{y}_h$ in Lemma 4.5 further imply that $\|\mathbf{A}_h\|_{L^2(\Omega)}^2 \lesssim h^2$ and $|\mathbf{y}_h|_{H_h^2}^2 \lesssim 1$, whence $E_h[\mathbf{y}_h] \lesssim h^2$ according to (4.14).

Existence of a recovery sequence $\mathbf{y}_h$ so that $E_h[\mathbf{y}_h] \lesssim h^2$ implies that global discrete minimizers $\mathbf{y}_h^*$ are uniformly bounded in the H_h^2-seminorm. The uniform bound means that a subsequence of $\mathbf{y}_h^*$ converges strongly in $H^1(\Omega)$, which bypasses the convexity issues of W_{str}. The tools to go from a discrete H^2-bound to additional compactness have been developed for bending problems [31]. We go over the relevant results in Lemmas 4.6 and 4.7.

We now connect our work with the existing literature. As in [66], energy scaling brings additional compactness, but the mechanism here is H^2-regularity of isometric immersions rather than the geometric rigidity result in [66]. We refer to [102] for a geometric rigidity result in the context of LCEs. Moreover, we learned from [102] that $\mathbf{R}$ is a suitable rotation to exploit frame indifference and perform a quadratic expansion of $\left|\mathbf{I}_3 + \mathbf{R}^T\mathbf{A}_h\right|^2$ around the identity.

4.3.1 Preliminaries

This section covers preliminaries to lay the groundwork for the main results later. Subsection 4.3.1.1 contains preliminaries on how to approximate an H^2-isometric immersion of g. The key question is

given $\mathbf{y} \in H^2(\Omega;\mathbb{R}^3)$ *that satisfies* $\nabla\mathbf{y}^T\nabla\mathbf{y} = g$*, how does one construct* $\mathbf{y}_h \in \mathbb{V}_h$ *such that* $\|\mathbf{y} - \mathbf{y}_h\|_{H^1(\Omega;\mathbb{R}^3)} \lesssim h$ *and* $J[\mathbf{y}_h] > 0$ *a.e. in* Ω*?*

This kind of approximation requires some control in $W^{1,\infty}(\Omega)$. To achieve control over $J[\mathbf{y}_h]$ in L^∞, we regularize $\mathbf{y}$ with a $\mathbf{y}^\mu \in W^{2,\infty}(\Omega;\mathbb{R}^3)$ such that $J[\mathbf{y}^\mu] \geq c$. One obstacle with such a regularization is that $J[\mathbf{y}] \geq c > 0$ is a nonconvex constraint, so convolution may not preserve it. We note that there has been work on approximating maps while preserving the existence of a normal vector [53]. In [53, Proposition 4.1], the authors are able to approximate maps by smooth maps with well-defined normal, but the approximation is in the L^∞-norm rather than H^1. In our context, however, we deal with functions that have higher regularity than [53]. Hence, we are able to take advantage of Lusin truncation of Sobolev functions and ideas used in the construction of a recovery sequence in [66].

Subsection 4.3.1.2 discusses the regularization of a piecewise constant matrix field by an H^1-matrix field. This regularization provides additional compactness and relies on a quasi-interpolant that has been used in previous works on DG methods for bending problems [31]. Our presentation is brief but selfcontained.

4.3.1.1 Preliminaries for energy scaling

We first establish a quadratic expansion of the neo-Hookean formula around the identity, thereby slight improving on [102, Proposition A.2].

Lemma 4.1 (scaling of neo-Hookean formula near identity)**.** *If* $\mathbf{A} \in \mathbb{R}^{3\times 3}$ *satisfies* $\det(\mathbf{I}_3 + \mathbf{A}) = 1$*, then*

$$\big|\mathbf{I}_3 + \mathbf{A}\big|^2 - 3 \leq 3\big|\mathbf{A}\big|^2.$$

Proof. Since $\det(\mathbf{I}_3 + \mathbf{A}) = 1$, we may apply Proposition 3.1 (bounds for $W^H_{3D}(\mathbf{F})$) to bound

$$|\mathbf{I}_3 + \mathbf{A}|^2 - 3 \leq 3\,\mathrm{dist}\left(\mathbf{I}_3 + \mathbf{A}, SO(3)\right)^2 \leq 3\big|\mathbf{I}_3 + \mathbf{A} - \mathbf{I}_3\big|^2 = 3\big|\mathbf{A}\big|^2,$$

which is the desired result. □

We next introduce without proof a truncation argument for Sobolev functions from [66, Proposition A.2]; this is a suitable form of Lusin Theorem. The original result is stated with boundary conditions but it is still valid without them. We also point to a similar result in [125, Theorem 3.11.6].

Lemma 4.2 (truncation of H^2-functions)**.** *Let* $\mathbf{y} \in H^2(\Omega;\mathbb{R}^3)$*. There exists* $\mathbf{y}^\mu \in W^{2,\infty}(\Omega;\mathbb{R}^3)$ *such that*

$$\|\mathbf{y}^\mu\|_{W^{2,\infty}(\Omega;\mathbb{R}^3)} \leq C\mu, \tag{4.21}$$

and for $S_\mu := \{x \in \Omega : \mathbf{y}(x) \neq \mathbf{y}^\mu(\mathbf{x})$ *or* $\nabla\mathbf{y}(x) \neq \nabla\mathbf{y}^\mu(\mathbf{x})\}$ *we have the estimate*

$$|S_\mu| \leq C\frac{\omega(\mu)}{\mu^2} \tag{4.22}$$

on the measure $|S_\mu|$ *of* S_μ*, where*

$$\omega(\mu) = \int_{\{|\mathbf{y}|+|\nabla\mathbf{y}|+|D^2\mathbf{y}|\geq\frac{\mu}{2}\}} \big(|\mathbf{y}| + |\nabla\mathbf{y}| + |D^2\mathbf{y}|\big)^2 \, d\mathbf{x}$$

satisfies $\omega(\mu) \to 0$ *as* $\mu \to \infty$.

Motivated by the proof of [66, Theorem 6.1(ii)], we refine Lemma 4.2 (truncation of H^2 functions) for our purposes. In our case, the isometric immersion $\mathbf{y}$ given by Assumption 4.1 satisfies $\mathbf{y} \in H^2(\Omega;\mathbb{R}^3) \cap W^{1,\infty}(\Omega,\mathbb{R}^3)$ and $J[\mathbf{y}] \geq c_{s,s_0} > 0$ by virtue of $\mathrm{I}[\mathbf{y}] = g$.

Lemma 4.3 (truncation of H^2-functions with Lipschitz control)**.** *If* $\mathbf{y} \in H^2(\Omega;\mathbb{R}^3) \cap W^{1,\infty}(\Omega;\mathbb{R}^3)$ *and* $J[\mathbf{y}] \geq c > 0$*, then the function* $\mathbf{y}^\mu \in W^{2,\infty}(\Omega;\mathbb{R}^3)$ *given by Lemma 4.2 satisfies the following bounds for* μ *sufficiently large:*

$$\|\mathbf{y}^\mu\|_{W^{2,\infty}(\Omega;\mathbb{R}^3)} \leq C\mu, \tag{4.23}$$

$$\|\mathbf{y}^\mu\|_{H^2(\Omega;\mathbb{R}^3)} \leq C\|\mathbf{y}\|_{H^2(\Omega;\mathbb{R}^3)}, \tag{4.24}$$

$$\|\mathbf{y}^\mu\|_{W^{1,\infty}(\Omega;\mathbb{R}^3)} \leq C\big(1 + \|\mathbf{y}\|_{W^{1,\infty}(\Omega;\mathbb{R}^3)}\big), \tag{4.25}$$

$$J[\mathbf{y}^\mu] \geq \frac{c}{2}, \tag{4.26}$$

$$\|\mathbf{y}^\mu - \mathbf{y}\|_{H^1(\Omega;\mathbb{R}^3)} \leq C\big(1 + \|\mathbf{y}\|_{W^{1,\infty}(\Omega;\mathbb{R}^3)}\big)\frac{\sqrt{\omega(\mu)}}{\mu}, \tag{4.27}$$

where C *are generic constants independent of the truncation parameter* μ.

Proof. We first invoke Lemma 4.2 (truncation of H^2 functions): For all $\mu > 0$, there exists a $\mathbf{y}^\mu \in W^{2,\infty}(\Omega;\mathbb{R}^3)$ such that $\mathbf{y}^\mu = \mathbf{y}$ and $\nabla\mathbf{y}^\mu = \nabla\mathbf{y}$ on a set $\Omega \setminus S_\mu$, where $|S_\mu| \leq C\omega(\mu)/\mu^2$ and $\lim_{\mu\to\infty}\omega(\mu) = 0$. Additionally, $\|\mathbf{y}^\mu\|_{W^{2,\infty}(\Omega;\mathbb{R}^3)} \leq C\mu$, which is (4.23).

We shall now prove that $\mathbf{y}^\mu$ satisfies the asserted properties starting with (4.24). Using properties of $\mathbf{y}^\mu$ on the good and bad sets yields

$$\begin{aligned}\|\mathbf{y}^\mu\|^2_{H^2(\Omega)} &= \int_{S_\mu} |\mathbf{y}^\mu|^2 + |\nabla \mathbf{y}^\mu|^2 + |\nabla^2 \mathbf{y}^\mu|^2 + \int_{\Omega\setminus S_\mu} |\mathbf{y}^\mu|^2 + |\nabla \mathbf{y}^\mu|^2 + |\nabla^2 \mathbf{y}^\mu|^2 \\ &\leq C|S_\mu|\mu^2 + \int_{\Omega\setminus S_\mu} |\mathbf{y}|^2 + |\nabla \mathbf{y}|^2 + |\nabla^2 \mathbf{y}|^2 \leq C|S_\mu|\mu^2 + \|\mathbf{y}\|^2_{H^2(\Omega)}.\end{aligned}$$

Since $C|S_\mu|\mu^2 = C\omega(\mu) \leq C\|\mathbf{y}\|^2_{H^2(\Omega)}$, (4.24) follows immediately.

In order to show (4.25) and (4.26), we first note that $J[\mathbf{y}^\mu(\mathbf{x})] \geq c$ and $|\nabla \mathbf{y}^\mu(\mathbf{x})| \leq C$ clearly hold for a.e. $\mathbf{x} \in \Omega \setminus S_\mu$. We now focus on $x \in S_\mu$. First, we proceed similarly to the proof of [66, Theorem 6.1(ii)] to show that there exists $\delta > 0$ such that $B(\mathbf{x}, R) \cap \Omega \setminus S_\mu \neq \emptyset$ for $R := \delta\sqrt{C\omega(\mu)}\mu^{-1}$ and all $x \in S_\mu$. Otherwise, $B(\mathbf{x}, R) \cap \Omega = B(\mathbf{x}, R) \cap S_\mu$ and, since Ω is Lipschitz, there exists $A > 0$ such that

$$AR^2 \leq |B(\mathbf{x}, R) \cap \Omega| = |B(\mathbf{x}, R) \cap S_\mu| \leq |S_\mu| \leq \frac{C\omega(\mu)}{\mu^2}.$$

Setting $\delta = \sqrt{(2/A)}$ produces a contradiction. Returning to $\mathbf{x} \in S_\mu$, we pick a $\mathbf{z} \in \Omega \setminus S_\mu$ such that $|\mathbf{x} - \mathbf{z}| \leq R$ and employ (4.21) to write

$$|\nabla \mathbf{y}^\mu(\mathbf{x}) - \nabla \mathbf{y}^\mu(\mathbf{z})| \leq C\mu R = C\mu\delta\sqrt{\omega(\mu)}\mu^{-1} = C\delta\sqrt{\omega(\mu)}. \tag{4.28}$$

Therefore,

$$
\begin{aligned}
|\nabla \mathbf{y}^\mu(\mathbf{x})| &\le |\nabla \mathbf{y}^\mu(\mathbf{x}) - \nabla \mathbf{y}^\mu(\mathbf{z})| + |\nabla \mathbf{y}^\mu(\mathbf{z})| \\
&\le C(\delta\sqrt{\omega(\mu)} + \|\nabla \mathbf{y}\|_{L^\infty(\Omega)}) \le C(1 + \|\nabla \mathbf{y}\|_{L^\infty(\Omega)}),
\end{aligned}
$$

for μ sufficiently large; this shows (4.25). Moreover,

$$
J[\mathbf{y}^\mu(\mathbf{x})] = J[\mathbf{y}^\mu(\mathbf{z})] + \big(J[\mathbf{y}^\mu(\mathbf{z})] - J[\mathbf{y}^\mu(\mathbf{x})]\big) \ge c - \big|J[\mathbf{y}^\mu(\mathbf{z})] - J[\mathbf{y}^\mu(\mathbf{x})]\big|. \tag{4.29}
$$

Exploiting the Lipschitz continuity of $J[\mathbf{y}^\mu(\mathbf{x})] = \det \mathrm{I}[\mathbf{y}^\mu(\mathbf{x})]$ within a ball of $W^{1,\infty}(\Omega)$ of radius proportional to $(1 + \|\nabla \mathbf{y}\|_{L^\infty(\Omega)}$, and combining the estimates (4.25) and (4.28) for $\mathbf{y}^\mu$ yields

$$
\big|J[\mathbf{y}^\mu(\mathbf{z})] - J[\mathbf{y}^\mu(\mathbf{x})]\big| \le C\big(1 + \|\nabla \mathbf{y}\|_{L^\infty(\Omega)}\big)\delta\sqrt{\omega(\mu)},
$$

whence the right-hand side is smaller than $c/2$ provided μ is sufficiently large. Inserting this back into (4.29) gives $J[\mathbf{y}^\mu(\mathbf{x})] \ge \frac{c}{2}$, which is (4.26).

It remains to prove (4.27). We first write the error $\|\mathbf{y}^\mu - \mathbf{y}\|^2_{H^1(\Omega;\mathbb{R}^3)}$ as

$$
\|\mathbf{y}^\mu - \mathbf{y}\|^2_{H^1(\Omega;\mathbb{R}^3)} = \int_{S_\mu} |\mathbf{y}^\mu - \mathbf{y}|^2 + |\nabla \mathbf{y}^\mu - \nabla \mathbf{y}|^2 d\mathbf{x},
$$

according to the definition of S_μ in Lemma (4.2) (truncation of H^2 functions). The $W^{1,\infty}$-bound (4.25) on $\mathbf{y}^\mu$ in conjunction with the estimate (4.22) on the measure of S_μ produces the bound

$$
\|\mathbf{y}^\mu - \mathbf{y}\|^2_{H^1(\Omega;\mathbb{R}^3)} \le C\big(1 + \|\mathbf{y}\|_{W^{1,\infty}(\Omega;\mathbb{R}^3)}\big)^2 |S_\mu| \le C\big(1 + \|\mathbf{y}\|_{W^{1,\infty}(\Omega;\mathbb{R}^3)}\big)^2 \, \frac{\omega(\mu)}{\mu^2}.
$$

Taking the square root of both sides yields the desired estimate. □

Remark 4.1. The argument in the proof of Lemma 4.3 is similar to that in the proof of [66, Theorem 6.1(ii)], while the key difference is the object of interest. We want control over $\|\nabla \mathbf{y}^\mu\|_{L^\infty(\Omega)}$ and $J[\mathbf{y}^\mu]$, while [66] needs the gradient of the recovery sequence to be in an L^∞-neighborhood of $SO(3)$.

Remark 4.2. We stress that the significance of (4.27) is to provide a rate of convergence in H^1 relative to the blow up of the parameter μ that controls the $W^{2,\infty}$ norm, for which it is crucial that $\mathbf{y} \in W^{1,\infty}(\Omega;\mathbb{R}^3)$. If $\mathbf{y} \in H^2(\Omega;\mathbb{R}^3)$ but not in $W^{1,\infty}(\Omega;\mathbb{R}^3)$, then Sobolev embedding combined with (4.24) gives the reduced rate for all $2 < p < \infty$

$$\|\mathbf{y}^\mu - \mathbf{y}\|_{H^1(\Omega;\mathbb{R}^3)} \le \|\mathbf{y}^\mu - \mathbf{y}\|_{W^{1,p}(\Omega;\mathbb{R}^3)} \big|S_\mu\big|^{\frac{p-2}{2p}} \le C\|\mathbf{y}\|_{H^2(\Omega;\mathbb{R}^3)}\mu^{-1+2/p}.$$

The next few results deal with numerical preliminaries that are important for energy scaling. The next result says that interpolating an H^2 function gives a discrete function that has a uniform discrete H^2-bound. We present the proof for completeness but the argument can be found in the proof of [31, Proposition 5.3].

Lemma 4.4 (Lagrange interpolation stability in H^2)**.** *Let* $\mathbf{y} \in H^2(\Omega;\mathbb{R}^3)$. *Then the Lagrange interpolant* $I_h\mathbf{y} \in \mathbb{V}_h$ *satisfies* $|I_h\mathbf{y}|_{H_h^2(\Omega)} \lesssim \|\mathbf{y}\|_{H^2(\Omega;\mathbb{R}^3)}$.

Proof. Consider an arbitrary edge $e \in \mathcal{E}_h$, and its neighboring elements $T_1, T_2 \in \mathcal{T}_h$. Since $\mathbf{y} \in H^2(\Omega;\mathbb{R}^3)$, the jump of $\nabla\mathbf{y}$ across e is zero. Then, by a trace inequality, interpolation estimate and the fact that $I_h\mathbf{y}$ is linear on each element,

$$
\begin{aligned}
\|[\nabla I_h\mathbf{y}]\|_{L^2(e)} &= \|[\nabla I_h\mathbf{y} - \nabla\mathbf{y}]\|_{L^2(e)} \\
&\le h^{-1/2}\|\nabla I_h\mathbf{y} - \nabla\mathbf{y}\|_{L^2(T_1\cup T_2)} + h^{1/2}\|D^2 I_h\mathbf{y} - D^2\mathbf{y}\|_{L^2(T_1\cup T_2)} \\
&\lesssim h^{1/2}\|D^2\mathbf{y}\|_{L^2(T_1\cup T_2)}.
\end{aligned}
$$

Dividing both sides by $h^{1/2}$, squaring and summing over edges gives the assertion in view of (4.16). □

We next establish other approximation properties of the Lagrange interpolant.

Lemma 4.5 (discrete approximation of H^2-maps)**.** *Let $\mathbf{y}\in H^2(\Omega;\mathbb{R}^3)$ satisfy $\mathbf{y}\in W^{1,\infty}(\Omega;\mathbb{R}^3)$ and $J[\mathbf{y}]\ge c$ a.e. in Ω. For all $h>0$ sufficiently small, there exists $\mathbf{y}_h\in\mathbb{V}_h$ such that $\|\mathbf{y}_h\|_{W^{1,\infty}(\Omega;\mathbb{R}^3)}\lesssim 1+\|\mathbf{y}\|_{W^{1,\infty}(\Omega;\mathbb{R}^3)}$ and the following estimates are valid*

$$
J[\mathbf{y}_h] \ge \frac{c}{4}, \tag{4.30}
$$

$$
\|\mathbf{y}_h - \mathbf{y}\|_{H^1(\Omega;\mathbb{R}^3)} \lesssim h\big(1+\|\mathbf{y}\|_{W^{1,\infty}(\Omega;\mathbb{R}^3)} + |\mathbf{y}|_{H^2(\Omega;\mathbb{R}^3)}\big), \tag{4.31}
$$

$$
|\mathbf{y}_h|_{H^2_h(\Omega)} \lesssim 1+\|\mathbf{y}\|_{H^2(\Omega;\mathbb{R}^3)}. \tag{4.32}
$$

Proof. We first invoke Lemma 4.3 (truncation of H^2-functions with Lipschitz control) with $\mu_h = \delta h^{-1}$ to regularize $\mathbf{y}$ with a $\mathbf{y}^{\mu_h}$; the constant $\delta>0$ will be determined soon. We choose $\mathbf{y}_h = I_h\mathbf{y}^{\mu_h}$ to be the discrete approximation of $\mathbf{y}$. Since $|\mathbf{y}^{\mu_h}|_{W^{2,\infty}(\Omega)}\le C\mu_h$, in light of (4.23), a standard error estimate for the Lagrange interpolant gives the $W^{1,\infty}$-error estimate

$$
\|\nabla\mathbf{y}_h - \nabla\mathbf{y}^{\mu_h}\|_{L^\infty(\Omega)} \lesssim h|\mathbf{y}^{\mu_h}|_{W^{2,\infty}(\Omega)} \lesssim h\mu_h = \delta.
$$

This, together with (4.25), implies uniform $W^{1,\infty}$-bounds for $\mathbf{y}_h, \mathbf{y}^{\mu_h}$, which in turn yield the following error estimate for $J[\mathbf{y}_h]$:

$$\|J[\mathbf{y}_h] - J[\mathbf{y}^{\mu_h}]\|_{L^\infty(\Omega)} \leq C\delta.$$

We choose δ sufficiently small, so that $C\delta < \frac{c}{4}$. Hence, for this choice of δ, we have

$$J[\mathbf{y}_h] \geq J[\mathbf{y}^{\mu_h}] - \|J[\mathbf{y}_h] - J[\mathbf{y}^{\mu_h}]\|_{L^\infty(\Omega)} \geq J[\mathbf{y}^{\mu_h}] - C\delta \geq \frac{c}{2} - \frac{c}{4} = \frac{c}{4},$$

provided h sufficiently small, and correspondingly $\mu_h = \delta h^{-1}$ is sufficiently large for (4.26) to be valid. This proves the first assertion (4.30).

For the second assertion (4.31), we apply the triangle inequality

$$\|\mathbf{y} - \mathbf{y}_h\|_{H^1(\Omega;\mathbb{R}^3)} \leq \|\mathbf{y} - \mathbf{y}^{\mu_h}\|_{H^1(\Omega;\mathbb{R}^3)} + \|\mathbf{y}^{\mu_h} - \mathbf{y}_h\|_{H^1(\Omega;\mathbb{R}^3)},$$

and observe that (4.27) from Lemma 4.3 implies

$$\|\mathbf{y} - \mathbf{y}^{\mu_h}\|_{H^1(\Omega;\mathbb{R}^3)} \leq C\mu_h^{-1}\big(1 + \|\mathbf{y}\|_{W^{1,\infty}(\Omega;\mathbb{R}^3)}\big).$$

For the remaining term we utilize a standard error estimate for the Lagrange interpolant, in conjunction with (4.24) from Lemma 4.3, to arrive at

$$\|\mathbf{y}^{\mu_h} - I_h\mathbf{y}^{\mu_h}\|_{H^1(\Omega;\mathbb{R}^3)} \lesssim h|\mathbf{y}^{\mu_h}|_{H^2(\Omega;\mathbb{R}^3)} \lesssim h\|\mathbf{y}\|_{H^2(\Omega;\mathbb{R}^3)}.$$

Combining the last two bounds with $\mu_h^{-1} = h\delta^{-1} \lesssim h$ yields the desired estimate

$$\|\mathbf{y} - \mathbf{y}_h\|_{H^1(\Omega;\mathbb{R}^3)} \lesssim h\big(1 + \|\mathbf{y}\|_{W^{1,\infty}(\Omega;\mathbb{R}^3)} + \|\mathbf{y}\|_{H^2(\Omega;\mathbb{R}^3)}\big)$$

because δ has already been fixed. Finally, the uniform H_h^2-bound (4.32) follows from Lemma 4.4 (Lagrange interpolation stability in H^2) and the H^2-bound (4.24) on $\mathbf{y}^\mu$ in Lemma 4.3 . $\square$

4.3.1.2 Preliminaries for compactness

The first result is to show that the stretching energy is coercive in H^1, which will be important for some weak compactness results in the proof of Theorem 4.2

Proposition 4.2 (coercivity)**.** *There exists $C(s, s_0) > 0$, $c \geq 0$ such that the stretching energy $E_{str}[\mathbf{y}]$ defined in (4.1) satisfies*

$$C(s, s_0)\left(\|\nabla\mathbf{y}\|^2_{L^2(\Omega;\mathbb{R}^{3\times 2})} + \|J[\mathbf{y}]^{-1/2}\|^2_{L^2(\Omega)}\right) - 3|\Omega| \leq E_{str}[\mathbf{y}] \qquad \forall\, \mathbf{y} \in H^1(\Omega;\mathbb{R}^3). \quad (4.33)$$

Proof. Recall the expression (4.38),

$$E_{str}[\mathbf{y}] = \int_\Omega \left(\left|\mathbf{L}_{\mathbf{n}}^{-1/2}[\nabla\mathbf{y}, \mathbf{b}]\mathbf{L}_{\mathbf{m}}^{1/2}\right|^2 - 3\right)\, d\mathbf{x}.$$

where $\mathbf{n} = \frac{\nabla\mathbf{y}\,\mathbf{m}}{|\nabla\mathbf{y}\,\mathbf{m}|}$ and $\mathbf{b} = \frac{\boldsymbol{\nu}}{\sqrt{J[\mathbf{y}]}}$.

We now invoke an elementary result for any matrix $\mathbf{A} \in \mathbb{R}^{d\times d}$ and an SPD matrix $\mathbf{B} \in \mathbb{R}^{d\times d}$, which is $|\mathbf{A}\mathbf{B}|^2 \geq \lambda_{min}(\mathbf{B})^2|\mathbf{A}|^2$ and $|\mathbf{B}\mathbf{A}|^2 \geq \lambda_{min}(\mathbf{B})^2|\mathbf{A}|^2$ where $\lambda_{min}(\mathbf{B}) = \min_{1\leq j\leq d}\{\lambda_j(\mathbf{B})\} >$

0. To see this, we decompose $\mathbf{B}$ in dyadic form

$$\mathbf{B} = \sum_{i=1}^{d} \lambda_i \mathbf{b}_i \otimes \mathbf{b}_i,$$

where $\{\mathbf{b}_i\}_{i=1}^{d}$ is an orthonormal set of eigenvectors of $\mathbf{B}$ in $\mathbb{R}^d$. Then,

$$\mathbf{AB} = \sum_{i=1}^{d} \lambda)i \mathbf{A}\mathbf{b}_i \otimes \mathbf{b}_i.$$

Since the dyads $\mathbf{b}_i \otimes \mathbf{b}_i$ are orthogonal in the Frobenius inner product, we can bound

$$\begin{aligned}
|\mathbf{AB}|^2 &= \sum_{i=1}^{d} \lambda_i^2 |\mathbf{A}\mathbf{b}_i \otimes \mathbf{b}_i|^2 \\
&\leq \lambda_{min}(\mathbf{B})^2 \sum_{i=1}^{d} |\mathbf{A}\mathbf{b}_i \otimes \mathbf{b}_i|^2 \\
&= \lambda_{min}(\mathbf{B})^2 \left| \sum_{i=1}^{d} \mathbf{A}\mathbf{b}_i \otimes \mathbf{b}_i \right|^2 \\
&= \lambda_{min}(\mathbf{B})^2 \left| \mathbf{A}\mathbf{I}_d \right|^2 = \lambda_{min}(\mathbf{B})^2 \left| \mathbf{A} \right|^2.
\end{aligned}$$

The same argument works for $|\mathbf{BA}|^2$.

These properties allow us write the lower bound

$$E_{str}[\mathbf{y}] \geq \int_\Omega \frac{\lambda_{min}(\mathbf{L_m})}{\lambda_{max}(\mathbf{L_n})} \left| [\nabla \mathbf{y}, \mathbf{b}] \right|^2 - 3 \, d\mathbf{x}.$$

In view of the forms of $\mathbf{L_m}, \mathbf{L_n}$ in (3.2) and (3.3), their eigenvalues are explicit, namey $(s_0 + 1)^{2/3}, (s_0 + 1)^{1/3}$ and $(s + 1)^{2/3}, (s + 1)^{2/3}$ respectively. Recall the assumptions on s, s_0 in (4.7), we have that there is a constant $C(s, s_0) > 0$ such that $\frac{\lambda_{min}(\mathbf{L_m})}{\lambda_{max}(\mathbf{L_n})} \geq C(s, s_0)$ for a.e. $\mathbf{x} \in \Omega$. Thus,

$$E_{str}[\mathbf{y}] \geq C(s, s_0) \int_\Omega \left|[\nabla \mathbf{y}, \mathbf{b}]\right|^2 - 3 \, d\mathbf{x}.$$

Using the fact that $|\mathbf{b}|^2 = J[\mathbf{y}]^{-1}$ completes the proof. □

We show now how to extract H^1-compactness for sequences of continuous piecewise linear functions which are not naturally in $H^2(\Omega)$. We proceed by discrete regularization via Clement interpolation as in [31].

Suppose first that we have a piecewise constant function v over $\mathcal{T}_h$, namely $v|_T \in \mathcal{P}_0$ for all $T \in \mathcal{T}_h$. Given a generic node $z \in \mathcal{N}_h$, with corresponding star (or patch) ω_z, let $\mathbb{V}_h(\omega_z)$ be the space of continuous piecewise linear functions over ω_z. We define the local L^2-projection over $\mathbb{V}_h(\omega_z)$ as follows:

$$v_z \in \mathbb{V}_h(\omega_z): \qquad \int_{\omega_z} (v_z - v) v_h = 0 \quad \forall v_h \in \mathbb{V}_h(\omega_z); \tag{4.34}$$

note that $v_z = v$ if $v \in \mathbb{V}_h(\omega_z)$. We define the Clement interpolant $\mathcal{I}_h v \in \mathbb{V}_h$ to be

$$\mathcal{I}_h v := \sum_{z \in \mathcal{N}_h} v_z(z) \phi_z, \tag{4.35}$$

where $\{\phi_z\}_{z \in \mathcal{N}_h}$ denotes the nodal basis of $\mathbb{V}_h$ associated with $z \in \mathcal{N}_h$.

Lemma 4.6 (regularization of piecewise constant functions)**.** *If v is a piecewise constant function over $\mathcal{T}_h$, then its piecewise linear quasi-interpolant $\mathcal{I}_h v \in C^0(\overline{\Omega})$ defined in (4.34) and (4.35)* *satisfies the error estimates*

$$\|v - \mathcal{I}_h v\|_{L^2(\Omega)} + h\|\nabla \mathcal{I}_h v\|_{L^2(\Omega)} \lesssim h\sqrt{\sum_{e\in\mathcal{E}_h} \frac{1}{h}\int_e [v]^2}. \tag{4.36}$$

Proof. This is a corollary of [31, Lemma 2.1]. □

This lemma is instrumental to derive compactness properties from sequences of functions with uniform H_h^2-bounds. This is what we establish next. The proof follows the proof of [31, Proposition 5.1], but we sketch it for completeness.

Lemma 4.7 (compactness properties)**.** *Let* $\mathbf{y}_h \in \mathbb{V}_h$ *satisfy the uniform bounds* $\|\nabla \mathbf{y}_h\|_{L^2(\Omega;\mathbb{R}^{3\times 2})} \lesssim 1$ *and* $|\mathbf{y}_h|_{H_h^2(\Omega)} \lesssim 1$*. Then there exists* $\mathbf{y} \in H^2(\Omega;\mathbb{R}^3)$ *such that a subsequence (not relabeled) of* $\mathbf{y}_h$ *converges strongly*

$$(\mathbf{y}_h - \overline{\mathbf{y}}_h) \to \mathbf{y}$$

in $H^1(\Omega;\mathbb{R}^3)$ *as* $h \to 0$*, where* $\overline{\mathbf{y}}_h := |\Omega|^{-1}\int_\Omega \mathbf{y}_h$ *is the mean value of* $\mathbf{y}_h$*.*

Proof. Let $\mathbf{y}_h$ be a sequence that satisfies the uniform bound $\|\nabla \mathbf{y}_h\|_{L^2(\Omega;\mathbb{R}^{3\times 2})} \lesssim 1$. Poincaré inequality further implies the uniform bound $\|\mathbf{y}_h - \overline{\mathbf{y}}_h\|_{H^1(\Omega;;\mathbb{R}^3)} \lesssim 1$. Therefore, there is $\mathbf{y} \in H^1(\Omega;\mathbb{R}^3)$ and a subsequence (not relabeled) of $(\mathbf{y}_h - \overline{\mathbf{y}}_h)$ such that $(\mathbf{y}_h - \overline{\mathbf{y}}_h) \to \mathbf{y}$ strongly in $L^2(\Omega;\mathbb{R}^3)$ and weakly in $H^1(\Omega;\mathbb{R}^3)$.

To extract additional regularity of $\mathbf{y}$, we consider $\mathbf{w}_h = \mathcal{I}_h(\nabla \mathbf{y}_h) \in [\mathbb{V}_h]^{3\times 2}$ with $\mathcal{I}_h$ defined in (4.35). In view of the uniform bound $|\mathbf{y}_h|_{H_h^2(\Omega)} \lesssim 1$, (4.36) of Lemma 4.6 implies that $\mathbf{w}_h$ is uniformly bounded in $H^1(\Omega;\mathbb{R}^{3\times 2})$ and $\mathbf{w}_h - \nabla \mathbf{y}_h \to 0$ strongly in $L^2(\Omega;\mathbb{R}^{3\times 2})$, whence $\mathbf{w}_h \to \nabla \mathbf{y}$ weakly in $L^2(\Omega;\mathbb{R}^{3\times 2})$. The uniform H^1-bound of $\mathbf{w}_h$ means that a subsequence (not relabeled) of $\mathbf{w}_h \to \nabla \mathbf{y}$ strongly in $L^2(\Omega;\mathbb{R}^{3\times 2})$ and $\nabla \mathbf{y} \in H^1(\Omega;\mathbb{R}^{3\times 2})$. Consequently, a subsequence (not relabeled) of $\nabla \mathbf{y}_h \to \nabla \mathbf{y}$ strongly in $L^2(\Omega; \mathbb{R}^{3\times 2})$ and completes the proof. $\square$

4.3.2 Energy scaling and compactness

Our next result is a crucial discrete energy scaling estimate. It states that if there is an H^2-deformation $\mathbf{y}$ that satisfies the target metric (i.e. an H^2-isometric immersion), then the discrete energy $E_h[\mathbf{y}_h]$ associated with the $\mathbf{y}_h$ of Lemma 4.5 (discrete approximation of H^2 maps) scales like $E_h[\mathbf{y}_h] \lesssim h^2$. In the language of Γ-convergence, this is a recovery sequence result.

Proposition 4.3 (recovery sequence). *If $\mathbf{y} \in H^2(\Omega; \mathbb{R}^3) \cap W^{1,\infty}(\Omega; \mathbb{R}^3)$ is the deformation of Assumption 4.1, then for any h sufficiently small there exists $\mathbf{y}_h \in \mathbb{V}_h$ such that*

$$E_h[\mathbf{y}_h] \lesssim h^2 \left(1 + \|\mathbf{y}\|_{W^{1,\infty}(\Omega;\mathbb{R}^3)} + |\mathbf{y}|_{H^2(\Omega;\mathbb{R}^3)}\right). \tag{4.37}$$

Proof. By Assumption 4.1, we know that $\mathbf{y} \in H^2(\Omega; \mathbb{R}^3)$ satisfies $\nabla \mathbf{y}^T \nabla \mathbf{y} = g$, whence $E_{str}[\mathbf{y}] = 0$ by Proposition 3.3 (target metric), as well as $J[\mathbf{y}] = \lambda \geq c_{s,s_0} > 0$ by Proposition 4.2 (coercivity) . By Lemma 4.5, for h sufficiently small, there exists $\mathbf{y}_h \in \mathbb{V}_h$ such that $J[\mathbf{y}_h(x)] \geq \frac{c_{s,s_0}}{4}$ and $|\mathbf{y}_h|_{H^2_h} \lesssim 1 + \|\mathbf{y}\|_{H^2(\Omega;\mathbb{R}^3)}$. The latter implies that $R_h[\mathbf{y}_h] = c_r h^2 |\mathbf{y}_h|^2_{H^2_h} \lesssim h^2(1 + \|\mathbf{y}\|_{H^2(\Omega;\mathbb{R}^3)})$ in (4.14). It thus remains to show that $\int_\Omega W_{str}(\mathbf{x}, \nabla \mathbf{y}_h) d\mathbf{x} \lesssim h^2$, for which we resort to (4.38)

$$W_{str}(\mathbf{x}, \nabla \mathbf{y}_h) = \left| \mathbf{L}_{\mathbf{n}_h}^{-1/2} [\nabla \mathbf{y}_h, \mathbf{b}_h] \mathbf{L}_{\mathbf{m}}^{1/2} \right|^2 - 3 \tag{4.38}$$

where the kinematic constraint reads $\mathbf{n}_h = \frac{(\nabla \mathbf{y}_h)\mathbf{m}}{|(\nabla \mathbf{y}_h)\mathbf{m}|}$. We split the proof into three steps.

Step 1. Error estimate of scaled normal vectors. We recall that these vectors are

$$\mathbf{b} = \frac{\partial_1 \mathbf{y} \times \partial_2 \mathbf{y}}{J[\mathbf{y}]}, \qquad \mathbf{b}_h = \frac{\partial_1 \mathbf{y}_h \times \partial_2 \mathbf{y}_h}{J[\mathbf{y}_h]},$$

with $J[\mathbf{y}] = |\partial_1 \mathbf{y} \times \partial_2 \mathbf{y}|^2$ and $J[\mathbf{y}_h] = |\partial_1 \mathbf{y}_h \times \partial_2 \mathbf{y}_h|^2$. We claim that $|\mathbf{b} - \mathbf{b}_h| \lesssim |\nabla \mathbf{y} - \nabla \mathbf{y}_h|$ pointwise for which we write

$$\big|\mathbf{b} - \mathbf{b}_h\big| \le \big|\partial_1 \mathbf{y} \times \partial_2 \mathbf{y}\big| \left| \frac{1}{J[\mathbf{y}]} - \frac{1}{J[\mathbf{y}_h]} \right| + \frac{1}{J[\mathbf{y}_h]} \big|\partial_1 \mathbf{y} \times \partial_2 \mathbf{y} - \partial_1 \mathbf{y}_h \times \partial_2 \mathbf{y}_h\big|.$$

Since $J[\mathbf{y}_h] \ge \frac{c_{s,s_0}}{4}$, according to (4.30), the Lipschitz bound on $\mathbf{y}$ yields

$$\big|\mathbf{b} - \mathbf{b}_h\big| \lesssim \left| \frac{1}{J[\mathbf{y}]} - \frac{1}{J[\mathbf{y}_h]} \right| + \big|\partial_1 \mathbf{y} \times \partial_2 \mathbf{y} - \partial_1 \mathbf{y}_h \times \partial_2 \mathbf{y}_h\big|.$$

We now add and subtract $\partial_1 \mathbf{y} \times \partial_2 \mathbf{y}_h$, and apply the triangle inequality along with the bound $\|\mathbf{y}_h\|_{W^{1,\infty}(\Omega;\mathbb{R}^3)} \lesssim 1 + \|\mathbf{y}\|_{W^{1,\infty}(\Omega;\mathbb{R}^3)}$ from Lemma 4.5, to further estimate

$$\big|\mathbf{b} - \mathbf{b}_h\big| \lesssim \left| \frac{1}{J[\mathbf{y}]} - \frac{1}{J[\mathbf{y}_h]} \right| + \big|\nabla \mathbf{y} - \nabla \mathbf{y}_h\big|.$$

Since $x \mapsto \frac{1}{x}$ is Lipschitz on $[\frac{c_{s,s_0}}{4}, \infty)$, we deduce

$$\left| \frac{1}{J[\mathbf{y}]} - \frac{1}{J[\mathbf{y}_h]} \right| \lesssim \big|J[\mathbf{y}] - J[\mathbf{y}_h]\big|.$$

Likewise, on bounded subsets of $\mathbb{R}^{3\times 2}$, the map $\mathbf{F} \mapsto J(\mathbf{F})$ is Lipschitz. Hence, we again use the uniform $W^{1,\infty}$-bound of $\mathbf{y}_h$ from Lemma 4.5 to obtain

$$\big|J[\mathbf{y}] - J[\mathbf{y}_h]\big| \lesssim \big|\nabla\mathbf{y} - \nabla\mathbf{y}_h\big|.$$

Combining these bounds gives the desired pointwise error estimate for the scaled normals

$$|\mathbf{b} - \mathbf{b}_h| \lesssim |\nabla\mathbf{y} - \nabla\mathbf{y}_h|.$$

Step 2. Estimate on the kinematic constraint. Since $J[\mathbf{y}_h] = \det \mathrm{I}[\mathbf{y}_h] \geq \frac{c}{4}$, according to (4.30), we deduce that $\mathrm{I}[\mathbf{y}_h]$ is uniformly positive definite and

$$\big|\nabla\mathbf{y}_h\mathbf{m}\big|^2 = \mathbf{m}^T\nabla\mathbf{y}_h^T\nabla\mathbf{y}_h\mathbf{m} = \mathbf{m}^T\mathrm{I}[\mathbf{y}_h]\mathbf{m} \geq c'$$

for a constant $c' > 0$ depending on c; a similar estimate is valid for $\big|\nabla\mathbf{y}\mathbf{m}\big|$. Since $\mathbf{y}_h \in W^{1,\infty}(\Omega;\mathbb{R}^3)$ is uniformly bounded, in view of Lemma 4.5, and the map $x \mapsto x/|x|$ is Lipschitz on bounded subsets of $\{x \in \mathbb{R}^2 : |x| \geq \sqrt{c'}\}$, we see that

$$|\mathbf{n} - \mathbf{n}_h| = \left|\frac{\nabla\mathbf{y}\mathbf{m}}{|\nabla\mathbf{y}\mathbf{m}|} - \frac{\nabla\mathbf{y}_h\mathbf{m}}{|\nabla\mathbf{y}_h\mathbf{m}|}\right| \lesssim |\nabla\mathbf{y}\mathbf{m} - \nabla\mathbf{y}_h\mathbf{m}| \leq |\nabla\mathbf{y} - \nabla\mathbf{y}_h|.$$

Step 3. Energy Scaling. We now rewrite the neo-Hookean relation (4.38) of $W_{str}(\mathbf{x}, \nabla\mathbf{y}_h)$ as follows after adding and subtracting $\mathbf{R} := \mathbf{L}_{\mathbf{n}}^{-1/2}[\nabla\mathbf{y},\ \mathbf{b}]\mathbf{L}_{\mathbf{m}}^{1/2} \in SO(3)$:

$$W_{str}(\mathbf{x}, \nabla\mathbf{y}_h) = \big|\mathbf{R} + \mathbf{A}_h\big|^2 - 3, \quad \mathbf{A}_h := \mathbf{L}_{\mathbf{n}_h}^{-1/2}[\nabla\mathbf{y}_h,\ \mathbf{b}_h]\mathbf{L}_{\mathbf{m}}^{1/2} - \mathbf{L}_{\mathbf{n}}^{-1/2}[\nabla\mathbf{y},\ \mathbf{b}]\mathbf{L}_{\mathbf{m}}^{1/2}.$$

The fact that $\mathbf{R} \in SO(3)$ is a consequence of Remark 3.2 (special rotations) provided $\mathrm{I}[\mathbf{y}] = \nabla\mathbf{y}^T\nabla\mathbf{y} = g$, or equivalently $W_{str}[\mathbf{y}] = 0$. We exploit frame indifference to multiply by $\mathbf{R}^T$ without changing the energy density

$$W_{str}(\mathbf{x}, \nabla\mathbf{y}_h) = |\mathbf{R}^T\mathbf{R} + \mathbf{R}^T\mathbf{A}_h|^2 - 3 = |\mathbf{I}_3 + \mathbf{A}_h|^2 - 3.$$

Note that $\det\left(\mathbf{I}_3 + \mathbf{R}^T\mathbf{A}_h\right) = \det(\mathbf{L}_{\mathbf{n}_h}^{-1/2}[\nabla\mathbf{y}_h,\ \mathbf{b}_h]\mathbf{L}_{\mathbf{m}}^{1/2}) = 1$, because (3.8), (3.9) and Proposition 3.2 (minimal energy extension) imply $\det\mathbf{L}_{\mathbf{n}_h} = \det\mathbf{L}_{\mathbf{m}} = \det[\nabla\mathbf{y}_h,\ \mathbf{b}_h] = 1$. We then apply Lemma 4.1 (scaling of neo-Hookean formula near identity) to obtain

$$\int_\Omega W_{str}(\mathbf{x}, \nabla\mathbf{y}_h)d\mathbf{x} = \int_\Omega |\mathbf{I} + \mathbf{R}^T\mathbf{A}_h|^2 - 3\;d\mathbf{x} \le 3\int_\Omega |\mathbf{R}^T\mathbf{A}_h|^2 = 3\int_\Omega |\mathbf{A}_h|^2.$$

It thus suffices to show $\int_\Omega |\mathbf{A}_h|^2 d\mathbf{x} \lesssim h^2$. Adding and subtracting $\mathbf{L}_{\mathbf{n}_h}^{-1/2}[\nabla\mathbf{y}, \mathbf{b}]\mathbf{L}_{\mathbf{m}}^{1/2}$, and using the triangle and Young's inequalities, yields

$$\begin{aligned}|\mathbf{A}_h|^2 &\lesssim \left|\mathbf{L}_{\mathbf{n}_h}^{-1/2}([\nabla\mathbf{y}_h,\ \mathbf{b}_h] - [\nabla\mathbf{y},\ \mathbf{b}])\mathbf{L}_{\mathbf{m}}^{1/2}\right|^2 + \left|(\mathbf{L}_{\mathbf{n}}^{-1/2} - \mathbf{L}_{\mathbf{n}_h}^{-1/2})[\nabla\mathbf{y},\ \mathbf{b}]\mathbf{L}_{\mathbf{m}}^{1/2}\right|^2 \\ &\lesssim \left|[\nabla\mathbf{y}_h,\ \mathbf{b}_h] - [\nabla\mathbf{y},\ \mathbf{b}]\right|^2 + \left|\mathbf{L}_{\mathbf{n}}^{-1/2} - \mathbf{L}_{\mathbf{n}_h}^{-1/2}\right|^2 \lesssim \left|\nabla\mathbf{y} - \nabla\mathbf{y}_h\right|^2,\end{aligned}$$

where the last inequality follows from the preceding steps. In fact, Step 1 implies

$$\left|[\nabla\mathbf{y}_h,\ \mathbf{b}_h] - [\nabla\mathbf{y},\ \mathbf{b}]\right| \lesssim \left|\nabla\mathbf{y}_h - \nabla\mathbf{y}\right|,$$

while Step 2, together with (3.10) and the assumptions (4.7) and $s \in L^\infty(\Omega)$ on s gives

$$\big|\mathbf{L}_{\mathbf{n}}^{-1/2} - \mathbf{L}_{\mathbf{n}_h}^{-1/2}\big| \lesssim \big|\mathbf{n} - \mathbf{n}_h\big| \lesssim \big|\nabla\mathbf{y} - \nabla\mathbf{y}_h\big|.$$

Finally, applying (4.31) of Lemma 4.5 (discrete approximation of H^2-maps) yields

$$\int_\Omega |\mathbf{A}_h|^2 d\mathbf{x} \lesssim \int_\Omega |\nabla\mathbf{y} - \nabla\mathbf{y}_h|^2 d\mathbf{x} = \|\mathbf{y} - \mathbf{y}_h\|_{H^1}^2 \lesssim h^2 \left(1 + \|\mathbf{y}\|_{W^{1,\infty}(\Omega;\mathbb{R}^3)} + |\mathbf{y}|_{H^2(\Omega;\mathbb{R}^3)}\right), \tag{4.39}$$

which is the desired estimate. $\square$

Remark 4.3 (regularity of $\mathbf{m}$)**.** It is worth realizing that the proof of Proposition 4.3 only requires regularity on $\mathbf{y}$, but not of $\mathbf{m}$ beyond $L^\infty(\Omega)$. We stress, however, that $\mathbf{y} \in H^2(\Omega;\mathbb{R}^3) \cap W^{1,\infty}(\Omega;\mathbb{R}^3)$ implies $g = \nabla\mathbf{y}^T\nabla\mathbf{y} \in H^1(\Omega;\mathbb{R}^{2\times2}) \cap L^\infty(\Omega;\mathbb{R}^{2\times2})$ with g given in (3.42) in terms of $\mathbf{m}$. This regularity is borderline and does not guarantee continuity of g (or $\mathbf{m}$) in Ω.

The next Proposition establishes compactness: if a discrete $\mathbf{y}_h$ satisfies an appropriate energy scaling, then a subsequence converges to a minimizer of E.

Proposition 4.4 (compactness)**.** *Let $\mathbf{y}_h \in \mathbb{V}_h$ satisfy $E_h[\mathbf{y}_h] \leq Ch^2$ for a positive constant C, and let $\overline{\mathbf{y}}_h := |\Omega|^{-1}\int_\Omega \mathbf{y}_h$. Then there is a subsequence (not relabeled) of $\mathbf{y}_h - \overline{\mathbf{y}}_h$ that converges in $H^1(\Omega;\mathbb{R}^3)$ strongly to a limit $\mathbf{y}^* \in H^2(\Omega;\mathbb{R}^3)$ and $E[\mathbf{y}^*] = 0$.*

Proof. Proposition 4.2 (coercivity) implies that $\|\nabla\mathbf{y}_h\|_{L^2(\Omega;\mathbb{R}^{3\times2})}^2 \lesssim 1$, whereas

$$h^2|\mathbf{y}_h|_{H_h^2}^2 \lesssim c_r h^2 |\mathbf{y}_h|_{H_h^2}^2 + \int_\Omega W_{str}(\mathbf{x}, \nabla\mathbf{y}_h) = E_h[\mathbf{y}_h] \lesssim h^2$$

yields $|\mathbf{y}_h|_{H_h^2}^2 \lesssim 1$. Therefore, Lemma 4.7 (compactness properties) guarantees the existence of

$\mathbf{y}^* \in H^2(\Omega;\mathbb{R}^3)$ such that a subsequence (not relabeled) $(\mathbf{y}_h - \overline{\mathbf{y}}_h) \to \mathbf{y}^*$ converges strongly in $H^1(\Omega;\mathbb{R}^3)$. It remains to show that $E[\mathbf{y}^*] = 0$.

We can choose a further subsequence $\mathbf{y}_h$ such that $\nabla \mathbf{y}_h \to \nabla \mathbf{y}$ a.e. in Ω, whence

$$J[\mathbf{y}_h] \to J[\mathbf{y}^*], \quad \nabla \mathbf{y}_h\, \mathbf{m} \to \nabla \mathbf{y}^*\, \mathbf{m}, \quad \text{a.e. in } \Omega.$$

Our goal is to show that $\int_\Omega W_{str}(\mathbf{x}, \nabla \mathbf{y}_h) \to \int_\Omega W_{str}(\mathbf{x}, \nabla \mathbf{y}^*)$, for which we recall that

$$W_{str}(\mathbf{x}, \nabla \mathbf{y}_h) + 3 = \left| \mathbf{L}_{\mathbf{n}_h}^{-1/2} [\nabla \mathbf{y}_h, \mathbf{b}_h] \mathbf{L}_{\mathbf{m}}^{1/2} \right|^2 \geq \frac{C(s, s_0)}{J[\mathbf{y}_h]},$$

where $C(s, s_0)$ is the constant from Proposition 4.2 (coercivity). The above inequality is a by-product of the proof of Proposition 4.2 (coercivity). We first show that $J[\mathbf{y}_h]$ does not vanish and the singular term $\frac{1}{J[\mathbf{y}_h]}$ is well defined. If $B_{h,\eta} := \{x \in \Omega : J[\mathbf{y}_h] < \frac{c_{s,s_0}}{\eta}\}$, then we define $\tilde{c}_{s,s_0} = \frac{C(s,s_0)}{c_{s,s_0}}$ and obtain

$$W_{str}(\mathbf{x}, \nabla \mathbf{y}_h) \geq \frac{C(s, s_0)}{J[\mathbf{y}_h]} - 3 \geq \eta \tilde{c}_{s,s_0} - 3 \quad \forall\, x \in B_{h,\eta},$$

where $\eta > 3\tilde{c}_{s,s_0}^{-1}$ is to be determined. This implies that

$$|B_{h,\eta}| \leq \frac{1}{\eta \tilde{c}_{s,s_0} - 3} \int_{B_{h,\eta}} W_{str}(\mathbf{x}, \nabla \mathbf{y}_h) \leq \frac{E_h[\mathbf{y}_h]}{\eta \tilde{c}_{s,s_0} - 3} \leq \frac{Ch^2}{\eta \tilde{c}_{s,s_0} - 3}.$$

Since $\nabla \mathbf{y}_h$ is piecewise constant, $B_{h,\eta}$ is a collection of N_η elements of the triangulation $\mathcal{T}_h$. By the shape regularity of $\{\mathcal{T}_h\}_h$, there is $\gamma > 0$ such that $|B_{h,\eta}| \geq N_\eta \gamma h^2$. Hence,

$$N_\eta \gamma h^2 \leq \frac{Ch^2}{\eta \tilde{c}_{s,s_0} - 3}.$$

Taking $\eta > 0$ sufficiently large implies that $N_\eta = 0$ and $J[\mathbf{y}_h] \geq \frac{c_{s,s_0}}{\eta}$ a.e. in Ω, whence we infer that $J[\mathbf{y}^*] \geq \frac{c_{s,s_0}}{\eta}$ a.e. in Ω. Likewise this implies that $|\nabla \mathbf{y}^* \mathbf{m}|^2 = C_{\mathbf{m}}[\mathbf{y}^*] > 0$ a.e. because $\frac{c_{s,s_0}}{\eta} \leq J[\mathbf{y}^*] \leq C_{\mathbf{m}}[\mathbf{y}^*] C_{\mathbf{m}_\perp}[\mathbf{y}^*]$ according to (4.5). Combined with continuity of $x \mapsto 1/x$ for positive x, we have $\frac{1}{J[\mathbf{y}_h]} \to \frac{1}{J[\mathbf{y}^*]}$ and $\frac{\nabla \mathbf{y}_h \mathbf{m}}{|\nabla \mathbf{y}_h \mathbf{m}|} \to \frac{\nabla \mathbf{y}^* \mathbf{m}}{|\nabla \mathbf{y}^* \mathbf{m}|}$ pointwise a.e. in Ω. Thus, both

$$\mathbf{L}_{\mathbf{n}_h}^{-1/2} [\nabla \mathbf{y}_h, \mathbf{b}_h] \mathbf{L}_{\mathbf{m}}^{1/2} \to \mathbf{L}_{\mathbf{n}^*}^{-1/2} [\nabla \mathbf{y}^*, \mathbf{b}^*] \mathbf{L}_{\mathbf{m}}^{1/2},$$

and

$$W_{str}(\mathbf{x}, \nabla \mathbf{y}_h) \to W_{str}(\mathbf{x}, \nabla \mathbf{y}^*)$$

pointwise a.e. in Ω.

Since $W_{str}(\mathbf{x}, \nabla \mathbf{y}_h) \geq 0$, by virtue of Corollary 3.3 (nondegeneray of stretching energy), we apply Fatou's Lemma to deduce the desired result

$$E[\mathbf{y}^*] = \int_\Omega W_{str}(\mathbf{x}, \nabla \mathbf{y}^*) d\mathbf{x} \leq \liminf_{h \to 0} \int_\Omega W_{str}(\mathbf{x}, \nabla \mathbf{y}_h) \leq \lim_{h \to 0} E_h[\mathbf{y}_h] = 0.$$

This concludes the proof. □

We are now ready to prove the convergence of discrete minimizers.

Proof of Theorem 4.1. The proof follows readily from Propositions 4.3 (recovery sequence), 4.4 (compactness), and 3.3 (target metric). □

4.4 Piecewise H^2-deformations: nonisometric origami

This section is dedicated to the analysis of piecewise H^2-deformations rather than globally H^2-deformations. The inspiration for this extension comes from [18] and [20]. For physical applications, the motivation comes from nonisometric origami [100, 101, 102].

Let $\Omega = \cup_{i=1}^n \Omega_i$ be a disjoint partition of Ω, where each Ω_i is polygonal. We denote by Γ the boundaries of all Ω_i's, which is the *set of creases or folding set*. We then define the space of piecewise H^2 functions to be

$$\mathbb{V}_\Gamma = \{\mathbf{y} \in W^{1,\infty}(\Omega;\mathbb{R}^3) : \mathbf{y}|_{\Omega_i} \in H^2(\Omega_i;\mathbb{R}^3) \text{ for all } i = 1,\dots,n\}. \tag{4.40}$$

We shall approximate minimizers $\mathbf{y}^* \in \mathbb{V}_\Gamma$ of (4.1) with folding across Γ. To this end, we make the geometric assumption

$$\Gamma \subset \bigcup_{e\in\mathcal{E}_h} e, \tag{4.41}$$

i.e. the triangulation is fitted to Γ. We denote by $\mathcal{E}_h^i$ the *interior* skeleton to each Ω_i (so that edges on Γ are excluded) and define the new discrete energy with folds as

$$E_{h,\Gamma}[\mathbf{y}_h] := \int_\Omega W_h(x,\nabla\mathbf{y}_h)d\mathbf{x} + R_{h,\Gamma}[\mathbf{y}_h], \tag{4.42}$$

where the regularization term is given by $R_{h,\Gamma}[\mathbf{y}_h] := c_r h^2 |\mathbf{y}_h|^2_{H_h^2(\Omega\setminus\Gamma)}$ and

$$|\mathbf{y}_h|^2_{H_h^2(\Omega\setminus\Gamma)} := \sum_{i=1}^n \sum_{e\in\mathcal{E}_h^i} \frac{1}{h}\int_e \left|[\nabla\mathbf{y}_h]\right|^2. \tag{4.43}$$

We point out that (4.43) does not include jumps across Γ, which in turn allows for folds across Γ without penalty on the energy. This modeling feature is responsible for the formation of nonisometric origami within this setting.

We next adjust the regularity Assumption 4.1 to the new framework.

Assumption 4.2. *There exists a* $\mathbf{y} \in W^{1,\infty}(\Omega;\mathbb{R}^3)$ *such that* $\mathrm{I}[\mathbf{y}] = g$ *a.e. in* Ω *and* $\mathbf{y}|_{\Omega_i} \in H^2(\Omega_i;\mathbb{R}^3) \cap C^1(\overline{\Omega}_i;\mathbb{R}^3)$ *for all* $i = 1,\ldots,n$.

We relax the H^2-regularity but observe that $\mathbf{y}|_{\Omega_i} \in C^1(\overline{\Omega}_i;\mathbb{R}^3)$ implies that $g|_{\Omega_i} \in C(\overline{\Omega}_i;\mathbb{R}^{2\times 2})$ is slightly stronger than the mere $L^\infty \cap H^1$-regularity of g as discussed in Remark 4.3. We point out that Assumption 4.2 might not be always satisfied. It is possible that such a piecewise H^2-isometric immersion does not exist if one of Ω_i has reentrant corners.

We now state the new recovery sequence result.

Proposition 4.5 (recovery sequence)**.** *If* $\mathbf{y} \in \mathbb{V}_\Gamma$ *is the deformation of Assumption 4.2, then for* h *sufficiently small the Lagrange interpolant* $\mathbf{y}_h = I_h\mathbf{y} \in \mathbb{V}_h$ *satisfies*

$$E_{h,\Gamma}[\mathbf{y}_h] \lesssim h^2 \left(1 + \sum_{i=1}^{n} \|\mathbf{y}\|_{C^1(\overline{\Omega}_i;\mathbb{R}^3)} + \|\mathbf{y}\|_{H^2(\overline{\Omega}_i;\mathbb{R}^3)} \right).$$

Proof. In view of (4.41) and $\mathbf{y}|_{\Omega_i} \in H^2(\Omega_i;\mathbb{R}^3)$ from Assumption 4.2, Lemma 4.4 (Lagrange interpolation stability in H^2) applied to each Ω_i gives $|\mathbf{y}_h|_{H^2_h(\Omega_i)} \lesssim \|\mathbf{y}\|_{H^2(\overline{\Omega}_i;\mathbb{R}^3)}$. Moreover, we also have the standard error estimate $\|\mathbf{y} - \mathbf{y}_h\|_{H^1(\Omega_i;\mathbb{R}^3)} \lesssim h|\mathbf{y}|_{H^2(\overline{\Omega}_i;\mathbb{R}^3)}$.

To derive the energy scaling, we first show that $J[\mathbf{y}_h] \geq c/2$ a.e. for sufficiently small h provided $J[\mathbf{y}] = \det g \geq c > 0$. Since $\mathbf{y} \in C^1(\overline{\Omega}_i;\mathbb{R}^3)$, the function $\nabla\mathbf{y}$ is uniformly continuous in Ω_i with modulus of continuity $\sigma(t)$ (i.e. $\sigma(t) \to 0$ as $t \to 0$). Therefore, $\|\nabla\mathbf{y} - \nabla\mathbf{y}_h\|_{L^\infty(\Omega)} \lesssim$

$\sigma(h)$ and, for h sufficiently small, we obtain

$$J[\mathbf{y}_h] \geq J[\mathbf{y}] - \big|J[\mathbf{y}_h] - J[\mathbf{y}]\big| \geq c - C\sigma(h) \geq \frac{c}{2},$$

because $J[\mathbf{y}]$ is Lipschitz continuous in $W^{1,\infty}(\Omega;\mathbb{R}^3)$ on bounded balls. Applying the arguments in Proposition 4.3 (recovery sequence), we deduce

$$\int_{\Omega_i} W_{str}(\mathbf{x}, \nabla\mathbf{y}_h)d\mathbf{x} + c_r h^2 |\mathbf{y}_h|^2_{H^2_h(\Omega_i)} \lesssim h^2$$

on each Ω_i. Summing over Ω_i yields the desired result. $\square$

The compactness result in the previous section carries over to the case with jumps, but with a small modification. The analog to Theorem 4.1 (convergence of discrete minimizers) reads as follows.

Theorem 4.2 (convergence of discrete minimizers with creases)**.** *Let Assumption 4.2 hold and let $\mathbf{y}_h$ be a minimizer of $E_{h,\Gamma}$ with $\overline{\mathbf{y}}_h = |\Omega|^{-1}\int_\Omega \mathbf{y}$. Then, as $h \to 0$, we have that*

$$E_{h,\Gamma}[\mathbf{y}_h] \lesssim h^2 \tag{4.44}$$

and $\mathbf{y}_h - \overline{\mathbf{y}}_h$ has a strongly convergent subsequence (not relabeled) $\mathbf{y}_h - \overline{\mathbf{y}}_h \to \mathbf{y}^*$ in $H^1(\Omega;\mathbb{R}^3)$ to a function $\mathbf{y}^* \in \mathbb{V}_\Gamma$ that satisfies $E[\mathbf{y}^*] = 0$ and $\mathrm{I}(\mathbf{y}^*) = g$ a.e. in Ω.

Proof. We first apply Proposition 4.5 (recovery sequence) to deduce that $E_{h,\Gamma}[\mathbf{y}_h] \leq E_{h,\Gamma}[I_h\mathbf{y}] \lesssim h^2$ because $\mathbf{y}_h$ is a minimizer of $E_{h,\Gamma}$. Moreover, since $E[\mathbf{y}_h] \leq E_{\Gamma,h}[\mathbf{y}_h] \lesssim h^2$ by definition (4.42), Proposition 4.2 (coercivity) implies the uniform bound $\|\nabla\mathbf{y}_h\|_{L^2(\Omega)} \lesssim 1$ and, hence, the weak convergence of a subsequence (not relabeled) of $\mathbf{y}_h - \overline{\mathbf{y}}_h$ to a function $\mathbf{y}^* \in H^1(\Omega; \mathbb{R}^3)$. We need to prove further regularity of $\mathbf{y}^*$.

Proceeding now as in Lemma 4.7 (compactness properties) and Proposition 4.4 (compactness) over each subdomain Ω_i, we can show that up to a subsequence $\nabla \mathbf{y}_h|_{\Omega_i} \to \nabla \mathbf{y}^*|_{\Omega_i}$ converges strongly in $L^2(\Omega_i; \mathbb{R}^{3\times 2})$ and that $\nabla \mathbf{y}^*|_{\Omega_i} \in H^1(\Omega_i; \mathbb{R}^{3\times 2})$ and $\mathrm{I}[\mathbf{y}^*|_{\Omega_i}] = g$ a.e. in Ω_i for each $i = 1, \ldots, n$. In view of Proposition 3.3 (target metric) we also obtain that $W_{str}(\mathbf{x}, \nabla \mathbf{y}^*|_{\Omega_i}) = 0$ for each $i = 1, \ldots, n$, whence $E[\mathbf{y}^*] = 0$.

It remains to show that $\mathbf{y}^* \in W^{1,\infty}(\Omega; \mathbb{R}^3)$ is globally Lipschitz. We note that $\mathbf{y}^*|_{\Omega_i} \in W^{1,\infty}(\Omega_i; \mathbb{R}^3)$ for each $i = 1, \ldots, n$ because $\mathrm{I}[\mathbf{y}^*|_{\Omega_i}] = g \in L^\infty(\Omega_i; \mathbb{R}^{2\times 2})$, which in turn implies that the trace of $\mathbf{y}^*|_{\Omega_i}$ on $\partial\Omega_i$ is continuous. Since $\mathbf{y}^* \in H^1(\Omega; \mathbb{R}^3)$, we infer that the jumps $[\mathbf{y}^*]|_\Gamma = 0$ must vanish, thereby showing that $\mathbf{y}^* \in C(\overline{\Omega}; \mathbb{R}^3)$ is uniformly continuous in Ω. This, in addition to being piecewise Lipschitz, proves that $\mathbf{y}^*$ is globally Lipschitz, whence $\mathbf{y}^* \in \mathbb{V}_\Gamma$ as asserted. $\square$

4.5 Iterative solver

We design a nonlinear discrete gradient flow to find a solution to (4.19) in this subsection. Due to the stretching energy being non-quadratic and non-convex, we end up with a nonlinear non-convex discrete problem to solve.

4.5.1 Nonlinear gradient flow.

Implicit gradient flows are robust methods to find stationary points of energy functionals E regardless of their convexity, and have the advantage of built-in energy stability; they belong to the class of energy descent methods. Consider the auxiliary evolution equation $\partial_t A[\mathbf{y}] + \delta E[\mathbf{y}] = 0$, where A is a symmetric elliptic operator, $\delta E[\mathbf{y}]$ stands for the first variation of E, and t is a pseudo-time. The backward Euler discretization reads: given $\mathbf{y}^n \in H$ solve for $\mathbf{y}^{n+1} \in H$

$$\frac{1}{\tau}\big(A\mathbf{y}^{n+1} - A\mathbf{y}^n\big) + \delta E[\mathbf{y}^{n+1}] = 0,$$

where τ is the time-step discretization parameter and H is a suitable Hilbert (or even metric) space. The weak formulation of this semi-discrete equation is equivalent to minimizing the augmented functional

$$L^n[\mathbf{y}] := \frac{1}{2\tau}\|\mathbf{y} - \mathbf{y}^n\|_A^2 + E[\mathbf{y}] \tag{4.45}$$

where $\|\cdot\|_A$ is the norm associated with the operator $A : H \to H^*$, i.e. $\|\mathbf{y}\|_A^2 := \langle A\mathbf{y}, \mathbf{y}\rangle$. This can be reinterpreted as finding a minimizer of E constrained to be closed to $\mathbf{y}^n$; so the first term in (4.45) penalizes the deviation of $\mathbf{y}$ from $\mathbf{y}^n$ in the A-norm.

Since the stretching energy E_{str} from (4.1) and (4.2) is formulated in $H = H^1(\Omega;\mathbb{R}^3)$, we choose $A = I - \Delta$ and the corresponding norm to be the $H^1(\Omega)$-norm. This choice has the property of making L^n convex in $H^1(\Omega;\mathbb{R}^3)$ provided $\mathbf{y}^n$ is sufficiently smooth and τ is sufficiently small. With this in mind, we devise a discrete counterpart of (4.45) to find stationary points of E_h in (4.14) under some additional assumptions on the current iterate $\mathbf{y}_h^n \in \mathbb{V}_h$ to be discussed below. We thus seek to solve

$$\mathbf{y}_h^{n+1} \in \operatorname{argmin}_{\mathbf{y}_h \in \mathbb{V}_h} L_h^n[\mathbf{y}_h] \tag{4.46}$$

where

$$L_h^n[\mathbf{y}_h] := \frac{1}{2\tau}\|\mathbf{y}_h - \mathbf{y}_h^n\|_{H^1(\Omega)}^2 + E_h[\mathbf{y}_h]. \tag{4.47}$$

The corresponding Euler-Lagrange equation results from computing the first order variation of $L_h^n[\mathbf{y}_h]$ in the direction $\mathbf{v}_h$

$$\delta L_h^n[\mathbf{y}_h](\mathbf{v}_h) = \frac{1}{\tau}(\mathbf{y}_h, \mathbf{v}_h)_{H^1(\Omega)} + \delta E_h[\mathbf{y}_h](\mathbf{v}_h) - F_h^n(\mathbf{v}_h) = 0 \quad \forall\, \mathbf{v}_h \in \mathbb{V}_h, \tag{4.48}$$

where $F_h^n \in \mathbb{V}_h^*$ is defined as

$$F_h^n(\mathbf{v}_h) := \frac{1}{\tau}(\mathbf{y}_h^n, \mathbf{v}_h)_{H^1(\Omega)},$$

and

$$\delta E_h[\mathbf{y}_h](\mathbf{v}_h) = \delta E_{str}[\mathbf{y}_h](\mathbf{v}_h) + \delta R_h[\mathbf{y}_h](\mathbf{v}_h).$$

A direct but tedious computation shown in Appendix A gives an explicit expression for $\delta E_{str}[\mathbf{y}_h](\mathbf{v}_h)$, which turns out to depend *nonlinearly* on $\mathbf{y}_h$. Therefore, (4.48) is a nonlinear discrete equation for $\mathbf{y}_h \in \mathbb{V}_h$.

We now state the energy stability of (4.47) provided (4.46) is solved exactly. This is a natural property for *implicit* gradient flows.

Theorem 4.3 (energy stability). *Given $\mathbf{y}_h^n \in \mathbb{V}_h$ for any $n \geq 0$, suppose $\mathbf{y}_h^{n+1} \in \mathbb{V}_h$ minimizes $L_h^n[\mathbf{y}_h]$ defined in (4.47). Then $E_h[\mathbf{y}_h^{n+1}] \leq E_h[\mathbf{y}_h^n]$, and the inequality is strict if $\mathbf{y}_h^{n+1} \neq \mathbf{y}_h^n$.*

Moreover, for any $N \geq 1$,

$$E_h[\mathbf{y}_h^N] + \frac{1}{2\tau}\sum_{n=0}^{N-1} \|\mathbf{y}_h^{n+1} - \mathbf{y}_h^n\|_{H^1(\Omega)}^2 \leq E_h[\mathbf{y}_h^0]. \tag{4.49}$$

Proof. Since $\mathbf{y}_h^{n+1}$ minimizes L_h^n, we have $L_h^n[\mathbf{y}_h^{n+1}] \leq L_h^n[\mathbf{y}_h^n]$, whence

$$\frac{1}{2\tau}\|\mathbf{y}_h^{n+1} - \mathbf{y}_h^n\|_{H^1(\Omega)}^2 + E_h[\mathbf{y}_h^{n+1}] = L_h^n[\mathbf{y}_h^{n+1}] \leq L_h^n[\mathbf{y}_h^h] = E_h[\mathbf{y}_h^n].$$

This proves monotonicity of $E_h[\mathbf{y}_h^n]$ and, adding over $n = 1 : N-1$, yields (4.49). $\square$

A corollary of this energy stability result is that there are subsequences of the iteration defined by (4.46) converge to critical points of E_h. This is also a standard property for implicit gradient flows.

Corollary 4.1 (critical points of E_h)**.** *Let $\mathbf{y}_h^0 \in \mathbb{V}_h$ satisfy $E_h[\mathbf{y}_h^0] < \infty$. Consider the sequence $\{\mathbf{y}_h^n\}_{n=0}^\infty$ defined recursively by (4.46). There is a constant $0 \leq C < \infty$ such that $\|\mathbf{y}_h^n\|_{H^1(\Omega)} \leq C$ for all $n \geq 0$.*

Additionally, let $\mathbf{y}_h^* \in \mathbb{V}_h$ be a cluster point of $\{\mathbf{y}_h^n\}_{n=0}^\infty$,namely there is a subsequence of $\{\mathbf{y}_h^n\}_{n=0}^\infty$ which converges to $\mathbf{y}_h^*$. Then $\mathbf{y}_h^*$ is a critical point of E_h in the sense that

$$\delta E_h[\mathbf{y}_h^*](\mathbf{v}_h) = 0, \quad \forall \mathbf{v}_h \in \mathbb{V}_h. \tag{4.50}$$

Proof. We break the proof into two steps.

Step 1. Uniform H^1 bound. Let $\mathbf{y}_h^0 \in \mathbb{V}_h$ satisfy $E_h[\mathbf{y}_h^0] < \infty$. Consider the sequence

$\{\mathbf{y}_h^n\}_{n=0}^\infty$ defined recursively by (4.46). For each $N \geq 1$, Theorem 4.3 (energy stability) tells us

$$E_h[\mathbf{y}_h^N] + \frac{1}{2\tau}\sum_{n=0}^{N-1} \|\mathbf{y}_h^{n+1} - \mathbf{y}_h^n\|_{H^1(\Omega)}^2 \leq E_h[\mathbf{y}_h^0]. \tag{4.51}$$

By Proposition 4.2 (coercivity), there is a constant $C(s, s_0) > 0$ such that

$$C(s, s_0)\left(\|\mathbf{y}_h\|_{H^1(\Omega)}^2 + \|J[\mathbf{y}_h]^{-1/2}\|_{L^2(\Omega)}^2\right) - 3|\Omega| \leq E_h[\mathbf{y}_h] \tag{4.52}$$

For $N \geq 1$, (4.51) combined with (4.52) yields

$$\|\mathbf{y}_h\|_{H^1(\Omega)}^2 \leq \frac{E_h[\mathbf{y}_h^0] + 3|\Omega|}{C(s, s_0)} < \infty, \tag{4.53}$$

which proves the uniform H^1 bound. We now have that $\{\mathbf{y}_h^n\}_{n=0}^\infty$ is a uniformly bounded sequence in the finite dimensional space $\mathbb{V}_h$ equipped with the H^1 norm. Hence, the sequence has cluster points in $\mathbb{V}_h$.

Step 2. Cluster points are critical points. Suppose $\mathbf{y}_h^* \in \mathbb{V}_h$ is a cluster point. There is a subsequence (not relabled) $\{\mathbf{y}_h^n\}_{n=0}^\infty$ such that $\mathbf{y}_h^n \to \mathbf{y}_h^*$ in $H^1(\Omega; \mathbb{R}^3)$. Since $\mathbb{V}_h$ has finite dimensions, we also have that $\mathbf{y}_h^n \to \mathbf{y}_h^*$ in $W^{1,\infty}(\Omega)$.

Let $\mathbf{v}_h \in \mathbb{V}_h$. To prove (4.50), it is sufficient to prove that $\lim_{n\to\infty} \delta E_h[\mathbf{y}_h^n](\mathbf{v}_h) = \delta E_h[\mathbf{y}_h^*](\mathbf{v}_h)$. To see this we recall that $\mathbf{y}_h^n$ solves the Euler Lagrange equation (4.48). Thus,

$$\frac{1}{\tau}(\mathbf{y}_h^n - \mathbf{y}_h^{n-1}, \mathbf{v}_h)_{H^1(\Omega)} + \delta E_h[\mathbf{y}_h^n](\mathbf{v}_h) = 0. \tag{4.54}$$

The energy decrease property in (4.51) and the nonnegativity of E_h from Corollary 3.3 (nondegeneracy) implies that

$$\frac{1}{2\tau}\sum_{n=0}^{\infty}\|\mathbf{y}_h^n-\mathbf{y}_h^{n-1}\|_{H^1(\Omega)}^2\le E_h[\mathbf{y}_h^0]<\infty,$$

and consequently, $\lim_{n\to\infty}\|\mathbf{y}_h^n-\mathbf{y}_h^{n-1}\|_{H^1(\Omega)}=0$. Passing the limit of (4.54) as $n\to\infty$ brings us to

$$\lim_{n\to\infty}\delta E_h[\mathbf{y}_h^n](\mathbf{v}_h)=0.$$

Hence, in order to prove (4.50), it suffices to show $\lim_{n\to\infty}\delta E_h[\mathbf{y}_h^n](\mathbf{v}_h)=\delta E_h[\mathbf{y}_h^*](\mathbf{v}_h)$. Recall from (4.53), there is a constant $C<\infty$ such that the sequence $\mathbf{y}_h^n$ satisfies

$$\|\mathbf{y}_h^n\|_{H^1(\Omega;\mathbb{R}^3)}+\|J[\mathbf{y}_h^n]^{-1}\|_{L^1(\Omega)}\le C.$$

Note that $\mathbf{y}_h^n\in\mathbb{V}_h$ and $J[\mathbf{y}_h^n]^{-1}$ is piecewise constant. We may apply global inverse inequalities

$$\|\mathbf{y}_h^n\|_{W^{1,\infty}(\Omega;\mathbb{R}^3)}\lesssim h^{-1}\|\mathbf{y}_h^n\|_{H^1(\Omega;\mathbb{R}^3)}\text{ and }\|J[\mathbf{y}_h^n]^{-1}\|_{L^\infty(\Omega)}\lesssim h^{-2}\|J[\mathbf{y}_h^n]^{-1}\|_{L^1(\Omega)}$$

to obtain the bound

$$\|\mathbf{y}_h^n\|_{W^{1,\infty}(\Omega;\mathbb{R}^3)}+\|J[\mathbf{y}_h^n]^{-1}\|_{L^\infty(\Omega)}\le Ch^{-2}<\infty, \tag{4.55}$$

for some $C<\infty$ that is independent of h. Passing a limit $n\to\infty$ also shows us that $\mathbf{y}_h^*$ satisfies the upper bound (4.55). We point to Appendix A for a lengthy derivation of $\delta E_h[\mathbf{y}_h^n](\mathbf{v}_h)$, but an important feature is that the map $\mathbf{y}_h\mapsto\delta E_h[\mathbf{y}_h](\mathbf{v}_h)$ is continuous at $\mathbf{y}_h^*$ if $\mathbf{y}_h^*$ satisfies (4.55).

Therefore, $\lim_{n\to\infty} \delta E_h[\mathbf{y}_h^n](\mathbf{v}_h) = \delta E_h[\mathbf{y}_h^*](\mathbf{v}_h)$, which completes the proof of (4.50). $\square$

It is worth realizing that a critical point of E_h may not be a global discrete minimizer of E_h. Finally, given a tolerance $\mathrm{tol}_1 > 0$, we stop the nonlinear gradient flow when

$$\frac{1}{\tau}\big|E_h[\mathbf{y}_h^N] - E_h[\mathbf{y}_h^{N-1}]\big| \ < \ \mathrm{tol}_1$$

is satisfied for some $N > 0$. The function $\mathbf{y}_h^N \in \mathbb{V}_h$ is the desired output. We next discuss how we solve the nonlinear equation (4.48).

4.5.2 Newton sub-iteration

We solve each step n of the iterative scheme (4.48) by a Newton-type sub-iteration. In fact, we let $\mathbf{y}_h^{n,0} := \mathbf{y}_h^n$ and assume $\mathbf{y}_h^{n,k} \in \mathbb{V}_h$ is given. We then solve for the increment $\delta\mathbf{y}_h^{n,k} \in \mathbb{V}_h$ by

$$\delta^2 L_h^n[\mathbf{y}_h^{n,k}](\delta\mathbf{y}_h^{n,k}, \mathbf{v}_h) = -\delta L_h^n[\mathbf{y}_h^{n,k}](\mathbf{v}_h) \quad \forall\, \mathbf{v}_h \in \mathbb{V}_h, \tag{4.56}$$

and update $\mathbf{y}_h^{n,k+1} := \mathbf{y}_h^{n,k} + \delta\mathbf{y}_h^{n,k}$. Equation (4.56) is *linear* in the unknown $\delta\mathbf{y}_h^{n,k}$ because $\mathbf{y}_k^{n,k}$ is known. Moreover, given a tolerance tol_2, we stop (4.56) when

$$\big|\delta L_h^n[\mathbf{y}_h^{n,M}](\delta\mathbf{y}_h^{n,M})\big|^{1/2} \le \mathrm{tol}_2,$$

for some integer $M > 0$ and set $\mathbf{y}_h^{n+1} := \mathbf{y}_h^{n,M}$. The expression of $\delta^2 L_h^n[\mathbf{y}_h](\mathbf{v}_h, \mathbf{w}_h)$ for $\mathbf{y}_h, \mathbf{v}_h, \mathbf{w}_h \in \mathbb{V}_h$ is tedious to compute but is given in Appendix A.

We next assess the performance of the Newton sub-iterations for solving (4.48). We base our comments below on our numerical experiments of Section 5. We present a thorough discussion of well-posedness and convergence for the Newton sub-iterations in this section, provided $\mathbf{y}_h^0 \in \mathbb{V}_h$ is close to the discrete solution. Below are some reasons why we expect the Newton sub-iteration to perform well.

- **Initialization.** When $\mathbf{y}_h^i \in \mathbb{V}_h$ is given in the gradient flow outer iteration, it is natural to choose $\mathbf{y}_h^{i,0} := \mathbf{y}_h^i$ as initial guess for the Newton's inner iterations that is designed to compute $\mathbf{y}_h^{i+1}$. If $\mathbf{y}_h^{i,*}$ is a local minimizer of (4.47) and $E_h[\mathbf{y}_h^0] \le \alpha$, then (4.49) implies

$$\frac{1}{2\tau}\|\mathbf{y}_h^{i,*} - \mathbf{y}_h^i\|_{H^1(\Omega)}^2 \le E_h[\mathbf{y}_h^i] \le E_h[\mathbf{y}_h^0] \le \alpha,$$

  whence the H^1-distance between $\mathbf{y}_h^{i,0}$ and the minimizer $\mathbf{y}_h^{i,*}$ is proportional to $\tau^{1/2}$. This not only reveals the crucial role of τ but also of the H^1-metric for the discrete flow (4.47), which is the norm governing the stretching energy (4.1).

- **Well-posedness and convergence.** In view of (4.46), the quadratic structure of the flow metric term $\tau^{-1}(\cdot,\cdot)_{H^1(\Omega)}$ may compensate for the lack of ellipticity of $\delta^2 E_h[\mathbf{y}_h](\cdot,\cdot)$ due to the lack of quasi-convexity of E_h, provided τ is sufficiently small. Therefore, we expect well-posedness and superlinear convergence of the proposed Newton method, when τ is small.

- **Moderate condition on τ.** Our simulations of Section 5 confirm solvability and convergence of the Newton sub-iterations (4.56) with moderate values of τ relative to the meshsize h. Consequently, the restriction on τ is mild for current simulations and yet prevents the use of backtracking techniques. This constrasts strikingly with our theoretical estimates below, which suggest an a priori relation $\tau \lesssim h^2$ for quadratic convergence; see Remark 4.4.

A natural question is whether the Newton equation (4.56) is well-posed in each sub-step n and $\mathbf{y}_h^{n,k}$ converges to a minimizer of (4.47) as $k \to \infty$ in a neighborhood of the previous iterate $\mathbf{y}_h^n$, provided τ is sufficiently small. Heuristically, the lack of convexity of the stretching energy works against the well-posedness and convergence of the Newton sub-iteration, but the flow metric $\tau^{-1}(\cdot,\cdot)_{H^1(\Omega)}$ in (4.48) is chosen to dominate $\delta E_h[\mathbf{y}_h^n]$ when τ is small enough.

We now discuss properties of the proposed Newton sub-iteration (4.56). We first state the following ellipticity of $\delta^2 L_h^n[\mathbf{y}_h](\cdot,\cdot)$ but prove it in Appendix A.

Theorem 4.4 (ellipticity)**.** *Given $\mathbf{y}_h \in \mathbb{V}_h$, let the piecewise constant eigenvalues $\lambda_1[\mathbf{y}_h] \leq \lambda_2[\mathbf{y}_h]$ of $\mathrm{I}[\mathbf{y}_h]$ over $\mathcal{T}_h$ satisfy*

$$0 < c_1 \leq \lambda_1[\mathbf{y}_h] \leq \lambda_2[\mathbf{y}_h] \leq c_2 \quad \forall T \in \mathcal{T}_h, \tag{4.57}$$

with c_1, c_2 independent of h and T. Then for τ small enough, there exists a constant $c > 0$ independent of h such that

$$\delta^2 L_h^n[\mathbf{y}_h](\mathbf{v}_h,\mathbf{v}_h) \geq c\|\mathbf{v}_h\|^2_{H^1(\Omega;\mathbb{R}^3)} \quad \forall\, \mathbf{v}_h \in \mathbb{V}_h. \tag{4.58}$$

We next state a Lipschitz property of $\delta^2 L_h^n$ but postpone its proof to Appendix A.

Theorem 4.5 (Lipschitz property)**.** *Let $\mathbf{y}_h, \widetilde{\mathbf{y}}_h \in \mathbb{V}_h$ be given and both satisfy (4.57). Then, there exists a constant M independent of h such that*

$$\big|\delta^2 L_h^n[\mathbf{y}_h] - \delta^2 L_h^n[\widetilde{\mathbf{y}}_h]\big|(\mathbf{v}_h,\mathbf{w}_h) \leq \frac{M}{h}\|\mathbf{y}_h - \widetilde{\mathbf{y}}_h\|_{H^1(\Omega;\mathbb{R}^3)}\|\mathbf{v}_h\|_{H^1(\Omega;\mathbb{R}^3)}\|\mathbf{w}_h\|_{H^1(\Omega;\mathbb{R}^3)}, \tag{4.59}$$

for any $\mathbf{v}_h, \mathbf{w}_h \in \mathbb{V}_h$.

With Theorems 4.4 (ellipticity) and 4.5 (Lipschitz property) at hand, we state an error estimate for each Newton sub-iteration (4.56) and refer to Appendix A for its proof.

Corollary 4.2 (quadratic estimate)**.** *If* $\mathbf{y}_h^{n,k}$ *satisfy* (4.57) *for any* $n \geq 0$ *and* $k \geq 0$*, then* (4.56) *is well-posed and* $\delta\mathbf{y}_h^{n,k}$ *is the unique solution. Moreover, if* $\mathbf{y}_h^{n,k+1} := \mathbf{y}_h^{n,k} + \delta\mathbf{y}_h^{n,k}$*, then*

$$\|\mathbf{y}_h^{n,k+1} - \mathbf{y}_h^{n,*}\|_{H^1(\Omega;\mathbb{R}^3)} \leq \frac{M}{2ch}\|\mathbf{y}_h^{n,k} - \mathbf{y}_h^{n,*}\|^2_{H^1(\Omega;\mathbb{R}^3)}, \tag{4.60}$$

where c, M *are the constants appearing in* (4.58) *and* (4.59) *and* $\mathbf{y}_h^{n,*}$ *is a local minimizer of* L_h^n*.*

Together with a further condition on the initialization $\mathbf{y}_h^{n,0}$, the estimate (4.60) guarantees the convergence of Newton sub-iterations.

Remark 4.4 (quadratic convergence)**.** If $\mathbf{y}_h^{n,0}$ satisfies

$$\|\mathbf{y}_h^{n,0} - \mathbf{y}_h^{n,*}\|_{H^1(\Omega)} \leq \frac{ch}{M}, \tag{4.61}$$

then for $k \geq 0$ an induction argument combined with (4.60) yields

$$\|\mathbf{y}_h^{n,k+1} - \mathbf{y}_h^{n,*}\|_{H^1(\Omega)} \leq \frac{1}{2}\|\mathbf{y}_h^{n,k} - \mathbf{y}_h^{n,*}\|_{H^1(\Omega)} < \frac{ch}{M}. \tag{4.62}$$

This implies that the Newton sub-iterations $\mathbf{y}_h^{n,k}$ remain within an H^1-ball of radius $\frac{ch}{M}$ centered at $\mathbf{y}_h^{n,*}$ and converge to $\mathbf{y}_h^{n,*}$; in view of (4.60) this convergence is quadratic. It remains to check whether the initialization condition (4.61) is realistic. Assume that $E_h[\mathbf{y}_h^0] \leq \alpha$ for a constant

$\alpha > 0$ and recall that $\mathbf{y}_h^{n,0} = \mathbf{y}_h^n$ to deduce

$$\frac{1}{2\tau}\|\mathbf{y}_h^{n,*} - \mathbf{y}_h^n\|_{H^1(\Omega)}^2 \le L_h^n[\mathbf{y}_h^{n,*}] \le L_h^n[\mathbf{y}_h^n] = E_h[\mathbf{y}_h^n] \le E_h[\mathbf{y}_h^0] \le \alpha.$$

Consequently, if

$$\tau \le \frac{c^2h^2}{2M^2\alpha}$$

then (4.61) is valid. However, quantitative numerical experiments in Section 5.2 reveal that the largest admissible value of τ is independent of h. This is strikingly better than our theoretical prediction.

Remark 4.5 (assumption (4.57))**.** We now argue heuristically that the crucial assumption (4.57) is realistic in practice for each iterate $\mathbf{y}_h^{n,k}$ and $n, k \ge 0$. Suppose that $\mathrm{I}[\mathbf{y}_h^{n,k}]$ is close to g pointwise in the sense that

$$\|\mathrm{I}[\mathbf{y}_h^{n,k}] - g\|_{L^\infty(\Omega)} \le \varepsilon, \tag{4.63}$$

for some $\varepsilon > 0$. We recall that the eigenvalues of g are λ^2, λ^{-1} with $\lambda > 0$ defined in (4.8). Then the eigenvalues of $\mathrm{I}[\mathbf{y}_h^{n,k}]$, denoted by $\lambda_1[\mathbf{y}_h^{n,k}] \le \lambda_2[\mathbf{y}_h^{n,k}]$, satisfy

$$c_1 = \min\{\lambda^2, \lambda^{-1}\} - c\varepsilon \le \lambda_1[\mathbf{y}_h^{n,k}] \le \lambda_2[\mathbf{y}_h^{n,k}] \le \max\{\lambda^2, \lambda^{-1}\} + c\varepsilon = c_2,$$

with some constant $c > 0$. This turns out to be (4.57) for $\mathbf{y}_h^{n,k}$ provided ε is sufficiently small so that the constants $c_1, c_2 > 0$. Computations in Section 5.7 show conclusively that $\|\mathrm{I}[\mathbf{y}_h^n] - g\|_{L^\infty(\Omega)}$ decreases monotonically as n increases when $\mathbf{m}$ is smooth. They also indicate that $\|\mathrm{I}[\mathbf{y}_h^n] - g\|_{L^1(\Omega)}$ decreases monotonically regardless of the regularity of $\mathbf{m}$. This gives computational support for (4.63) and all iterates $\mathbf{y}_h^{n,k}$ provided $\mathrm{I}[\mathbf{y}_h^0]$ is close to the target metric g in the max-norm.

We conclude this section by summarizing the proposed strategy in Algorithm 2.

Algorithm 2: (nonlinear gradient flow scheme)

Given a pseudo time-step $\tau > 0$ and target tolerances tol_1 and tol_2;
Choose initial guess $\mathbf{y}_h^0 \in \mathbb{V}_h$;
while $\tau^{-1}\big|E_h[\mathbf{y}_h^{n+1}] - E_h[\mathbf{y}_h^n]\big| > tol_1$ **do**
  Set $\mathbf{y}_h^{n,0} = \mathbf{y}_h^n$, $k = 0$;
  while $\big|\delta L_h^n[\mathbf{y}_h^{n,k}](\delta \mathbf{y}_h^{n,k})\big|^{1/2} > tol_2$ **do**
    Solve (4.56) for $\delta \mathbf{y}_h^{n,k}$;
    Update $\mathbf{y}_h^{n,k+1} \leftarrow \mathbf{y}_h^{n,k} + \delta \mathbf{y}_h^{n,k}$, $k = k+1$;
  end
  Update $\mathbf{y}_h^{n+1} := \mathbf{y}_h^{n,k}$, where k is the index of last sub-iterate.
end

Chapter 5: Computation of Thin Liquid Crystal Polymer Networks

In this chapter, we investigate computationally the wealth of shapes that can be created upon actuation of an LCN, with special emphasis on the effect of defects and creases. We have implemented Algorithm 2 using the multiphysics finite element software Netgen/NGSolve [109], and the visualization relies on ParaView [7]. We focus on the ability of our discrete reduced model (4.19) to capture quite appealing and practical physical phenomena related to shape formation. We also present insightful numerical experiments that show quantitative properties of Algorithm 2 and document the convergence of the proposed method.

In order to allow for locally refined triangulations, which are instrumental for some simulations, we modify the regularization term in (4.15) as follows

$$R_h[\mathbf{y}_h] = c_r \sum_{e \in \mathcal{E}_h} h_e \int_e |[\nabla \mathbf{y}_h]|^2, \tag{5.1}$$

and similarly for $R_{h,\Gamma}$ in (4.43). In some experiments we measure the deviation of $\mathrm{I}[\mathbf{y}_h^\infty]$ from the target metric g for the final iterate $\mathbf{y}_h^\infty$ as an indicator of error between an approximate solution and an exact global minimizer to (4.1). We quantify the metric deviation via

$$e_h^p[\mathbf{y}_h^\infty] \ := \ \|\mathrm{I}[\mathbf{y}_h^\infty] \ - \ g\|_{L^p(\Omega\mathbb{R}^{2\times 2})}, \tag{5.2}$$

for $p = 1, \infty$. Since global minimizers to (4.1) are characterized by the metric constraint (3.44) of Corollary 3.4 (immersions of g are minimizers with vanishing energy), a small metric deviation (5.2) implies that the approximate solution $\mathbf{y}_h^N$ is close to an exact global minimizer.

5.1 Rotationally symmetric director fields and defects

Let $\Omega \subset \mathbb{R}^2$ be the unit disc. Motivated by [46, 88, 91, 122], we let the blueprinted director field $\mathbf{m}$ be a rotation of (3.56) by an angle α, namely

$$\mathbf{m}(r,\theta) = \big(\cos(n(\theta+\alpha)), \sin(n(\theta+\alpha))\big); \tag{5.3}$$

recall that n is the defect degree and that $\mathbf{m}$ is discontinuous at the origin. We run Algorithm 2 with several values of α and n and display the output in Fig. 5.1. To illustrate the effectiveness of Algorithm 2 to capture physical phenomena, we also compare the computed shapes with experimental and expected configurations in [91, 122] and find striking similarities. We use the following physical and numerical parameters

$$s = 0.1,\ s_0 = 1; \quad \text{tol}_1 = 10^{-6},\ \text{tol}_2 = 10^{-10},\ \tau = 0.1,\ h = 1/32,\ c_r = 1,$$

let $\mathbf{x} = (x_1, x_2) \in \Omega$, and initialize Algorithm 2 with $\mathbf{y}_h^0 = I_h \mathbf{y}^0$, where

$$\mathbf{y}^0(\mathbf{x}) \ = \ \big(\mathbf{x}, 0.05(1-|\mathbf{x}|^2)\big) \tag{5.4}$$

is a small perturbation of a flat disc (i.e. $\mathbf{y}(\Omega) = \Omega$).

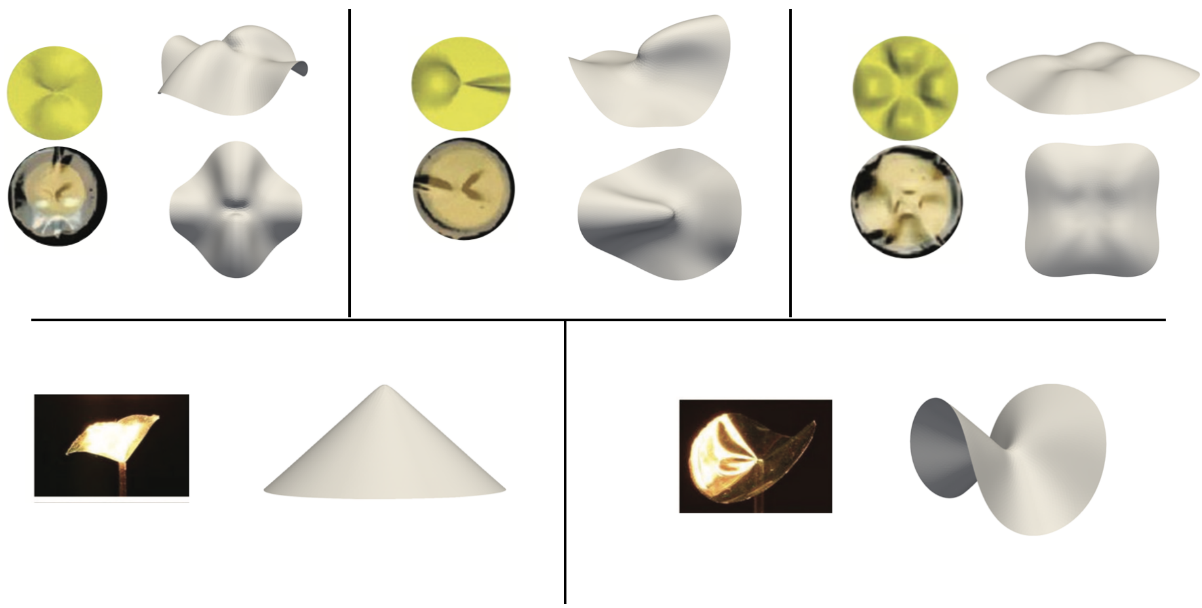

Figure 5.1: *Director fields with point defects of degree* n. First row displays $n = 2, 3/2, -1$ and $\alpha = 0$ (from left to right). Each panel shows experimental and expected configurations from [88] as well as two views of the computed solution. Second row depicts experimental pictures from [58] and our simulations of the cone structure $n = 1, \alpha = \frac{\pi}{2}$ (left) and anti-cone structure $n = 1, \alpha = 0$ (right). The numerical model reproduces experimental observations well.

5.2 Quantitative properties

In this subsection, we investigate computationally some quantitative properties of the proposed method, and in particular the role of meshsize h and pseudo time step τ. Our goals are as follows.

- **Convergence of metric deviation**. We measure the metric deviation $e_h[\mathbf{y}_h^\infty]$ defined in (5.2) as an error between computed solutions $\mathbf{y}_h^\infty$ and global minimizers, and recall that g is given by (3.42). We expect convergence of $e_h[\mathbf{y}_h^\infty]$ as $h \to 0$.

- **Convergence of energy**. We know that the exact minimum energy is 0 from discussions of Section 3.2.2. Therefore, we also expect convergence of the energy error $|E_h[\mathbf{y}_h^\infty]| := |E_h[\mathbf{y}_h^\infty] - 0|$ as $h \to 0$.

- **Role of pseudo time-step** τ. We expect that the well-posedness and convergence of Newton method (4.56) depend on τ. We thus disclose the influence of τ on the final energy $E_h(\mathbf{y}_h^\infty)$, metric deviation $e_h(\mathbf{y}_h^\infty)$ and the number of gradient flow iterations N.

We consider three experiments to explore these issues computationally.

Experiment 1: smooth $\mathbf{m}$. Let Ω be the unit square $\Omega = [-0.5, 0.5]^2$ and

$$\mathbf{m} = (x+1, y+1)/\sqrt{(x+1)^2 + (y+1)^2}. \tag{5.5}$$

We take parameters

$$s = 0.1, \quad s_0 = 1; \quad c_r = 0, \quad \mathrm{tol}_1 = 10^{-10}, \quad \mathrm{tol}_2 = 10^{-9},$$

and the initialization $\mathbf{y}_h^0 = I_h \mathbf{y}^0$ with

$$\mathbf{y}^0(x_1, x_2) = \big(x_1, x_2, 0.8(x_1 - 0.5)(x_1 + 0.5)(x_2 - 0.5)(x_2 + 0.5)\big). \tag{5.6}$$

Tables 5.1 and 5.2 display the results. We see that in Table 5.1 both $e_h[\mathbf{y}_h^\infty]$ and $|E_h[\mathbf{y}_h]|$ are rather insensitive to τ but N decreases with increasing τ. The fact that performance does not improve for smaller τ motivates us to explore the largest admissible time step $\tau_{\max}$ with various h in Table 5.2, which also reveals the convergence of our method.

τ	$e_h[\mathbf{y}_h^\infty]$	$\lvert E_h[\mathbf{y}_h^\infty]\rvert$	N
0.2	4.66909E-3	2.3484E-5	2304
0.4	4.66909E-3	2.3484E-5	1151
0.8	4.66910E-3	2.3484E-5	574
1.6	4.66918E-3	2.3482E-5	286
3.2	diverge	diverge	diverge

Table 5.1: Experiment 1 with the blueprinted director field (5.5). This reveals influence of τ on the energy error, metric deviation e_h, and the number of gradient flow iterations N with fixed $h = 1/32$.

h	$\tau_{\max}$	$e_h(\mathbf{y}_h^\infty)$	$\lvert E_h(\mathbf{y}_h^\infty)\rvert$	N
1/16	2.23	9.45213E-3	8.7909E-5	267
1/32	2.11	4.66924E-3	2.3482E-5	216
1/64	2.10	2.30916E-3	5.7742E-6	130
1/128	2.09	1.22053E-3	1.5746E-6	129

Table 5.2: Experiment 1 with the blueprinted director field (5.5). This gives the largest admissible time step $\tau_{\max}$ that guarantees the well-posedness and convergence of Newton step for various h. Convergence of errors as $h \to 0$ are observed with corresponding $\tau_{\max}$, which change slowly with h.

Experiment 2: effect of regularization. We consider the same set-up as *Experiment 1* but instead of $c_r = 0$ we take $c_r = 1$.

Experiment 3: $\mathbf{m}$ with defects. We consider the set-up in Section 5.1. The director field $\mathbf{m}$ is the degree $3/2$ defect given in (5.3). The parameters are as those from Section 5.1:

$$s = 0.1, \; s_0 = 1; \quad \text{tol}_1 = 10^{-6}, \; \text{tol}_2 = 10^{-10}.$$

However, we take $c_r = 0$ instead of $c_r = 1$.

The energy errors $|E_h[\mathbf{y}_h^\infty]|$ and metric deviation $e_h[\mathbf{y}_h^\infty]$ for *Experiments 1,2,3* are plotted in Fig. 5.2 for meshsizes $h = 1/16, 1/32, 1/64, 1/128$. We discuss them next.

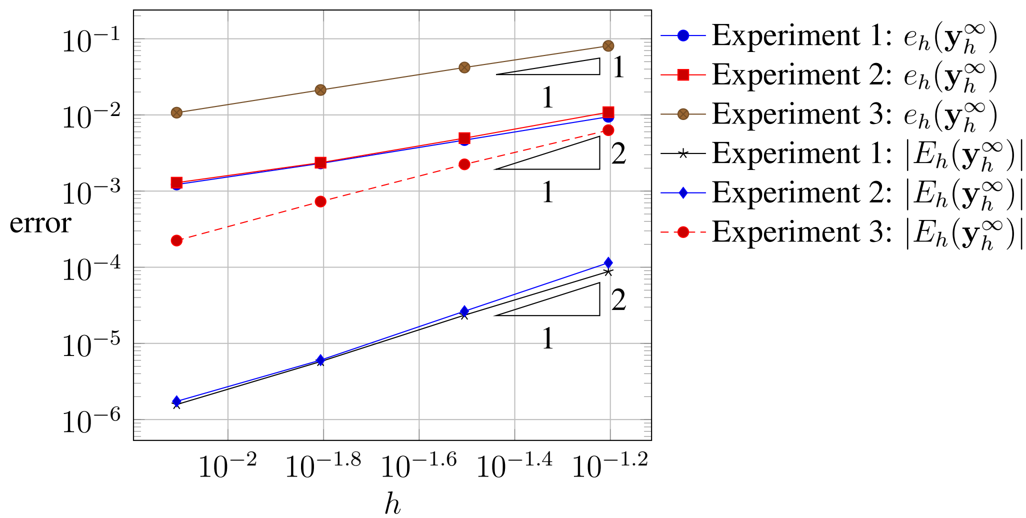

Figure 5.2: Convergence of errors for *Experiments 1,2,3*. We can see that the regularization has almost no influence on convergence rates, while it results in a slightly larger value of errors. For *Experiment 3* with discontinuous $\mathbf{m}$ the errors are significantly larger. In all cases we observe that $e_h[\mathbf{y}_h^\infty]$ is linear in h, while $|E_h[\mathbf{y}_h^\infty]|$ is quadratic in h for *Experiments 1,2* and has a rate slightly worse than quadratic (it is approximately $\mathcal{O}(h^{\log_2 3})$) for *Experiment 3*.

We conclude with a summary of quantitative observations.

- The metric deviation $e_h[\mathbf{y}_h^\infty]$ converges as $\mathcal{O}(h)$. The energy error $|E_h(\mathbf{y}_h^\infty)|$ converges as $\mathcal{O}(h^2)$ or sub-quadratically, depending on the regularity of $\mathbf{m}$.

  – $|E_h[\mathbf{y}_h^\infty]|$ converges as $\mathcal{O}(h^2)$ in Experiments 1 and 2, when $\mathbf{m}$ is smooth and g is likely to admit a H^2 isometric immersion. This computational result corroborates the validity of Assumption 4.1 and the energy scaling in Proposition 4.3.

  - $|E_h[\mathbf{y}_h^\infty]|$ converges sub-quadratically in Experiment 3, when $\mathbf{m}$ has a degree $3/2$ defect. It is plausible that g does not admit a H^2 isometric immersion, and if so the validity of Assumption 4.1 is questionable. It is worth realizing that this assumption is responsible for the quadratic energy scaling in Proposition 4.3 (recovery sequence).

- The Newton sub-iteration is well-posed and convergent when τ is small enough. The influence of h on $\tau_{\max}$ is negligible. This is much better than $\tau \lesssim h^2$, the theoretical prediction in Remark 4.4 (quadratic convergence).

- Once τ is chosen such that the Newton method is well-posed and convergent, further decreasing of τ has only a negligible influence on errors.

- For fixed h, the number of gradient flow iterations $N = \mathcal{O}(\tau^{-1})$, and so does the computational time. Minimizing N is crucial for computational efficiency.

These conclusions corroborate convergence of the proposed finite element method with nonlinear solver and the fact that an ideal choice of τ is its largest admissible value $\tau_{\max}$ for various problems. We do not need to take $\tau \to 0$ as triangulations refine, and $\tau_{\max}$ provides a moderate upper bound for τ. This is an advantage compared to a linearized gradient flow (e.g. [29]) and a fixed point sub-iteration scheme (e.g. [19]) in that both require τ depending on h.

5.3 Compatible nonisometric origami

Recall in Section 4.4, we introduced a modification to E_h, that allows for *folds or creases* along some polygonal set $\Gamma = \cup_{i=1}^{N} \gamma_i$, which is the union of line segments γ_i. This section is dedicated to computing configurations of compatible nonisometric origami, which we explain below.

Compatibility: We assume the blueprinted director field $\mathbf{m}$ to be constant in each subdomain. We say the set-up of nonisometric origami is *compatible* if

- $\mathbf{m}$ satisfies the compatibility condition proposed in [102, formula (6.3)], namely

$$|\mathbf{m}_{\gamma_i^+} \cdot \mathbf{t}_{\gamma_i}| = |\mathbf{m}_{\gamma_i^-} \cdot \mathbf{t}_{\gamma_i}|,$$

  for any $i = 1, \ldots, N$, where $\mathbf{t}_{\gamma_i}$ represents a unit tangent vector to γ_i and $\mathbf{m}_{\gamma_i^\pm}$ denote $\mathbf{m}$ restricted to the two subdomains that share γ_i;

- The actuation parameters s, s_0, and thus the parameter λ defined in (4.8), are continuous across γ_i for $i = 1, \ldots, N$.

The compatibility condition means that the tangential component of the line field $\mathbf{m} \otimes \mathbf{m}$ and parameter λ are continuous across γ_i. Therefore, since any equilibrium configuration satisfies the metric constraint (3.44) with metric g defined in (3.42), such configuration sustains *compatible* stretching on both sides of a folding line γ_i.

In Section 4.4, we exploit the fact that the regularization parameter c_r may depend on the edge e to incorporate the creases Γ in the discrete energy $E_{h,\Gamma}$ in (4.42). We thus take regularization parameter $c_r = 0$ along the folding lines Γ and $c_r = 100$ in the rest of domain, i.e., we rewrite (4.43) as

$$R_{h,\Gamma}[\mathbf{y}_h] = c_r h \sum_{e \in \mathcal{E}_h \setminus \Gamma} \int_e [\nabla \mathbf{y}_h]^2. \tag{5.7}$$

In fact, the zero regularization (no jumps of gradient) models a weakened (or damaged) material on creases [18], and mathematically this allows for the formation of kinks. On the other hand, the large regularization in the subdomains serves as a mechanism to force small bending energy on minimizers of the discrete stretching energy E_h. Consequently, equilibrium configurations prefer flat surfaces and folds to meet the target metric (3.44), namely nonisometric origami.

5.3.1 Pyramids

We consider piecewise constant blueprinted director fields $\mathbf{m}$ and set-up creases Γ and subdomains Ω_i as depicted in Fig.5.13. In this experiment, we take $\Omega = [0,1]^2$,

$$s = 0.1, \quad s_0 = 1, \quad h = 1/64, \mathrm{tol}_1 = 10^{-10}, \quad \mathrm{tol}_2 = 10^{-6}.$$

Case 1. We first consider the set-up on the left of Fig.5.3, $\tau = 1$, and use initialization $\mathbf{y}_h^0 = I_h \mathbf{y}^0$ with

$$\mathbf{y}^0(x_1, x_2) \;=\; \big(x_1, x_2, 0.8x_1(1-x_1)x_2(1-x_2)\big)\,. \tag{5.8}$$

Case 2. We then consider the set-up on the right of Fig.5.3, $\tau = 0.4$, and use the same initialization as (5.8), *Case 3.* We also apply another initialization

$$\mathbf{y}^0(x_1, x_2) \;=\; 0.2\cos\big(7\pi(x_1 - 0.5)\big)\, x_2(x_2 - 1) \tag{5.9}$$

to the set-up on the right of Fig.5.3 and take $\tau = 0.5$.

The computed solutions for all three cases are shown in Fig.5.4. We get pyramid-like final configuration for *Case 1*, which is consistent with the prediction in [92]. For *Cases 2* and *3*, we obtain different equilibria starting from different initial states, but the difference in final energies is about 10^{-6}. They are indeed global minimizers, because computed metric deviations $e_h^\infty[\mathbf{y}_h^\infty]$ are $1.6 \times 10^{-3}, 2.5 \times 10^{-3}, 2.4 \times 10^{-3}$ for *Cases 1,2,3* respectively. Therefore, this gives an example where global minimizers to (4.19) are non-unique, and computed equilibrium shapes depend on initializations. This verifies the heuristic discussion in Section 4.1.1, confirms the lack of quasi-convexity of this model, and illustrates capability and accuracy of our numerical method for computing origami structures.

Case 4. To confirm that the pyramid-like origami structure is *not* an effect due to the triangulation, we generate a triangulation with $h = 1/64$ unfitted to the two diagonals Γ of the square. We consider the same set-up as in *Case 1* except that the regularization parameter $c_r(\mathbf{x}) = 0$ if $\mathbf{x} \in \Gamma_{0.02}$ and $c_r(\mathbf{x}) = 100$ otherwise, where $\Gamma_d := \{\mathbf{x} \in \Omega : \text{dist}(\mathbf{x}, \Gamma) < d\}$ is a strip surrounding the crease Γ.

The computed solution for the *Case 4* is also displayed in Fig. 5.4 (third row). We still get the pyramid-like configuration, but with tiny wrinkling appearing in the strips $\Gamma_{0.02}$, due to the lack of regularization in this region. We present a thorough discussion of the computational effect of regularization in Section 5.6.

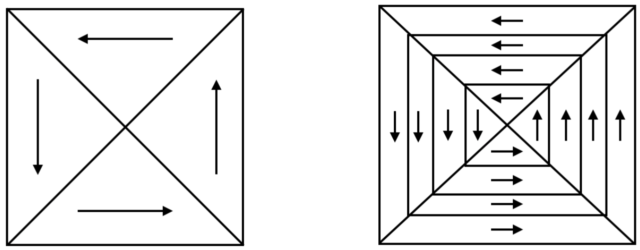

Figure 5.3: This is the set-up for experiments in Subsection 5.3.1. Solid lines inside the square represent the locations of the creases, and arrows shows the piecewise constant director field $\mathbf{m}$ in each subdomain. In this case, $\mathbf{m} = (0, -1), (-1, 0), (0, 1), (1, 0)$ in different subdomains.

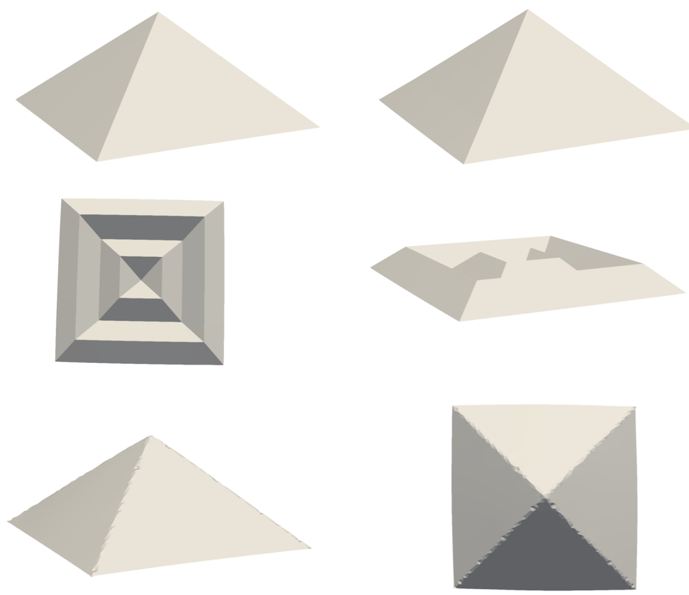

Figure 5.4: Non-isometric origami: First row, pyramid-like final configurations for *Case 1* and *Case 2*. Second row, different views of final configuration for *Case 3* exhibiting multiple folds. Third row, different views of final configuration for *Case 4*, thereby confirming that the pyramid-like configuration is not an effect due to the triangulation.

5.3.2 Folding table.

The set-up of blueprinted director field $\mathbf{m}$, creases Γ and subdomains of $\Omega = [0,1] \times [0,2]$ are displayed in Fig.5.5 (left). We choose parameters

$$s = 0.1,\ s_0 = 1;\ h = 1/64,\ \tau = 0.5,\ \mathrm{tol}_1 = 10^{-6},\ \mathrm{tol}_2 = 10^{-10}.$$

Case 1. We use the initialization $\mathbf{y}_h^0 = I_h \mathbf{y}^0$ with

$$\mathbf{y}^0(x_1, x_2) = \big(x_1, x_2, 0.8x_1(1-x_1)x_2(2-x_2)\big). \tag{5.10}$$

Case 2. We use the initialization $\mathbf{y}_h^0 = I_h \mathbf{y}^0$ with

$$\mathbf{y}^0(x_1, x_2) = \big(x_1, x_2, 0.8x_1(1-x_1)x_2(1-x_2)\big). \tag{5.11}$$

Simulations for both cases are presented in Fig.5.5. We get final configurations consistent with the predicted and experimental shapes in [103, Figure 5.2]. The two distinct final states correspond to different initial configurations. However, final energies are $E_h[\mathbf{y}_h^\infty] = 8.27 \times 10^{-6}, 5.97 \times 10^{-6}$ and the metric deviations are $e_h^1[\mathbf{y}_h^\infty] = 4.5 \times 10^{-3}, 3.7 \times 10^{-3}$ for the two cases. Consequently, this provides yet another example of non-unique minimizers due to the non-convex nature of the discrete model (4.19).

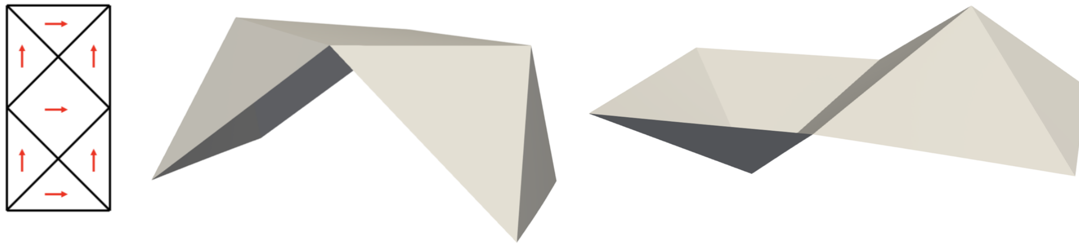

Figure 5.5: *Folding table*: Setting for origami in Subsection 5.3.2 (left). Final configurations for *Case 1* (middle) and *Case 2* (right).

5.3.3 Folding cube.

We now consider the design in [101] whose folded shape is an origami cube. The set-up is given in Fig.5.6 (left), where the domain Ω is a rhombus with vertices $(0,1)$, $(0,2)$, $(\sqrt{3},0)$, $(\sqrt{3},1)$. We take a *graded triangulation* such that $h = 1/128$ near the creases and $h = 1/32$ everywhere else. We choose the parameters

$$s = -1/3,\ s_0 = 1;\ \tau = 0.1,\ \text{tol}_1 = 10^{-8},\ \text{tol}_2 = 10^{-10},$$

and use the initialization $\mathbf{y}_h^0 = I_h \mathbf{y}^0$ with

$$\mathbf{y}^0(x_1, x_2) \ = \ \Big(x_1, x_2, 0.8x_1(x_1 - \sqrt{3})\big(x_2 + \frac{\sqrt{3}}{3}x_1 - 1\big)\big(x_2 + \frac{\sqrt{3}}{3}x_1 - 2\big)\Big). \tag{5.12}$$

The evolution of our nonlinear gradient flow is displayed in Fig.5.6 (right). We reach the desired cube equilibrium configuration with final energy $E_h[\mathbf{y}_h^\infty] = 7.34 \times 10^{-8}$ and metric defect $e_h^1[\mathbf{y}_h^\infty] = 3.6 \times 10^{-4}$. This relaxation dynamics is not physically motivated, but it is meaningful for an evolution without intertial effects.

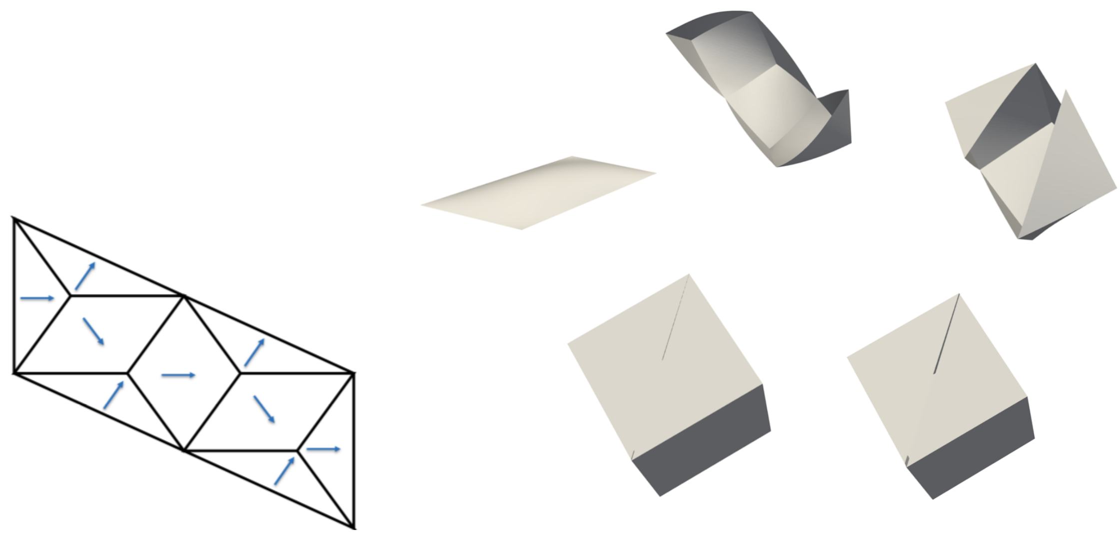

Figure 5.6: *Folding cube*: Rhombus Ω, creases Γ and director field $\mathbf{m}_\perp$ (left). Gradient flow iterates $\mathbf{y}_h^0, \mathbf{y}_h^{110}, \mathbf{y}_h^{310}, \mathbf{y}_h^{1010}$ and final configuration $\mathbf{y}_h^{1287}$ displayed clockwise.

The choice $s = -1/3$ and $s_0 = 1$ is crucial for the shape to form a perfect cube. This can be justified in the spirit of [92] as follows. We expect that rhombi subdomains in Fig. 5.6 to deform into faces of the cube, which are squares; this is depicted in Fig. 5.7. We assume that the diagonals of undeformed rhombi are parallel to $\mathbf{m}_\perp, \mathbf{m}$ and denote their lengths by L_1, L_2. If $s < s_0$ then $\lambda = \left(\frac{s+1}{s_0+1}\right)^{1/3} < 1$ according to (4.8), whence the expression (3.42) of the metric g reveals that the material stretches in the direction $\mathbf{m}_\perp$ and shrinks along $\mathbf{m}$ with ratios $1/\sqrt{\lambda}, \lambda$. If ℓ_1, ℓ_2 stand for the diagonals of the deformed square, then they satisfy $\ell_1 = (1/\sqrt{\lambda})L_1$ and $\ell_2 = \lambda L_2$ as well as $\ell_1 = \ell_2$. Consequently, we see that $\lambda^{-3/2} = L_2/L_1 = \sqrt{3}$ upon choosing $s_0 = 1$, that $s = -1/3$ as asserted.

5.3.4 Curved creases

The creases are arcs in this example motivated by [76]. The set-up in Fig. 5.8 (left) shows that the domain Ω is a square and the creases Γ are curved solid lines. We use a *graded* tri-

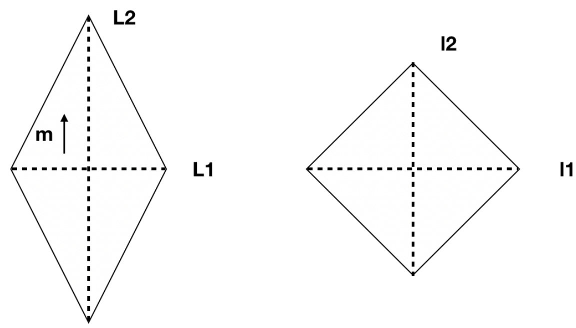

Figure 5.7: *Folding cube*: rhombus with diagonals L_1, L_2 deforms into a square with diagonals $\ell_1 = \ell_2$ to match the target metric and thus minimize the stretching energy.

angulation such that $h = 1/128$ near the arcs and $h = 1/32$ everywhere else. We choose the parameters

$$s = 0.1,\ s_0 = 1;\ \tau = 0.5,\ \text{tol}_1 = 10^{-6},\ \text{tol}_2 = 10^{-10},$$

and use the initialization (5.11). The equilibrium shape is displayed in Fig. 5.8, which is like a tent. This examples shows the ability of our discrete model (4.19) to deal with curved creases.

5.4 Incompatible nonisometric origami

In this section, we allow the physical quantities $\mathbf{m}, s, s_0$ to *violate* the compatibility condition in Section 5.3, namely to be discontinuous across creases Γ. This entails a discontinuity of g and requires the material to sustain *incompatible* stretching on both sides of the creases. In light of Corollary 3.4 (immersions of g are minimizers with vanishing energy) and the discussion after it, the existence of an H^1 isometric immersion $\mathbf{y}$ of such a discontinuous g is questionable, and we would hypothesize that there is no deformation $\mathbf{y} \in H^1(\Omega; \mathbb{R}^3)$ such that $\mathrm{I}[\mathbf{y}] = g$ and correspondingly $E_{str,\Gamma}[\mathbf{y}] = 0$, due to the incompatible stretching. Computational evidence given

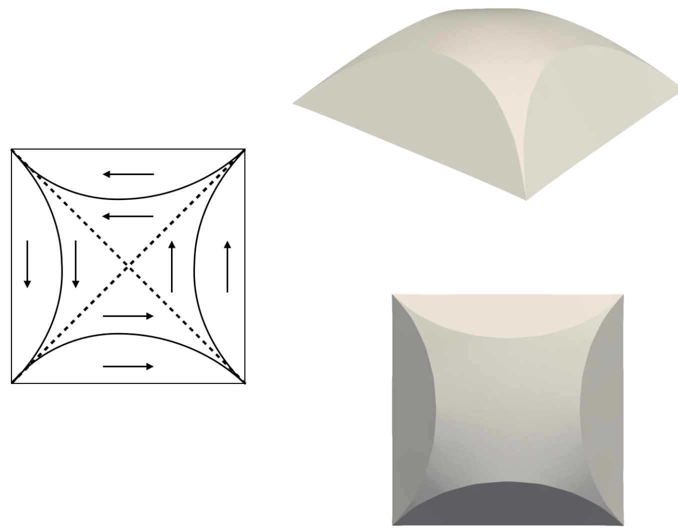

Figure 5.8: *Curved creases*: Square domain Ω, curved creases Γ (solid lines), and director field $\mathbf{m}$ (left). The dashed lines are lines of discontinuity of $\mathbf{m}$ rather than creases. Two views of final tent equilibrium configuration (right).

below shows that the discrete energy $E_h[\mathbf{y}_h]$ and metric defect $e_h^1[\mathbf{y}]$ decrease with meshsize to a positive value and the discrete solution $\mathbf{y}_h$ converges, at least weakly, in view of Proposition 4.2 (coercivity). We present two simulations and discuss the structure of this limit. To this end, we again consider the modified regularization (5.7) with $c_r = 0$ along the folding lines and $c_r = 100$ in the rest of the domain.

5.4.1 Lifted square origami.

Let $\Omega := [0, 1]^2$ be the unit square and the creases and subdomains be as depicted in Fig. 5.9 (left). The latter are concentric squares with vertices connected by folding lines. We take $s = s_0 = 1$ in the inner square (ideally no deformation) and $s = 0.1, s_0 = 1$ in the annulus between the two squares so that $\lambda < 1$ in this region. This implies shrinking along the direction of the director field $\mathbf{m}$, hence parallel to the sides, and stretching in the orthogonal direction $\mathbf{m}_\perp$.

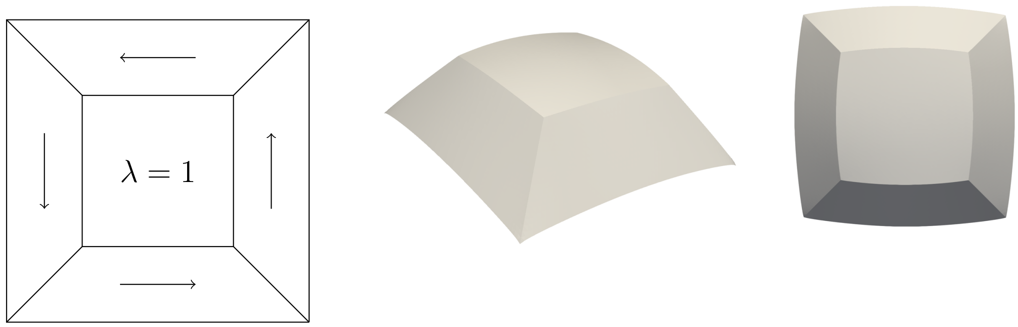

Figure 5.9: *Lifted square origami*: Lines indicate creases and arrows indicate the blueprinted director field $\mathbf{m}$ in regions where $\lambda < 1$ (left). The inner square has $\lambda = 1$ (no internal deformation). Two views of equilibrium configuration show that buckling takes place to accommodate the lack of data compatibility.

We use the initialization (5.11) and choose the parameters to be

$$h = 1/64, \ \tau = 0.1, \ \text{tol}_1 = 10^{-6}, \ \text{tol}_2 = 10^{-10}.$$

We plot two views of the final configuration on the middle and right of Fig. 5.9. We see that the inner region has no internally-induced deformation but shrinks and lifts up out of plane to accommodate itself to the change in the outer region.

h	$E_h[\mathbf{y}_h^\infty]$	$e_h^1[\mathbf{y}_h^\infty]$
1/32	0.0277	0.177
1/64	0.0127	0.103
1/128	0.00751	0.0754
1/256	0.00525	0.0626

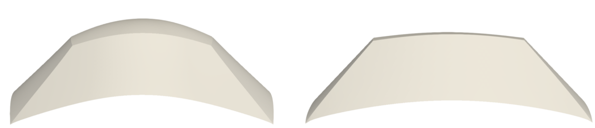

Figure 5.10: *Lifted square origami*: The table shows a monotone decrease of discrete energy $E_h[\mathbf{y}_h^\infty]$ and metric defect $e_h^1[\mathbf{y}_h^\infty]$ in terms of h, which stabilizes to a positive value. Side views of the deformations for $h = 1/128$ (middle) and $h = 1/64$ (right). The buckling is more pronounced for smaller h.

To explore the asymptotic behavior of $\mathbf{y}_h^\infty$ as $h \to 0$ we run a series of experiments reported in Fig. 5.10. We see that the energy $E_h[\mathbf{y}_h^\infty]$ is $\mathcal{O}(10^{-2})$ and decreases but not quadratically; in fact, it seems that it stabilizes to a positive value. Recall that the quadratic scaling $E_h[\mathbf{y}_h] \lesssim h^2$ of (4.44) in Theorem 4.2 (convergence of discrete minimizers with creases) leads to strong convergence in $H^1(\Omega;\mathbb{R}^3)$ to a piecewise H^2-limit $\mathbf{y}^*$ such that $E_{str,\Gamma}[\mathbf{y}^*] = 0$ and $\mathrm{I}[\mathbf{y}^*] = g$. This reveals that g may not admit an isometric immersion, at least not with the regularity stated in Theorem 4.2. This in turn contrasts with the compatible origami shapes in Section 5.3 for which the final energies are $\mathcal{O}(10^{-5})$ and $\mathcal{O}(10^{-7})$, making it likely that $E_{str,\Gamma}[\mathbf{y}^*] = 0$.

Fig. 5.10 also shows that buckling is more pronounced for smaller regularization, which happens for smaller $h = 1/128$. Finally, we view the regularization term $R_{h,\Gamma}[\mathbf{y}_h]$ as a numerical mechanism that selects some equilibrium configurations in the limit $h \to 0$. This process is related to the quasiconvex envelope of E_{str}, which is not known for E_{str} given by (4.1) and (4.2) and is hard to find. We refer to Section 4.1.1 for a discussion of quasiconvexity.

5.4.2 Lifted M-origami

We explain now how to exploit the idea in Subsection 5.4.1 as a building block to design lifted configurations of any polygonal shapes. In fact, for any polygonal subdomain $P \subset \Omega := [0,1]^2$ with $\operatorname{dist}(P, \partial\Omega) > 0$, we can always construct a dilation P' of P so that it is "concentric" with P and $P \subset P'$ with $\operatorname{dist}(P', \partial\Omega) > 0$. Then we further connect corresponding vertices of P and P' with folding lines, and also let all the sides of ∂P and $\partial P'$ be creases. We finally take $\mathbf{m}$ parallel to the sides of ∂P and $\lambda < 1$ in $P' \setminus P$, while $\lambda = 1$ in P and $\Omega \setminus P'$. The discontinuity of λ across creases implies again $E_{str}[\mathbf{y}] > 0$ for all $\mathbf{y} \in H^1(\Omega;\mathbb{R}^3)$.

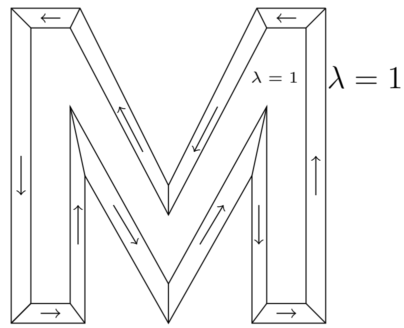

Figure 5.11: *Lifted M-origami*: Lines indicate creases and arrows indicate the blueprinted director field $\mathbf{m}$ in regions where $\lambda < 1$, whereas $\lambda = 1$ within and outside the M.

We apply this procedure to an M-shaped subdomain. The set-up is shown in Fig. 5.11 and all the parameters are the same as in Subsection 5.4.1. In particular $s = 0.1$ inside the M-annulus region while $s = 1$ in the rest of domain. We use a graded triangulation of size $h = 1/256$ near the creases and otherwise $h = 1/32$.

We display the computed solution in Fig. 5.12, which is the desired lifted M-shape. We stress that the background and solid M are not completely flat due to the same buckling effect already discussed in Section 5.4.1. However, this effect is not so pronounced because the shrinking layer is thin relative to the rest of the M and background. We emphasize that the current procedure is different from the construction of lifted surfaces in Section 3.3.1. The latter requires $|\nabla\phi| = \sqrt{\lambda^3 - 1}$ a.e. in Ω, which makes it harder to implement; recall the discussion after (3.47).

5.5 Actuation parameters s and s_0

Parameters s and s_0 encode the effect of environment actuation, such as light and heat, and determine the magnitude of stretches or shrinks in the directions $\mathbf{m}_\perp$ or $\mathbf{m}$ for equilibrium configurations. Therefore, when s is close to s_0 we can only expect a minor deformation; on the other hand, the material deforms significantly if s is far away from s_0. In this Subsection, we

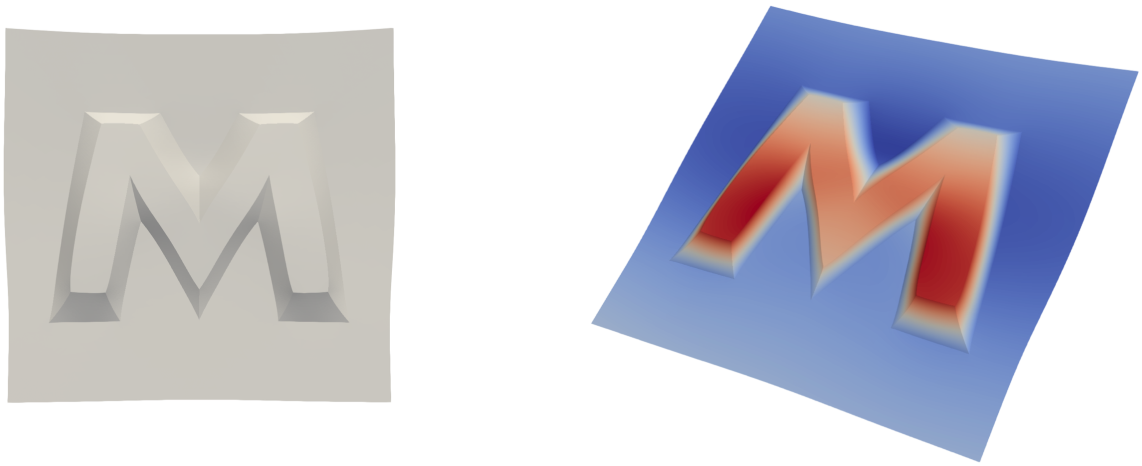

Figure 5.12: *Lifted M-origami*: Two views of final equilibrium configuration. Color on the right picture represents the value of y_3 and shows that the solid M and background are not completely flat.

explore the role of s and s_0 by our discrete model (4.19).

5.5.1 Pyramids with different s.

We consider the set-up of Fig.5.13: the domain is the square $\Omega = [0,1]^2$, its diagonals are the creases Γ, and the blueprinted director field $\mathbf{m}$ is parallel to the sides of Ω. We choose the parameters

$$s_0 = 1;\ h = 1/64, \tau = 1,\ \mathrm{tol}_1 = 10^{-6},\ \mathrm{tol}_2 = 10^{-10},$$

regularization constants $c_r = 0$ along the creases and $c_r = 100$ everywhere else, and initialization (5.11). We take $s = 0.9, 0.5, 0.1, -0.3$ and compare the results.

With arguments similar to those in Subsection 5.3.3 related to Fig. 5.7, one can easily see that the length of each side of the pyramid base should be $\lambda = (\frac{s+1}{s_0+1})^{\frac{1}{3}}$. In Fig. 5.14, we compare this theoretical value with computations of such lengths for different values of s, and display

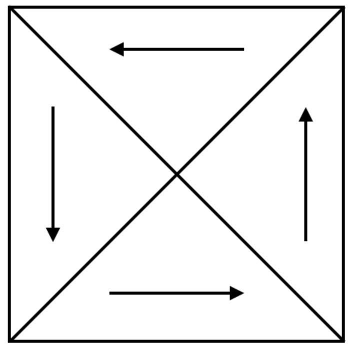

Figure 5.13: Set-up for experiments in Subsection 5.5.1. Square domain Ω with solid diagonals representing the creases and arrows parallel to the sides indicating the piecewise constant blueprinted director field $\mathbf{m}$.

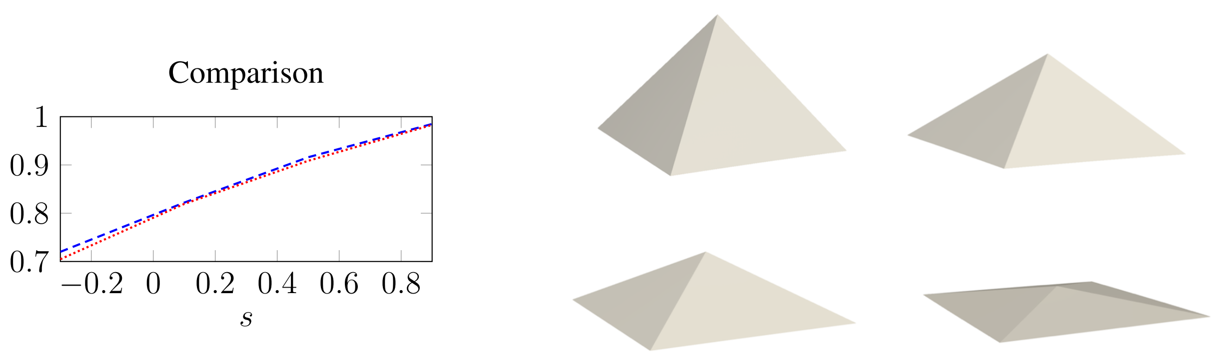

Figure 5.14: *Pyramids with varying actuation parameter* s: Comparison between computed length (blue dashed) and theoretical value $\lambda = (\frac{s+1}{s_0+1})^{\frac{1}{3}}$ (pink dots) of the pyramids base for several values of s (left). Computed pyramid solutions for values $s = -0.3, 0.1, 0.5, 0.9$ approaching $s_0 = 1$ (right).

the final equilibrium configurations for $s = -0.3, 0.1, 0.5, 0.9$; the agreement is remarkable. We observe that the pyramid height decreases to 0 as s increases toward $s_0 = 1$, and thus $\lambda \to 1$ (no deformation).

5.5.2 Pyramids with space varying s.

All preceding simulations assume s constant in space. We now consider the effect of varying s in space, while keeping all other parameters in Subsection 5.5.1 unchanged. This corresponds, for instance, to the situation that light stimulus is applied non-uniformly to the material. We take

$$s = 1 - 14.4x_1(1 - x_1)x_2(1 - x_2). \tag{5.13}$$

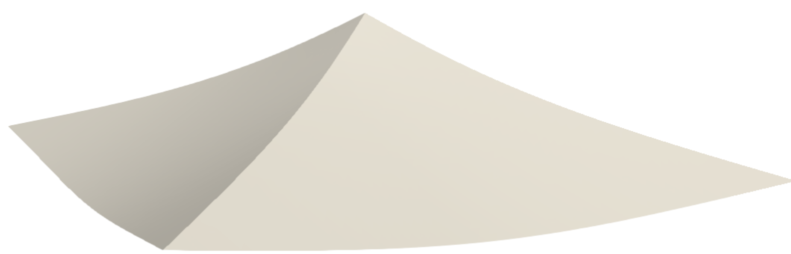

Figure 5.15: *Pyramid with space varying* s: The resulting pyramid for s given in (5.13) has curved faces, creases and sides.

The computed solution, displayed in Fig.5.15, consists of a pyramid with curved faces, creases and sides. For the flat pyramids of Fig 5.14, following [92], we can predict the opening angle ϕ of the pyramid to satisfy $\sin\phi = \sqrt{\frac{s+1}{s_0+1}}$. The opening angle is formed by two line segments: the vertical line from the vertex of the pyramid to the center of the base and the line segment from the vertex to the midpoint of the side of the base. Since $s_0 = 1$ and s decreases monotonically towards the center of the base from $s = 1$ on the base boundary, we realize that ϕ should decrease as well. This is consistent with our computed solution.

5.5.3 Four cones.

In this case, we take $\Omega := [-0.5, 0.5]^2$ and parameters

$$s_0 = 1;\ h = 1/64,\ \tau = 0.1,\ \text{tol}_2 = 10^{-10},\ \text{tol}_1 = 10^{-6}.$$

We choose the parameters $s = 0.1$ and $c_r = 1$ inside the four circles with radius 0.2 and centers $(\pm 0.25, \pm 0.25)$, and $s = 1$ and $c_r = 100$ everywhere else in the domain. We set the blueprinted director field as in (5.3), with $n = 1$ and $\alpha = \pi/2$

$$\mathbf{m}(x_1, x_2) = \big(\cos(\theta_i + \pi/2), \sin(\theta_i + \pi/2)\big) \tag{5.14}$$

where $\theta_i := \theta_i(x_1, x_2)$ for $i = 1 : 4$ is the angle between the positive x_1-axis and the line connecting (x_1, x_2) with $(0.25, 0.25)$, $(-0.25, 0.25)$, $(-0.25, -0.25)$, $(0.25, -0.25)$ in each quadrant, respectively. For instance,

$$\theta_1(x_1, x_2) := \begin{cases} \arctan(\frac{x_2 - 0.25}{x_1 - 0.25}) & x_1 > 0.25 \\ \arctan(\frac{x_2 - 0.25}{x_1 - 0.25}) + \pi & x_1 \leq 0.25. \end{cases} \tag{5.15}$$

Moreover, we initialize the discrete gradient flow with $\mathbf{y}_h^0 = I_h \mathbf{y}^0$ and

$$\mathbf{y}^0(x_1, x_2) \ = \ \big(x_1, x_2, 0.8(x_1 - 0.5)(x_1 + 0.5)(x_2 - 0.5)(x_2 + 0.5)\big). \tag{5.16}$$

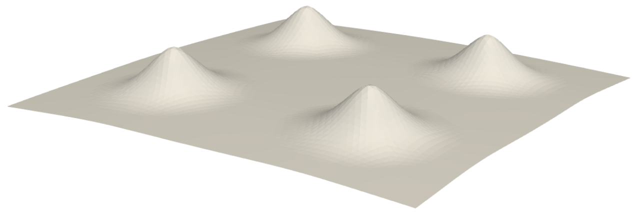

Figure 5.16: *Four cones*: Equilibrium shape showing four rotationally symmetric cones with vertices at $(\pm 0.5, \pm 0.5)$ and curved lateral surfaces. The parameter s and metric g are discontinuous across the boundaries of four circles of radius 0.2 centered at the vertices.

The equilibrium shape is displayed in Fig. 5.16, and consists of four cones with vertices at the four prescribed points $(\pm 0.25, \pm 0.25)$. Locally around each vertex, the shape is a rotationally symmetric cone as in Subsection 5.1 with $n = 1$ and $\alpha = \pi/2$, but the lateral surface flattens out as it meets the background substrate. This is due to the incompatibility created by the discontinuous parameter s and metric g cross the boundary of the four circles. This configuration is similar to the experimental one in [117].

5.6 Wrinklings and regularizations

We now elaborate on the role of the regularization term R_h defined in (4.15) in the formation of equilibrium configurations.

5.6.1 Degree -1 defect

First, we consider a blueprinted director field $\mathbf{m}$ with a defect of degree $n = -1$ rotated by an angle $\alpha = 0$ as described in (5.3) of Section 5.1. Fig. 5.17 compares two simulations with Algorithm 2 and regularization parameter $c_r = 0$ (left) and $c_r = 1$ (right). We observe the formation of wrinklings (or micro-structure) at the scale h in final configurations produced when $c_r = 0$ and a smooth shape for $c_r = 1$. We conclude that the regularization term R_h can effectively remove such oscillations.

Figure 5.17: *Degree* -1 *defect*: Final configurations with $c_r = 0$ (left) and $c_r = 1$ (right) for a director field $\mathbf{m}$ with degree $n = -1$ and $\alpha = 0$ in (5.3). The regularization term removes oscillations.

5.6.2 Incompatible square origami

We repeat the simulations of Section 5.4.1 with the same parameters except for $c_r = 1$ away from creases Γ (top) and $c_r = 0$ (bottom) of Fig. 5.18. We learned in Section 5.4.1 that this setting gives rise to *buckling* but, comparing with Fig. 5.9 when $c_r = 100$ in $\Omega \setminus \Gamma$, we now realize that a smaller regularization parameter leads to a more significant buckling. Moreover, the regularization R_h with $c_r = 1$ removes wrinklings observed for $c_r = 0$.

An illuminating discussion follows about $e_h^1[\mathbf{y}_h^\infty]$ and $E_h[\mathbf{y}_h^\infty]$. We obtain

$$c_r = 100,\ 1,\ 0 \ \Rightarrow\ e_h^1[\mathbf{y}_h^\infty] \approx 0.1,\ 0.035,\ 0.01;\ \ E_h[\mathbf{y}_h^\infty] \approx 0.012,\ 0.0026,\ 8.9 \times 10^{-4}.$$

Does this mean that the final configuration of Fig. 5.18 for $c_r = 0$ is closer to a true global minimizer of the stretching energy $E_{str,\Gamma}$ than the others? To elucidate this question, we conduct a refinement analysis for $c_r = 0$ and $c_r = 100$ and report it in Fig. 5.19. We see that $E_h[\mathbf{y}_h^\infty]$ and $e_h^1[\mathbf{y}_h^\infty]$ converge linearly to 0 for $c_r = 0$, whereas these quantities seem to decrease to a positive value for $c_r = 100$. In contrast, for the compatible pyramid origami of Example 4.2, displayed in Fig. 5.4, $E_h[\mathbf{y}_h^\infty]$ and $e_h^1[\mathbf{y}_h^\infty]$ can reach the value 10^{-14} by simply reducing the stopping tolerance tol_1, even for a very coarse meshsize $h = 1/16$. The reason is that an exact solution $\mathbf{y}^*$ for the compatible pyramid origami is *piecewise affine* over $\mathcal{T}_h$, because $\mathcal{T}_h$ matches the creases, so that $\mathbf{y}^* \in \mathbb{V}_h$. We resort to Corollary 3.4 (isometric immersions are minimizers with vanishing energy) and Theorem 4.2 (convergence of discrete minimizers with creases) to infer that there exists a piecewise H^2 isometric immersion for the compatible pyramid origami but not for the incompatible square origami.

We further wonder about the limit of $\mathbf{y}_h^\infty$ as $h \to 0$ for $c_r = 0$. Although coercivity of the energy $E_h[\mathbf{y}_h^\infty]$ implies that $\{\mathbf{y}_h^\infty\}_h$ have a weakly convergent subsequence in $H^1(\Omega;\mathbb{R}^3)$, and we do observe computationally that $E_{str}[\mathbf{y}_h^\infty] \to 0$, the weak limit $\mathbf{y}$ might not have zero stretching energy due to the lack of quasi-convexity of E_{str}. To illustrate this point we consider again the explicit example of compatible folding pyramids of Example 4.2 with vanishing stretching energy. The sequence $\{\mathbf{y}_i^*\}_{i=1}^\infty$ consists of flat pyramids folding across dyadic concentric creases Γ_i at distance 2^{-i} from each other and matched by the triangulation $\mathcal{T}_h$. The first three discrete solutions $\mathbf{y}_{i,h}^*$ computed by our method are displayed in Fig. 5.4 and satisfy $\mathbf{y}_{i,h}^* = \mathbf{y}_i^* \in \mathbb{V}_h$ for $i = 1, 2, 3$. The sequence $\{\mathbf{y}_i^*\}_{i=1}^\infty$ converges weakly in $H^1(\Omega;\mathbb{R}^3)$ to $\mathbf{y}^*(\mathbf{x}') = (\lambda\mathbf{x}', 0)^T$ as $i \to \infty$, but the limit satisfies $E_{str}[\mathbf{y}^*] > 0$. This lack of weak lower semicontinuity of E_{str} in H^1 is related to the lack of quasiconvexity of E_{str}; we refer to Section 4.1.1 for details. We can now create a sequence of discrete minimizers $\mathbf{y}_h \in \mathbb{V}_h$ that converge weakly to $\mathbf{y}^*(\mathbf{x}') = (\lambda\mathbf{x}', 0)^T$

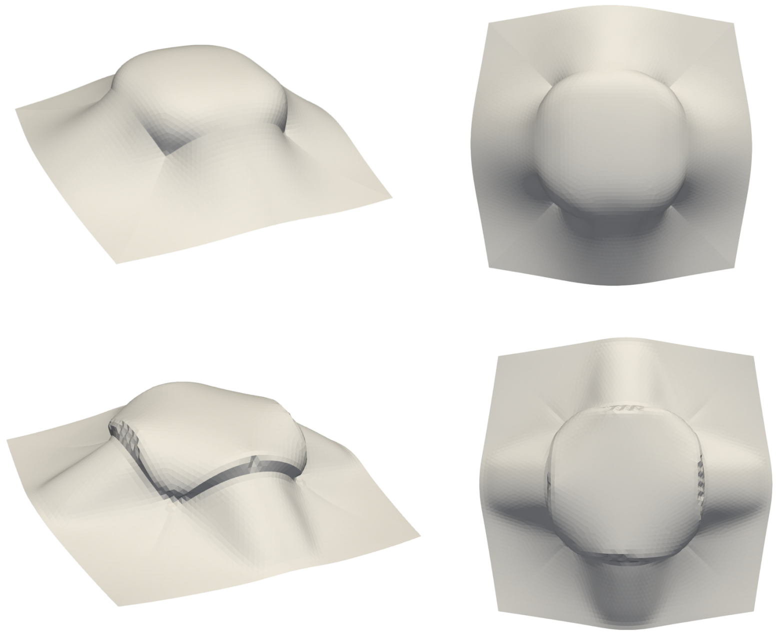

Figure 5.18: *Incompatible square origami*: Two views of the final configurations with regularization parameter $c_r = 1$ (top) and $c_r = 0$ (bottom) away from the creases. Wrinkling occurs for $c_r = 0$.

as $h \to 0$: (a) let $\mathcal{T}_h$ be a uniform dyadic partition of Ω made of right triangles with cartesian edges of size $h = 2^{-i}$ for $i \in \mathbb{N}$; (b) let $i(h) = \log_2(1/h)$ and $\mathbf{y}^*_{i(h)}$ be a folding pyramid with creases $\Gamma_{i(h)}$; (c) take $\mathbf{y}_h := \mathbf{y}^*_{i(h)} \in \mathbb{V}_h$ and note that $E_h[\mathbf{y}_h] = 0$. We expect a similar behavior for the incompatible square origami, except that we are not able to characterize the weak limit. Computing the quasiconvex envelope, a key step in this regard, is still open for this problem.

We now justify heuristically the shape of $\mathbf{y}$ in Figs. 5.9 and 5.18. We observe that any side of the inner square has to shrink by a factor $\lambda < 1$ due to the annulus but remain constant due to the inner square. This incompatible deformation can be realized by developing wrinkles in the inner square with increasing frequency towards the sides so that the length is maintained but accommodated in a shorter interval; a similar mechanism consisting of rapid oscillations

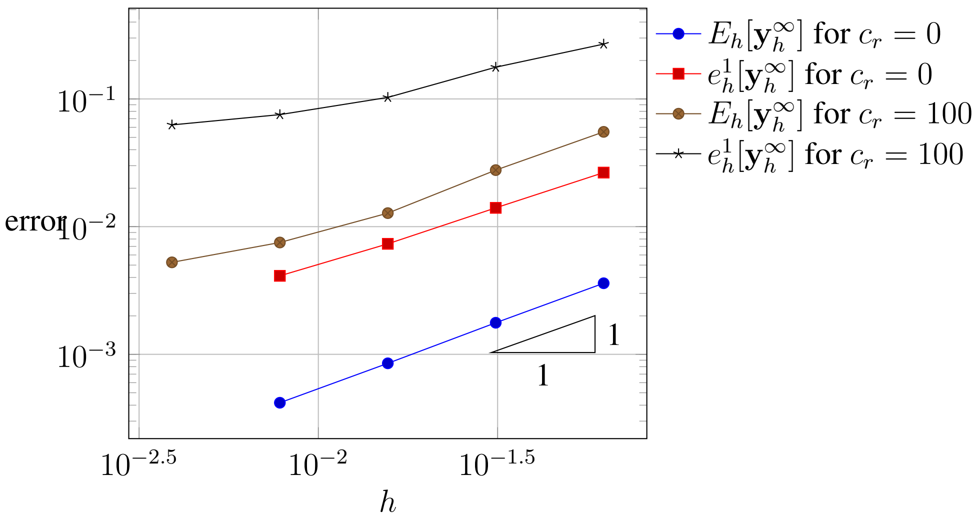

Figure 5.19: *Incompatible square origami*: Plots of $E_h[\mathbf{y}_h^\infty]$ and $e_h^1[\mathbf{y}_h^\infty]$ with several meshsizes h and regularization parameters $c_r = 0, 100$. For $c_r = 0$ we observe that $E_h[\mathbf{y}_h^\infty]$ and $e_h^1[\mathbf{y}_h^\infty]$ are both $\mathcal{O}(h)$, whereas for $c_r = 100$ they stabilize to a positive value as h decreases.

towards the domain boundary is studied in [79] for a simplified model. Any approximation of this deformation within the finite element space $\mathbb{V}_h$ introduces the triangulation scale h and the effect of regularization $R_h[\mathbf{y}_h]$. The former suppresses infinite wrinkling while the latter prevents the formation of wrinkles at any scale and favors piecewise smooth deformations. Since discrete solutions do not allow infinite oscillations near creases, buckling out of plane is then a natural phenomenon to occur to accommodate incompatible stretching. Figs. 5.9 and 5.18 depict the final configuration and show that the faces and creases are not flat but curved, although all the creases are straight lines in the undeformed configuration.

We may conclude that the regularization (4.15) serves as a mechanism to select minimizers of stretching energy for *compatible* origami, while a competition between stretching and bending energies determines the final shape for *incompatible* origami.

5.7 Metric errors in the flow

We take $\Omega = [-0.5, 0.5]^2$ and parameters

$$s = 0.1,\ s_0 = 1;\ h = 1/64,\ \tau = 0.48,\ c_r = 1,\ \text{tol}_1 = 10^{-6},\ \text{tol}_2 = 10^{-10}.$$

Analogously to (5.10) and (5.8), we initialize the discrete gradient flow with a perturbation of the flat square $\mathbf{y}_h^0 = I_h \mathbf{y}^0$ where

$$\mathbf{y}^0(x_1, x_2) \ = \ \big(x_1, x_2, 0.8(x_1 - 0.5)(x_1 + 0.5)(x_2 - 0.5)(x_2 + 0.5)\big). \tag{5.17}$$

Case 1: Smooth $\mathbf{m}$. We choose the smooth blueprinted director field

$$\mathbf{m}(x_1, x_2) := (x_1 + 1, x_2 + 1)/\sqrt{(x_1 + 1)^2 + (x_2 + 1)^2}. \tag{5.18}$$

Case 2: Rough $\mathbf{m}$. We consider a defect of degree $n = 3/2$ and $\alpha = 0$ in (5.3).

Fig. 5.20 contains plots of the metric errors and energies in the discrete gradient flow for both cases. We observe that the energy $E_h[\mathbf{y}_h^n]$ always decays monotonically as expected from Theorem 4.3 (energy stability). The metric defect $e_h^1[\mathbf{y}_h^n]$ also converges monotonically as n increases in both cases. In contrast, the error $e_h^\infty[\mathbf{y}_h^n]$ decreases monotonically in Case 1 (smooth $\mathbf{m}$) but not in Case 2 (rough $\mathbf{m}$). The latter is due to the discontinuity of $\mathbf{m}$ at the origin, hence of the target metric g, but occurs only at the beginning of the flow. The error $e_h^\infty[\mathbf{y}_h^n]$ stabilizes asymptotically but is much larger than $e_h^1[\mathbf{y}_h^n]$. This behavior is consistent with the discontinuity of g but against assumption (4.63) of Remark 4.5 and assumption (4.57), in the sense that satisfying (4.63) for $\mathbf{y}_h^0$ might not be enough to guarantee (4.63) for all iterates $\mathbf{y}_h^{n,k}$. Nonetheless, we emphasize again that our Newton sub-iterations always work properly in practice with a simple and straightforward choice of τ rather insensitive to h.

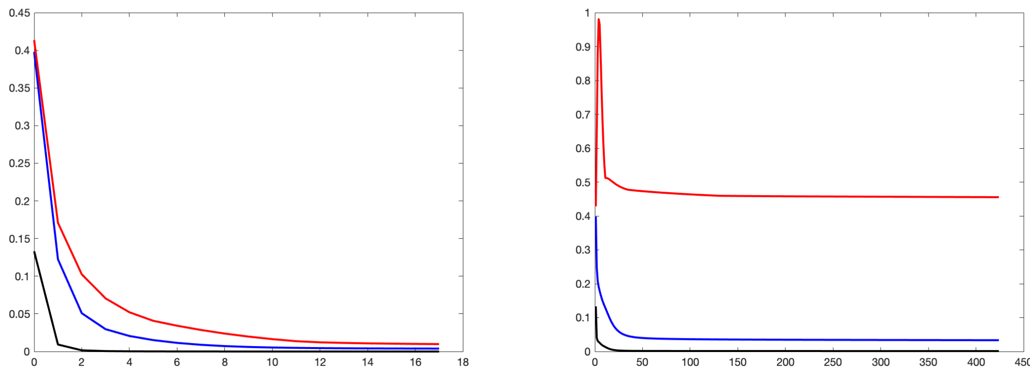

Figure 5.20: Plots of metric errors of $e_h^1[\mathbf{y}_h^n]$ (blue curve), $e_h^\infty[\mathbf{y}_h^n]$ (red curve) and energy $E_h[\mathbf{y}_h^n]$ (black curve) of the gradient flow for $n \geq 0$. Case 1: $\mathbf{m}$ smooth (left) and Case 2: $\mathbf{m}$ rough (right). Except for $e_h^\infty[\mathbf{y}_h^n]$ in Case 2, the behaviors ofthe metric errors and energy errors is monotone.

Appendix A: Gradient flow and Newton method: discussion and proofs

In this appendix we present the lengthy explicit expressions of δE_h and $\delta^2 L_h^n$, as well as proofs of the theorems in Section 4.5. To aid in the derivation, we introduce the notation

$$K[\mathbf{y}_h, \mathbf{v}_h] = \nabla \mathbf{y}_h^T \nabla \mathbf{v}_h + \nabla \mathbf{v}_h^T \nabla \mathbf{y}_h, \tag{A.1}$$

which is the linearization of $\mathrm{I}[\mathbf{y}_h]$.

We first show the expressions of the first variation

$$\delta E_h[\mathbf{y}_h](\mathbf{v}_h) = \delta E_{str}[\mathbf{y}_h](\mathbf{v}_h) + \delta R_h[\mathbf{y}_h](\mathbf{v}_h)$$

at $\mathbf{y}_h \in \mathbb{V}_h$ along the variational direction (or test function) $\mathbf{v}_h \in \mathbb{V}_h$. Since the regularization term $R_h[\mathbf{y}_h]$ in (5.1) is quadratic, its first variation reads

$$\delta R_h[\mathbf{y}_h](\mathbf{v}_h) = 2 \sum_{e \in \mathcal{E}_h} c_r h_e \int_e [\nabla \mathbf{y}_h] : [\nabla \mathbf{v}_h].$$

The first variation of the nonlinear and nonconvex energy E_{str} reads instead

$$\delta E_{str}[\mathbf{y}_h](\mathbf{v}_h) = T_1[\mathbf{y}_h, \mathbf{v}_h] + T_2[\mathbf{y}_h, \mathbf{v}_h] + T_3[\mathbf{y}_h, \mathbf{v}_h] + T_4[\mathbf{y}_h, \mathbf{v}_h],$$

where

$$T_1[\mathbf{y}_h,\mathbf{v}_h] := -\int_\Omega J[\mathbf{y}_h]^{-1}\mathrm{tr}\Big(\mathrm{I}[\mathbf{y}_h]^{-1}K[\mathbf{y}_h,\mathbf{v}_h]\Big)$$
$$T_2[\mathbf{y}_h,\mathbf{v}_h] := \frac{1}{s+1}\int_\Omega \Big(2\nabla\mathbf{y}_h : \nabla\mathbf{v}_h + s_0\mathbf{m}\cdot K[\mathbf{y}_h,\mathbf{v}_h]\mathbf{m}\Big)$$
$$T_3[\mathbf{y}_h,\mathbf{v}_h] := -\frac{s}{s+1}\int_\Omega \frac{J[\mathbf{y}_h]}{C_\mathbf{m}[\mathbf{y}_h]^2}\,\mathbf{m}\cdot K[\mathbf{y}_h,\mathbf{v}_h]\mathbf{m}$$
$$T_4[\mathbf{y}_h,\mathbf{v}_h] := \frac{s}{s+1}\int_\Omega \frac{J[\mathbf{y}_h]}{C_\mathbf{m}[\mathbf{y}_h]}\mathrm{tr}\Big(\mathrm{I}[\mathbf{y}_h]^{-1}K[\mathbf{y}_h,\mathbf{v}_h]\Big),$$

and $J[\mathbf{y}_h], C_\mathbf{m}[\mathbf{y}_h]$ are defined in (3.19) and $K[\mathbf{y}_h,\mathbf{v}_h]$ in (A.1).

We next compute the second order variation of L_h^n at $\mathbf{y}_h \in \mathbb{V}_h$. In fact, we obtain

$$\begin{aligned}\delta^2 L_h^n[\mathbf{y}_h](\mathbf{v}_h,\mathbf{w}_h) = {} & \frac{1}{\tau}(\mathbf{w}_h,\mathbf{v}_h)_{H^1(\Omega)} \\ & + \delta^2 E_{str}[\mathbf{y}_h](\mathbf{v}_h,\mathbf{w}_h) + \delta^2 R_h[\mathbf{y}_h](\mathbf{v}_h,\mathbf{w}_h),\end{aligned} \tag{A.2}$$

for arbitrary $\mathbf{v}_h, \mathbf{w}_h \in \mathbb{V}_h$. In view of (5.1), the last term is actually independent of $\mathbf{y}_h$ and reads

$$\delta^2 R_h[\mathbf{y}_h](\mathbf{v}_h,\mathbf{w}_h) = 2\sum_{e\in\mathcal{E}_h}\int_e c_r h_e[\nabla\mathbf{v}_h] : [\nabla\mathbf{w}_h]. \tag{A.3}$$

Moreover, the second variation of E_{str} can be written as follows

$$\delta^2 E_{str}[\mathbf{y}_h](\mathbf{v}_h,\mathbf{w}_h) = \sum_{i=1}^4 \delta_{\mathbf{y}_h} T_i[\mathbf{y}_h,\mathbf{v}_h](\mathbf{w}_h), \tag{A.4}$$

in terms of the first variations of the earlier quantities T_i

$$\begin{aligned}
\delta_{\mathbf{y}_h} T_1[\mathbf{y}_h, \mathbf{v}_h](\mathbf{w}_h) &= \int_\Omega J[\mathbf{y}_h]^{-1} \mathrm{tr}\Big(\mathrm{I}[\mathbf{y}_h]^{-1} K[\mathbf{y}_h, \mathbf{w}_h]\Big) \mathrm{tr}\Big(\mathrm{I}[\mathbf{y}_h]^{-1} K[\mathbf{y}_h, \mathbf{v}_h]\Big) \\
&\quad + \int_\Omega J[\mathbf{y}_h]^{-1} \mathrm{tr}\Big(\mathrm{I}[\mathbf{y}_h]^{-1} K[\mathbf{y}_h, \mathbf{v}_h]\, \mathrm{I}[\mathbf{y}_h]^{-1} K[\mathbf{y}_h, \mathbf{w}_h]\Big) \\
&\quad - \int_\Omega J[\mathbf{y}_h]^{-1} \mathrm{tr}\Big(\mathrm{I}[\mathbf{y}_h]^{-1} K[\mathbf{v}_h, \mathbf{w}_h]\Big), \\
\delta_{\mathbf{y}_h} T_2[\mathbf{y}_h, \mathbf{v}_h](\mathbf{w}_h) &= \frac{1}{s+1} \int_\Omega \Big(2\nabla \mathbf{w}_h : \nabla \mathbf{v}_h + s_0 \mathbf{m} \cdot K[\mathbf{v}_h, \mathbf{w}_h]\mathbf{m}\Big), \\
\delta_{\mathbf{y}_h} T_3[\mathbf{y}_h, \mathbf{v}_h](\mathbf{w}_h) &= -\frac{s}{s+1} \int_\Omega \frac{J[\mathbf{y}_h]}{C_{\mathbf{m}}[\mathbf{y}_h]^2} \mathrm{tr}\Big(\mathrm{I}[\mathbf{y}_h]^{-1} K[\mathbf{y}_h, \mathbf{w}_h]\Big)\, \mathbf{m} \cdot K[\mathbf{y}_h, \mathbf{v}_h]\mathbf{m} \\
&\quad + 2\frac{s}{s+1} \int_\Omega \frac{J[\mathbf{y}_h]}{C_{\mathbf{m}}[\mathbf{y}_h]^3} \big(\mathbf{m} \cdot K[\mathbf{y}_h, \mathbf{v}_h]\mathbf{m}\big)\big(\mathbf{m} \cdot K[\mathbf{y}_h, \mathbf{w}_h]\mathbf{m}\big) \\
&\quad - \frac{s}{s+1} \int_\Omega \frac{J[\mathbf{y}_h]}{C_{\mathbf{m}}[\mathbf{y}_h]^2}\, \mathbf{m} \cdot K[\mathbf{v}_h, \mathbf{w}_h]\mathbf{m},
\end{aligned}$$

and

$$\begin{aligned}
\delta_{\mathbf{y}_h} T_4[\mathbf{y}_h, \mathbf{v}_h](\mathbf{w}_h) &= \frac{s}{s+1} \int_\Omega \frac{J[\mathbf{y}_h]}{C_{\mathbf{m}}[\mathbf{y}_h]} \mathrm{tr}\Big(\mathrm{I}[\mathbf{y}_h]^{-1} K[\mathbf{y}_h, \mathbf{w}_h]\Big)\, \mathrm{tr}\Big(\mathrm{I}[\mathbf{y}_h]^{-1} K[\mathbf{y}_h, \mathbf{v}_h]\Big) \\
&\quad - \frac{s}{s+1} \int_\Omega \frac{J[\mathbf{y}_h]}{C_{\mathbf{m}}[\mathbf{y}_h]} \mathrm{tr}\Big(\mathrm{I}[\mathbf{y}_h]^{-1} K[\mathbf{y}_h, \mathbf{v}_h]\, \mathrm{I}[\mathbf{y}_h]^{-1} K[\mathbf{y}_h, \mathbf{w}_h]\Big) \\
&\quad + \frac{s}{s+1} \int_\Omega \frac{J[\mathbf{y}_h]}{C_{\mathbf{m}}[\mathbf{y}_h]} \mathrm{tr}\Big(\mathrm{I}[\mathbf{y}_h]^{-1}\, K[\mathbf{v}_h, \mathbf{w}_h]\Big) \\
&\quad - \frac{s}{s+1} \int_\Omega \frac{J[\mathbf{y}_h]}{C_{\mathbf{m}}[\mathbf{y}_h]^2} \mathrm{tr}\Big(\mathrm{I}[\mathbf{y}_h]^{-1}\, K[\mathbf{y}_h, \mathbf{v}_h]\Big)\, \mathbf{m} \cdot K[\mathbf{y}_h, \mathbf{w}_h]\mathbf{m}.
\end{aligned}$$

We are ready to discuss the proof of ellipticity of $\delta^2 L_h^n$, which requires time-step τ small enough and guarantees the Newton method to be well-posed.

Proof of Theorem 4.4 (ellipticity). If $\mathbf{w}_h = \mathbf{v}_h$ in (A.3), this regularization term gives

$$\delta^2 R_h[\mathbf{y}_h](\mathbf{v}_h, \mathbf{v}_h) = 2R_h[\mathbf{v}_h] > 0.$$

We only need to estimate the four terms in the expansion of $\delta^2 E_{str}[\mathbf{y}_h](\mathbf{v}_h, \mathbf{v}_h)$ by replacing $\mathbf{w}_h = \mathbf{v}_h$ in (A.4), and using the flow metric term to control them.

We compute for the piecewise constant quantities $J[\mathbf{y}_h]^{-1}$ and $C_{\mathbf{m}}[\mathbf{y}_h]^{-1}$

$$J[\mathbf{y}_h]^{-1} = \lambda_1^{-1}\lambda_2^{-1} \le c_1^{-2} \text{ for all } T \in \mathcal{T}_h,$$

where $0 < c_1 \le \lambda_1 = \lambda_1[\mathbf{y}_h] \le \lambda_2 = \lambda_2[\mathbf{y}_h] \le c_2$ according to (4.57), and

$$C_{\mathbf{m}}[\mathbf{y}_h]^{-1} \le \lambda_1^{-1} \le c_1^{-1} \text{ for all } T \in \mathcal{T}_h.$$

Moreover, one can easily verify that for any SPD matrices $A, B, C \in \mathbb{R}^{2\times 2}$,

$$\operatorname{tr}(AB) \le \lambda_{\max}(A)|B|, \quad \operatorname{tr}(ABAC) \le \lambda_{\max}(A)^2|B||C|.$$

We apply this property to $A = \mathrm{I}[\mathbf{y}_h]^{-1}$, $B = K[\mathbf{y}_h, \mathbf{v}_h]$ and $C = K[\mathbf{y}_h, \mathbf{w}_h]$. Since $\lambda_{\max}(\mathrm{I}[\mathbf{y}_h]^{-1}) \le \lambda_1^{-1} < c_1^{-1}$. we obtain

$$\left|\delta_{\mathbf{y}_h} T_1[\mathbf{y}_h, \mathbf{v}_h](\mathbf{v}_h)\right| \le 2c_1^{-4}\|K[\mathbf{y}_h, \mathbf{v}_h]\|^2_{L^2(\Omega)} + c_1^{-3}\|K[\mathbf{v}_h, \mathbf{v}_h]\|_{L^1(\Omega)}.$$

Moreover, for any 3×2 matrices A, B we have

$$|A^T B| \leq \sigma_{max}(A)|B|,$$

where $\sigma_{max}(A) := \lambda_{\max}(A^T A)^{\frac{1}{2}}$ is the largest singular value of A. We apply this estimate to $A = \nabla \mathbf{y}_h$ and $B = \nabla \mathbf{v}_h$ to arrive at

$$\big|K[\mathbf{y}_h, \mathbf{v}_h]\big|^2 \leq 4\big|\nabla \mathbf{y}_h^T \nabla \mathbf{v}_h\big|^2 \leq 4\lambda_2\big|\nabla \mathbf{v}_h\big|^2 \leq 4c_2\big|\nabla \mathbf{v}_h\big|^2, \tag{A.5}$$

whence $\|K[\mathbf{y}_h, \mathbf{v}_h]\|^2_{L^2(\Omega;\mathbb{R}^{2\times 2})} \leq 4c_2\|\nabla \mathbf{v}_h\|^2_{L^2(\Omega;\mathbb{R}^{3\times 2})}$. Therefore,

$$\big|\delta_{\mathbf{y}_h} T_1[\mathbf{y}_h, \mathbf{v}_h](\mathbf{v}_h)\big| \leq \big(8c_1^{-4}c_2 + 2c_1^{-3}\big)\|\nabla \mathbf{v}_h\|^2_{L^2(\Omega;\mathbb{R}^{3\times 2})}.$$

Similarly, one can estimate the other terms, and conclude that

$$\big|\delta_{\mathbf{y}_h} T_j[\mathbf{y}_h, \mathbf{v}_h](\mathbf{v}_h)\big| \leq C(s, s_0, c_1, c_2, \mathbf{m})\|\nabla \mathbf{v}_h\|^2_{L^2(\Omega;\mathbb{R}^{3\times 2})} \quad j = 2, 3, 4. \tag{A.6}$$

Recalling the expression (A.2) for $\delta^2 L_h^n[\mathbf{y}_h](\mathbf{v}_h, \mathbf{v}_h]$, we realize that

$$\delta^2 L_h^n[\mathbf{y}_h](\mathbf{v}_h, \mathbf{v}_h) \geq \left(\frac{1}{\tau} - C(s, s_0, c_1, c_2, \mathbf{m})\right)\|\nabla \mathbf{v}_h\|^2_{L^2(\Omega;\mathbb{R}^{3\times 2})}$$

and choosing τ sufficiently small depending on $s, s_0, c_1, c_2, \mathbf{m}$ yields the desired estimate (4.58).

$\square$

We next prove the Lipschitz property of $\delta^2 L_h^n$. This is a crucial step towards the convergence of Newton method.

Proof of Theorem 4.5 (Lipschitz property). To prove (4.59), we first note that

$$\delta^2 L_h^n[\mathbf{y}_h](\mathbf{v}_h,\mathbf{w}_h) - \delta^2 L_h^n[\widetilde{\mathbf{y}}_h](\mathbf{v}_h,\mathbf{w}_h) = \delta^2 E_{str}[\mathbf{y}_h](\mathbf{v}_h,\mathbf{w}_h) - \delta^2 E_{str}[\widetilde{\mathbf{y}}_h](\mathbf{v}_h,\mathbf{w}_h),$$

as the flow metric and regularization terms both canceled because they are independent of $\mathbf{y}_h, \tilde{\mathbf{y}}_h$. Therefore, we only need to check first variations of T_1, T_3, T_4, because that of T_2 does not depend on $\mathbf{y}_h$. Since the many ensuing terms can be treated with similar techniques, we illustrate the process with a typical one, namely the second term of $\delta_{\mathbf{y}_h} T_1$. In fact, we denote

$$T_5[\mathbf{y}_h;\mathbf{v}_h,\mathbf{w}_h] := \operatorname{tr}\big(\mathrm{I}[\mathbf{y}_h]^{-1}\, K[\mathbf{y}_h,\mathbf{v}_h]\, \mathrm{I}[\mathbf{y}_h]^{-1}\, K[\mathbf{y}_h,\mathbf{w}_h]\big), \tag{A.7}$$

and observe that $\big|T_5[\mathbf{y}_h;\mathbf{v}_h,\mathbf{w}_h]\big| \le 4c_1^{-2}c_2\big|\nabla\mathbf{v}_h\big|\big|\nabla\mathbf{w}_h\big|$, in view of (A.5). We now estimate the second term of $\delta_{\mathbf{y}_h} T_1[\mathbf{y}_h,\mathbf{v}_h](\mathbf{w}_h)$ as follows:

$$\begin{aligned}
\Big|\int_\Omega & J[\mathbf{y}_h]^{-1} T_5[\mathbf{y}_h;\mathbf{v}_h,\mathbf{w}_h] - J[\widetilde{\mathbf{y}}_h]^{-1} T_5[\widetilde{\mathbf{y}}_h;\mathbf{v}_h,\mathbf{w}_h]\Big| \\
&\le \int_\Omega \Big|\frac{J[\widetilde{\mathbf{y}}_h] T_5[\mathbf{y}_h;\mathbf{v}_h,\mathbf{w}_h] - J[\mathbf{y}_h] T_5[\widetilde{\mathbf{y}}_h;\mathbf{v}_h,\mathbf{w}_h]}{J[\mathbf{y}_h] J[\widetilde{\mathbf{y}}_h]}\Big| \\
&\le c_1^{-4}\int_\Omega \Big|J[\mathbf{y}_h]\big(T_5[\mathbf{y}_h;\mathbf{v}_h,\mathbf{w}_h] - T_5[\widetilde{\mathbf{y}}_h;\mathbf{v}_h,\mathbf{w}_h]\big)\Big| \\
&+ c_1^{-4}\int_\Omega \Big|\big(J[\widetilde{\mathbf{y}}_h] - J[\mathbf{y}_h]\big) T_5[\mathbf{y}_h;\mathbf{v}_h,\mathbf{w}_h]\Big| \\
&\le c_1^{-4}c_2^2\int_\Omega \Big|T_5[\mathbf{y}_h,\mathbf{v}_h,\mathbf{w}_h] - T_5[\widetilde{\mathbf{y}}_h,\mathbf{v}_h,\mathbf{w}_h]\Big| \\
&+ 4c_1^{-6}c_2\int_\Omega \Big|J[\widetilde{\mathbf{y}}_h] - J[\mathbf{y}_h]\Big|\Big|\nabla\mathbf{v}_h\Big|\Big|\nabla\mathbf{w}_h\Big|.
\end{aligned}$$

We can easily rewrite

$$\Big|T_5[\mathbf{y}_h,\mathbf{v}_h,\mathbf{w}_h]-T_5[\widetilde{\mathbf{y}}_h,\mathbf{v}_h,\mathbf{w}_h]\Big| \le \sum_{i=6}^{9} T_i[\mathbf{y}_h,\widetilde{\mathbf{y}}_h,;\mathbf{v}_h,\mathbf{w}_h], \tag{A.8}$$

where

$$\begin{aligned}
T_6[\mathbf{y}_h,\widetilde{\mathbf{y}}_h,;\mathbf{v}_h,\mathbf{w}_h] &= \Big|\mathrm{tr}\Big((\mathrm{I}[\mathbf{y}_h]^{-1}-\mathrm{I}[\widetilde{\mathbf{y}}_h]^{-1})\, K[\mathbf{y}_h,\mathbf{v}_h]\, \mathrm{I}[\mathbf{y}_h]^{-1} K(\mathbf{y}_h,\mathbf{w}_h)\Big)\Big|,\\
T_7[\mathbf{y}_h,\widetilde{\mathbf{y}}_h,;\mathbf{v}_h,\mathbf{w}_h] &= \Big|\mathrm{tr}\Big(\mathrm{I}[\widetilde{\mathbf{y}}_h]^{-1}(K[\mathbf{y}_h,\mathbf{v}_h]-K[\widetilde{\mathbf{y}}_h,\mathbf{v}_h])\mathrm{I}[\mathbf{y}_h]^{-1}K[\mathbf{y}_h,\mathbf{w}_h]\Big)\Big|,\\
T_8[\mathbf{y}_h,\widetilde{\mathbf{y}}_h,;\mathbf{v}_h,\mathbf{w}_h] &= \Big|\mathrm{tr}\Big(\mathrm{I}[\widetilde{\mathbf{y}}_h]^{-1}K[\widetilde{\mathbf{y}}_h,\mathbf{v}_h](\mathrm{I}[\mathbf{y}_h]^{-1}-\mathrm{I}[\widetilde{\mathbf{y}}_h]^{-1})K[\mathbf{y}_h,\mathbf{w}_h]\Big)\Big|,\\
T_9[\mathbf{y}_h,\widetilde{\mathbf{y}}_h,;\mathbf{v}_h,\mathbf{w}_h] &= \Big|\mathrm{tr}\Big(\mathrm{I}[\widetilde{\mathbf{y}}_h]^{-1}K[\widetilde{\mathbf{y}}_h,\mathbf{v}_h]\mathrm{I}[\widetilde{\mathbf{y}}_h]^{-1}\big(K[\mathbf{y}_h,\mathbf{w}_h]-K[\widetilde{\mathbf{y}}_h,\mathbf{w}_h]\big)\Big)\Big|.
\end{aligned}$$

Note that for SPD matrices $A,B,C\in\mathbb{R}^{2\times 2}$, there holds

$$|\mathrm{tr}((A^{-1}-B^{-1})C)| = |\mathrm{tr}(A^{-1}(B-A)B^{-1}C)| \le \lambda_{\max}(A^{-1})\lambda_{\max}(B^{-1})|B-A||C|.$$

Using this property and (A.5), we obtain

$$\begin{aligned}
T_6[\mathbf{y}_h,\widetilde{\mathbf{y}}_h,;\mathbf{v}_h,\mathbf{w}_h] &\le c_1^{-2}\big|\mathrm{I}[\mathbf{y}_h]-\mathrm{I}[\widetilde{\mathbf{y}}_h]\big|\,\big|K[\mathbf{y}_h,\mathbf{v}_h]\,\mathrm{I}[\mathbf{y}_h]^{-1}\,K[\mathbf{y}_h,\mathbf{w}_h]\big|\\
&\le 4c_1^{-3}c_2\big|\mathrm{I}[\mathbf{y}_h]-\mathrm{I}[\widetilde{\mathbf{y}}_h]\big|\,\big|\nabla\mathbf{v}_h\big|\,\big|\nabla\mathbf{w}_h\big|\\
&\le 4c_1^{-3}c_2^2\big|\nabla\mathbf{y}_h-\nabla\widetilde{\mathbf{y}}_h\big|\,\big|\nabla\mathbf{v}_h\big|\,\big|\nabla\mathbf{w}_h\big|,
\end{aligned}$$

and a similar estimate for $T_8[\mathbf{y}_h, \widetilde{\mathbf{y}}_h, ; \mathbf{v}_h, \mathbf{w}_h]$. Likewise, we can derive

$$T_7[\mathbf{y}_h, \widetilde{\mathbf{y}}_h, ; \mathbf{v}_h, \mathbf{w}_h] \leq 4c_1^{-2}c_2^{1/2}\big|\nabla\mathbf{y}_h - \nabla\widetilde{\mathbf{y}}_h\big|\,\big|\nabla\mathbf{v}_h\big|\,\big|\nabla\mathbf{w}_h\big|,$$

and a similar estimate for $T_9[\mathbf{y}_h, \widetilde{\mathbf{y}}_h, ; \mathbf{v}_h, \mathbf{w}_h]$.

Finally, collecting these estimates and resorting to an inverse inequality yields

$$\int_\Omega \Big|T_5[\mathbf{y}_h, \mathbf{v}_h, \mathbf{w}_h] - T_5[\widetilde{\mathbf{y}}_h, \mathbf{v}_h, \mathbf{w}_h]\Big| \\ \lesssim h^{-1}\|\nabla\mathbf{y}_h - \nabla\widetilde{\mathbf{y}}_h\|_{L^2(\Omega;\mathbb{R}^{3\times2})}\|\nabla\mathbf{v}_h\|_{L^2(\Omega;\mathbb{R}^{3\times2})}\|\nabla\mathbf{w}_h\|_{L^2(\Omega;\mathbb{R}^{3\times2})},$$

with a hidden constant depending on c_1, c_2. Moreover, we can easily estimate

$$|J[\widetilde{\mathbf{y}}_h] - J[\mathbf{y}_h]| \lesssim |\nabla\widetilde{\mathbf{y}}_h - \nabla\mathbf{y}_h|,$$

with a hidden constant depending on c_1, c_2. This further implies that

$$\Big|\int_\Omega \frac{T_5[\mathbf{y}_h, \mathbf{v}_h, \mathbf{w}_h]}{J[\mathbf{y}_h]} - \frac{T_5[\widetilde{\mathbf{y}}_h, \mathbf{v}_h, \mathbf{w}_h]}{J[\widetilde{\mathbf{y}}_h]}\Big| \lesssim h^{-1}\|\mathbf{y}_h - \widetilde{\mathbf{y}}_h\|_{H^1(\Omega;\mathbb{R}^3)}\|\mathbf{v}_h\|_{H^1(\Omega;\mathbb{R}^3)}\|\mathbf{w}_h\|_{H^1(\Omega;\mathbb{R}^3)}.$$

We can apply the same procedure to all the other terms in $\delta_{\mathbf{y}_h}T_j$ for $j = 1, 3, 4$ to conclude the proof of (4.59). □

Theorems 4.4 (coercivity) and 4.5 (Lipschitz property) are instrumental to proof the following quadratic estimate of the Newton sub-iterations.

Proof of Corollary 4.2 (quadratic estimate). Since (4.57) is satisfied for any $\mathbf{y}_h^{n,k}$ with fixed

$n, k \geq 0$ by assumption, Theorem 4.4 (coercivity) implies that $\delta^2 L_h^n[\mathbf{y}_h]$ is coercive at $\mathbf{y}_h^{n,k}$, whence the Newton step (4.56) is well-posed when τ is small enough.

We then rewrite (4.56) as

$$\delta^2 L_h^n[\mathbf{y}_h^{n,k}](\mathbf{y}_h^{n,k+1} - \mathbf{y}_h^{n,*}, \mathbf{v}_h) = \delta^2 L_h^n[\mathbf{y}_h^{n,k}](\mathbf{y}_h^{n,k} - \mathbf{y}_h^{n,*}, \mathbf{v}_h) - \delta L_h^n[\mathbf{y}_h^{n,k}](\mathbf{v}_h),$$

and also

$$\delta L_h^n[\mathbf{y}_h^{n,k}](\mathbf{v}_h) = \int_0^1 \delta^2 L_h^n\big[\mathbf{y}_h^{n,*} + s(\mathbf{y}_h^{n,k} - \mathbf{y}_h^{n,*})\big](\mathbf{y}_h^{n,k} - \mathbf{y}_h^{n,*}, \mathbf{v}_h) ds,$$

as $\delta L_h^n[\mathbf{y}_h^{n,*}](\mathbf{v}_h) = 0$ for all $\mathbf{v}_h \in V_h$. Substituting this into the preceding equality gives

$$\begin{aligned}
&\delta^2 L_h^n[\mathbf{y}_h^{n,k}](\mathbf{y}_h^{n,k+1} - \mathbf{y}_h^{n,*}, \mathbf{v}_h) \\
&\qquad = \int_0^1 \Big(\delta^2 L_h^n[\mathbf{y}_h^{n,k}] - \delta^2 L_h^n\big[\mathbf{y}_h^{n,*} + s(\mathbf{y}_h^{n,k} - \mathbf{y}_h^{n,*})\big]\Big)(\mathbf{y}_h^{n,k} - \mathbf{y}_h^{n,*}, \mathbf{v}_h) ds.
\end{aligned}$$

Taking $\mathbf{v}_h = \mathbf{y}_h^{n,k+1} - \mathbf{y}_h^{n,*}$ and using Theorem 4.4 (coercivity) to estimate the left-hand side from below and Theorem 4.5 (Lipschitz property) to bound the right-hand side from above yields

$$c\|\mathbf{y}_h^{n,k+1} - \mathbf{y}_h^{n,*}\|_{H^1(\Omega;\mathbb{R}^3)}^2 \leq \frac{M}{2h}\|\mathbf{y}_h^{n,k} - \mathbf{y}_h^{n,*}\|_{H^1(\Omega;\mathbb{R}^3)}^2 \, \|\mathbf{y}_h^{n,k+1} - \mathbf{y}_h^{n,*}\|_{H^1(\Omega;\mathbb{R}^3)}.$$

This concludes the proof. □

Bibliography

[1] James H. Adler, Timothy J. Atherton, David B. Emerson, and Scott P. MacLachlan. An energy-minimization finite-element approach for the Frank–Oseen model of nematic liquid crystals. *SIAM Journal on Numerical Analysis*, 53(5):2226–2254, 2015.

[2] Virginia Agostiniani and Antonio DeSimone. Rigorous derivation of active plate models for thin sheets of nematic elastomers. *Mathematics and Mechanics of Solids*, 25(10):1804–1830, 2020.

[3] Virginia Agostiniani, Antonio DeSimone, and Konstantinos Koumatos. Shape programming for narrow ribbons of nematic elastomers. *Journal of Elasticity*, 127(1):1–24, 2017.

[4] Hillel Aharoni, Eran Sharon, and Raz Kupferman. Geometry of thin nematic elastomer sheets. *Physical Review Letters*, 113(25):257801, 2014.

[5] Hillel Aharoni, Yu Xia, Xinyue Zhang, Randall D Kamien, and Shu Yang. Universal inverse design of surfaces with thin nematic elastomer sheets. *Proceedings of the National Academy of Sciences*, 115(28):7206–7211, 2018.

[6] James Ahrens, Berk Geveci, and Charles Law. Paraview: An end-user tool for large data visualization. *The visualization handbook*, 717(8), 2005.

[7] James Ahrens, Berk Geveci, and Charles Law. ParaView: An end-user tool for large data visualization. In Charles D. Hansen and Chris R. Johnson, editors, *Visualization Handbook*, pages 717–731. Elsevier, 2005.

[8] François Alouges. A new algorithm for computing liquid crystal stable configurations: the harmonic mapping case. *SIAM journal on numerical analysis*, 34(5):1708–1726, 1997.

[9] François Alouges and Jean-Michel Ghidaglia. Minimizing Oseen-Frank energy for nematic liquid crystals: algorithms and numerical results. In *Annales de l'IHP Physique théorique*, volume 66, pages 411–447, 1997.

[10] Harbir Antil, Sören Bartels, and Armin Schikorra. Approximation of fractional harmonic maps. *arXiv preprint arXiv:2104.10049*, 2021.

[11] John M Ball. The calculus of variations and materials science. *Quarterly of Applied Mathematics*, 56(4):719–740, 1998.

[12] Marco Barchiesi and Antonio DeSimone. Frank energy for nematic elastomers: a nonlinear model. *ESAIM: Control, Optimisation and Calculus of Variations*, 21(2):372–377, 2015.

[13] Sören Bartels. Stability and convergence of finite-element approximation schemes for harmonic maps. *SIAM journal on numerical analysis*, 43(1):220–238, 2005.

[14] Sören Bartels. Finite element approximation of large bending isometries. *Numerische Mathematik*, 124(3):415–440, 2013.

[15] Sören Bartels. *Numerical methods for nonlinear partial differential equations*, volume 47. Springer, 2015.

[16] Sören Bartels. Projection-free approximation of geometrically constrained partial differential equations. *Mathematics of Computation*, 85(299):1033–1049, 2016.

[17] Sören Bartels, Klaus Böhnlein, Christian Palus, and Oliver Sander. Benchmarking numerical algorithms for harmonic maps into the sphere. *arXiv preprint arXiv:2209.13665*, 2022.

[18] Sören Bartels, Andrea Bonito, and Peter Hornung. Modeling and simulation of thin sheet folding. *Interfaces and Free Boundaries*, 2022.

[19] Sören Bartels, Andrea Bonito, and Ricardo H. Nochetto. Bilayer plates: Model reduction, γ-convergent finite element approximation, and discrete gradient flow. *Communications on Pure and Applied Mathematics*, 70(3):547–589, 2017.

[20] Sören Bartels, Andrea Bonito, and Philipp Tscherner. Error estimates for a linear folding model. *arXiv preprint arXiv:2205.05720*, 2022.

[21] Sören Bartels, Max Griehl, Jakob Keck, and Stefan Neukamm. Modeling and simulation of nematic lce rods. *arXiv preprint arXiv:2205.15174*, 2022.

[22] Sören Bartels, Max Griehl, Stefan Neukamm, David Padilla-Garza, and Christian Palus. A nonlinear bending theory for nematic lce plates. *arXiv preprint arXiv:2203.04010*, 2022.

[23] Sören Bartels and Christian Palus. Stable gradient flow discretizations for simulating bilayer plate bending with isometry and obstacle constraints. *IMA Journal of Numerical Analysis*, 42(3):1903–1928, 2022.

[24] Sören Bartels, Christian Palus, and Zhangxian Wang. Quasi-optimal error estimates for the approximation of stable harmonic maps. *arXiv preprint arXiv:2209.11985*, 2022.

[25] Kaushik Bhattacharya and Richard D James. A theory of thin films of martensitic materials withapplications to microactuators. *Journal of the Mechanics and Physics of Solids*, 47(3):531–576, 1999.

[26] Kaushik Bhattacharya and Richard D. James. The material is the machine. *Science*, 307(5706):53–54, 2005.

[27] Kaushik Bhattacharya, Marta Lewicka, and Mathias Schäffner. Plates with incompatible prestrain. *Archive for Rational Mechanics and Analysis*, 221(1):143–181, 2016.

[28] P Bladon, EM Terentjev, and M Warner. Deformation–induced orientational transitions in liquid crystals elastomer. *Journal de Physique II*, 4(1):75–91, 1994.

[29] Andrea Bonito, Diane Guignard, Ricardo H. Nochetto, and Shuo Yang. Numerical analysis of the LDG method for large deformations of prestrained plates. *arXiv preprint arXiv:2106.13877*, 2021.

[30] Andrea Bonito, Diane Guignard, Ricardo H. Nochetto, and Shuo Yang. LDG approximation of large deformations of prestrained plates. *Journal of Computational Physics*, 448:110719, 2022.

[31] Andrea Bonito, Ricardo H. Nochetto, and Dimitrios Ntogkas. Dg approach to large bending plate deformations with isometry constraint. *Mathematical Models and Methods in Applied Sciences*, 31(01):133–175, 2021.

[32] Andrea Bonito, Ricardo H Nochetto, and Shuo Yang. Γ-convergent LDG method for large bending deformations of bilayer plates. *arXiv preprint arXiv:2301.03151*, 2023.

[33] Juan Pablo Borthagaray, Ricardo H. Nochetto, and Shawn W. Walker. A structure-preserving fem for the uniaxially constrained Q-tensor model of nematic liquid crystals. *Numerische Mathematik*, 145(4):837–881, 2020.

[34] Lucas Bouck and Ricardo H. Nochetto. Projection free method for the full Frank-Oseen model of liquid crystals. *To be submitted*, 2023.

[35] Lucas Bouck, Ricardo H. Nochetto, and Shuo Yang. Convergent fem of a membrane model of liquid crystal polymer networks. *arXiv preprint arXiv:2209.04754*, 2022.

[36] Lucas Bouck, Ricardo H. Nochetto, and Shuo Yang. Reduced membrane model for liquid crystal polymer networks: asymptotics and computation. *arXiv preprint arXiv:2210.02710*, 2022.

[37] Andrea Braides. *Gamma-convergence for beginners*, volume 22. Clarendon Press, 2002.

[38] Andrea Braides. *Local minimization, variational evolution and Γ-convergence*, volume 2094. Springer, 2014.

[39] Susanne C Brenner, L Ridgway Scott, and L Ridgway Scott. *The mathematical theory of finite element methods*, volume 3. Springer, 2008.

[40] Haïm Brezis, Jean-Michel Coron, and Elliott H. Lieb. Harmonic maps with defects. *Communications in Mathematical Physics*, 107(4):649–705, 1986.

[41] M. Carme Calderer, Carlos A. Garavito Garzón, and Baisheng Yan. A Landau–de Gennes theory of liquid crystal elastomers. *Discrete and Continuous Dynamical Systems - S*, 8(2):283–302, 2015.

[42] Miguel Camacho-Lopez, Heino Finkelmann, Peter Palffy-Muhoray, and Michael Shelley. Fast liquid-crystal elastomer swims into the dark. *Nature Materials*, 3(5):307–310, 2004.

[43] Carsten Carstensen. Clément interpolation and its role in adaptive finite element error control. In *Partial differential equations and functional analysis*, pages 27–43. Springer, 2006.

[44] Pierluigi Cesana, Paul Plucinsky, and Kaushik Bhattacharya. Effective behavior of nematic elastomer membranes. *Archive for Rational Mechanics and Analysis*, 218(2):863–905, 2015.

[45] Yunmei Chen. The weak solutions to the evolution problems of harmonic maps. *Mathematische Zeitschrift*, 201(1):69–74, 1989.

[46] Hayoung Chung, Jung-Hoon Yun, Joonmyung Choi, and Maenghyo Cho. Finite-element analysis of the optical-texture-mediated photoresponse in a nematic strip. *Computational Mechanics*, 59(1):147–160, 2017.

[47] Fehmi Cirak, Quan Long, Kaushik Bhattacharya, and Mark Warner. Computational analysis of liquid crystalline elastomer membranes: Changing gaussian curvature without stretch energy. *International Journal of Solids and Structures*, 51(1):144–153, 2014.

[48] Philippe Clément. Approximation by finite element functions using local regularization. *Revue française d'automatique, informatique, recherche opérationnelle. Analyse numérique*, 9(R2):77–84, 1975.

[49] Bernardo Cockburn, George E Karniadakis, and Chi-Wang Shu. *Discontinuous Galerkin methods: theory, computation and applications*, volume 11. Springer Science & Business Media, 2012.

[50] Robert Cohen, Robert Hardt, David Kinderlehrer, San-Yin Lin, and Mitchell Luskin. Minimum energy configurations for liquid crystals: Computational results. In *Theory and Applications of Liquid Crystals*, pages 99–121. Springer, 1987.

[51] Robert Cohen, San-Yih Lin, and Mitchell Luskin. Relaxation and gradient methods for molecular orientation in liquid crystals. *Computer Physics Communications*, 53(1-3):455–465, 1989.

[52] Sergio Conti, Antonio DeSimone, and Georg Dolzmann. Soft elastic response of stretched sheets of nematic elastomers: a numerical study. *Journal of the Mechanics and Physics of Solids*, 50(7):1431–1451, 2002.

[53] Sergio Conti and Georg Dolzmann. Derivation of elastic theories for thin sheets and the constraint of incompressibility. In *Analysis, Modeling and Simulation of Multiscale Problems*, pages 225–247. Springer, 2006.

[54] Sergio Conti and Georg Dolzmann. An adaptive relaxation algorithm for multiscale problems and application to nematic elastomers. *Journal of the Mechanics and Physics of Solids*, 113:126–143, 2018.

[55] Bernard Dacorogna. *Direct methods in the calculus of variations*, volume 78. Springer Science & Business Media, 2007.

[56] Timothy A. Davis and Eugene C. Gartland Jr. Finite element analysis of the Landau–de Gennes minimization problem for liquid crystals. *SIAM Journal on Numerical Analysis*, 35(1):336–362, 1998.

[57] Pierre-Gilles De Gennes and Jacques Prost. *The physics of liquid crystals*. Number 83. Oxford University Press, 1993.

[58] Laurens T. de Haan, Carlos Sánchez-Somolinos, Cees M.W. Bastiaansen, Albertus P.H.J. Schenning, and Dirk J. Broer. Engineering of complex order and the macroscopic deformation of liquid crystal polymer networks. *Angewandte Chemie*, 124(50):12637–12640, 2012.

[59] Antonio DeSimone and Georg Dolzmann. Macroscopic response of nematic elastomers via relaxation of a class of SO(3)-invariant energies. *Archive for Rational Mechanics and Analysis*, 161(3):181–204, 2002.

[60] Manfredo P. Do Carmo. *Differential geometry of curves and surfaces: revised and updated second edition*. Courier Dover Publications, 2016.

[61] Howard C. Elman, David J. Silvester, and Andrew J. Wathen. *Finite elements and fast iterative solvers: with applications in incompressible fluid dynamics*. Oxford Science Publications, 2014.

[62] Jerald L. Ericksen. Nilpotent energies in liquid crystal theory. *Archive for Rational Mechanics and Analysis*, 10(1):189–196, 1962.

[63] Jerald L. Ericksen. Liquid crystals with variable degree of orientation. *Archive for Rational Mechanics and Analysis*, 113(2):97–120, 1991.

[64] Frederick C. Frank. I. liquid crystals. on the theory of liquid crystals. *Discussions of the Faraday Society*, 25:19–28, 1958.

[65] Vsevolod Fréedericksz and V Zolina. Forces causing the orientation of an anisotropic liquid. *Transactions of the Faraday Society*, 29(140):919–930, 1933.

[66] Gero Friesecke, Richard D James, and Stefan Müller. A theorem on geometric rigidity and the derivation of nonlinear plate theory from three-dimensional elasticity. *Communications on Pure and Applied Mathematics*, 55(11):1461–1506, 2002.

[67] Roland Glowinski, Ping Lin, and Xing-Bin Pan. An operator-splitting method for a liquid crystal model. *Computer physics communications*, 152(3):242–252, 2003.

[68] Tyler Guin, Michael J Settle, Benjamin A Kowalski, Anesia D Auguste, Richard V Beblo, Gregory W Reich, and Timothy J White. Layered liquid crystal elastomer actuators. *Nature communications*, 9(1):2531, 2018.

[69] Qing Han and Jia-Xing Hong. *Isometric embedding of Riemannian manifolds in Euclidean spaces*, volume 13. American Mathematical Soc., 2006.

[70] Robert Hardt and David Kinderlehrer. Mathematical questions of liquid crystal theory. In *Theory and applications of liquid crystals*, pages 151–184. Springer, 1987.

[71] Robert Hardt, David Kinderlehrer, and Fang-Hua Lin. Existence and partial regularity of static liquid crystal configurations. *Communications in mathematical physics*, 105(4):547–570, 1986.

[72] Matthieu Hébert, Rama Kant, and Pierre-Gilles De Gennes. Dynamics and thermodynamics of artificial muscles based on nematic gels. *Journal de Physique I*, 7(7):909–919, 1997.

[73] Frédéric Hélein. Minima de la fonctionelle energie libre des cristaux liquides. *CR Acad. Sci. Paris*, 305:565–568, 1987.

[74] Qiya Hu, Xue-Cheng Tai, and Ragnar Winther. A saddle point approach to the computation of harmonic maps. *SIAM Journal on Numerical Analysis*, 47(2):1500–1523, 2009.

[75] Qiya Hu and Long Yuan. A Newton-penalty method for a simplified liquid crystal model. *Advances in Computational Mathematics*, 40(1):201–244, 2014.

[76] Martin Kilian, Aron Monszpart, and Niloy J Mitra. String actuated curved folded surfaces. *ACM Transactions on Graphics*, 36(3):1–13, 2017.

[77] David Kinderlehrer and Biao Ou. Second variation of liquid crystal energy at $x/|x|$. *Proceedings of the Royal Society of London. Series A: Mathematical and Physical Sciences*, 437(1900):475–487, 1992.

[78] Wilhelm Klingenberg. *A course in differential geometry*, volume 51. Springer Science & Business Media, 2013.

[79] Robert V. Kohn and Stefan Müller. Surface energy and microstructure in coherent phase transitions. *Communications on Pure and Applied Mathematics*, 47(4):405–435, 1994.

[80] Arda Kotikian, Ryan L. Truby, John William Boley, Timothy J. White, and Jennifer A. Lewis. 3d printing of liquid crystal elastomeric actuators with spatially programed nematic order. *Advanced Materials*, 30(10):1706164, 2018.

[81] Xiao Kuang, Devin J. Roach, Jiangtao Wu, Craig M. Hamel, Zhen Ding, Tiejun Wang, Martin L. Dunn, and Hang Jerry Qi. Advances in 4d printing: materials and applications. *Advanced Functional Materials*, 29(2):1805290, 2019.

[82] Isabel Kundler and Heino Finkelmann. Strain-induced director reorientation in nematic liquid single crystal elastomers. *Macromolecular rapid communications*, 16(9):679–686, 1995.

[83] Hervé Le Dret and Annie Raoult. The nonlinear membrane model as variational limit of nonlinear three-dimensional elasticity. *Journal de Mathématiques Pures et Appliquées*, 74(6):549–578, 1995.

[84] Hervé Le Dret and Annie Raoult. The membrane shell model in nonlinear elasticity: a variational asymptotic derivation. *Journal of Nonlinear Science*, 6(1):59–84, 1996.

[85] Hui Li. The Kirchhoff theory for elastic pre-strained shells. *Nonlinear Analysis: Theory, Methods & Applications*, 78:1–16, 2013.

[86] Min-Hui Li and Patrick Keller. Artificial muscles based on liquid crystal elastomers. *Philosophical Transactions of the Royal Society A: Mathematical, Physical and Engineering Sciences*, 364(1847):2763–2777, 2006.

[87] Chong Luo and Maria-Carme Calderer. Numerical study of liquid crystal elastomers by a mixed finite element method. *European Journal of Applied Mathematics*, 23(1):121–154, 2012.

[88] Michael E McConney, Angel Martinez, Vincent P Tondiglia, Kyung Min Lee, Derrick Langley, Ivan I Smalyukh, and Timothy J White. Topography from topology: photoinduced surface features generated in liquid crystal polymer networks. *Advanced Materials*, 25(41):5880–5885, 2013.

[89] Joselle M. McCracken, Brian R. Donovan, and Timothy J. White. Materials as machines. *Advanced Materials*, 32(20):1906564, 2020.

[90] L. Angela Mihai and Alain Goriely. A plate theory for nematic liquid crystalline solids. *Journal of the Mechanics and Physics of Solids*, 144:104101, 2020.

[91] Carl D. Modes, Kaushik Bhattacharya, and Mark Warner. Gaussian curvature from flat elastica sheets. *Proceedings of the Royal Society A: Mathematical, Physical and Engineering Sciences*, 467(2128):1121–1140, 2011.

[92] Carl D Modes and Mark Warner. Blueprinting nematic glass: Systematically constructing and combining active points of curvature for emergent morphology. *Physical Review E*, 84(2):021711, 2011.

[93] Cyrus Mostajeran. Curvature generation in nematic surfaces. *Physical Review E*, 91(6):062405, 2015.

[94] Cyrus Mostajeran, Mark Warner, Taylor H. Ware, and Timothy J. White. Encoding gaussian curvature in glassy and elastomeric liquid crystal solids. *Proceedings of the Royal Society A: Mathematical, Physical and Engineering Sciences*, 472(2189):20160112, 2016.

[95] Ricardo H. Nochetto, Michele Ruggeri, and Shuo Yang. Gamma-convergent projection-free finite element methods for nematic liquid crystals: The Ericksen model. *SIAM Journal on Numerical Analysis*, 60(2):856–887, 2022.

[96] Ricardo H. Nochetto, Shawn W Walker, and Wujun Zhang. A finite element method for nematic liquid crystals with variable degree of orientation. *SIAM Journal on Numerical Analysis*, 55(3):1357–1386, 2017.

[97] Carl W. Oseen. The theory of liquid crystals. *Transactions of the Faraday Society*, 29(140):883–899, 1933.

[98] Olivier Ozenda, André M Sonnet, and Epifanio G. Virga. A blend of stretching and bending in nematic polymer networks. *Soft Matter*, 16(38):8877–8892, 2020.

[99] Christopher C. Paige and Michael A. Saunders. Solution of sparse indefinite systems of linear equations. *SIAM journal on numerical analysis*, 12(4):617–629, 1975.

[100] Paul Plucinsky, Benjamin A Kowalski, Timothy J White, and Kaushik Bhattacharya. Patterning nonisometric origami in nematic elastomer sheets. *Soft Matter*, 14(16):3127–3134, 2018.

[101] Paul Plucinsky, Marius Lemm, and Kaushik Bhattacharya. Programming complex shapes in thin nematic elastomer and glass sheets. *Physical Review E*, 94(1):010701, 2016.

[102] Paul Plucinsky, Marius Lemm, and Kaushik Bhattacharya. Actuation of thin nematic elastomer sheets with controlled heterogeneity. *Archive for Rational Mechanics and Analysis*, 227(1):149–214, 2018.

[103] Paul P. Plucinsky. *The deformations of thin nematic elastomer sheets*. PhD thesis, California Institute of Technology, 2017.

[104] Annie Raoult. Quasiconvex envelopes in nonlinear elasticity. In *Poly-, Quasi-and Rank-One Convexity in Applied Mechanics*, pages 17–51. Springer, 2010.

[105] Martin Rumpf, Stefan Simon, and Christoph Smoch. Finite element approximation of large-scale isometric deformations of parametrized surfaces. *SIAM Journal on Numerical Analysis*, 60(5):2945–2962, 2022.

[106] Martin Schadt. Liquid crystal materials and liquid crystal displays. *Annual review of materials science*, 27(1):305–379, 1997.

[107] Cody D. Schimming, Jorge Viñals, and Shawn W. Walker. Numerical method for the equilibrium configurations of a maier-saupe bulk potential in a Q-tensor model of an anisotropic nematic liquid crystal. *Journal of Computational Physics*, 441:110441, 2021.

[108] Joachim Schöberl. C++ 11 implementation of finite elements in ngsolve. *Institute for Analysis and Scientific Computing, Vienna University of Technology*, 30, 2014.

[109] Joachim Schöberl et al. Netgen/ngsolve. *Software hosted at https://ngsolve. org*, 2017.

[110] Francesca Serra, Mohamed A. Gharbi, Yimin Luo, Iris B. Liu, Nathan D. Bade, Randall D. Kamien, Shu Yang, and Kathleen J. Stebe. Curvature-driven, one-step assembly of reconfigurable smectic liquid crystal compound eye lenses. *Advanced Optical Materials*, 3(9):1287–1292, 2015.

[111] Yi-Chung Shu. Heterogeneous thin films of martensitic materials. *Archive for Rational Mechanics and Analysis*, 153(1):39–90, 2000.

[112] Harmeet Singh and Epifanio G. Virga. A ribbon model for nematic polymer networks. *Journal of Elasticity*, pages 1–22, 2022.

[113] G.C. Verwey and Mark Warner. Compositional fluctuations and semisoftness in nematic elastomers. *Macromolecules*, 30(14):4189–4195, 1997.

[114] Epifanio G. Virga. *Variational theories for liquid crystals*, volume 8. CRC Press, 1995.

[115] Shawn W. Walker. A finite element method for the generalized ericksen model of nematic liquid crystals. *ESAIM: Mathematical Modelling and Numerical Analysis*, 54(4):1181–1220, 2020.

[116] Wei Wang, Lei Zhang, and Pingwen Zhang. Modelling and computation of liquid crystals. *Acta Numerica*, 30:765–851, 2021.

[117] Taylor H. Ware, Michael E. McConney, Jeong Jae Wie, Vincent P. Tondiglia, and Timothy J. White. Voxelated liquid crystal elastomers. *Science*, 347(6225):982–984, 2015.

[118] Mark Warner. Topographic mechanics and applications of liquid crystalline solids. *Annual Review of Condensed Matter Physics*, 11:125–145, 2020.

[119] Mark Warner and Cyrus Mostajeran. Nematic director fields and topographies of solid shells of revolution. *Proceedings of the Royal Society A: Mathematical, Physical and Engineering Sciences*, 474(2210):20170566, 2018.

[120] Mark Warner and Eugene Terentjev. Thermal and photo-actuation in nematic elastomers. In *Macromolecular Symposia*, volume 200, pages 81–92. Wiley Online Library, 2003.

[121] Mark Warner and Eugene Michael Terentjev. *Liquid crystal elastomers*, volume 120. Oxford University Press, 2007.

[122] Timothy J White and Dirk J Broer. Programmable and adaptive mechanics with liquid crystal polymer networks and elastomers. *Nature Materials*, 14(11):1087–1098, 2015.

[123] Jingmin Xia, Patrick E. Farrell, and Florian Wechsung. Augmented lagrangian preconditioners for the Oseen–Frank model of nematic and cholesteric liquid crystals. *BIT Numerical Mathematics*, 61(2):607–644, 2021.

[124] Yao Zhao, Yinding Chi, Yaoye Hong, Yanbin Li, Shu Yang, and Jie Yin. Twisting for soft intelligent autonomous robot in unstructured environments. *Proceedings of the National Academy of Sciences*, 119(22):e2200265119, 2022.

[125] William P Ziemer. *Weakly differentiable functions: Sobolev spaces and functions of bounded variation*, volume 120. Springer Science & Business Media, 1989.